Damping of Composite Mast Structures

PhD Thesis

$$(EIv'')'' = q - \rho A\ddot{v}$$

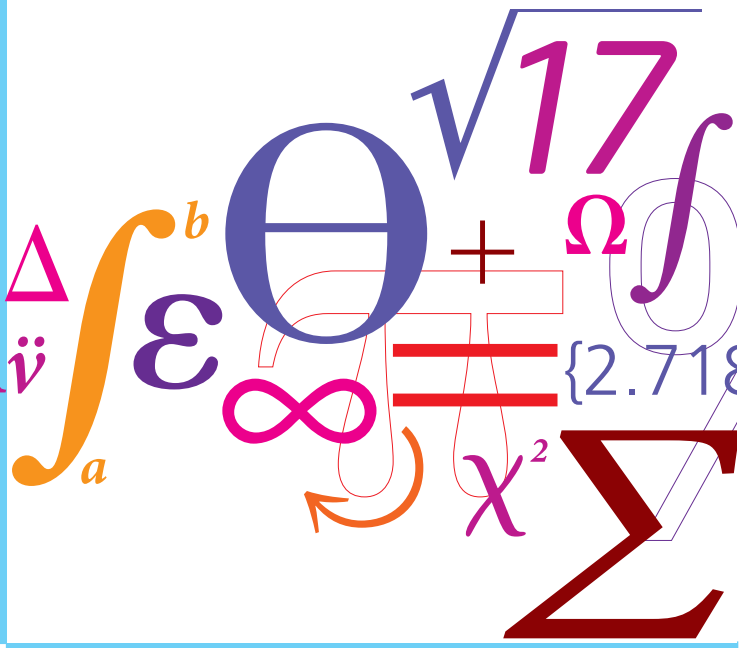

Mathias Kliem
DCAMM Special Report No. S240
March 2018

DTU Mechanical Engineering
Department of Mechanical Engineering

Damping of composite mast structures

Mathias Kliem

PhD Thesis
Section of Solid Mechanics
Department of Mechanical Engineering
Technical University of Denmark
March 2018

Section of Solid Mechanics
Department of Mechanical Engineering
Technical University of Denmark
Nils Koppels Alle, Building 404, DK-2800 Kongens Lyngby, Denmark
Phone +45 4525 1960, Telefax +45 4593 1475
WWW: `http://www.mek.dtu.dk/`

Publication Reference Data
Mathias Kliem
Damping of composite mast structures
Ph.D. Thesis
Technical University of Denmark, Section of Solid Mechanics.
March, 2018
ISBN 978-87-7475-522-7
DCAMM Special report no. S240
Keywords: Damping analysis, composite material, fibre direction dependent damping, modal strain energy approach, cross-section analysis, nanoclay, resin material, dynamic mechanical analysis, Conductor line galloping, bend-twist coupling

Preface

This thesis is submitted in partial fulfilment of the Ph.D. degree from the Technical University of Denmark. The work has been carried out primarily at the Section of Solid Mechanics (FAM), Department of Mechanical Engineering (MEK) at the Technical University of Denmark (DTU). The work has been performed in the period of January 2015 to March 2018 under the supervision of Associate Professor Jan Høgsberg as main supervisor and Associate Professor Christian Berggreen as co-supervisor.

I owe my deepest gratitude to Prof. Jan Høgsberg and Prof. Christian Berggreen for their guidance and support and for openly sharing their knowledge on mechanics of structures with me. Both have provided me with invaluable advice and constructive feedback.

The PhD project was funded by the Innovation Fund Denmark as part of the project 'Power Pylons of the Future' (PoPyFu) (grant no. 106-2013-3). The financial support and the collaboration of the project partners involved in PoPyFu has been greatly appreciated.

I would like to thank Dr. Edith-Roland Fotsing from the Department of Mechanical Engineering at Polytechnique Montréal, Canada who received me for a rewarding two month external stay in his research group. I am also thankful to Joachim Vanwalleghem who was hosting me at University Gent, Belgium for a short term period to carry out forced vibration experiments. I am equally grateful to my former colleagues at Technical University Dresden, Germany for their kind and helpful collaboration during several short term stays. Finally, I would like to thank Tom Løgstrup Andersen and co-workers from the Department of Wind Energy at DTU Risø Campus for their technical support.

Furthermore, I would like to thank my colleagues at the department for their companionship which created a pleasant and stimulant working environment.

Finally I would like to express my deepest thanks to my family for their unconditional support and encouragement during my studies. A special thank you to my beloved wife Ricarda and both our kids Silja and Theo for moving to Denmark to remain by my side during this endeavour. They were continuous sources of inspiration and motivation to me.

Kgs. Lyngby, March 2018

Mathias Kliem

Resumé

Den nødvendige udvidelse på 50,000 km af det Europæiske elektriske net de næste 10 år, giver muligheden for at installere visuelt innovative og flotte kraftpyloner, som vil medføre offentlig accept. Brugen af kompositmaterialer, der ikke er elektriske ledere, til de nye kraftpyloner, vil muliggøre en direkte tilslutning af lederledninger, uden klassisk isolering, og føre til en reduktion af pylonens størrelse. Brugen af en direkte ledning-pylon tilslutning, vil øge den dynamiske interaktion. Dermed vil vindinducerede vibrationer, såsom galloping fænomenet, kunne føre til skader på konstruktionen, forårsaget af en store amplitude af vibrationerne. Den nødvendige foranstaltning for at forhindre galloping af lederledninger, antages at kunne opnås ved at introducere dæmpning direkte i den krydsende kompositarm.
For at designe kraftpylonen, tages potentielle galloping hændelser i betragtning. Dertil er fiberretningsafhngig dæmpning undersøgt grundigt, i forhold til de typiske miljøbetingelser ved galloping. Supplerende dæmpning kan opnås ved at anvende eller implementere adskillige dæmpnings øgende indgreb. I denne afhandling er potentielle dæmpnings indgreb vurderet til anvendelse i et miljø med høj spænding, i forhold til opførelsen af dmpning ved lave temperaturer og frekvenser, som er de typiske betingelser for galloping. Opførelsen af dæmpning af sammensatte kompositprøver og sub-strukturer, er derfor numerisk og eksperimentelt undersøgt.
Den præsenterede afhandling er opdelt i fire dele, som hver især vedrører hvordan galloping i lederledninger forhindres, ved forbedret dæmpning i kompositmaterialer og sub-strukturer.

Den første del viser et udvalg af lovende dæmpnings indgreb til kompositmaterialer og strukturer, velegnet til højspndings brug, og effektive under de typiske miljøbetingelser ved galloping af ledningsledninger. Gennemførligheden ved produktion og de potentielle bivirkninger af indgrebene, er vurderet ved brug af eksempler.

I den anden del, er den dynamisk-mekaniske karakterisering beskrevet til dæmpningsmodificerede kompositmaterialer og sub-strukturer af master. Denne er beskrevet ved typiske temperaturer og frekvenser for galloping, med focus på indgreb på mikro-skala, meso-skala og makro-skala niveau.

Den tredje del præsenterer en fremgangsmåde til numerisk simulering af dmpning, ved brug af modal tøjningsenergi metoden. De numeriske resultater sammenlignes med de eksperimentelle resultater af prøvestænger og strukturelle tests.

I den sidste del af afhandlingen, udføres en numerisk galloping analyse, med henblik på evaluering af dæmpningens effekt, og forskellige understøtningsforhold af kabler til potentiel forhindre af galloping af ledningsledninger.

Abstract

The required expansion of the European electrical grid by 50.000 km within the next 10 years provides the opportunity to install visually innovative and beautified power pylons, generating a broad public acceptance. The use of non-conductive composite materials for the novel power pylon will enable the direct attachment of the conductor lines without classic insulators and, consequently, a reduction in its size. The use of a direct cable-pylon connection will increase in the dynamic interaction, so that wind-induced vibrations like the severe galloping phenomenon, may lead to structural damage due to excessive vibration amplitudes. The necessary measure to mitigate conductor line galloping is assumed to be achieved by introducing damping into the directly linked composite cross arm.
In order to design the power pylon for potential galloping events, the fibre direction dependent damping properties of the non-conductive composite materials is thoroughly investigated for environmental conditions typical for galloping. Additional damping may be achieved by the application or implementation of several damping enhanced treatments. In the thesis, potential damping treatments for an application in high-voltage environment are evaluated with regard to the damping behaviour at low temperatures and frequencies, typical for galloping conditions. The damping behaviour of composite coupon specimens and sub-structures is therefore numerically and experimentally investigated.
The present thesis is organized in four parts, all concerning the mitigation of conductor-line galloping by the damping enhancement in composite materials and (sub-)structures.

The first part presents a selection of promising damping treatments for composite materials and structures, suitable in high-voltage applications and effective at environmental conditions typical for conductor-line galloping. The manufacturing feasibility and potential side effects of the treatments are assessed using examples.

In the second part the dynamic-mechanical characterisation is described for damping-modified composite materials and mast sub-structures at temperatures and frequencies typical for galloping, focusing on treatments at micro-scale, meso-scale and macro-scale level.

The third part presents a numerical damping simulation approach using the modal strain energy method. The numerical results are thereby compared with experimental results of coupon specimens and structural tests.

In the final part of the thesis a numerical galloping analysis is conducted to evaluate the effect of damping and different cable support conditions for a potential mitigation of conductor-line galloping.

Publications

Appended journal papers

[P1] Mathias Kliem, Jan Høgsberg, Qian Wang, Martin Dannemann: Characterization of Clay-modified thermoset polymers under various environmental conditions for the use in high-voltage power pylons, *Advances in Mechanical Engineering*, **9**:1–16, 2017.

[P2] Mathias Kliem, Marvin Rüppel, Jan Høgsberg, Christian Berggreen, Sina Baier: Damping properties of non-conductive composite materials for applications in power transmission pylons, *Journal of Composite Materials*, First published online: March 25, 2018; DOI: 10.1177/0021998318766635.

[P3] Mathias Kliem, Jan Høgsberg, Joachim Vanwalleghem, Angelos Filippatos, Stefan Hoschützky, Edith-Roland Fotsing, Christian Berggreen: Damping analysis of cylindrical composite structures with enhanced viscoelastic properties, *Applied Composite Materials*, In press, DOI: 10.1007/s1044301896842

[P4] Mathias Kliem, Daniel Johansen, Jan Høgsberg: Mitigation of conductor line galloping by enhanced damping in composite power pylons, submitted.

Additional contributions

Conference papers and posters

[C1] Mathias Kliem, Jan Høgsberg, Christian Berggreen, Composite Power Pylons for High-Voltage Transmission Lines, *Poster, 15th DCAMM Symposium*, March 16-18, 2015, Horsens, Denmark.

[C2] Mathias Kliem, Jan Høgsberg, Martin Dannemann, Characterization of fibre direction dependent damping of glass fibre composites at low temperatures and low frequencies, *Proceedings of 17th European Conference on Composite Materials*, June 26-30, 2016, Munich, Germany.

[C3] Mathias Kliem, Jan Høgsberg, Stefan Hoschützky, Joachim Vanwalleghem, Angelos Filippatos, Experimental analysis of passive constrained layer damping treatments for composite power pylon structures, *Proceedings of 10th Canadian-International conference on composite materials and products*, July 17-20, 2017, Ottawa, Canada.

[C4] H. Skouboe, F. M. F. Da Silva, M. H. Mikkelsen, C. Berggreen, C. L. Bak, J. P. Waldbjørn, Q. Wang, M. Manouchehr, T. Jahangiri, M. Kliem, The composite pylon, *Proceedings of CIGRE Session, SC B2 OVERHEAD LINES*, 2018, Paris, (accepted).

Data publication

[D1] Mathias Kliem, Experimental data for analysing the damping behaviour of non-conductive composite materials, *Mendeley Data*
doi: 10.17632/65t5zzxvm5.1

[D2] Mathias Kliem, Data for: Damping analysis of cylindrical composite structures with enhanced viscoelastic properties, *Mendeley Data*
doi:10.17632/jxy3m76dg5.1

[D3] Mathias Kliem, Fortran-, Python- and Abaqus-Codes for: Mitigation of conductor line galloping by enhanced damping in composite power pylons, *Mendeley Data*
doi:10.17632/3gg4mc2n8t.1

List of abbreviations

AF	Aramid fibre
BD	Bidirectional
CA	Cross arm
CAT	Computer axial tomography
CL	Constraining layer
CLD	Constrained layer damping
COS	Coordinate system
CNC	Computerised numerical controlled
CT	Computerised axial tomography
DMTA	Dynamic mechanical thermal analysis
EP	Epoxy
FE	Finite element
FEA	Finite element analysis
FRP	Fibre reinforced plastic
FVR	Fibre-volume-ratio
GF	Glass fibre
GFRP	Glass fibre-reinforced plastic
LVDT	Linear variable differential transformer
NC	Nanoclay
NT	Nanotube
PU	Polyurethane
RT	Room temperature
SEM	Scanning electron microscopy
TEM	Transmission electron microscopy
UD	Unidirectional
UV	Ultraviolet
VBT	Vibrating beam testing
VE	Vinyl-ester
VEM	Viscoelastic material
XRD	X-ray diffraction

Contents

Chapter 1

Introduction and background

The design of standard steel lattice transmission towers, dominating the landscape today, has not been changed over the last 60 years in terms of visual impact [1]. A recently growing political opposition and civil society [2] exerts pressure on transmission system operators to reassess the use of standard lattice towers for the required expansion of the European electrical grid by 50.000 km within the next 10 years, in particular due to the increasing demand for renewable energies [3–5]. A redesign using non-conductive composite materials will provide the opportunity to install visually innovative and beautified power pylons, generating a broader public acceptance. Furthermore, a reduction in size will be achieved due to the integration of insulators by using non-conductive structural materials, instead of applying classical long insulators (see Fig. 1.1).

Figure 1.1: Composite power pylon with directly attached overhead transmission line bundles, [6].

Composite-based power pylons are, at the same time, assumed to be cost-competitive relative to standard steel lattice towers and may therefore provide an attractive alternative to underground cables, which are many times more expensive [7].
However, a direct and rigid connection of conductor lines to the composite power pylon, enabled by non-conductive composite materials, may significantly increase the dynamic interaction compared to the classic lattice tower design using long in-

sulators. Wind-induced vibrations of conductor lines, such as the severe galloping instability, may therefore be directly transferred into the composite masts.
Galloping vibrations may cause phase flash overs between adjacent phase conductors up to structural damage of the cable clamps or the entire power pylon due to excessive vibration amplitudes at resonance. Galloping is therefore one of the main design drivers for the overall architecture of large high-voltage power transmission systems. At the same time, the horizontal spacing between adjacent phase conductors as well as the vertical safety clearance to the ground is partly determined by the vibration amplitudes of the galloping conductor lines, in order to prevent flash-overs.

A reduction in galloping amplitudes is thereby highly desired as it may enable a closer spacing of conductor lines and a reduction in power pylon size, due to a reduced vertical safety clearance. It is assumed that galloping vibrations may be mitigated by sufficiently high damping within the composite pylon structure, as the self-damping capability of conductor lines can be ignored [8]. Composite materials are thereby particularly suited due to the highly flexible design space, where potentially opposing design parameters like damping, stiffness and weight may be tuned according to the requirements. Furthermore, composite materials provide the unique feature of tailoring the products material properties to special demands like flame retardancy or enhanced damping behaviour by adding fillers to the resin or modifying the reinforcement during manufacturing [9].

With increasing complexity of the component geometry and laminate architecture, the use of analytical design approaches is only feasible to a limited extent. The dynamic design of composite mast (sub-)structures, described in the thesis, is therefore based on numerical finite element simulations for the investigation of galloping conductor lines (see [P4]) and the fibre direction dependent damping using the modal strain energy approach (see [P2] and [P3]). All numerical damping simulations are verified by various experimental investigations (see [P1], [P2], [P3]).

1.1. Galloping conductor lines

Galloping is a wind induced vibration phenomenon potentially leading to critical and costly damage such as broken conductors and fittings, damaged tower components or even entire tower collapses [10]. The low-frequent galloping vibration with large amplitudes is typically initiated by asymmetrical ice aggregations along conductor lines, exposed to steady cross winds with moderate to strong wind conditions. The typical temperature for galloping to happen is below the freezing point and is therefore considered between - 20 °C and 0 °C, leading to cable vibrations at frequencies between 0.5 Hz and 2 Hz. Peak-to-peak vibration amplitudes in magnitude similar to the cable sag have usually been observed for galloping modes with

up to 3-loops. The amplitude decreases for higher modes. In Fig. 1.2, a galloping incidence of a 345 kV transmission line system is shown, representing a 1-loop galloping mode.

Figure 1.2: Documented galloping event: 345 kV transmission line system with galloping conductor lines in a 1-loop mode (South Dakota, USA), [11].

The galloping motion is characterised by a dominating vertical component and a small horizontal component, forming the so called galloping ellipse. Once galloping is initiated, the vibration may occur up to 24 h, fatiguing the materials and structures [12].

1.2. Damping mechanisms in composite materials and structures

The damping in composite materials can be up to several orders of magnitudes higher than in traditional engineering materials such as metals and alloys [13]. Several sources of energy dissipation within fibre reinforced plastic materials (FRP), characterised by its highly non-homogeneous and anisotropic nature, can be identified [14, 15]:

1) Viscoelastic properties of the polymer matrix, fibre and interface material

(dependent on its relative proportions).

2) Interface related damping.

3) Damping due to damage.

4) Viscoplastic damping.

5) Thermoelastic damping.

The primary damping source for a non-damaged composite mast structure vibrating with small amplitudes at low frequencies, can be related to 1) the viscoelastic behaviour of the individual components of the composite material. The viscoelastic propteries of the polymer matrix are hence considered to dominate the global damping behaviour. Therefore, the damping of a representative unidirectional (UD) ply is highly dependent on its fibre direction: The damping transverse to the fibre direction is higher due to the matrix dominated properties compared to the direction parallel to the fibres. Aramid fibres (AF) are reported to exhibit a higher damping capacity than glass (GF) and carbon fibres (CF).
The addition of filler materials, such as nanoclays (NC), to the resin leads to a large interfacial area, providing frictional damping due to local sliding effects specified under 2). The damping sources identified in 3), 4) and 5) may be neglected based on the assumptions mentioned above.
Besides the listed internal damping sources in composite materials, additional damping treatment for composite structures should be mentioned [16]: Damping layers of soft viscoelastic material (VEM) can either be integrated into the laminate as interleaved films or applied to an existing structure as constrained layer damping (CLD). Energy is thereby increasingly dissipated by transverse shear deformations of the VEM due to structural bending, providing an increasing structural loss factor.
However, the damping of composite materials can be tuned the same way as the stiffness by choosing the relevant design variables: The properties of each individual component of the composite, the layup of the plies as well as the global fibre volume ratio. Due to opposing objective functions of stiffness, strength and damping, a suitable trade-off has to be found in the dynamic design of composite structures.

1.3. Research hypotheses and related objectives of the PhD study

Although composite materials exhibit considerably higher damping properties compared to conventional engineering materials like steel, the damping capacity in one

account may be insufficient to significantly mitigate conductor line vibration amplitudes at low frequencies and temperatures, requiring additional damping treatments.
A dynamic pre-design of the power pylon, based on damping properties available in the literature, is thereby not feasible, as the fibre direction dependent damping of non-conductive composite materials at temperatures and frequencies typical for galloping (- 20 °C to 0 °C and 0.5 Hz to 2 Hz) have not been investigated yet. In the effort of applying promising damping treatments to composite materials and mast sub-structures, the following research hypotheses are defined:

1) The fibre direction dependent damping properties of composite materials, determined on coupon level, may be used to predict the trend in damping of composite sub-structures by numerical simulations.

2) The dynamic-mechanical properties of composite materials thereby highly depend on the used characterisation techniques.

3) Additional passive damping treatments, suitable for high-voltage applications, may increase the damping capacity of non-conductive composite laminates and structures, leading to a mitigation of conductor line galloping.

4) Damping in composite power pylon structures is required, as galloping induced power pylon vibrations may be close to the natural frequencies of the structure.

5) Galloping vibrations may be reduced by rigidly clamping the conductor line to the composite arm instead of applying classical long insulators.

The aim of this research is to mitigate galloping vibrations by enhanced damping properties of the composite power pylon. The focus of the present research includes the characterisation of the damping properties of non-conductive composite materials and sub-structures at temperatures and frequencies typical for galloping, with and without additional damping treatments. Based on the above listed research hypotheses the following objectives are defined:

1) Evaluation of damping enhanced treatments to improve the damping properties of composite materials and structures for a potential application at high-voltage.

2) Investigation of the fibre direction dependent damping properties of non-conductive composite materials, with and without applied damping treatments, by different characterisation methods at environmental conditions typical for galloping.

3) Derivation and assessment of constructive measures in the composite cross arm design in order to further enhance damping.

4) Implementation of the modal strain energy approach into a commercial finite element software to calculate the damping behaviour of laminates and composite sub-structures.

5) Demonstration of a potential mitigation of conductor line galloping by rigidly connected cables to the composite cross arm with enhanced damping properties.

1.4. Structure of the thesis

The thesis consists of an extended summery covering the following two main aspects: (1) The numerical and experimental analysis of damping enhanced treatments on composite materials and structures used in high-voltage applications and (2) the associated potential to reduce the vibration amplitudes of galloping conductor lines and thereby prevent costly damage of the power system.
Four journal papers are attached, denoted [P1] to [P4], which are covering the presented topics in greater detail. The extended summary is organised as follows:
First, potentially usable damping enhanced treatments for composite materials and structures in high-voltage applications, presented in [P1] to [P3], are summarised in Chapter 2. A selection of the most promising methods are evaluated by means of examples, regarding the manufacturing feasibility and potential side effects on the material properties.
Next, the dynamic-mechanical characterisation of the damping-modified composite materials and generic sub-structures is summarised in Chapter 3 for both, environmental conditions typical for galloping and at room temperatures for verification purposes with numerical simulations. While the focus in [P1] is only on micro-scale level, analysing the matrix material, the damping on meso-scale (ply level) and macro-scale (sub-structural level) is studied in [P2] and [P3], respectively.
The numerical damping simulation, presented in [P2] and [P3], is described in Chapter 4: The modal strain energy approach is thereby applied to predict the damping of bidirectional (BD) coupon specimens and generic mast sub-structures with constrained layer damping treatments. The numerical models are compared against experimental test results.
Finally, in Chapter 5 the effect of a direct cable-pylon connection as well as damping within the composite arm structure on the galloping vibration amplitudes is summarised, based on work presented in [P4]. In the last section of the extended summery, Chapter 6, concluding remarks with regard to the main results are presented together with an outlook towards possible future directions.

Chapter 2

Selected damping enhanced treatments

The relatively high damping properties of composite materials compared to metallic materials, provided by the viscoelastic nature of the polymer resin, may further be increased by additional damping enhanced treatments. However, their application in high voltage composite power pylon structures limits the selection of potentially available damping treatments due to the following restrictions:

1) High-voltage: The dispersion of carbon nano tubes into the polymer resin, reported to enhance the structural damping properties [14,17], is not practical due to associated increase in electrical conductivity.

2) Harsh environmental conditions: The organic flax fibre, with its substantial vibration damping properties [18], is limited for external applications due to potential humidity retention [19, 20].

3) Low cost, robustness, reliability and free of maintenance: Active vibration control is therefore not appropriate.

4) Complex loading conditions: The application of tuned mass dampers in the pylon structure, each with its tuned frequency, is not feasible to damp galloping vibrations, as the wind-induced cable vibration frequencies considerably depend on the ambient temperature, the cable tension and sag, the galloping mode and the mass of the ice accretion. Furthermore, the galloping frequencies are expected to be significantly lower than the natural frequencies of the power pylon structure.

However, the remaining damping enhanced treatments for composite materials, to be used in high voltage applications, may act at different scaling levels. The addition of non-conductive nanoclay (NC) to the polymer resin system will mainly affect the matrix dominated properties of a lamina on nano-scale level, thoroughly investigated in [P1], whereas an application of constrained layer damping treatments may enhance the damping behaviour independent from the fibre direction on a (sub-)structural level, as represented in [P3]. However, three different and electrically non-conductive damping enhanced treatments are summarised in Chapter 2, based on investigations presented in [P1] on nanoscale level, [P2] on laminate level and [P3] on sub-structural level.

Further relevant dependencies of the static- and dynamic-mechanical properties of the used materials on the temperature, the frequency, various ageing conditions such as water immersion and UV-exposure are presented in [P1] and [P2].

2.1. Matrix modification by Nanoclay

2.1.1. Introduction

The application of nanotechnology provides the possibility to enhance specific material properties of resin or composite materials by employing nano-scale materials as reinforcements [13]. Nanoclays (NC) are thereby particularly attractive as they are cheap, widely available and are reported to provide both enhanced damping and static material properties in polymer matrices [21, 22]. Furthermore, the desired increase in electrical non-conductivity for the application in composite power pylon structures is also reported [23].
Most clay minerals, which are commonly used as reinforcement within polymer matrix materials, consist of a layered or ribbon-like structure of individual single clay layers, also known as platelets [24]. In order to mostly benefit from the property enhancing effect of NC, the initially agglomerated clay within the unmixed matrix material needs to be broken up ideally into single clay platelets, providing an extremely high aspect ratio. Frictional sliding at these clay platelet-matrix interfaces, called stick-slip behaviour, is seen as the main mechanism of NC within the polymer matrix, which leads to enhanced damping properties. However, an improvement of these dynamic-mechanical properties thereby mainly depends on the quality of the clay dispersion in the matrix, as remaining clay aggregations are weakening the polymer host material the same way as e.g. the presence of voids.
The high-speed homogeniser technology is chosen for the preparation of all NC samples used in [P1] and [P2], as it is reported to effectively disperse nanoclay into standard thermosetting resin systems, such as Epoxy (EP) and Vinyl-ester (VE) [25, 26]. However, the dispersion processes has in turn been evaluated in the presented investigation [P1] to be the bottle neck for a feasible application on large scale. In order to obtain a highly qualitative NC-matrix dispersion with regard to a sufficient amount of single platelets, the mixing duration simply takes too long.
This section summarises the processing, the quality assurance and the characterisation of nano-composites and NC-modified AF-EP and AF-VE composite samples with special regard to the enhancement of the dynamic-mechanical properties at temperatures and frequencies typical for conductor line galloping, based on the work presented in [P1] and [P2].

2.1.2. Processing and quality assurance

The effect of NC on the damping properties of neat EP and VE is investigated in [P1] for different weight percentages (0 wt. %, 1 wt. %, 2 wt. % and 3 wt. %) of an alkyl ammonium-based NC, commercially available as 'Garamite 1958'. In [P2], the damping enhancing properties are verified on laminate level for UD composite samples considering five different fibre directions (0 °, 30 °, 45 °, 60 ° and 90 °) by adding 2 wt. % of NC. However, the preparation of two NC modified resin materials, EP and VE, is made in the same way, using a high-speed homogeniser. Several quality assurance technologies, such as the scanning electron microscopy (SEM), the transmission electron microscopy (TEM), the X-ray diffraction (XRD) and rheological measurements are used to study the morphology of the obtained NC-resin dispersion (see Fig. 2.1).

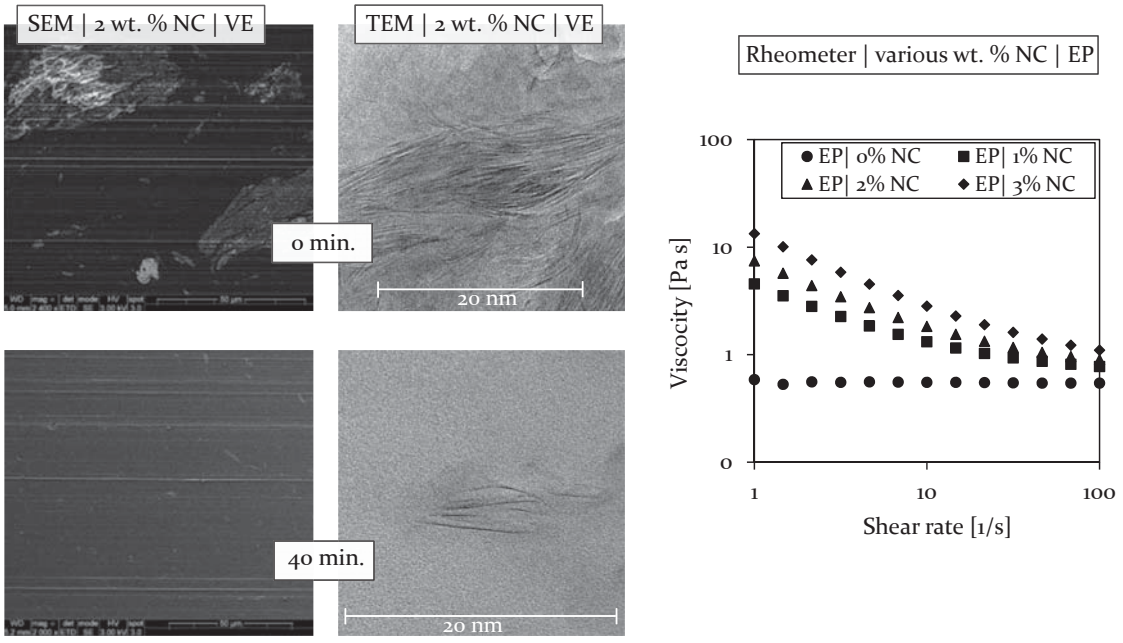

Figure 2.1: Quality assurance techniques such as SEM (left), TEM (middle) and rheological measurements (right) to analyse the level of clay exfoliation within the VE and EP matrix. From [P1].

The samples, used for the SEM and TEM microscopy, are taken from the cured matrix material on a random basis, demonstrating the effectiveness of the mixing process. After 40 min of mixing the initially present clay agglomerates are broken up into single platelets or packages of a few clay layers. These levels of clay platelet-separation are also known as exfoliation or intercalation, respectively, whereas the presence of exfoliated clay platelets lead to the highest improvement of material properties.
A rheological analysis of the non-cured clay-resin dispersion may also be used to

draw conclusions on the level of exfoliation. The observed decrease in viscosity with increasing shear rate, called shear-thinning, is found to be directly linked to a large portion of exfoliated clay platelets [27, 28]. However, the achieved clay-resin dispersion is assumed to be of high quality in order to relate the change in the static and dynamic material properties directly to the addition of nanoclay.
The NC-modified resin is used to manufacture two different sample plate types, from which specimens for static and dynamic tests are cut out: 1) NC-modified EP and VE and 2) unidirectional plates made of aramid fibre reinforced plastic (AFRP) and glass fibre reinforced plastic (GFRP). The dynamic-mechanical testing procedure is summarised in chapter 3 in more detail.

2.1.3. Enhanced damping properties

The effect of NC on the dynamic-mechanical properties of standard thermosetting resin systems, such as EP and VE, and AF-composites is discussed in the following for vibration frequencies and temperatures typical for galloping, based on experimental results. The effect of NC on the static-mechanical properties of EP- and VE-nanocomposites with regard to harsh environmental conditions, such as UV-exposure and water immersion, which will be experienced by composite power pylons during an expected life time of 100 years, is thoroughly investigated in [P1] and will not be discussed in the following section.

On matrix-material level

The diagrams in Fig. 2.2 represent the damping properties obtained by the Dynamic-Mechanical-Thermal-Analysis (DMTA) of NC-modified EP and VE at temperatures and frequencies typical for galloping events (- 20 °C and 0 °C at 0.5 Hz). The damping properties of non-aged VE and EP samples increase proportional to the amount of added NC at all investigated temperatures. Whereas the addition of 3 wt. % NC lead to an increase in loss factor of about 23 % and 28 % for VE at 0 °C and - 20 °C, respectively, the damping is only slightly enhanced by about 5 % for EP at both temperatures. The increasing effect of water immersion on the damping behaviour of VE and EP is as expected, due to the swelling and softening behaviour of polymer materials by absorbing water molecules [29]. An additional NC-modification leads to a slight amplification of the effect. In contrast, UV-light exposure decreases the damping properties of VE and EP, independent on any NC modification, due to related embrittlement of the polymer.
It can be concluded that an addition of NC may potentially enhance the damping properties of thermosetting resin systems like EP and VE. The degrading effect of environmental ageing on the matrix properties, in particular by UV-light, may effectively be prevented by the application of coatings on the composites cross arm [30].

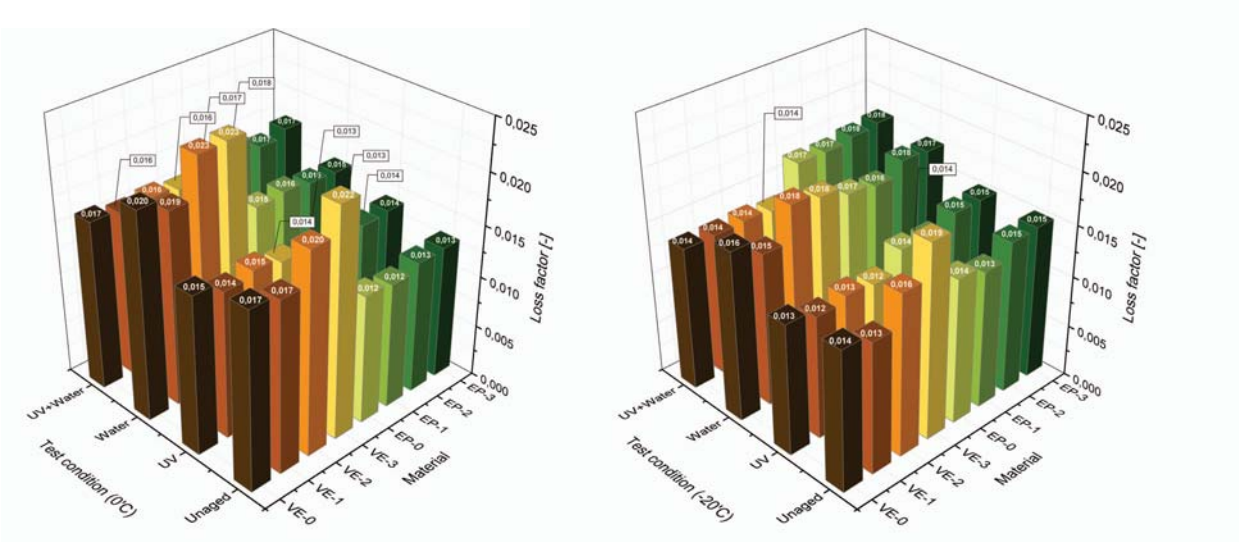

Figure 2.2: Damping properties of NC-modified EP and VE resin samples before and after ageing [DMTA, 0 °C (left) and -20 °C (right) at 0.5 Hz]. From [P1].

On laminate level

The material properties, such as the vibrational damping characteristics, of fibre reinforced plastic (FRP) materials highly depend on the fibre direction φ (see Fig. 2.3).

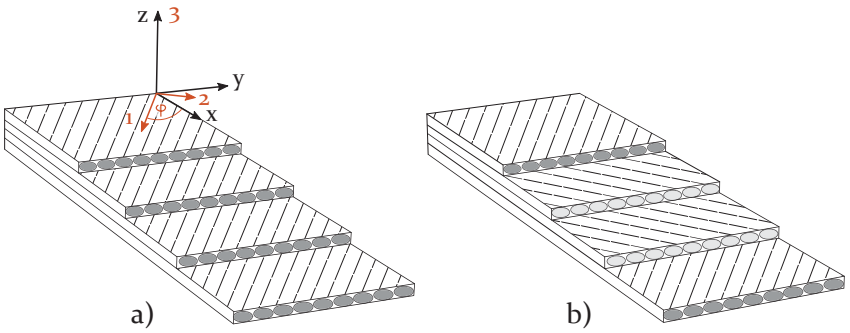

Figure 2.3: Variation of the stacking sequence: a) Off-axis stack (unidirectional (UD) and unbalanced, $[\varphi]_n$) and b) angle-ply stack (bidirectional (BD), balanced, $[\pm\varphi]_{ns}$) with regard to the global and local material coordinate system (COS). From [P2].

The fibre direction dependent damping properties are thereby required as input pa-

rameters, in order to numerically model the damping behaviour of FRP structures by using the modal strain energy method (discussed in more detail in chapter 4). The frequencies and temperatures during the experimental characterisation should therefore be chosen to represent the environmental conditions of interest. As the focus of the PhD is on the structural vibration damping of conductor line galloping, the dynamic-mechanical characterisation is carried out at frequencies and temperatures typical for galloping (-20 °C to 0 °C and 0.5 Hz to 1 Hz). The effect of 2 wt. % NC on the fibre-direction dependent damping properties of AFRP is shown in Fig. 2.4, further discussed in detail in [P2]. The plotted results for AF-EP-0 and AF-VE-0 (0 wt. % NC) as well as AF-EP-2 and AF-VE-2 (2 wt. % NC) are based on measurements using a DMTA (see section 3.1).
The loss factor η of a representative UD lamina is usually higher in transverse direction (fibre angle $\varphi = 90\,^\circ$) than in the fibre dominated longitudinal direction ($\varphi = 0\,^\circ$), represented by

$$\eta_{90} = \left(\frac{E''}{E'}\right)_{90} > \left(\frac{E''}{E'}\right)_{0} , \tag{2.1}$$

where E' and E'' represent the storage and loss modulus of the lamina, respectively. The properties in transverse direction are matrix dominated, leading to higher damping due to the viscoelastic nature of the polymer. Therefore, an NC-modification of the polymer matrix mainly improves the matrix dominated properties, leading to enhanced damping properties at $\varphi \geq 30\,^\circ$, as shown in Fig. 2.4.

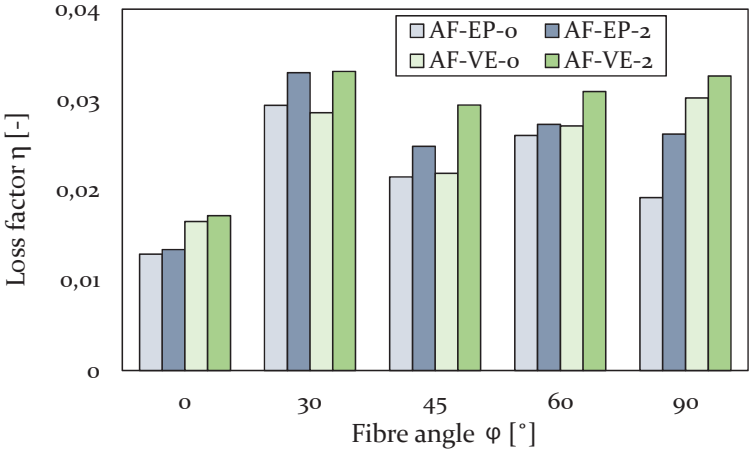

Figure 2.4: Effect of NC modification on the fibre direction dependent damping behaviour of AF-EP and AF-VE specimens [DMTA, -20 °C at 1 Hz]. From [P2].

The damping enhancement in fibre direction ($\varphi = 0\,^\circ$) by 2 wt. % NC is with 4 % much lower than the average increase in damping in the matrix dominated direction $30\,^\circ \leq \varphi \leq 90\,^\circ$ with 14 % and 15 % for AF-EP-2 and AF-VE-2. This is close to the

findings of the nanocomposite damping properties (see Fig. 2.2). The addition of 2 wt. % NC to EP and VE at -20 °C lead to an increase in damping by about 12 % and 14 %, respectively.
However, the overall loss factor η for AF-EP and AF-VE composites in the matrix dominated direction ($\varphi \geq 30\,°$) is with about 0.027 almost twice as high as the damping of the neat EP and VE matrix (see Fig. 2.2). This may be due to the high damping properties of AF in the direction transverse and parallel to the anisotropic fibre [31]. For a better understanding, the damping in the matrix and the fibre may be illustrated by two parallel connected dampers, representing the overall damping by the sum of the single dampers. The higher the fibre damping, the higher the overall damping, although the damping in the matrix remains constant.
To summarise, the addition of 2 wt. % NC to the matrix is observed to increase the matrix dominated damping properties by about 14 % to 15 %. However, the damping properties in the fibre direction are almost unaffected by an NC modification.

2.2. Hybridisation of the fibre reinforcement

2.2.1. Introduction

AF composites are already used in high voltage insulators due to its non-conductive nature and excellent mechanical properties [32]. Their considerable vibration damping capacity and the good fatigue resistance, both higher compared to GF composites, are substantial arguments for an application in composite power pylons. In contrast, higher material costs, the poor compressive strength and the tendency to absorb moisture are potential draw backs for a large scale application in high voltage power pylons [33, 34].
A hybridisation of the fibre reinforcement may be an excellent alternative, providing the possibility to combine desired material properties of different fibres in order to achieve a greater efficiency [35] and to reduce potential downsides by specifically treating and placing each material within the laminate according to its characteristics. However, the fibre hybridisation is reported to be an effective tool to enhance the dynamic-mechanical properties of composite materials [36, 37]. The addition of AF, with their beneficial damping and fatigue properties, to glass fibre (GF) composites is reported to increase in the vibration damping capacity and the stiffness of the laminate [38].
In the following section, the fibre direction dependent damping enhancement of unidirectional AF-GF-hybrid composite materials is evaluated for environmental conditions typical for galloping, based on the work presented in [P2].

2.2.2. Experimental results

Two AF-GF-EP hybrid stacking sequences are evaluated with regard to its damping behaviour at low frequencies and temperatures and are compared to its non-hybrid AF-EP and GF-EP counterparts. The fibre direction dependent damping for all four stacking configurations is represented in Fig. 2.5.

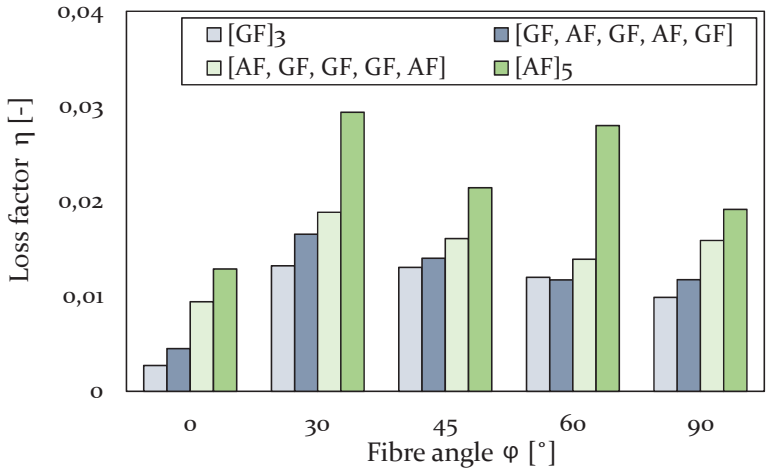

Figure 2.5: Effect of fibre-hybridisation on the fibre direction dependent damping behaviour of GF-EP, AF-EP and AF-GF-EP [DMTA, -20 °C at 1 Hz]. From [P2].

As expected, the loss factor of the laminate gradually increases proportional to the amount of AF. In comparison to a pure GF-EP laminate, the damping of a pure AF-EP laminate is observed to increase by a factor of 4.8 in the direction parallel to the fibre ($\varphi = 0\,^\circ$) and by a factor of 2.0 in average for fibre directions $\varphi \geq 30\,^\circ$. The reduced difference between the two fibre angles $\varphi_1 = 0\,^\circ$ and $\varphi_2 \geq 30\,^\circ$ is due to the contribution of the viscoelastic matrix to the damping.
The hybridisation of the fibre reinforcement is obtained by the addition of two unidirectional AF layers to the reference GF-EP laminate, corresponding to an increase of only 15 wt. %. The damping enhancement thereby strongly depends on the position of the AF layers within the stack. By placing two AF layers at the outer most location [AF, GF, GF, GF, AF], an increase by a factor of 3.5 and 1.4 in average is achieved for $\varphi_1 = 0\,^\circ$ and $\varphi_2 \geq 30\,^\circ$, respectively, compared to the reference laminate GF-EP. The increasing factor reduces to 1.7 and 1.1 in average for $\varphi_1 = 0\,^\circ$ and $\varphi_2 \geq 30\,^\circ$, respectively, when placing the AF layers to the inside [GF, AF, GF, AF, GF]. This is expected, as the outer layers experience larger deformations in bending, therefore dominating the structural behaviour. The low compressive strength of aramid is of minor importance, as the cross arm is designed for stiffness with a maximum allowable tip deflection.
It can therefore be concluded that a hybridisation of AF and GF may be a cost-

effective way to increase the damping properties of the composite material, used in the power pylon cross arm, by in average 36 % for the off-axis direction and up to 3.5 times in fibre direction, compared to the reference GF-EP laminate.

2.3. Constrained layer damping treatment

2.3.1. Introduction

Mechanical energy may effectively be dissipated from a vibrating structure by introducing soft damping layers made of viscoelastic materials (VEM), which are sandwiched between the structure and a stiff constraining layer [39]. The damping treatment is therefore called constrained layer damping (CLD). When the structure flexes due to vibration, shear strains are introduced into the damping layer, converting kinetic energy into heat and thereby introducing damping. The CLD treatment may effectively be applied to high voltage composite power pylons, as it is a low cost, robust, reliable and maintenance-free structural vibration control method [40], using a rubber-like damping layer with electrical non-conductive properties [41]. It is reported that a CLD treatment is most effective when the viscoelastic damping layer operates close to its glass transition temperature T_g [42], which characterises the transition from the glassy state to a viscous and rubbery state. As conductor line galloping typically occurs at temperatures below the freezing point, the viscoelastic damping material DYAD 601 from Soundcoat with its T_g close to the freezing point is used in the analysis (see [P3] for further details).
The aim of this section is to demonstrate the effectiveness of CLD treatments on generic composite cylinders, representing the composite cross arm of the power pylon in the scale 1:10 with respect to dimensions and stacking sequences of the laminate. The damping in the generic composite cylinders, restricted by the design specifications to a circular outer geometry, is maximised by the use of well located CLD treatments in combination with structural modifications on the inside of the structure. Several cross-sectional design concepts are thereby presented and tested in order to identify the concept with the highest damping. This concept may be used in composite power pylons to potentially mitigate wind induced cable vibrations such as galloping. More information about the manufacturing and experimental damping analysis are provided in [P3].

2.3.2. Cross-sectional design concepts

The application of CLD treatments to a host structure should preferably be considered at locations with potentially high shear deformations within the damping layer. This may either be far from the neutral plane for structures undergoing flexural vibrations [43], or close to the neutral plane due to the presence of maxi-

mum shear stresses [44]. However, the design flexibility for potential CLD locations along the circumference is limited for hollow and cylindrical composite cylinders. Based on existing damping concepts, which consider the addition of sub-structural components for the application of CLD treatments [45–47], composite shear webs are introduced into the neutral plane of the generic composite cylinder in order to provide a stiff structure for a potential application of CLD treatments. The highest damping may thereby be observed when the structure flexes in the direction perpendicular to the shear web, introducing maximum shear deformations to the damping layer along the entire width of the CLD treated web.
Eight potential CLD configurations for the generic composite cylinder are derived (cross sectional design A to I), considering the effective CLD locations mentioned above. An overview of the different cross sectional designs (design A to I) is presented in Fig. 2.6.

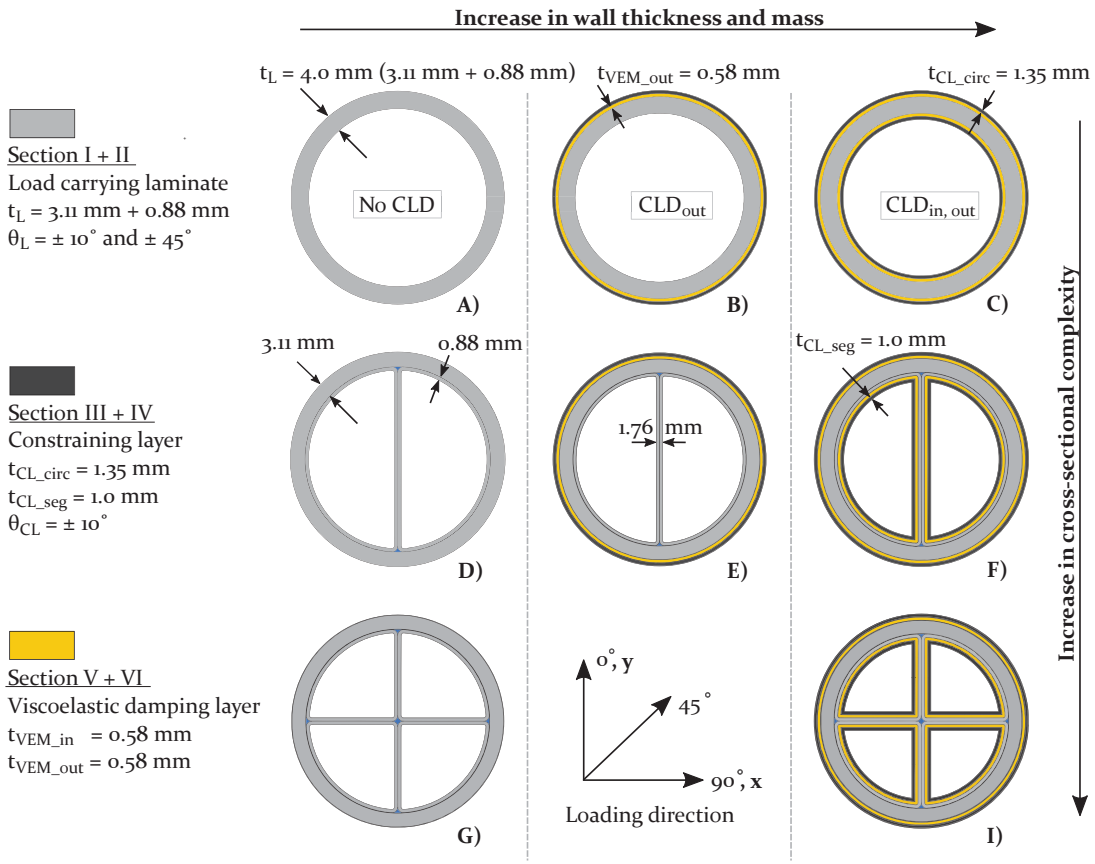

Figure 2.6: Overview of the different cross-sectional designs with details of the stacking sequence and loading direction (not drawn to scale). From [P3].

One or two shear webs may potentially be integrated into the generic composite cylinder (concept D and E or G and I), as bending loads on the cross arm are expected in the x- and y- directions due to the directly attached and potentially

Table 2.1: Geometric and stacking properties of the generic composite cylinder. From [P3].

Parameter	Layup and Dimensions
Free specimen length l	950 ± 5 mm
Constant inner diameter D_i	79.0 mm
Wall thickness 'host structure'	4.0 mm
Host structure layup	$[\pm 45\,^\circ, \pm 45\,^\circ, \pm\ 10\,^\circ, \pm 45\,^\circ]$
Constraining layer (CL) layup	$[\pm 10\,^\circ]$
Layer thickness GFRP $[\pm 45\,^\circ]$	0.88 mm
Layer thickness GFRP $[\pm 10\,^\circ]$	1.00 mm (segment) - 1.35 mm (circular)
Layer thickness VEM	0.58 mm
Spacer plate thickness	3.0 mm

galloping conductor lines (see Fig. 1.1). The viscoelastic damping layers are required to be placed only at the out- or inside of the composite structure, keeping the VEM out of the load carrying laminate. This specification is due to the safe load introduction of overhead transmission lines into the cross arm over the expected structural lifetime of 100 years.
Although an interleaving of VEM into the load carrying structure is often used to increase the damping, it considerably weakens the laminate and may reduce the load carrying capacity drastically. For the sake of simplicity, a constant wall thickness of the load carrying laminate for all generic composite cylinders is assumed. All dimensions and layups are specified in Tab. 2.1. An application of CLD treatments onto the generic composite cylinders without changing the load carrying laminate may potentially lead to an increase in stiffness and a changed vibration behaviour. In order to fairly compare the damping enhancement of the different design concepts, the specimens are grouped based on the level of applied CLD treatments (no CLD, $\mathrm{CLD_{out}}$, $\mathrm{CLD_{in,out}}$). This approach is considered as a trade-off between the structural requirements mentioned above and the scientific evaluation of the damping enhanced treatments.

2.3.3. Experimental investigation

The potential of CLD treatments is demonstrated based on the results of the experimental damping analysis. All generic GF-composite cylinders were therefore manufactured using a wet filament winding process and a segmentable mandrel, in order to enable the implementation of the shear webs and the VEM in one 'shot' (see [P3] for details regarding the manufacturing process). The viscoelastic damping layer was applied during the manufacturing process and co-cured with the GFRP

host structure. A selection of generic composite cylinders, reinforced at the end for a reliable free-fixed clamping, and a microsection of the cross section of the cross-sectional design concept I) are presented in Fig. 2.7.

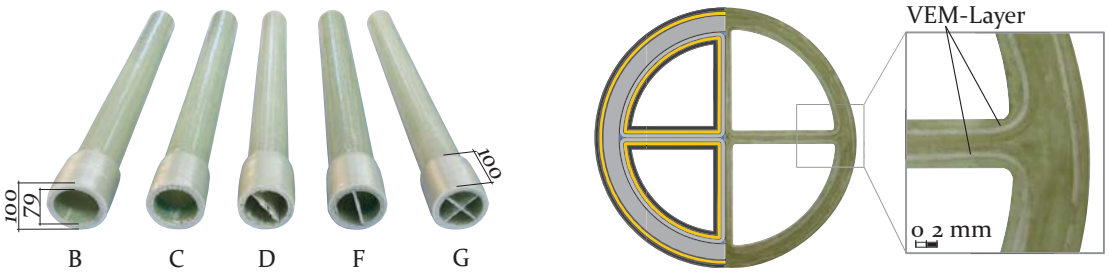

Figure 2.7: Selection of different manufactured cylindrical composite design concepts (left) and cross-sectional distribution of the VEM for the design concept I) (see Fig. 2.6) with a zoom into the interesting area (right). From [P3].

The damping of all composite cylinders is experimentally determined by exciting the cantilever structure by an impact and analysing its free decay. The dynamic-mechanical characterisation process is summarised in detail in section 3.2.

2.3.4. Experimental results

The experimentally determined modal loss factors η_1 of the generic composite cylinder for the first flexural mode (with frequency f_1) are represented in Fig. 2.8 for all eight cross-sectional design concepts, classified into three groups. The number in the sample notation defines the loading direction (see Fig. 2.6). The gradually increasing trend in damping by the application of CLD treatments from group 'No CLD' to group '$\text{CLD}_{\text{in,out}}$' is clearly observed and as expected. The CLD-free reference concept A exhibits thereby the lowest damping with $\eta = 0.013$, whereas the highest damping is observed for concept F.90 with $\eta = 0.038$. The implementation of shear webs (D.90, D.0 and G.45) seems to slightly increase the damping in the group 'No CLD', due to its matrix dominated material properties of the $\pm 45\,^\circ$ laminates. The application of CLD treatments circularly to the outside of the structure leads to an increase in damping of about 90 % compared to the reference concept A. A beneficial contribution of additional shear webs is thereby not observed (concept E.90 and E.0) due to the dominant effect of the outer CLD treatment.
As expected, the highest damping is observed for F.90 with an increase of about 190 % compared to concept A., representing the concept with the highest amount of VEM subjected to shear deformation: 1) Far away from the neutral axis at the out- and inside of the cylindrical section and 2) close to the neutral plane along the shear web.

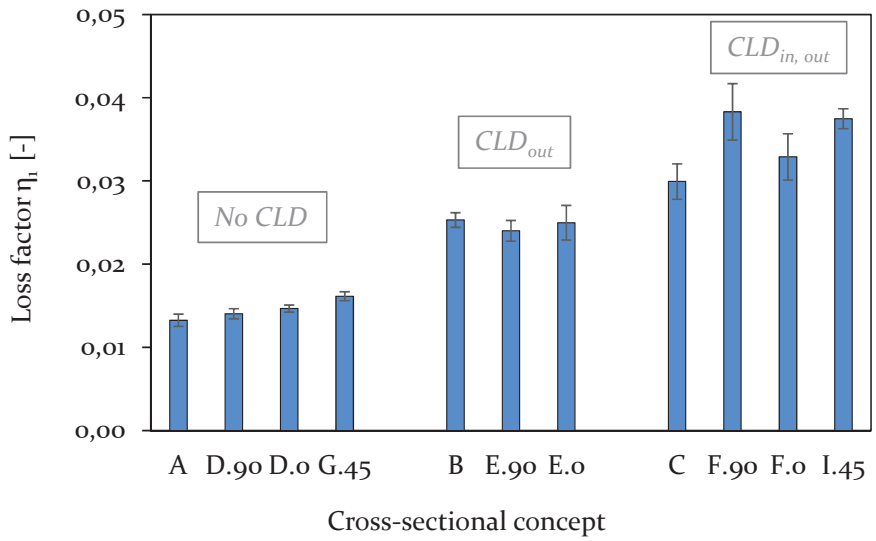

Figure 2.8: Results of the modal loss factor η_1 related to the first flexural mode for all cross-sectional design concepts. From [P3].

The additional amount of VEM and stiff constraining layers consequently leads to an increase in the sample weight (see Tab. 2.2).

Table 2.2: Design-related properties of the different generic composite cylinders. From [P3].

Parameter	Cross-sectional design							
	A	B	C	D	E	F	G	I
Mass [kg]	2.04	3.00	3.69	2.32	3.36	4.67	2.56	5.30
Fibre volume content [%]	51.0	45.6	51.3	50.4	53.4	48.4	48.8	42.4

The increase in static stiffness on one side and the increase in sample weight on the other side almost equalises under dynamic flexing conditions of the structure as only small changes in the natural frequencies for all cross-sectional concepts are observed (see Fig. 2.9). At the same time, the damping increases by almost a factor 3 for concept F.90.
It can therefore be concluded that an application of CLD in combination with additional shear webs may considerably increase the damping behaviour of composite cross arm structures, represented by generic composite cylinders with various CLD treatment configurations (concept A to I), while the related natural frequencies remain almost unchanged. As always, the final design of the cross arm is based on a trade-off between additional costs, due to an increased complexity of structure (F.90) and an increased material consumption, and an enhanced damping behaviour

of almost factor 3 on the other side.

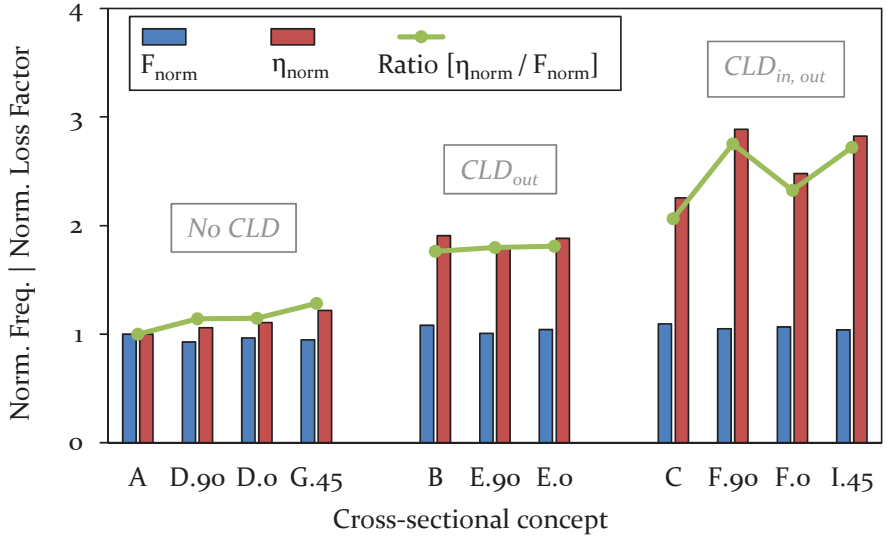

Figure 2.9: Results of the normalised frequency and loss factor (with respect to the reference design concept A) and its related damping-frequency-ratio. From [P3].

Concluding remarks

The presented selection of non-conductive damping enhanced treatments demonstrates the potential of each approach with its individual characteristics for the use in high voltage composite power pylons. A nanoclay modification mainly enhances the damping performance in the off-axis fibre direction, whereas the hybridisation of the fibre-reinforcement leads primarily to a damping increase in the fibre direction. In both cases, the stiffness and damping may cost-effectively be enhanced, though the nanoclay modification is evaluated not to be suitable for mass production of large scale structures. In contrast, CLD treatments are highly suitable for the application on large scale structures and may lead to an increase in damping by a factor 3 compared to a non-treated reference structure, based on the results summarised above.

Chapter 3

Dynamic-mechanical characterisation

The damping properties of composite materials strongly depend on the fibre direction, the temperature and, to some extend, on the frequency. An increase in temperature will soften the matrix, enhance the damping, but considerably decrease the stiffness [48]. Below the glass transition temperature T_g of the sample, a change in frequency is reported to only slightly influence the damping properties [49].
For the design of composite structures, used in specific environmental conditions, the knowledge about the dynamic-mechanical properties is essential. For instance, the fibre direction dependent in-plane damping properties η_1, η_2 and η_{12} at low temperature (between -20 °C to 0 °C) and low frequencies (0.5 Hz to 2 Hz) are required as input parameters in order to numerically predict the damping behaviour of composite power pylons during the severe galloping phenomenon. However, only insufficient data for the composite materials of interest are available in the literature with regard to the temperature and frequency range typical for galloping vibrations. Therefore, the dynamic-mechanical characterisation of various composite materials is summarised in this section, based on two typically used techniques: Vibration beam testing (VBT) and Dynamic-Mechanical-Thermal Analysis (DMTA), both described in detail in [P1] and [P2]. Furthermore, the damping behaviour of unbalanced off-axis and balanced angle-ply laminates for five different fibre directions is presented, in order to discuss the influence of the bend-twist-coupling on the damping. Finally, the technique to determine the damping properties of the generic composite cylinder, representing the power pylon cross arm in the scale 1:10, is described based on the same boundary conditions as used for the VBT method.

3.1. On coupon level

The standardised DMTA [50] and VBT [51] method are used to analyse the damping of various GF- and AF-composite materials at environmental conditions, which are typical for galloping (see section 2.1.3 and 2.2.2). The main purpose of using two different damping characterisation techniques is due to the following points:

1) Partly contradictory results of VBT and DMTA measurements are reported in the literature:

   a) Amplitude dependent differences: While the 'intra fibre friction mechanism' dominates the damping at small deformations (DMTA), 'intra and inter-yarn friction mechanisms' are typical for larger deformations (VBT) [52].

   b) Frequency dependent differences: An increase in damping proportional to the frequency is reported for GF-EP and AF-EP using VBT measurements [53], whereas the opposite trend is reported for characterising carbon fibre reinforced plastics (CFRP) by DMTA measurements [54]. The mismatch may be explained by different support conditions and highly different vibration amplitudes (see 1.a)

2) The VBT is used to verify an equivalent numerical model with free-clamped support conditions, using the modal strain energy approach (see section 4.2.1). The approach has later been extended to a numerical model of the vibrating generic composite cylinder (see section 4.2.2), representing the power pylon cross arm (see [P3]).

Both characterisation techniques with their different working principles, support conditions, sample sizes and vibration amplitudes, are used to determine the damping in the following five fibre directions $\varphi = 0\,^\circ$, $30\,^\circ$, $45\,^\circ$, $60\,^\circ$ and $90\,^\circ$.
The damping, provided by the DMTA, is based on the measured phase lag δ between the applied stress and the responding strain. In contrast, the dynamic response of the free vibrating composite beam, represented by a declining sine curve, is used to calculate the damping ratio ζ by fitting an exponential envelope $g(t)$ to the decay, represented by

$$g(t) = X_0 e^{-\zeta\omega_1 t}\,, \tag{3.1}$$

where ω_1, ζ and X_0 represents the natural frequency, the damping ratio and the initial displacement, respectively [55]. The time history of the tip displacement is contactless measured by a laser sensor, as it is reported to give the most accurate displacement measures [56]. For low damping, the loss factor η may be represented by the other damping definitions

$$\eta \approx \frac{\psi}{2\pi} \approx \frac{\lambda}{\pi} \approx 2\zeta \approx \tan\,\delta\,, \tag{3.2}$$

with ψ being the specific damping capacity, λ being the logarithmic decrement, ζ being the damping ratio and δ being the phase angle [57]. In Fig. 3.1, the setups for the DMTA and the VBT methods are shown.

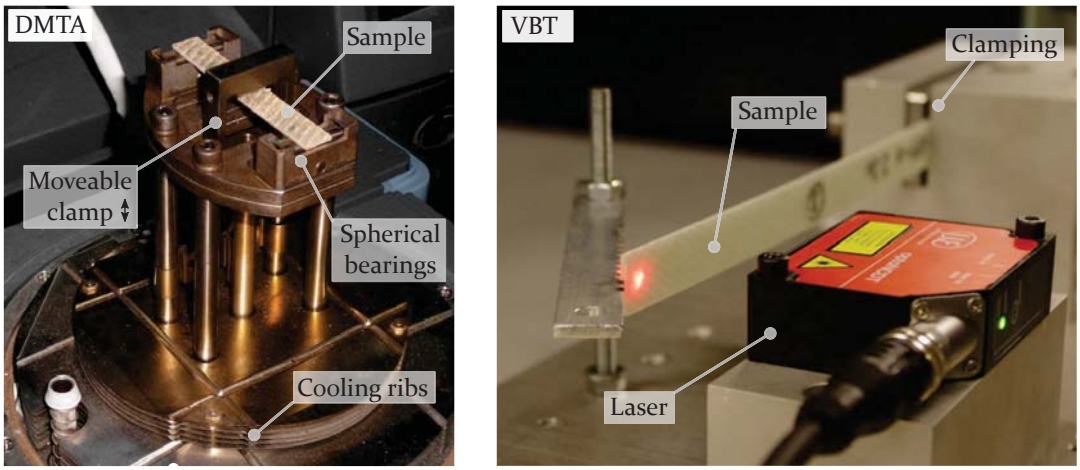

Figure 3.1: Left: Dynamic mechanical thermal analysis (DMTA) with a three-point-bending configuration (forced vibration) | Right: Vibration beam testing (free vibration). From [P2].

The results of the fibre direction dependent damping based on the two damping methods are represented in Fig. 3.2 for a GF-VE composite material. Also, the influence of different initial tip displacements is shown for the VBT method. The frequency is kept constant at 20 Hz for both measurement. The length of the vibrating beam is thereby varied for VBT.

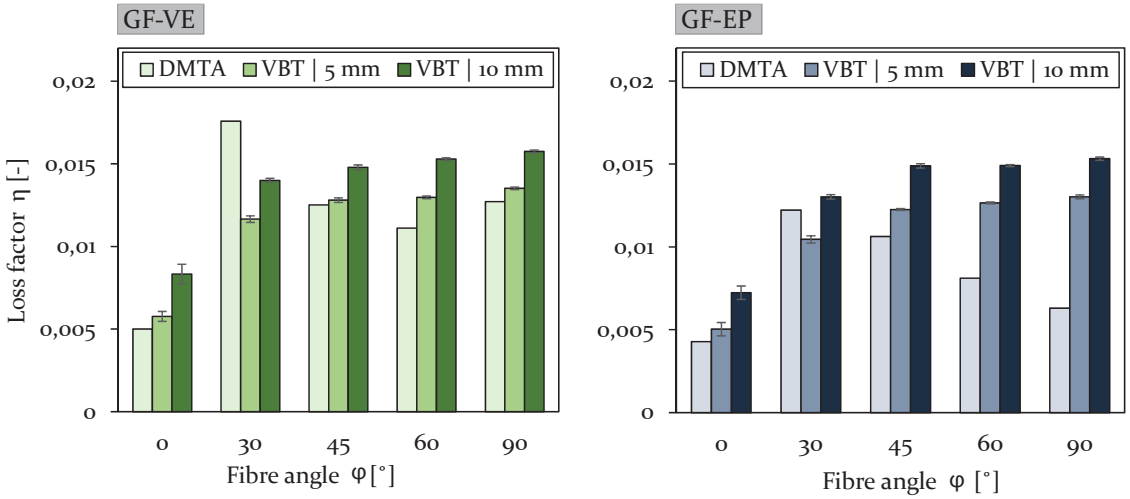

Figure 3.2: Effect of the test method (DMTA vs. VBT with 5 mm and 10 mm initial tip displacement) on the fibre direction dependent damping properties of GF-VE and GF-EP at 20 °C at 20 Hz. From [P2]

A reduction from 10 mm to 5 mm initial tip displacement leads to reduced damping properties of about 20 % for all fibre directions. This may be explained by a reduced influence of air damping, clamping effects and tip deflection dependent non-linearities. In order to minimise such external effects on material damping measurements, the vibration amplitudes are proposed to be small. The observed peak value for the damping at $\varphi \approx 30\,^\circ$ is due to the bend-twist coupling of off-axis laminates. This effect, surprisingly only captured by DMTA measurements, is discussed in the section 3.1.1 on bend-twist coupling.
To summarise, no major differences, except from the peak at $\varphi \approx 30\,^\circ$ for DMTA results, are observed for GF-VE, analysed by VBT and DMTA measurements at the frequency of 20 Hz. The trend of both damping techniques is well captured. A similar trend is observed for GF-EP, presented in [P2], although increasing differences are observed for fibre angles $\varphi \geq 60\,^\circ$. However, the results appear in a different light when plotting the fibre direction dependent damping with regard to DMTA and VBT measurements for different frequencies (see Fig. 3.3).

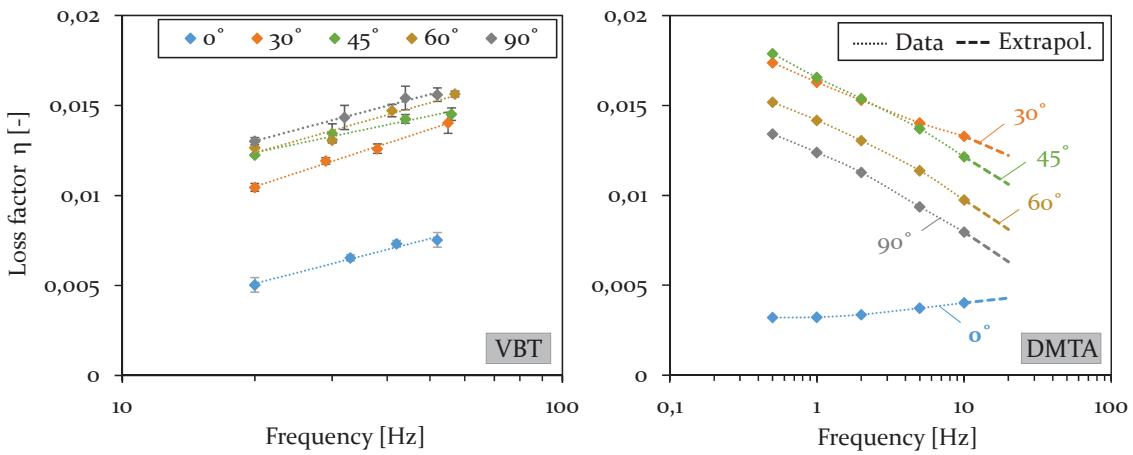

Figure 3.3: Frequency dependent damping results of off-axis GF-EP samples, obtained by VBT (left) and DMTA measurements (right). From [P2] and [P3].

Although the frequency range for the presented VBT and DMTA results is not the same, the contrary trend in the fibre direction dependent damping properties is clearly observed. Only for the fibre direction $\varphi = 0\,^\circ$ similar results are achieved. The discrepancy may be explained by highly differing vibration amplitudes with $a_{DMTA} = 0.15\,\text{mm}$ and $a_{VBT} = 5\,\text{mm}$ and different support conditions for DMTA (simple supported) and VBT (clamped-free). However, the results of both damping characterisation methods are used as input parameters for the numerical damping prediction of composite coupons and (sub-)structures (see chapter 4).

3.1.1. Bend-twist coupling

The damping results, obtained by DMTA measurements, show a characteristic peak at the fibre angle $\varphi \approx 30\,^\circ$ (see Fig. 3.2). The observation is in agreement with the literature [54,58] and explained by the bend-twist coupling of off-axis laminates, subjected to bending loads (see Fig. 2.3). It is unexpected that the coupling related damping is only observed by DMTA measurements with its spherical bearings at both sides (see Fig. 3.1), as coupling-induced deformations are also unrestricted during VBT. However, the numerical damping prediction of composite structures consisting of angle-ply laminate is often reported to be based on the material properties of off-axis laminates with its characteristic bend-twist coupling [54, 59]. It is therefore assumed that a systematic error is introduced as the bend-twist coupling effects are erroneously considered, potentially leading to an overestimation of the damping properties of composite structures. In order to quantify the potential error, the damping is measured by VBT and DMTA for coupons with two different stacking sequences: a) Off-axis stack (UD, unbalanced, $[\varphi]_3$) and b) angle-ply stack (BD, balanced, $[\pm\varphi]_s$) (see Fig. 2.3). The results for GF-VE are presented in Fig. 3.4.

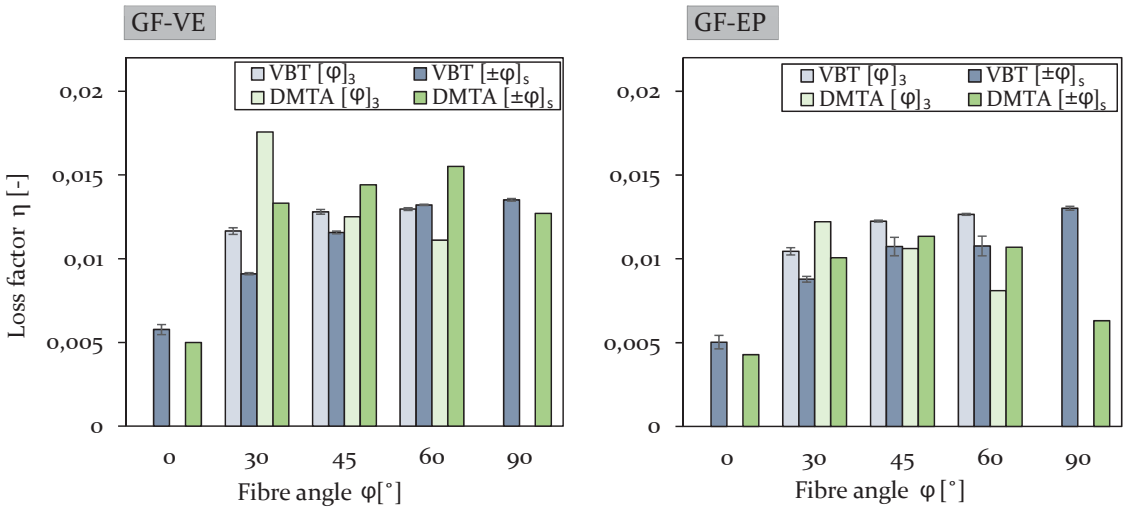

Figure 3.4: Effect of the stacking sequence (unbalanced $[\varphi]_3$ vs. balanced $[\pm\varphi]_s$) on the fibre direction dependent damping behaviour of GF-VE (left) and GF-EP (right) [DMTA and VBT (5 mm), 20 °C at 20 Hz].

The same trend is observed for GF-EP, although the damping properties, obtained by DMTA, decrease for fibre angles $\varphi \geq 60\,^\circ$. Angle-ply laminates ($[\pm\varphi]_s$), investigated by DMTA, lead to slightly higher damping properties compared to off-axis laminates $[\varphi]_3$ (except for $\varphi \approx 30\,^\circ$), whereas for VBT it is the other way around. A clear trend is thereby not observed, partly because of the potential differences in the measuring techniques.

However, the four different sets of results, presented in Fig. 3.4, are used to calculate the fibre direction dependent input parameters η_1, η_2 and η_{12}, as described in the following section. Based on the four input parameter sets, the damping of a freely vibrating beam with an angle-ply stack $[\pm\varphi]_s$ is numerically predicted (see section 4.2.1). The differences are evaluated in order to quantify the expected error mentioned above.

3.1.2. Fibre direction dependent damping

In order to numerically predict the damping behaviour of (thin-walled) composite structures by using the modal strain energy method (see chapter 4), the fibre direction dependent (in-plane) damping properties of each individual material η_1, η_2 and η_{12} are required as input parameters for the simulation. Theses in-plane damping properties may be approximated by the Adams-Bacon-approach [60],

$$\begin{aligned} \eta_\varphi \;=\; E^{'}(\varphi)\; \Bigg[\frac{\eta_1}{E_1^{'}} (\cos\varphi)^4 \;+\; \frac{\eta_2}{E_2^{'}}\, (\sin\varphi)^4 + \\ \left(\frac{\eta_{12}}{G_{12}^{'}} \;-\; (\eta_1 \;+\; \eta_2)\; \frac{\nu_{12}}{E_1^{'}} \right) (\sin\varphi)^2\, (\cos\varphi)^2 \Bigg] \;, \end{aligned} \tag{3.3}$$

where E_1', E_2', G_{12}' and ν_{12} are the static material properties, φ represents the fibre direction and η_φ corresponds to the experimentally determined damping properties by VBT or DMTA for different fibre directions, e.g. $\varphi = 0\,^\circ, 30\,^\circ, 45\,^\circ, 60\,^\circ$ and $90\,^\circ$. The related $E^{'}(\varphi)$ represents the fibre direction dependent Young's modulus, which may be determined by previously conducted tensile tests. The approach is thereby only restricted to 'free-flexure' conditions: The resulting torsional deformation of structures with an unbalanced stacking sequence is allowed, when subjected to pure bending. This is the case for both measurement methods: For VBT with beams clamped in a fixed-free support condition and for DMTA with simple supported specimens by spherical bearings. The mismatch between the measured damping $\eta_{\varphi\,exp}$ and the calculated damping η_φ is minimised by using the method of least squares,

$$\min_{\vec{x}} \sum_{j=1}^{n} (\eta_{\varphi j\,exp} \;-\; \eta_{\varphi j}(\vec{x}))^2 \quad \text{with} \quad \vec{x} = [\eta_1, \eta_2, \eta_{12}] \quad \text{and} \quad n \geq 3 \;. \tag{3.4}$$

The out-of-plane damping properties for the presented thin walled structure may be approximated by the in-plane equivalents: $\eta_{22} \approx \eta_{33}$, $\eta_{12} \approx \eta_{13} \approx \eta_{23}$ [61]. The resulting fibre direction dependent material damping properties η_1, η_2 and η_{12} are used as input parameters for the numerical damping simulation described in chapter 4. An equivalent shear damping $\eta_{12_{eq}}$ is introduced for angle-ply laminates $[\pm\varphi]_s$.

3.2. On sub-structural level

As mentioned in section 3.1, the principle of the VBT approach is extended to a larger scale, due to the same support conditions, for determining the damping properties of the generic composite cylinders with its different CLD design concepts. The beam-like structures are thereby clamped in fixed-free support condition (see Fig. 3.5).

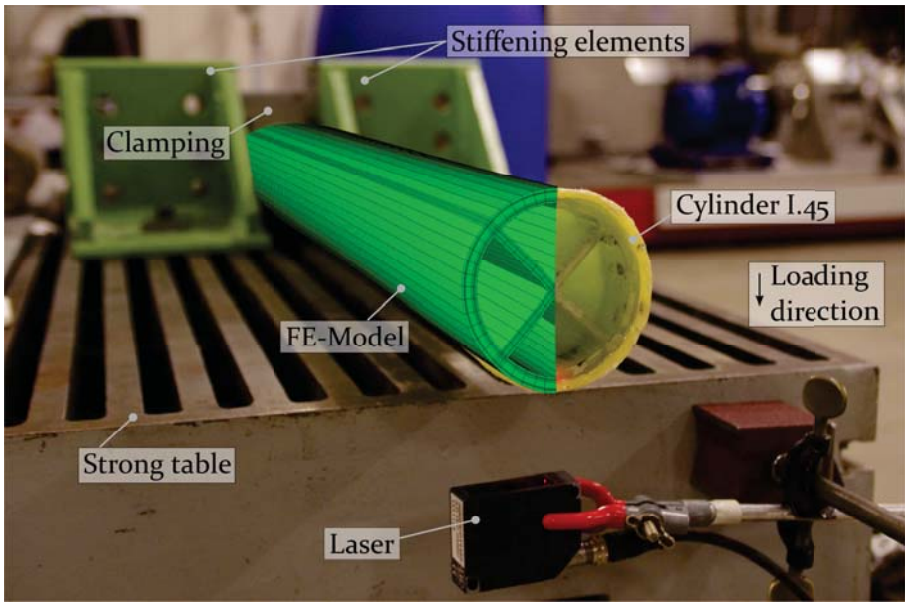

Figure 3.5: Free vibration test rig of the cylindrical sub-structure (cross sectional concept I.45) in a clamped-free support condition. From [P3].

The same approach, used for structures with similar dimensions as the generic composite cylinders, is reported to generate damping results which are in good agreement with numerical results [62, 63].
The choice of testing the generic composite cylinder in a cantilever support condition is also inspired by its original design purpose, representing the (cantilever) cross arm of the power pylon (see Fig. 1.1). The joint section between both sub-structures provides additional (friction) damping. Therefore, fixed-free support conditions are assumed to represent the original cross arm application more realistically than the idealised and often proposed free-free support. This support condition results in a considerable change of the structural vibration behaviour: The significant increase in natural frequency (e.g. factor 10 reported in [64]) leads to unrepresentative damping results due to the highly frequency dependent damping properties of the viscoelastic damping layer.
Furthermore, the effectiveness of CLD treatments is based on the shear deformation of the damping layer. In case of a free-free supported structure, which is excited by an impact, the overall deflection of the structure is very low and, to some extend,

local due to the impact. The level of shear deformation in the damping layer may therefore be very small and locally limited. It is therefore questionable if the performance of CLD treatments may sufficiently be represented by testing the composite cylinder in a free-free-support condition.
The damping characterisation of the generic composite cylinder is thereby carried out using a fixed-free support condition. A proper clamping is particularly of high importance, in order to minimise the friction damping at the fixed end of the generic composite structure [13]. Metallic inserts are used at the end sections of the composite cylinders in order to allow radial clamping, as also used in [63]. Furthermore, the flanges are reinforced and processed as accurately as possible. All samples are clamped the same way (same procedure, same torque) in order to allow comparability, as potential errors due to non-ideal clamping conditions may affect each single test result the same way.
The excitation of the clamped structure to vibrate in a bending mode is performed by a rubber block impulse in vertical direction on the reinforced tip section of the cylinder. The damping is thereby calculated based on the free decay of the vibrating generic composite cylinder by fitting an exponential envelope $g(t)$, defined in Eq. (3.1), to the declining sine curve. As several modes are thereby excited, of which the higher modes (torsional modes, axial modes) will quickly die out, the first 10 periods are neglected for the calculation of the damping properties. In order to verify the assumption, a Fast Fourier Transformation (FFT) of the experimentally determined time history is carried out for the cross sectional concept A to demonstrate the dominance of the first bending mode (see Fig. 3.6).

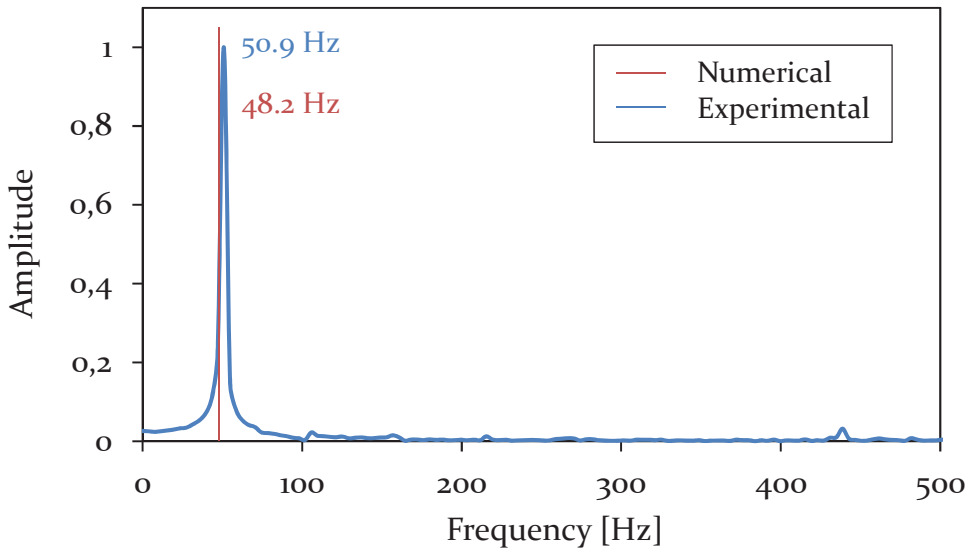

Figure 3.6: FFT analysis of the experimental time history of the cross-sectional concept A for the period range $P_{10} < P_{analysed} < P_{30}$. From [P3].

Table 3.1: Results of the numerical frequency analysis of the cross-sectional design concept A.

Mode	1	2	3	4	5	6	7	8
Frequency [Hz]	48.2	48.2	285.1	285.1	468.2	699.6	699.6	708.3
Mode type	Bending (out-of-plane)				Torsion	Bending (in-plane)		Axial

No other dominant modes besides the activated first flexural mode are observed. Only at around 450 Hz, a small peak is visible, potentially representing the first torsional mode (see Tab. 3.1). Due to the height of the peak, an influence on the damping behaviour can be neglected. The dynamic-mechanical properties of the VEM, used as damping layer for the CLD treatment, are characterised by DMTA with a shear sandwich clamp (see [P3]). The damping shows its peak value with $\zeta_{VEM} = \frac{1}{2}\,\eta_{VEM} = 0.35$ at low frequencies and temperatures around the freezing point (see Fig. 3.7).

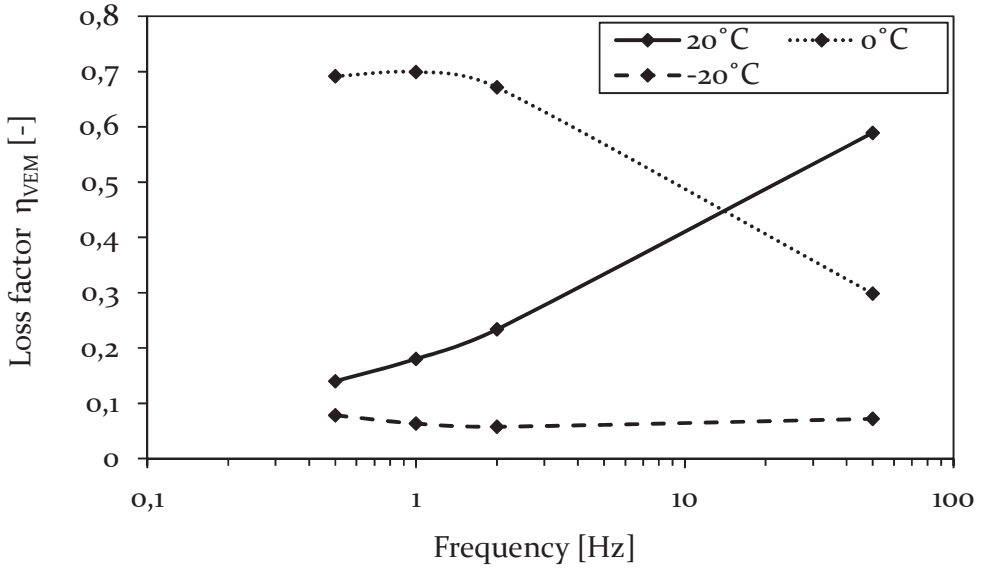

Figure 3.7: Frequency dependent loss factor of the VEM η_{VEM} for - 20 °C, 0 °C and 20 °C. From [P3].

The damping properties of the VEM and the composite material are required as individual input parameters for the numerical damping prediction of composite structures, as the modal strain energy is determined material-wise. In order to determine the damping at galloping relevant frequencies between 0.5 Hz and 2.0 Hz, additional forced vibration bending tests of the generic composite cylinders are carried out. The specimens are thereby clamped in a fixed-free support condition, representing the same clamping conditions as used for the free decay test at around

50 Hz (see Fig. 3.5). Furthermore, an actuator is horizontally connected to the tip of the cylinder by spherical bearings, introducing dynamic bending loads. The test setup is shown in Fig. A1 in the Appendix. The load is measured by a 2 kN load cell, mounted between the actuator and composite cylinder. Linear variable differential transformers (LVDT) are placed at the tip and the root end section, in order to measures the displacements during dynamic loading. The damping is calculated for each specimen by the ratio of dissipated energy to stored energy, obtained by an average of 20 hysteresis loops (see Eq. (A1) and Fig. A3 in the Appendix). However, no difference and trend is observed in the damping results for all cylinder specimens with varying CLD designs, indicating a major error in the test setup or the measuring equipment (see Fig. A2). The LVDT, located at the root end section of the cylinder, reveals high displacements during testing, obviously caused by relative displacement in the soft (aluminium) base element. The final results of the tests may therefore not be used to characterise the damping behaviour of the composite cylinder, as the damping in the clamping is obviously measured.

Concluding remarks

VBT and DMTA measurements may be used to characterise the fibre direction dependent damping of composite materials, although a discrepancy in the frequency domain has been observed. This may be explained by differences with regard to the working principles of the two damping characterisation techniques, the related amplitudes, the specimen dimensions and the support conditions. Irrespective of the differences, the damping results, obtained by either DMTA or VBT may be used to evaluate and qualitatively compare the effect of additional damping treatments or changed fibre/ matrix materials on the fibre direction dependent damping. Damping measurements by DMTA seem to be very sensitive for specimens with high Young's modulus, as an effect of bend-twist coupling is only captured by this method.
However, the results of VBT measurements are used to verify an equivalent numerical VBT model, using the modal strain energy method (see chapter 4). The fibre direction dependent damping input parameters η_1, η_2 and η_{12} may be obtained by VBT and DMTA measurements of samples with both off-axis and angle-ply stacking sequences. The final evaluation, which damping input parameter set may predict the damping with the smallest error, will be discussed in chapter 4.
Furthermore, the VBT method is extended to larger scale in order characterise the damping properties of the generic composite cylinders in a fixed-free support condition. The quality of the clamping is thereby of paramount importance. Based on an FFT analysis, it is demonstrated that the generic composite cylinder is vibrating only in the first flexural mode. It is therefore assumed, that the determined loss factor may correctly be associated with the first bending mode.

Chapter 4

Numerical damping prediction

The damping of composite materials and structures may be predicted by various models such as linear viscoelastic models, the complex modulus method or the modal strain energy approach. The latter allows an integration into finite element codes for the damping estimation of complex composite structures [65, 66]. The in-plane fibre direction dependent damping parameters η_1, η_2 and η_{12}, calculated based on VBT and DMA damping measurements for several fibre directions, are therefore used as input data for the numerical simulation (see section 3.1).
In this section the numerical damping prediction for composite structures, based on the modal strain energy approach, is summarised based on the investigations presented in [P2] and [P3]. The numerical results are compared with the experimental findings based on two numerical models: 1) Composite coupons with angle-ply stacks in accordance to the VBT method and 2) generic composite cylinders with different CLD design concepts, both models in fixed-free support conditions.

4.1. Modal strain energy approach

Most of the commercial available finite element (FE) software tools provide the implementation of the damping by means of mass and stiffness proportional coefficients, also known as Rayleigh damping. However, the Rayleigh damping is not well suited to predict the damping of composite structures, due to the orthotropic nature of composite materials. Instead, the modal strain energy approach, first introduced by Ungar and Kerwin [67], is used for the numerical damping analysis of the composite coupon and the generic composite cylinder. The damping is thereby represented by the ratio of the dissipated energy ΔU to the stored strain energy U within one cycle. The loss factor η is then calculated by

$$\eta = \frac{1}{2\pi} \frac{\Delta U}{U}. \tag{4.1}$$

The Adams-Bacon approach [60], already described in section 3.1 for the determination of the damping parameter input sets η_1, η_2 and η_{12} for off-axis laminates,

proposes the decomposition and the association of the dissipated energy with the principle stress components. This approach may be applied to finite element models, where the decomposition of the dissipated energy is performed individually for each finite element. The direction dependent, dissipated energy $\Delta U_{ij}^{[m]}$ may thereby be calculated by

$$\Delta U_{ij}^{[m]} = \eta_{ij}\, U_{ij}^{[m]} \ , \tag{4.2}$$

where η_{ij} and $U_{ij}^{[m]}$ represent the fibre direction dependent damping parameter input sets and the strain energy for the m'th finite element, respectively, with regard to the tensor components in all directions ($i, j = 1, 2, 3$) [61,65]. For thin-walled structures, only the in-plane components ($i, j = 1, 2$) are considered. The contributions to the total strain energy are calculated for the m'th finite element using a finite element software by

$$U_{ij}^{[m]} = \frac{1}{2}\, \sigma_{ij}^{[m]}\, \epsilon_{ij}^{[m]}\, V^{[m]}, \tag{4.3}$$

with $\sigma_{ij}^{[m]}$, $\epsilon_{ij}^{[m]}$ representing the direction dependent (in-plane) stress and strain components, respectively, within the element volume $V^{[m]}$ of the m'th finite element. The modal loss factor of a composite structure with k UD-layers, vibrating at the n'th mode, may thereby be calculated by

$$\eta_n = \frac{\sum_{m=1}^{N_e} \sum_{k=1}^{N} \sum_{i=1}^{3} \sum_{j=1}^{3} (\Delta U_{ij}^{[m]\,(k)})_n}{\sum_{m=1}^{N_e} \sum_{k=1}^{N} \sum_{i=1}^{3} \sum_{j=1}^{3} (U_{ij}^{[m]\,(k)})_n} \ , \tag{4.4}$$

where N_e and N are the total number of finite elements and the number of layers, respectively. The commercially available software Abaqus and the object-oriented programming language Python are used to numerically study the damping behaviour of the composite coupons and the generic composite cylinders. The implementation of a parametrical Python code thereby provides the automated determination and plotting of the overall modal damping in the post-processing step.

4.2. Numerical examples

The aim of the work, presented in [P2] and [P3], is to predict the modal damping of composite structures, based on the dynamic-mechanical material properties, obtained by DMTA and VBT measurements for different fibre directions. The freely vibrating composite beams and generic composite cylinders (see section 3.1 and 3.2) are thereby numerically modelled to demonstrate the feasibility of the implemented modal strain energy method into Abaqus.
Both composite parts are modelled using fully integrated, 8-node C3D8I hexahedral elements, characterised by internally added incompatible deformation modes.

This element type is therefore a cost effective way to model the flexing behaviour of structures, even with one element through the thickness [68]. The numerical model and the Python code for calculating the modal loss factor of the composite based on the modal strain energy method are available in [D1] and [D2] and may be used to verify the results presented in [P2] and [P3] or to apply the code to any other structure.

4.2.1. Coupon samples

The damping properties of GF-EP and GF-VE, obtained by DMTA and VBT measurements for different fibre angles and frequencies (see Fig. 3.3 and 3.4), differ to some extent significantly. In this section, the different numerical and experimental damping results, presented in [P2], are compared and summarised. It is furthermore evaluated, which of the four damping input parameter sets (see I to IV below), based on the fibre direction dependent damping presented in Fig. 3.4, predicts the modal damping of a numerical VBT model with best accuracy. Therefore, GF-VE and GF-EP composite beams, each with angle-ply stacks ($\varphi = \pm 30\,^\circ$, $\pm 45\,^\circ$ and $\pm 60\,^\circ$) and equivalent VBT support conditions, are numerically modelled using Abaqus. The numerical VBT model is furthermore compared to equivalent VBT experiments with the same angle-ply stacking sequence (VBT exp. $[\pm\varphi]_s$). As mentioned in section 3.1.1, four different damping input parameter sets η_1, η_2 and η_{12} are implemented, based on the following stack and measurement configurations:

I) DMTA $[\varphi]_3$ (samples with off-axis stacking sequence (UD, unbalanced)).

II) DMTA $[\pm\varphi]_s$ (samples with angle-ply stacking sequence (BD, balanced)).

III) VBT $[\varphi]_3$ (samples with off-axis stacking sequence (UD, unbalanced)).

IV) VBT $[\pm\varphi]_s$ (samples with angle-ply stacking sequence (BD, balanced)).

The numerical results of the freely vibrating beam model with the three different angle-ply stacks ($\varphi = \pm 30\,^\circ$, $\pm 45\,^\circ$ and $\pm 60\,^\circ$) are presented in Fig. 4.1. The application of the damping input parameter sets based on DMTA measurements (I and II) leads to either numerical overestimated or an underestimated modal damping compared to experimental VBT results (VBT exp. $[\pm\varphi]_s$). The observed trend depends on the analysed material (GF-EP vs. GF-VE) and the fibre direction ($\pm 30\,^\circ$ vs. $\pm 45\,^\circ$ vs. $\pm 60\,^\circ$). A difference is observed between the input concepts I and II. For fibre angles in the interval $\pm 30\,^\circ \leq \varphi \leq \pm 45\,^\circ$, the use of the input parameter set based on I leads to higher damping compared to II due to bend-twist coupling, which is getting maximum at $\varphi \approx 30\,^\circ$. The damping-enhancing bend-twist coupling effect diminishes at $\varphi \approx \pm 60\,^\circ$, which surprisingly leads to even lower modal damping by using I compared to the input parameter set II.

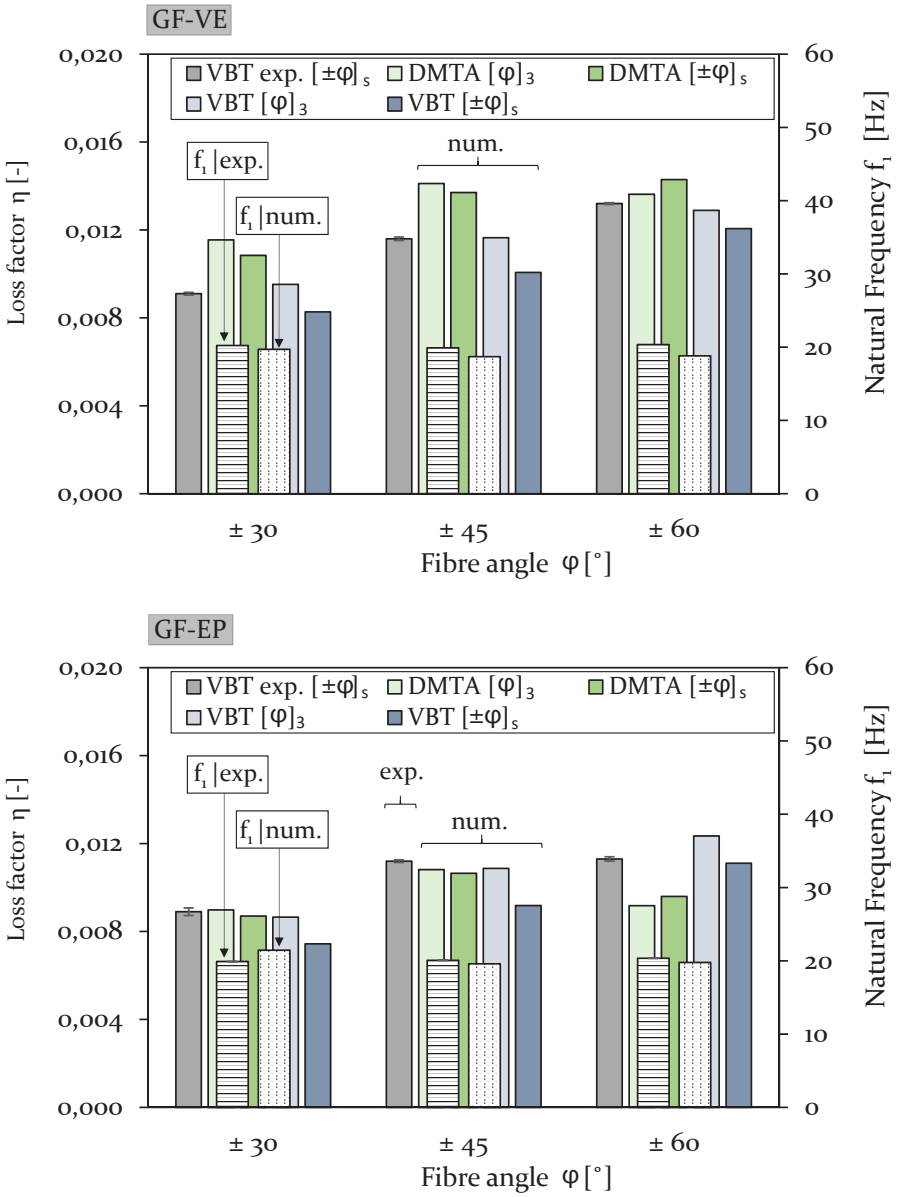

Figure 4.1: Comparison of the experimental and numerical results for the modal damping η and the natural frequency f_1 for GF-VE beams (above) and GV-EP (below) [VBT (5 mm), $\pm\varphi_s$, 20 °C at $\approx$ 20 Hz] based on the fibre direction dependent damping input parameters η_1, η_2 and $\eta_{12}/\eta_{12_{eq}}$ calculated by the following four input parameter sets: I) DMTA $[\varphi]_3$, II) DMTA $[\pm\varphi]_s$, III) VBT $[\varphi]_3$ and IV) VBT $[\pm\varphi]_s$.

However, a clear trend of the different numerical results with regard to the experimental VBT results is hardly observed. A reliable damping prediction of freely vibrating composite structures, based on the damping properties obtained by DMTA, is therefore not necessarily given.

Table 4.1: Average error of the damping results between the numerical VBT model with the four different input parameter sets and the equivalent VBT experiment.

Damping input set		DMTA		VBT	
		$[\varphi]_3$	$[\pm\varphi]_s$	$[\varphi]_3$	$[\pm\varphi]_s$
Avg. Error [%]	GF-EP	7.7	7.4	4.7	12.1
(Num. vs. Exp.)	GF-VE	14.0	13.0	2.4	10.3

In contrast, a trend in the numerical damping is clearly visible compared to the experimental VBT results, when applying the damping input parameter set based on VBT measurements (III and IV) to the numerical VBT model. The damping with the smallest deviation compared to the VBT experiment (VBT exp. $[\pm\varphi]_s$) is predicted, when applying the input parameter set III, based on VBT measurements of beams with an off-axis stack ($[\varphi]_3$). This may be due to the same test-, sample- and support conditions for the dynamic-mechanical characterisation by VBT and the numerical VBT model.
In contrast, the application of the damping parameter input set IV, based on angle-ply laminates, leads to under-predicted damping values for the two materials and all three stacking sequences $\varphi = \pm 30\,^\circ$, $\pm 45\,^\circ$ and $\pm 60\,^\circ$. This may be explained by a generally higher stiffness of angle-ply laminates compared to off-axis laminates in the range between $0\,^\circ < \varphi \leq 60\,^\circ$, which consequently results in slightly lower damping values. The numerical damping prediction, using damping properties which are based on dynamic-mechanically characterised angle-ply laminates, is therefore not recommended.
In Tab. 4.1, the average deviations between the numerical and experimental damping results are summarised with regard to the different fibre direction dependent damping parameter input sets (I to IV). The implementation of damping properties into the numerical VBT model, obtained by the DMTA of samples with off-axis (input set I) and angle-ply stacks (input set II), result in an average error of about 7.5 % for GF-EP and 13.5 % for GF-VE. As already mentioned, a trend in deviation is thereby not observed so that these damping properties may not be suited for the damping prediction of composite structures, clamped in a free-fixed support condition.
In contrast, the use of damping properties, based on VBT measurements of beams with off-axis stacks (input set III)), leads to the lowest deviation with 4.7 % for GF-EP and 2.4 % for GF-VE. The numerical damping prediction of the generic composite cylinders is therefore carried out using the damping input parameter set III. The numerical damping analysis, using VBT measurements of angle-ply laminates (input set IV), results in an underprediction of the damping due to its higher stiffness compared to off-axis laminates. The initial concern regarding a potential overprediction of the structural model damping, due to the characterisation of bend-twist coupling affected specimens (input concept I and III) is apparently

unfounded: Although a damping enhancing bend-twist coupling effect is observed in DMTA measurements (at $\varphi \approx 30\,^\circ$) (see Fig. 3.4), the influence of bend-twist coupling on the numerical damping prediction seems to be neglectable. It rather seems that the damping measurement method (VBT or DMTA) for the fibre direction dependent damping characterisation has a much higher impact on the final numerically predicted damping results. The choice should therefore be made based on potential test similarities with regard to the support condition and the expected vibration amplitude (see section 3.1 and Fig. 3.1).

4.2.2. Generic composite cylinders

Depending on the cross-sectional design concept (A to I, see Fig. 2.6), the filament wound generic composite cylinders consist of several unidirectional GF-EP layers with fibre directions of $\varphi = \pm 10\,^\circ$ and $\pm 45\,^\circ$ as well as viscoelastic damping layers. Both materials are fully characterised with regard to their frequency and temperature dependent damping behaviour (see section 3.1). Due to the good correlation of numerical and experimental results on coupon level, the fibre direction damping input parameter set III, based on VBT measurements of off-axis laminates (see section 4.2.1), are implemented into the post-processing script to calculate the modal damping η of the generic composite cylinders. In order to demonstrate the accuracy of the numerical cylinder models, each with its individual cross-sectional design concept, the numerically predicted and the experimentally determined first natural frequencies are compared (see Fig. 4.2).

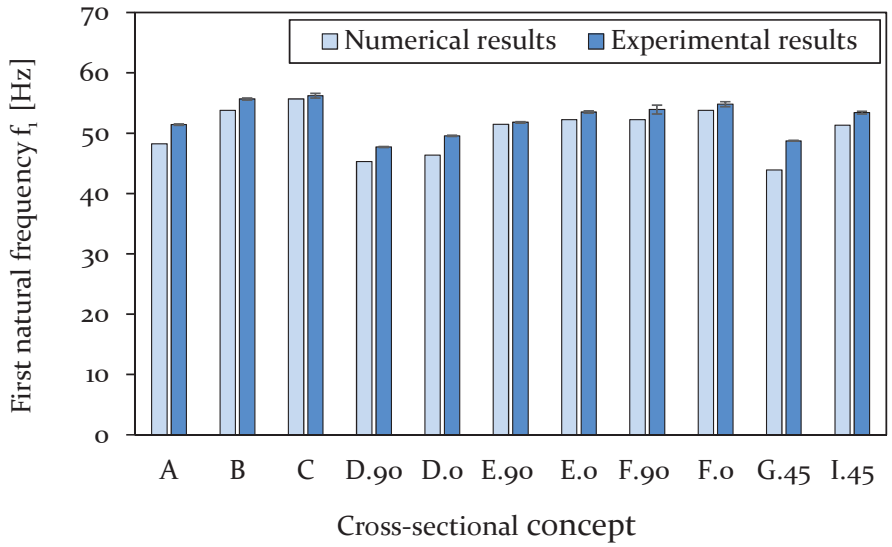

Figure 4.2: Numerical and experimental results of the natural frequency f_1 related to the first flexural mode. From [P3].

The numerically predicted natural frequencies are in good agreement with the exper-

imentally obtained results, although a slight underprediction of about 4 % in average is observed for all cross-sectional design concepts. The consistency of the underpredicted natural frequency indicates a general inaccuracy in the model, which may be related to inexact material properties or imprecisions during the manufacturing process by e.g. potential fibre misalignments or slightly changed layer thicknesses. An underestimation of the damping is also observed when comparing the numerical modal damping with the experimental results (see Fig. 4.3).

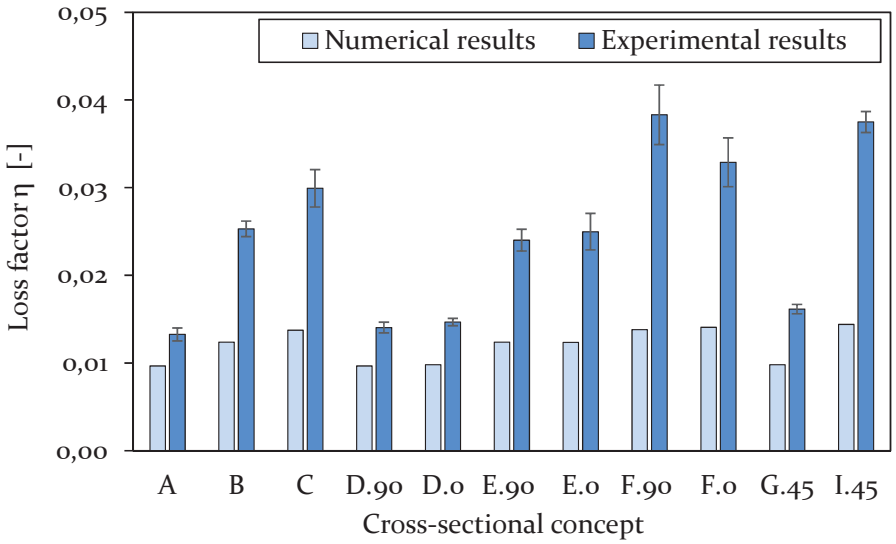

Figure 4.3: Numerical and experimental results of the modal loss factor related to the first flexural mode. From [P3].

Although the numerically determined loss factors follow the same trend as the experimental results, the differences disproportionally increase with the amount of applied VEM damping layers (concept B, C, E, F and I). Whereas the predicted damping for composite cylinders without CLD treatments is maximum 39 % lower than the experimental results (concept G.45), the difference increases to 64 % for concept F.90 with CLD treatments on the in- and outside. The increasing mismatch may be attributed to the following numerical and experimental issues:

1) Numerical: Simplified boundary conditions in the numerical model do not capture the complex stress state in the clamping area.

2) Experimental: Relative displacement in the clamping area due to insufficiently rigid clamping, caused by the continuous VEM damping layers over the entire cylinder length.

3) Experimental: Characterised material properties of the VEM may be imprecise, as the difference increases with increasing amount of VEM.

An interference of other modes can be excluded as potential source of error since the dominance of only the first mode is verified (see Fig. 3.6).

Concluding remarks

The modal damping of composite coupons and (sub-)structures is numerically predicted by the implementation of the modal strain energy approach into the commercially available finite element software Abaqus. The investigated structures are therefore modelled using hexahedral elements in order to calculate the direction dependent strain energy components. The dissipated energy is calculated by incorporating the fibre direction dependent damping, represented by input parameters η_1, η_2 and η_{12}.
Four different input parameter sets, based on DMTA or VBT measurements of samples with off-axis or angle-ply laminates, are used to predict the modal damping of a numerical VBT model, in order to determine the set, which leads to the smallest error compared to the measured damping of the equivalent experiment. The modal damping of freely vibrating GF-EP and GF-VE beams with three different angle-ply laminates are well predicted with an error of 4 % in average compared to the experiment, using the input parameter set III of VBT samples with off-axis laminates. This input parameter set is implemented into the numerical damping models of the generic composite cylinders with its different cross-sectional design concepts. The numerical damping results are constantly underpredicted for all cross-sectional design concepts compared to the experimentally obtained damping, resulting in differences between 27 % for design concept A up to 64 % for concept F.90.
Potential error sources are therefore identified, such as the use of simplified boundary conditions in the numerical model, insufficiently rigid clamping during cylinder testing and inaccurately determined damping properties of the VEM by DMTA measurements.

Chapter 5

Damping of wind-induced vibrations

Power pylon structures made of non-conductive composite materials, such as the thoroughly investigated GFRP and AFRP with regard to its dynamic-mechanical properties (see chapter 3), may be well suited for innovative designs with a potential reduction in size due to a possible integration of insulators. However, the ensuing direct cable-pylon connection leads to an increased dynamic interaction compared to the application of hanging insulators typical for standard steel lattice towers.
Galloping of conductor lines, vibrating at frequencies between 0.5 and 2.0 Hz and at temperatures below the freezing point [10], may potentially excite the composite power pylon structure, possibly leading to severe damage on the clamping or the entire power line system.
The galloping motion typically describes a vertically oriented ellipse with a small horizontal component, also known as the galloping ellipse. The general measure for the galloping intensity may be defined by the size of the galloping ellipse with regard to the vertical and horizontal component. A reduction in size is therefore desired due to the following aspects:

1) Minimising damage at the cable clamp, the structure and the entire power line system [10].

2) Potential downsizing of the composite power pylon, due to the reduced risk of flash overs: In the vertical direction because of the safety clearance to the ground and in the horizontal direction for safety distance to adjacent phase conductors.

The latter point is of great interest for the design of composite power pylons since a reduction of the horizontal galloping component may enable a closer spacing of adjacent phase conductors, resulting in a desired reduction in cross arm length.
In general, it is assumed that galloping amplitudes may be mitigated by rigid cable-pylon connections, as some kinetic energy of vibrating cables leads to deformation of the stiff composite cross arm. A further reduction of galloping vibrations is expected by the damping implementation into the cross arm structure. The potential damping capacity of composite materials and structures, eventually modified by

additional damping enhanced treatments (see chapter 2), is substantially compared to its metallic counterparts (see chapter 3) and therefore well suited for the use in vibration-susceptible power pylons. In order to verify the assumptions mentioned above, the numerical galloping analysis, using Abaqus and Fortran, is summarised in the following sections, based on the work presented in [P4].
Furthermore, a redesign of the composite cross arm is proposed based on the findings of the numerical galloping analysis: The galloping vibration amplitudes may further be mitigated by the reduction of the horizontal cross arm stiffness.

5.1. Numerical simulation of conductor line galloping

The aim of the numerical galloping study is to investigate the effect of different cable support conditions with and without added damping on the vibration amplitudes of galloping conductor lines. A representative 400 kV power line system, consisting of 3 x 300 m spans, is modelled using two different cable support conditions: 1) Cable attachment to a flexible insulator string, typical for standard steel lattice power pylons and 2) cable attachment directly to a stiff composite power pylon structure. The effect of damping is studied by the implementation of reasonable damping properties to the composite cross arm with regard to the cable support condition 2). The latter configuration is illustrated in Fig. 5.1.

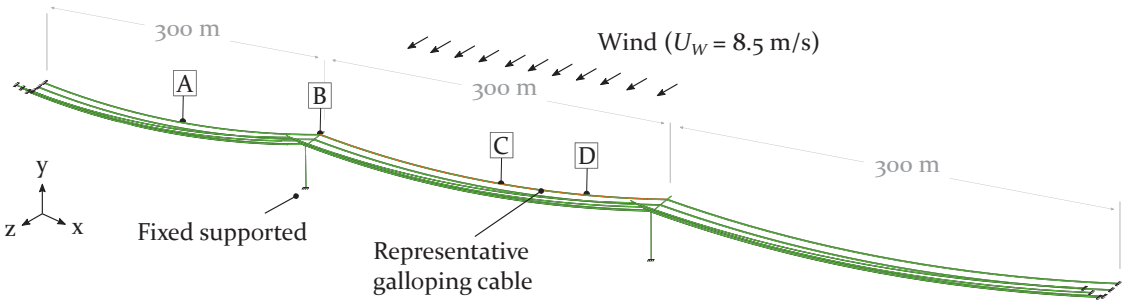

Figure 5.1: Representative double 400 kV three-span system of 3x 300m with a representative center-span-cable exposed to aerodynamic loads, where displacements due to galloping are analysed at the center (1/2) of an adjacent cable [A], at the cable attachment point (CAP) of the power pylon [B], at the center (1/2) of the galloping cable [C] and at a quarter point (1/4) of the galloping cable [D]. From [P4].

The dimensions and properties of the composite pylon, the representative insulator strings and the iced conductor lines, used in the numerical galloping simulation, are

listed in [P4].

5.1.1. Support condition specifications

In the following section, the two different cable support conditions: 1) Insulator strings and 2) direct cable-pylon connections, are summarised. The main difference with regard to the galloping vibration amplitudes is related to the apparent flexibility of the individual support conditions.

Model 1 - Insulator string connection

Conductor lines connected to hanging insulator strings are free to move in the horizontal x-z plane (see Fig. 5.1) and are only restricted by the stiffness from the adjacent cables, resulting in a sensitive coupling between adjacent spans. An excitation of various spans is thereby possible, even for light cable vibrations. However, the insulator string support conditions may be represented in the numerical model by static springs in the x- and z-direction [69], assuming the insulator string and the tower structure to be ideally stiff (see Fig. 5.2). The static springs are determined by

$$k_{i_x} = \frac{1}{L_i}\left(mgL_x + \frac{m_i g}{2}\right), \tag{5.1}$$

$$k_{i_z} = k_{i_x} + \frac{2H_x}{L_x}, \tag{5.2}$$

with L_i being the length of the insulator string, m_i being the weight of the insulator string, m being the mass per unit length of the cable, g being the constant of gravity, L_x being the span length and H_x representing the horizontal cable tension.

Model 2 - Direct cable-pylon connection

In contrast, the power pylon is modelled using spatial beam elements in order to realistically represent the direct cable-pylon connection, characterised by the stiffness of the steel tower and the composite cross arm (see Fig. 5.2). The representative conductor line, subjected to aerodynamic loads in order to initiate galloping vibrations, is modelled at the outer most position along the composite cross arm. The remaining conductor lines are represented by equivalent point masses and static springs in the x-direction. The equivalent spring stiffness k_x of a taut conductor line may be calculated by

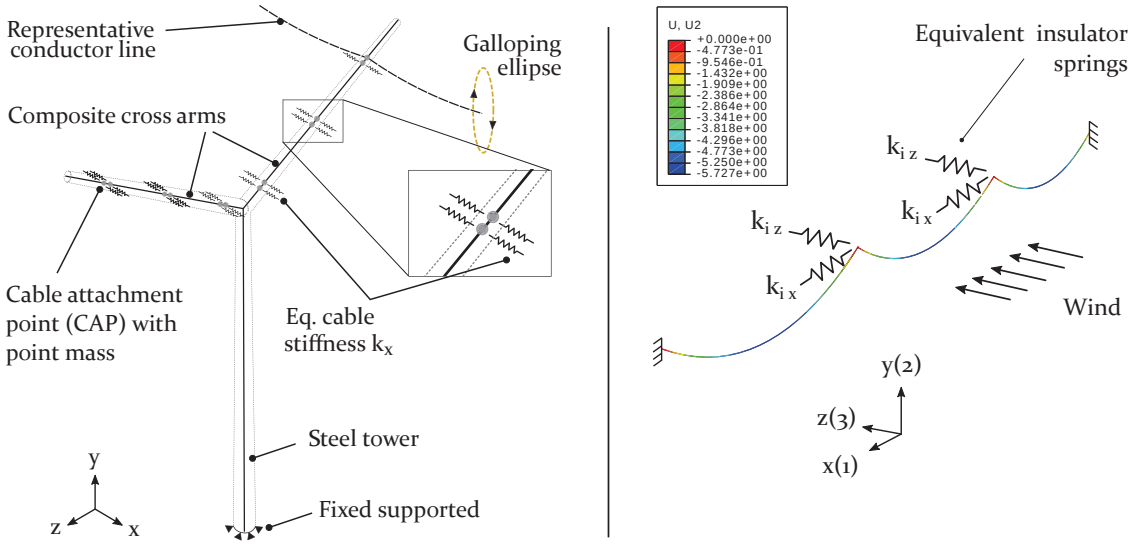

Figure 5.2: Left: Schematic power pylon model with boundary conditions for the composite power pylon with conductor lines represented by springs and point masses (left) | Right: Schematic insulator-string model with maximum static deflection of a 3 x 300 m conductor line connected to insulator strings represented by static springs with the inner span subjected to aerodynamic loads. From [P4].

$$k_x = k_e \left[1 + \frac{mgL_x^3 k_e}{12H_x^3 \left(1 + \frac{8}{3} \left(\frac{s}{L_x} \right)^2 \right)} \right]^{-1} \tag{5.3}$$

The horizontal stiffness of a perfectly taut cable and the cable sag at the center of the span is thereby represented with k_e and s, respectively [70]. The horizontal stiffness of a perfectly taut cable k_e may thereby be represented by

$$k_e = \frac{AE}{L_x} \left(\cos \varphi \right)^2 , \tag{5.4}$$

where AE and φ defines the axial stiffness of the conductor line and the angle between the chord line and a horizontal reference. The natural frequencies of the power pylon with attached conductor lines are determined using a numerical frequency analysis.

Model 3 - Direct cable-pylon connection with cross arm damping

In order to demonstrate the effect of additional damping of pylon structures on the galloping vibration amplitude, a reasonable damping ratio of $\zeta_{CA} = 0.03$ is assigned to the composite cross arm (CA). The additional cross arm damping, achieved by application of the potential damping treatments summarised in chapter 2, is thereby the only difference between Model 3 and Model 2. The damping is implemented into the numerical model in Abaqus using Rayleigh damping.

5.1.2. Conductor line model

The necessary condition for galloping to happen is an asymmetric ice accretion along the conductor line. The presented numerical galloping analysis is based on the frequently used D-shaped ice model (see Fig. 5.3) [71, 72]. The iced conductor line is modelled using beam elements. In order to account for the modified cable dimensions and properties due to icing, equivalent properties for the diameter, the density, E-modulus and the G-modulus are introduced. Therefore, the same axial stiffness, torsional rigidity, moment of inertia and mass per unit length is maintained. Ice accretions along conductor lines are reported to increase the damping [73–76]. Based on the reported values between $\zeta_{c_1} = 0.004$ and $\zeta_{c_2} = 0.06$, an average damping ratio for the iced conductor line of $\zeta_c = 0.032$ was implemented by Rayleigh damping.
The aerodynamic loads F_L, F_D and M, illustrated in Fig. 5.3 and necessary to initiate conductor line galloping, are defined in Eq. (5.5) by the aerodynamic coefficients C_L, C_D and C_M, the density of the air ρ_{air}, the velocity of the wind U_w and the height h of the wind-exposed object.

$$\begin{bmatrix} F_L \\ F_D \\ M \end{bmatrix} = \frac{1}{2}\rho_{air} U_w^2 h \begin{bmatrix} C_L(\alpha) \\ C_D(\alpha) \\ h\, C_M(\alpha) \end{bmatrix} \tag{5.5}$$

A typical wind velocity for Denmark with $U_w = 8.5\,\mathrm{m/s}$ is used for the numerical galloping analysis [77]. The wind speed independent aerodynamic coefficients are characterised by the instantaneous angle of attack α, which in turn may be approximated by

$$\alpha \approx \theta_0 - \left(\frac{R\dot{\theta} + \dot{V}}{U_w} \right), \tag{5.6}$$

with R representing the radius of the bare conductor, θ_0 representing the initial angle of attack, $\dot{\theta}$ representing the torsional angular velocity and $\dot{V}$ representing the vertical velocity of the conductor line [78, 79]. The vertical and torsional angular

velocity as well as the nodal displacement and torsional angle, describing the time dependent state of motion of the conductor line, are obtained for time t by numerical time integration. In order to calculate the angle of attack α at time $t + \Delta t$, the vertical velocity $\dot{V}$ and the torsional angular velocity $\dot{\theta}$ of the conductor line need to be predicted.
User elements (UEL) are therefore introduced into Abaqus [80] by a user subroutine, generating dummy elements without mass and stiffness to share the same nodes as the beam elements used for modelling the conductor line (see Fig. 5.3).

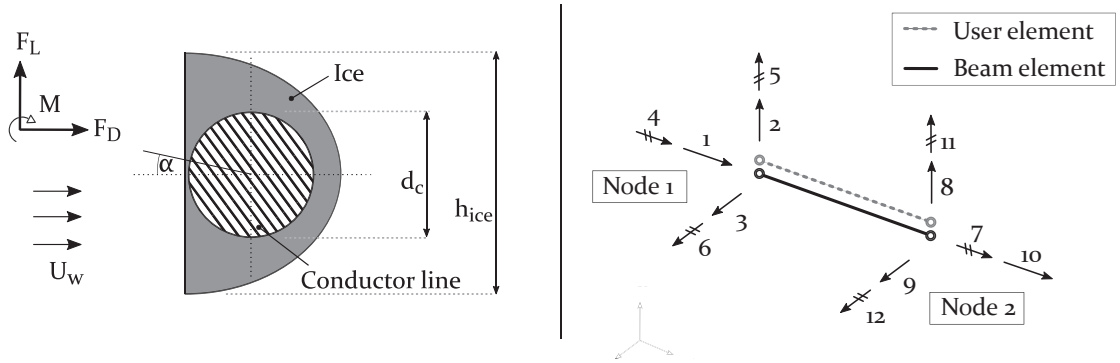

Figure 5.3: Left: Schematic conductor line model with a D-shaped ice accretion and the resulting aerodynamic loads (F_L, F_D and M) due to wind loads with the velocity U_W | Right: Schematic implementation of beam and user elements. From [P4].

The user-defined element subroutine allows access to the time-dependent state-of-motion parameters at time t for each node along the conductor line. Furthermore, the vertical velocity $\dot{V}$ and the torsional angular velocity $\dot{\theta}$ may be predicted for each node at time $t + \Delta t$, providing the calculation of the angle of attack α by Eq. (5.6) at time $t + \Delta t$. The related aerodynamic loads F_L, F_D and M may finally be applied to the nodes of the user elements, sharing the same nodes as the beam elements used to model the conductor line.

5.1.3. Results

The mode shape of the first natural frequency of the power pylon, characterised by bending motion of the cross arm in the y-direction, is with $f_1 = 1.32\,\text{Hz}$ very close to the vibration response of the cross arm at Location (Loc.) B (see Fig. 5.1) in the y-direction at a frequency of $f = 1.23\,\text{Hz}$ due to galloping (see Fig. 5.4). In order to prevent potential resonance vibrations to happen, an increase in vertical bending stiffness by locally reinforcing the composite cross arm is required, which consequently leads to an increase of the first natural frequency f_1. Furthermore, it is hereby demonstrated that damping in the pylon structure is essential as the

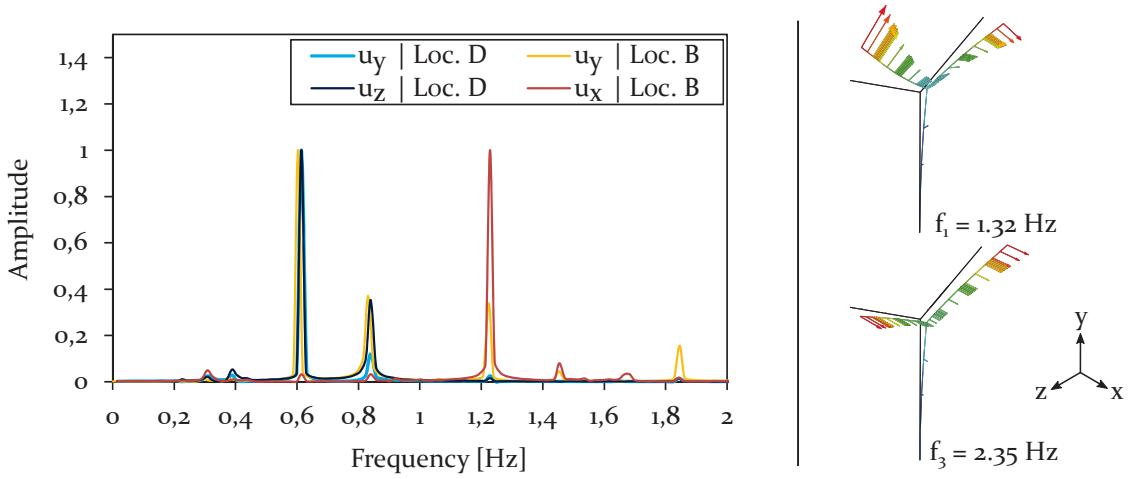

Figure 5.4: Left: Results of the Fast Fourier Transformation of Model 2, based on the time histories of displacements in vertical u_y and horizontal u_x, u_z directions at location B (CAP) and D (1/4 of the galloping cable span) (see Fig. 5.1) | Right: First natural frequencies and related mode shapes of the power pylon with attached conductor lines, represented by springs and point masses. From [P4].

resonance frequency and the vibration response frequency are closely spaced.
The evaluation of the galloping vibration amplitudes are based on the time history plots of the vertical and horizontal displacements for the three numerical models (Model 1 - 3, see section 5.1.1) at different locations along the three-span system (Loc. A - D). Two representative time history plots of the vertical and the horizontal displacements for Model 1 and Model 2 are shown in Fig. 5.5 and 5.6.

The galloping vibrations of Model 1 and 2, representing two different cable support conditions, differ widely in the galloping modes and amplitude values within the investigated time range of 1500 s. Conductor lines, connected to hanging insulators, exhibit a monotonous galloping behaviour vibrating in a 3-loop mode during steady state (phase II). As expected, the adjacent spans are quickly excited, leading to vertical amplitudes of 1.1 m in vertical direction.
In contrast, the galloping behaviour of Model 2, with its direct and rigid power-cable connection, is much more complex. After a longer initial build-up phase with a chaotic vibration behaviour (phase I), the conductor line is galloping in a 3-loop mode over a period of about 500 s (phase II), before changing to a 2-loop mode at steady state (phase IV). The vertical and horizontal amplitudes at the center of the span (Loc. C) thereby almost vanish (see Fig. 5.6), demonstrating a well balanced 2-loop condition. The observed unsteady vibration behaviour of Model 2 is assumed to be due the galloping conductor line rigidly connected to the stiff power pylon. In contrast to Model 1, the limited displacement at the CAP in the xy-plane leads to long period until steady state is reached. Furthermore, the adjacent spans (Loc. A)

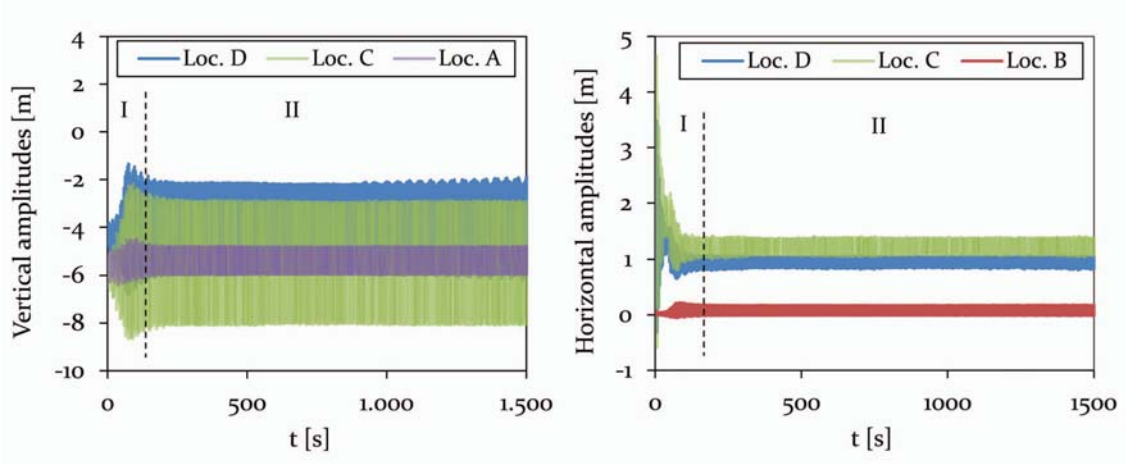

Figure 5.5: Time history plot of the vertical (left) and horizontal (right) displacements of Model 1 (insulator-cable connection) at location A (Center, adjacent span), location B (CAP, Power pylon), C (Center, mid span) and D (1/4, mid span), representing different vibration conditions (phase I - II). From [P4].

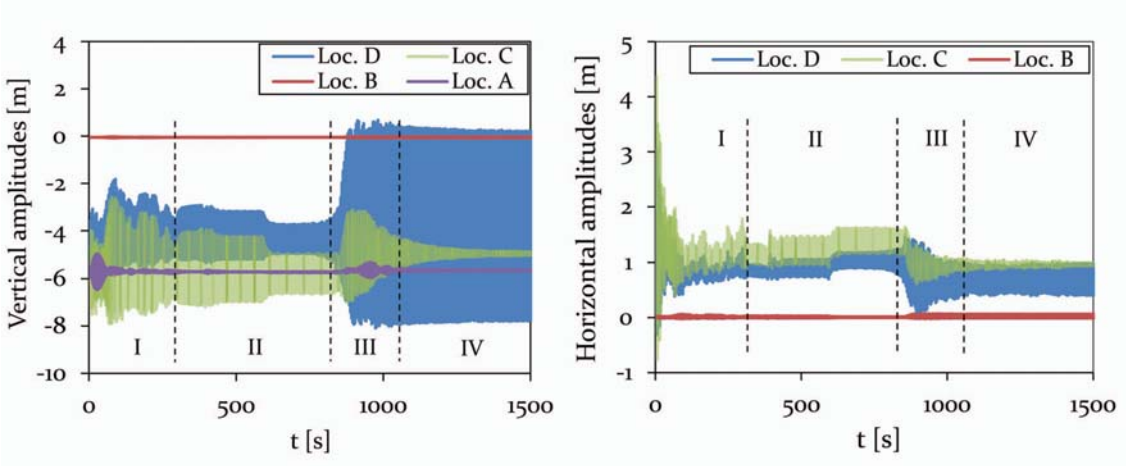

Figure 5.6: Time history plot of the vertical (left) and horizontal (right) displacements of Model 2 (direct pylon-cable connection) at location A (Center, adjacent span), location B (CAP, Power pylon), C (Center, mid span) and D (1/4, mid span), representing different vibration conditions (phase I - IV). From [P4].

are hardly excited. Only in the transition phases I and III, short vertical galloping amplitudes are observed.
The galloping vibration behaviour of Model 3 is very similar to Model 2, slightly differing in amplitude values and duration of the four phases I - IV. In order to fairly compare the effect of the cable support condition, the evaluation of the galloping amplitudes is focussed on phase II, where the galloping conductor lines of Model 1, 2 and 3 are vibrating commonly in a 3-loop mode.

Comparison

The galloping ellipses of the Models 1, 2 and 3 are compared in order to quantify the potential mitigation of conductor line galloping due to cross arm damping and a rigid cable-pylon connection. In Fig. 5.7, the three galloping ellipses are presented at a time of about 500 s (phase II in Fig. 5.5 and 5.6) with its local maxima at Loc. C and Loc. D (see Fig. 5.1) in a 3-loop mode.

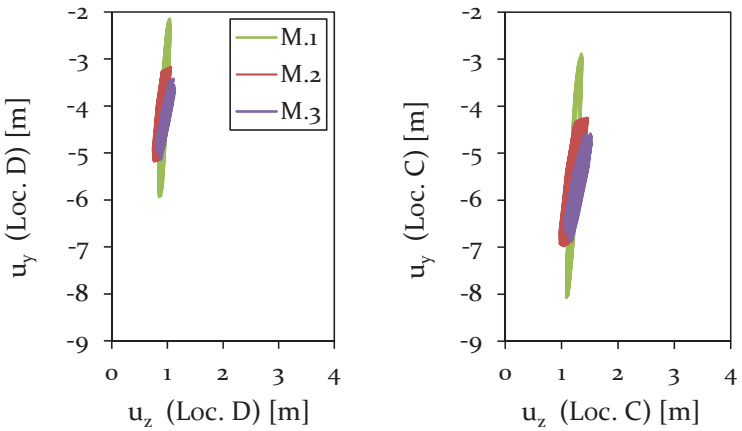

Figure 5.7: Comparison of the galloping ellipses of Model 1 (Insulator string connection), Model 2 (direct connection without cross arm damping) and Model 3 (direct connection with cross arm damping $\zeta_{CA} = 0.03$) with regard to a 3-loop condition at Loc. D (left) and C (right), each at about 500 s (phase II). From [P4].

A significant reduction in galloping amplitude by about 48 % is observed at both locations C and D by considering a direct cable-pylon connection (Model 2) instead of an insulator string connection (Model 1). The galloping amplitudes may further be reduced by about 15 % due to an implementation of damping to the composite cross arm by $\zeta_{CA} = 0.03$ (Model 3). An increasing rotation of the galloping ellipse towards the z-axis is observed from Model 1 to Model 2 by 7 % and from Model 2 to 3 by additional 2.3 %. The small horizontal vibration amplitudes increase by 53 % from Model 1 to 2, but decrease by 8 % due to the implementation of damping.

Concluding remarks

It can be concluded that a change in cable support condition from an insulator string connection to a direct cable-pylon connection may lead to a size reduction of the vertically oriented galloping ellipse by about 50 % for the analysed 3-loop galloping mode. The reduction thereby mainly affects the vertically oriented component of the galloping amplitudes. The application of damping to the composite cross arm reduces the galloping amplitudes even further by 15 %. In contrast, an increasing rotation of the galloping ellipse from Model 1 to 2 and 3 leads to an increase in the horizontal component of galloping vibration amplitude. It is therefore demonstrated that a rigid cable-pylon connection, modified by additional damping, not necessarily leads to a reduction of the horizontal galloping vibration component.
In contrast, the implementation of damping to the power pylon is shown to be of high importance as the vibration response of the cross arm in vertical direction (y-direction) and the first natural frequency of the power pylon almost coincide.
However, the initial idea of using the power pylon structure as tuned mass damper is seen critically due to the following points:

1) The natural frequencies of the power pylon significantly change with the cable tension, the cable type and potential ice accretions. In turn, the galloping frequencies strongly depend on several factors such as the wind speed, span length and the cable tension. It is therefore very likely that the natural frequency and the vibration response frequency do not coincide.

2) The vibration response of the cross arm in horizontal and vertical direction (x- and y-direction) highly differ in frequency (see Fig. 5.4). The vibration frequency of the cross arm, related to vibrations in vertical direction, might partly coincide with a natural frequency showing a similar mode shape (1.21 Hz vs. 1.32 Hz). However, the cross arm vibration in horizontal direction can have considerably different frequencies for similar vibration modes (1.21 Hz vs. 2.35 Hz).

The numerical model of the three-span cable-pylon system with different cable support conditions and the Fortran- and Python codes for simulating the conductor line galloping and extracting the relevant data in the post-processing step are freely available [D3]. The model files and the codes may be used to verify the results presented in [P4] or to simulate different galloping scenarios by e.g. modifying the wind speed or to study the effect of different ice accretions and cable types.

5.2. Re-design of the composite cross arm

The significant mitigation of conductor line galloping by a direct cable-pylon connection in combination with reasonable damping in the composite cross arm is demonstrated in section 5.1, based on the work presented in [P4]. It is shown that the composite cross arm vibrates in the horizontal x-direction with twice the amplitude (0.07 m vs. 0.035 m, see Fig. 5.6) and frequency (1.21 Hz vs. 0.61 Hz, see Fig. 5.4) compared to the vertically oriented component. It is assumed that the effect of implemented cross arm damping on the mitigation of conductor line galloping highly depends on the stiffness of the composite cross arm. A reduction in flexural stiffness consequently leads to higher vibration amplitudes of the cross arm structure, indicating the transfer of kinetic energy from the vibrating cable-pylon-system. Thus, the more kinetic energy is dissipated by potentially implemented damping treatments, the lower the vibration amplitudes of the galloping conductor lines will be.
However, the flexural stiffness of the cross arm in vertical direction (y-direction) may not be reduced, as the vertical tip deflection is restricted by the designers due to visual aspects. In contrast, a reduction in the horizontal flexural stiffness (in x-direction) may obviously not affect the visual appearance of the power pylon under static conditions, as the cable loads from adjacent spans balance out.
Due to that fact, the cross-sectional design of the composite cross arm may be modified, in order to obtain a direction dependent flexural stiffness: While the flexural stiffness remains unchanged in the vertical y-direction, the stiffness may be reduced in the horizontal x-direction. Potential cross-sectional designs of the cross arm are presented in Fig. 5.8, showing a reduced wall thickness in the x-direction, parallel to the directly attached conductor lines.

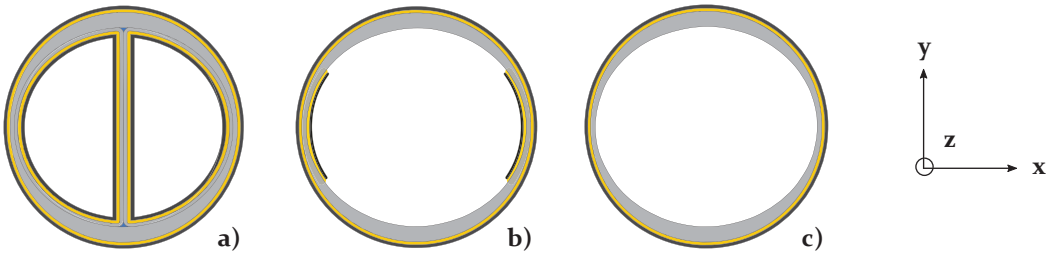

Figure 5.8: Proposed cross-sectional designs of the composite cross arm (a to c) based on the results presented in [P4].

The three potential cross-sectional designs exhibit the required circular outer shape. The feasibility to manufacture the cross arm by a filament winding process is demonstrated in [P4].
The structural complexity of the cross section, thus proportionate to additional

manufacturing costs, thereby gradually reduces from concept a) to concept c). Whereas a segmentable mandrel for the filament winding process is required to manufacture concept a), a monolithic tool may be used for concept b) and c), accompanied by gradually reduced damping properties compared to concept a) (see [P3]).

Chapter 6

Conclusion and future work

In the present thesis the damping enhancement in composite materials and sub-structures is experimentally and numerically investigated, targeting a real life application of innovatively designed composite high-voltage power pylons. As power line systems are prone to wind-induced vibrations, such as the severe galloping phenomenon, a damping enhancement in the structure is therefore required and may even lead to a mitigation of conductor line galloping to prevent costly damage in the tower structure and the rigidly connected transmission lines.

Due to the special characteristics of conductor line galloping, vibrating at very low frequencies and at temperatures below the freezing point, the damping behaviour of non-conductive composite materials is experimentally characterised at these conditions with regard to its orthotropic nature. Additional damping treatments, suitable for an application in high voltage power pylons, are furthermore investigated on material and (sub-) structural level (Chapter 2). The implementation of hybrid fibre reinforcements, consisting of non-conductive GF and AF, and the application of CLD treatments are therefore demonstrated to effectively increase the damping. The use of NC is, from the authors perspective, not suitable for large scale applications due to e.g. the time consuming mixing procedure.

The fibre direction dependent damping properties are obtained by DMTA and VBT measurements, resulting in partly contrary trends with regard to the measuring frequency (Chapter 3). In order to evaluate the reliability of the results, various numerical damping simulations, using the FE-software Abaqus, and equivalent experiments are carried out (Chapter 4). The damping results, obtained by DMTA and VBT measurements, are thereby used as input parameters for the prediction of the modal damping of coupon specimens and generic composite cylinders in a fixed-free support condition. It is observed that the calculated damping exhibits the smallest error, when the chosen damping characterisation technique has a similar specimen support condition and working principle compared to the equivalent experiment. With regard to the hypotheses drawn in chapter 1, the fibre direction dependent damping properties may be used to predict the trend in damping of composite coupon specimens and sub-structures. The damping characterisation technique should in turn be carefully chosen.

Based on the approximate idea of the achievable damping within the composite cross arm, a numerical galloping analysis is carried out in order to study the effect of cross arm damping and different cable support conditions on a potential mitigation of conductor line galloping. A standard insulator string connection, typical for steel lattice structures, is compared to a rigid and direct cable-pylon connection on composite pylon arms, with and without reasonable damping properties. It is found for the specifically investigated case, that the vertically oriented galloping ellipse may be reduced in size by about 50 % just by rigidly clamping the cable to the stiff cross arm. The application of damping reduces the amplitudes by additional 13 %. In contrast, a reduction in the horizontal component of the galloping ellipse is however not observed. However, it can be concluded that a direct cable-pylon connection in combination with realistic damping properties may lead to significant mitigation of conductor line galloping in the vertical direction. A potential downsizing of the power pylon is thereby enabled, as a re-definition of the safety clearance may be achieved.

Future work

The presented re-design in section 5.2, leading to an increased flexibility in the cable direction, may be considered in the numerical galloping model to evaluate the effect on the mitigation of conductor line galloping. A more realistic model, including the T-section of the power pylon and existing joints, may also be considered in the simulation.
An investigation on various span- and cable configurations may be of interest in order to verify the positive effect of cross arm damping and a rigid cable-pylon connection on the galloping mitigation for different galloping modes. A variation of different galloping parameters such as a modified ice accretion and a changed wind speed may help to understand the impact of the individual parameters on a potential reduction of the galloping amplitudes.
Finally, a more detailed feasibility study of the selected damping enhanced treatments for the large scale application in the composite cross arms might also be a next step. At the same time, a comprehensive life time analysis, including fatigue experiments in a high-voltage environment, will be necessary when proposing a realistic service life of 100 years.

References

[1] W. Taenzer, F. Fielitz, H. Mors, *Stahlmaste für Starkstrom-Freileitungen*, Springer-Verlag Berlin Heidelberg GmbH, 1960, 3rd Edition.

[2] Danish Energy Agency, *Nye retningslinjer for kabellægning og udbygning af transmissionsnettet*, 8. October 2008, j.nr. 022520/78028-001.

[3] Z. Liu, *Global Energy Interconnection*, Academic Press, 2015, 1st Edition.

[4] A. Bettencourt, *The Global Smart Grid Federation Report*, SmartGrid Canada, 2012.

[5] European Network of Transmission System Operators for Electricity, *Ten-Year Network Development Plan 2012*, www.entsoe.eu, 2012.

[6] H. Skouboe, BYSTRUP Design, Power Pylons of the Future, *E-mail: hs@bystrup.dk*, 16.11.2017.

[7] R.K. Kumar, G.A. Kulkarni: Overhead versus Underground Transmission Lines, *Journal of the Indian Electrical and Electronics Manufacturers Association*, **6**:46–52, 2015.

[8] F. Weber, H. Distl: Damping Estimation from Free Decay Responses of Cables with MR Dampers, *Scientific World Journal*, **861954**, doi: 10.1155/2015/861954, 2015.

[9] K. K. Kar, *Composite Materials - Processing, Applications, Characterizations*, Springer-Verlag Berlin Heidelberg, 2017, 1st Edition.

[10] J. L. Lilien, P. Van Dyke, J. M. Asselin, M. Farzaneh, K. Halsan, D. G. Havard, D. Hearnshaw, A. Laneville, M. Mito, C. B. Rawlins, M. St-Louis, D. Sunkle, A. Vinogradov: State of the art of conductor galloping. *Cigré TFB2.11.06, Électra, technical brochure no 322*, 2007.

[11] Basin Electric, www.basinelectric.com: Galloping Basin Electric transmission lines due to wind. *published 11.04.2013*.

[12] J. P. Den Hartog, *Mechanical Vibrations*, McGraw-Hill Book Company Inc., 4th Edition, 1956.

[13] A. Treviso, B.V. Genechten, D. Mundo, M. Tournour: Damping in Composite Materials: Properties and Models. *Composites Part B*, **78**:144–152, 2015.

[14] U. A. Khashaba: Toughness, flexural, damping and interfacial properties of hybridized GFRE composites with MWCNTs. *Composites: Part A* **68**:164–176, 2015.

[15] R. Chandra: Damping studies in Fiber-reinforced composite. *Composite Structures* **46**:41–51, 1999.

[16] B.R. Sher, R.A.S Moreira: Dimensionless analysis of constrained damping treatments. *Composite Structures* **99**:241–254, 2013.

[17] S. U. Khan, C. Y. Li, N. A. Siddiqui, J.-K. Kim: Vibration damping characteristics of carbon fiber-reinforced composites containing multi-walled carbon nanotubes. *Composites Science and Technology* **71**:1486–1494, 2011.

[18] S. Prabhakarana, V. Krishnaraj, M. Senthil kumar, R. Zitoune: Sound and Vibration Damping Properties of Flax Fiber Reinforced Composites, *Procedia Engineering*, **97**:573–581, 2014.

[19] A. Moudood, W. Hall, A. Öchsner, H. Li, A. Rahman, G. Francucci: Effect of Moisture in Flax Fibres on the Quality of their Composites. *Journal of Natural Fibers*, DOI: 10.1080/15440478.2017.1414651, 2017.

[20] C. A. Fuentes, K. W. Ting, C. Dupont Gillain, M. Steensma, A. G. Talma, R. Zuijderduin, A. W. Van Vuure: Effect of humidity during manufacturing on the interfacial strength of non-pre-dried flax fibre/unsaturated polyester composites. *Composites Part A: Applied Science and Manufacturing* **84**:209–215, 2016.

[21] J. Chandradass, M. R. Kumar, R. Velmurugan: Effect of Clay Dispersion on Mechanical, Thermal and Vibration Properties of Glass Fiber-Reinforced Vinyl Ester Composites, *Journal of Reinforced Plastics and Composites*, **27**:1585–1601, 2008.

[22] A. Kabir, S. V. Hoa: Improvement of Vibration Damping and Flexural Fatigue Property Incorporating Nanoclay into Glass-Epoxy Composite, *26th International Committee on Aeronautical Fatigue and Structural Integrity Symposium*, Montreal, Canada, June 2011.

[23] A. Guevara-Morales, A. C. Taylor: Mechanical and dielectric properties of epoxy-clay nanocomposites. *J Mater Sci* **49**:1574–1584, 2014.

[24] S. U. Khan: Multiscale Carbon Fiber-reinforced Epoxy Composites Containing Nanofillers, *Dissertation*, The Hong Kong University of Science and Technology, Department of Mechanical Engineering, 2011.

[25] W. Keyoonwong, Y. Guo, M. Kubouchi: Corrosion behavior of three nanoclay dispersion methods of epoxy-organoclay nanocomposites. *Int J Corros*, doi:10.1155/2012/924283, 2012.

[26] T.-D. Ngo, M.-T. Ton-That, S. V. Hoa, K. C. Cole: Effect of temperature, duration and speed of pre-mixing on the dispersion of clay/epoxy nanocomposites. *Composites Science and Technology* **69**:1831–1840, 2009.

[27] S. Ingram, H. Dennis, I. Hunter: Influence of clay type on exfoliation, cure and physical properties of in situ polymerised poly(methyl methacrylate) nanocomposites. *Polym Int* **57**:1118–1127, 2008.

[28] H. T. Huynh, K. Benzarti, M. S. Duc: Role of interfacial chemistry on the rheology and thermo-mechanical properties of clay-polymer nanocomposites for building applications. *Chem Pap* **66**:519–531, 2012.

[29] B. A. Zai, M. K. Park, H. S. Choi: Effect of moisture absorption on damping and dynamic stiffness of carbon fiber/epoxy composites. *J Mech Sci Technol* **23**:2998–3004, 2009.

[30] B. Zhang: Using graphene in coating materials to prevent UV degradation on advanced composite materials. *In Proceedings: 6th Annual Symposium: Graduate Research and Scholarly Projects*, Wichita, Wichita State University, p. 205-206, 2010.

[31] K. K. Chang, *Aramid Fibers*, ASM Handbook Volume 21, Composites (ASM International), 2001.

[32] T. Turba, P. Fracz: Comparative analysis of cellulose pressboard and aramid paper used in air insulation systems of high-voltage devices. *International Conference Energy, Environment and Material Systems* **19**, doi.org/10.1051/e3sconf/20171901044, 2017.

[33] A. Baker, S. Dutton, D. Kelly, *Composite Materials for Aircraft structures*, American Institute of Aeronautics and Astronautics, 2004, 2nd Edition.

[34] T. Kruckenberg, R. Paton, *Resin Transfer Moulding for Aerospace Structures*, Springer Netherlands, 1998, 1st Edition.

[35] K. J. Sandesh, K. S. Umashankar, B. J. Manujesh, C. K. Thejesh, N. M. Mohan Kumar: Mechanical Charaterisation of Kevlar/Glass Hybrid Reinforced Polymer composite laminates. *International Advanced Research Journal in Science, Engineering and Technology* **3**:90–97, 2016.

[36] E. M. Abderrahim, A. Mustapha, S. E. Youssef: Damping analysis of orthotropic composite materials and laminates. *Composite: Part B* **39**:1069–1076, 2008.

[37] E. C. Botelho, A. N. Campo: Damping behavior of continuous fiber/metal composite materials by the free vibration method. *Composite: Part B* **37**:255–263, 2006.

[38] M. Bulut, A. Erklig, E. Yeter: Experimental investigation on influence of Kevlar fiber hybridization on tensile and damping response of Kevlar/glass/epoxy resin composite laminates. *Journal of Composite Materials* **50**:1875–1886, 2016.

[39] D. G. Jones, *Handbook of Viscoelastic Vibration Damping*, Wiley, 1st Edition, 2001.

[40] M. A. Trindade, A. Benjeddou: Hybrid Active-Passive Damping Treatments Using Viscoelastic and Piezoelectric Materials: Review and Assessment. *Journal of Vibration and Control* **8**:699–745, 2002.

[41] M. D. Rao: Recent applications of viscoelastic dampin gfor noise control in automobiles and commercial airplanes. *Journal of Sound and Vibration* **262**:457–474, 2003.

[42] M. Hao, M. D. Rao: Vibration and Damping Analysis of a Sandwich Beam Containing a Viscoelastic Constraining Layer. *Journal of Composite Materials* **39**:1621–1643, 2004.

[43] R. A. S. Moreira, J. D. Rodrigues: Partial Constrained Viscoelastic Damping Treatment of Structures: A Modal Strain Energy Approach. *International Journal of Structural Stability and Dynamics* **6**:397–411, 2006.

[44] F. Cortes, M. J. Elejabarrieta: Structural vibration of flexural beams with thick unconstrained layer damping. *International Journal of Solids and Structures* **45**:5805–5813, 2008.

[45] E. R. March, L. C. Hale: Damping of Flexural Waves With Imbedded Viscoelastic Materials. *Journal of Vibration and Acoustics* **120**:188–193, 1998.

[46] J. Ruzicka: Damping Structural Resonances Using Viscoelastic Shear-Damping Mechanisms: Part I - Design Configurations. *Journal of Engineering for Industry* **83**:403–413, 1961.

[47] J. Ruzicka: Damping Structural Resonances Using Viscoelastic Shear-Damping Mechanisms: Part I - Experimental Results. *Journal of Engineering for Industry* **83**:414–424, 1961.

[48] Y. Sefrani, J. M. Berthelot: Temperature effect on the damping properties of unidirectional glass fibre composites. *Composite: Part B* **37**:346–355, 2006.

[49] J. Feng, Z. Guo: Effects of temperature and frequency on dynamic mechanical properties of glass/epoxy composites. *J Mater Sci*, **51**:2747–2758, 2016.

[50] ASTM D5023 Standard: Standard Test Method for Plastics: Dynamic Mechanical Properties: In Flexure (Three-Point Bending). *ASTM International*, 2007.

[51] ASTM E756 Standard: Standard Test Method for Measuring Vibration-Damping Properties of Materials. *ASTM International*, 2010.

[52] F. Duc, P.-E. Bourban, J.-A. E. Manson: Damping performance of flax fibre composites, *ECCM-16th European conference on composite materials*, Seville, Spain, June 2014.

[53] J.M. Berthelot, Y. Sefrani: Damping analysis of unidirectional glass and Kevlar fibre composites. *Composites Science and Technology* **64**:1261–1278, 2004.

[54] J. D. D. Melo, D. W. Radford: Time and temperature dependence of the viscoelastic properties of CFRP by dynamic mechanical analysis. *Composite Structures* **70**:240–253, 2005.

[55] C.F. Beards, *Engineering Vibration Analysis with Application to Control Systems*, Wiley - Technology and Engineering, 1st Edition, 1996.

[56] M. R. Maheri, R. D. Adams: Finite-element prediction of modal response of damped layered composite panels. *Composites Science and Technology* **55**:13–23, 1995.

[57] F. Duc, P.-E. Bourban, J.-A. E. Manson: The role of twist and crimp on the vibration behaviour of flax fibre composites. *Composites Science and Technology* 102:94–99, 2014.

[58] S. J. Hwang, R. F. Gibson: Influence of bending-twisting and extension-bending coupling on damping of laminated composites. *Journal of Materials Science* **28**:1–8, 1993.

[59] T. Wollmann, N. Modler, M. Dannemann, A. Langkamp, S. Nitschke, A. Filippatos: Design and testing of composite compressor blades with focus on the vibration behaviour. *Composites Part A: Applied Science and Manufacturing* **92**:183–189, 2017.

[60] R. D. Adams, D. G. C. Bacon: Effect of Fibre Orientation and Laminate Geometry on the Dynamic Properties of CFRP. *Journal of Composite Materials* **7**:402–428, 1973.

[61] M. Dannemann: Zur vibroakustischen Auslegung von Faserverbund-Leichtbaustrukturen. *Dissertation* Technische Universitaet Dresden, 2012.

[62] V. Alwan, A. Gupta, A. S. Sekhar, R. Velmurugan: Dynamic analysis of shafts of composite materials. *Journal of Reinforced Plastics and Composites* **29**:3364–3379, 2010.

[63] K. J. Balkema: Design and Analysis of constrained layer damping treatments for bending and torsion. *Dissertation* Air Force Institute of Technology, Ohio, USA, 1994.

[64] R. Kottner, J. Vacik, R. Zem: Improvement of the damping properties of carbon-fibre-reinforced laminated plastics using damping layers. *Materials and Technology* **47**:189–193, 2013.

[65] H. Z. Zhang, H. L. Chen: A study on the damping characteristics of laminated composites with integral viscoelastic layers. *Composite Structures* **74**:63–69, 2006.

[66] J. M. Berthelot, M. Assarar, Y. Sefrani, A. E. Mahi: Damping analysis of composite materials and structures. *Composite Structures* **85**:189–204, 2008.

[67] E. E. Ungar, M. Kerwin: Loss factors of viscoelastic systems in terms of energy concepts. *The Journal of the Acoustical Society of America* **34**:954–7, 1962.

[68] T. Heistermann: Stiffness of reverse channel connections at room and elevated temperatures. *Dissertation* Luleå University of Technology, 2013.

[69] A. S. Veletsos, G. R. Darbret: Dynamic stiffness of parabolic cables. *Earthquake Engineering and Structural Dynamics* **11**:367–401, 1983.

[70] M. K. S. Madugula, *Dynamic Response of Lattice Towers and Guyed Masts*, American Society of Civil Engineers, 1st Edition, 2001.

[71] X. M. Li, K. J. Zhu, L. Bin: Experimental Simulation on Aerodynamic Character of D-Shaped Iced Conductor. *Applied Mechanics and Materials* **614**:622–627, 2013.

[72] D.G Havard, J.L Lilien, *Conductor galloping*, Tutorial given at IEEE ESMOL and TPC Meeting, Las Vegas, January 2008.

[73] M. B. Waris, T. Ishihara, M. W. Sarwar: Galloping response prediction of ice-accreted transmission lines. *The 4th International Conference on Advances in Wind and Structures(AWAS'08)* Jeju, Korea, May 29-31, 2008.

[74] H. Zhang, X. Liu, L. Zhang, L. He: Theoretical and Numerical Analysis of Galloping of Bundle Conductors. *Asia-Pacific Power and Energy Engineering Conference* Wuhan, China, March 25-28, 2011.

[75] C. B. Gurung, H. Yamaguchi, T. Yukino: Identification of large amplitude wind-induced vibration of ice-accreted transmission lines based on field observed data. *Engineering Structures* **24**:179–188, 2001.

[76] B. Yan, X. Liu, X. Lv, L. Zhou: Investigation into galloping characteristics of iced quad bundle conductors. *Journal of Vibration and Control* **22**:965–987, 2014.

[77] J. Swinkels, L. v. d. Eijnden: A journey towards sustainable energy security - Lessons learned from Denmark, *Interdisciplinary research* Utrecht University, Mechanical Engineering, 2014.

[78] R. D. Blevins, *Flow-induced vibration*, Van Nostrand Reinhold, New York, 2nd Edition, 1990.

[79] D. Srivastava, D. Chandra: Transmission Line Conductor Galloping Analysis using FEM. *International Journal of Applied Engineering Research* **11**:6972–6982, 2016.

[80] J. Hu, B. Yan, S. Zhou, H. Zhang: Numerical Investigation on Galloping of Iced Quad Bundle Conductors. *IEEE TRANSACTIONS ON POWER DELIVERY* **27**:784–792, 2012.

Appendix A

Forced vibration testing

The test rig for damping measurement by forced vibration at galloping relevant frequencies (from 0.5 Hz to 2 Hz) is provided by the University of Ghent for a short term stay (see Fig. A1).

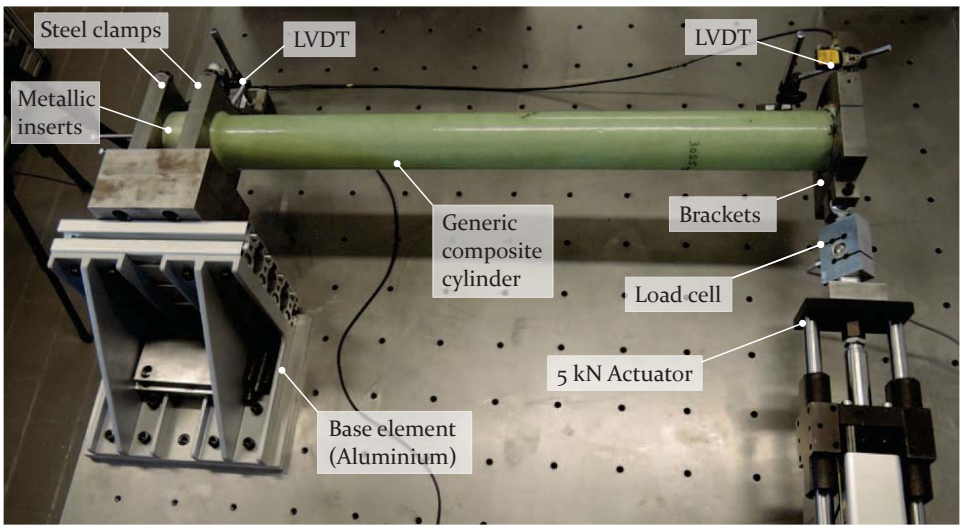

Figure A1: Fixed-Free clamped composite cylinder for a forced vibration test at low frequencies typical for galloping.

However, the aluminium base element is apparently too soft to precisely measure the structural loss factor of the composite beam during forced vibration. Instead, the damping in the aluminium clamping device is measured, as no differences in damping results of the various cross section concepts is observed (see Fig. A2).

The damping is calculated by

$$\eta = \frac{1}{2\pi} \frac{\Delta U}{U}, \tag{A1}$$

with U and ΔU representing the stored and dissipated energy per cycle, respectively. These values may be determined by the obtained hysteresis loop (see Fig. A1),

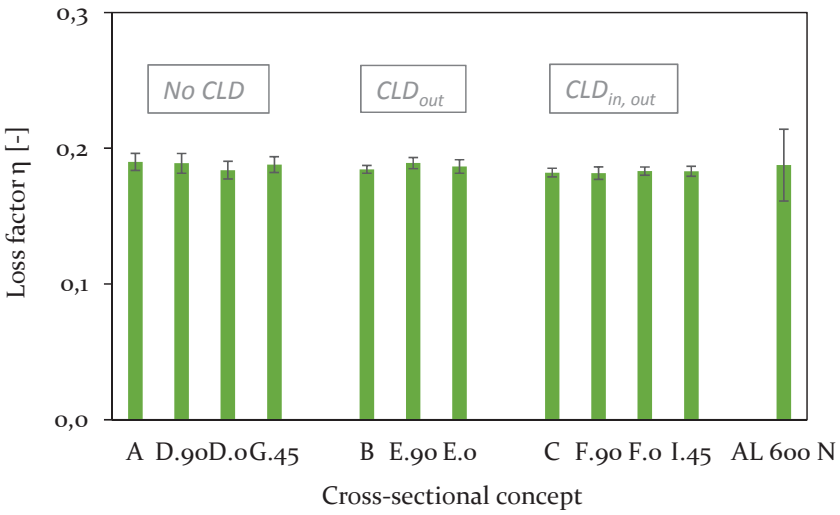

Figure A2: Damping results of the forced vibration test of all composite cylinders with reference aluminium shaft.

where U and ΔU are represented be the enclosed area of the triangle and the ellipse, respectively.

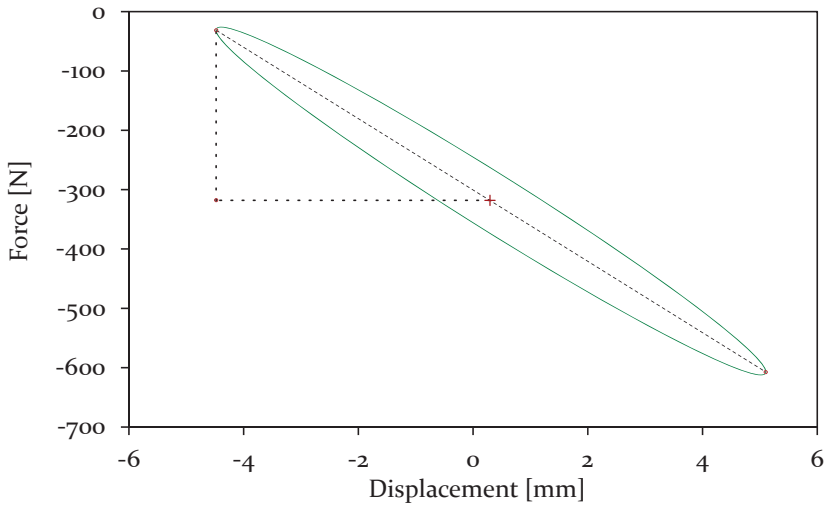

Figure A3: Representative hysteresis loop for the cross-sectional design concept A., tested at 2 Hz with an amplitude of 10 mm.

The plotted damping in Fig. A2 is averaged over 20 hysteresis loops.

P1

Characterization of Clay-modified thermoset polymers under various environmental conditions for the use in high-voltage power pylons

Mathias Kliem, Jan Høgsberg, Qian Wang, Martin Dannemann

Advances in Mechanical Engineering,
Vol **9**:1–16, 2017.

Special Issue Article

Advances in Mechanical Engineering

Advances in Mechanical Engineering
2017, Vol. 9(5) 1–16

DOI: 10.1177/1687814017698890
journals.sagepub.com/home/ade
SAGE

Characterization of clay-modified thermoset polymers under various environmental conditions for the use in high-voltage power pylons

Mathias Kliem[1], Jan Høgsberg[1], Qian Wang[2] and Martin Dannemann[3]

Abstract

The effect of nanoclay on various material properties like damping and strength of typical thermoset polymers, such as epoxy and vinyl ester, was investigated. Different environmental conditions typical for high-voltage transmission pylons made of composite materials were taken into account. Resin samples were prepared with various clay weight fractions ranging from 0% to 3%. Scanning electron microscopy, transmission electron microscopy, X-ray diffraction and rheological analysis were used to study the morphology and the structure of the nanocomposites. For all nanoclay-modified thermoset polymers, the morphology was found to be of exfoliated structure mainly. Static, uniaxial tensile tests showed that the addition of nanoclay to thermoset polymers led to a beneficial effect on the stiffness, whereas the tensile strength and ductility significantly decreased. When exposed to different environmental conditions, nanoclay was found to have a positive influence on the dynamic properties, analysed by a dynamic mechanical thermal analysis. The addition of nanoclay to the thermoset resin led to an increase of the damping properties by up to 28% for vinyl ester and up to 6% for epoxy at -20°C. The dielectric properties were evaluated by electrical breakdown strength tests resulting in 11% better insulating behaviour for nanoclay-modified vinyl ester.

Keywords

Nanoclay, thermoset polymers, material testing, environmental ageing

Date received: 14 October 2016; accepted: 13 February 2017

Academic Editor: Mohammad Talha

Introduction

Glass fibre–reinforced plastic (GFRP) materials are of non-conductive nature and well suited for use in high-voltage applications, such as insulators and power transmission pylons.[1] Thus, overhead transmission lines can be attached directly to the cross arms of each composite pylon because of the inherent non-conductivity of the raw material. Due to a rigid connection of the transmission lines to the pylon, any wind-induced vibration and motion will be directly transferred to the slender composite mast structure. As a consequence, the severe cable vibration phenomenon known as 'galloping' can lead to catastrophic failure of the entire structure due to excessive vibration amplitudes at resonance.[2,3] Therefore, galloping is

[1]Department of Mechanical Engineering, Technical University of Denmark, Kongens Lyngby, Denmark
[2]Department of Energy Technology, Aalborg University, Aalborg, Denmark
[3]Institute of Lightweight Engineering and Polymer Technology, Technische Universität Dresden, Dresden, Germany

Corresponding author:
Mathias Kliem, Department of Mechanical Engineering, Technical University of Denmark, Anker Engelunds Vej 1, 2800 Kongens Lyngby, Denmark.
Email: mkliem@mek.dtu.dk

considered as a major design parameter for the overall transmission line system.[4] Galloping occurs at temperatures around or below 0°C, as non-symmetrical ice aggregations along the transmission lines are usually initiating this low frequent vibration phenomenon associated with large vibration amplitudes (0.1–1 Hz).[5,6] The increase of structural damping is an effective way to raise the critical wind speed for the onset of galloping.[7] Nanoparticles, such as nanoclay (NC) and nanotubes (NT) within composite materials, have been found to enhance the static and dynamic material properties, specifically with regard to damping.[8–13] Kabir and colleagues[14,15] have been investigating the damping behaviour of GFRP beams with different laminate configurations by a free decay test and a dynamic mechanical thermal analysis (DMTA) at room temperature and have observed an increase in damping for a quasi-isotropic laminate by up to 36% in combination with a stiffness enhancement of 10% when reinforced by 2 wt% NC.

Another central issue of this article is a sensibility analysis of an NC modification of thermoset polymers to various environmental conditions and the resulting change in material properties, although this has been partially addressed in Singh et al.[16] and Tcherbi-Narteh et al.[17] Composite structures designed for an external application are being exposed to different environmental conditions like ultraviolet (UV) radiation, moisture and pollution, inducing material degradation. Although coatings are widely used for protection against environmental degradation,[18,19] the structural material to be used is required to be resistant against the weathering conditions mentioned above, especially as power transmission pylons are designed for life times of $\geq$50 years. NC has been found to enhance the barrier properties within the polymer, such as the resistance to moisture transport, and has been leading to a reduction of material degradation by UV exposure. These material properties play an important role for the design of high-voltage power pylons exposed to harsh environmental conditions, such as moisture, UV irritation and strong electromagnetic fields. Furthermore, an easy and inexpensive availability, processability and non-toxicity of NC is of high importance among other things, as it has been reported in Dasan[20] and Bensadoun et al.,[21] resulting in commercial attention towards these materials. Nowadays, NC is increasingly used in various industries, for example, in automotive, packaging, coating and paints, electronics and aerospace,[22–24] to enhance cost-effective, specific material properties, such as stiffness,[25] strength,[26] limited flammability and thermal stability,[27] fracture toughness[28] and viscosity.[29] Furthermore, NC is also of electrical non-conductive nature.[30] The overall dielectric material property of NC-modified Epoxy (EP) has been observed to be 20% higher compared to neat EP.[31] The use of NTs, for example, carbon NTs, is not conducive, as the material properties like non-conductivity and inexpensive availability are required for the design of the power transmission pylons. In summary, NC is a suitable and promising additive for the enhancement of static and dynamic material properties to be used in connection with high-voltage power pylons.

It has been reported in Velmurugan and Mohan[11] that NC modified with an organic modifier results in improved performance in terms of dispersion, thermal stability, stiffness and hardness compared to non-modified NC. This modification, for example, by an organic quaternary ammonium salt, has lead to an enhanced interaction between the clay surface and the matrix.[32] Therefore, the organomodified NC Garamite 1958 has been chosen in the following investigations due to its potential to enhance the relevant material properties of the neat polymer.[33,34]

Already small amounts of NC (of a few wt%) can lead to considerable improvements due to the high aspect ratio of layered silicate, resulting in a huge network of interfacial surface area.[13,14] Clay nanocomposites can be grouped into three different morphologies (see Figure 1) depending on the remaining agglomerate sizes of NC particles and the related interplanar distances (d-spacing) between clay platelets representing the crystal lattice planes (see Figure 3). The exfoliated clay–polymer morphology is the most desirable for improved material properties,[12,34,35] whereas in practice the final dispersion consists probably of all three morphologies with different percentage proportions.[12]

A number of investigations have dealt with various dispersion techniques to maximize the dispersion quality in terms of amount of exfoliated clay particles within the polymer.[36,37] It has been found that the mixing speed is one of the driving parameters for achieving an

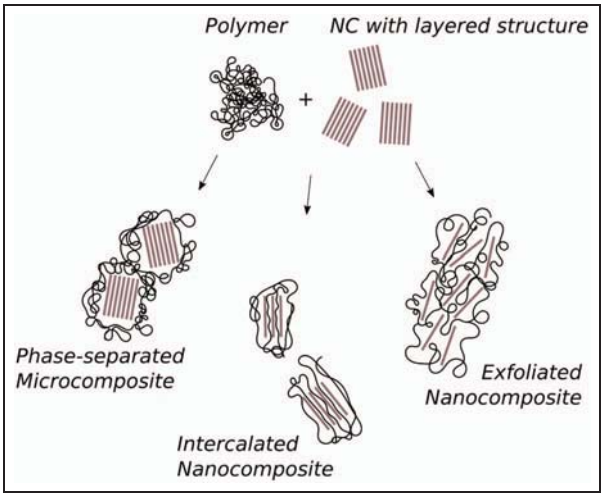

Figure 1. Scheme of different clay–polymer morphologies.

exfoliated clay–polymer morphology realizable with the high-speed homogenization technique used for this investigation.[38] The just mentioned dispersion quality, the type of polymer and clay as well as its pretreatment may all have a significant influence on the final material properties of the NC-modified polymer.[39] Therefore, the aim of this study is to present an evaluation on the effect of NC on the static and dynamic material properties by keeping those parameters constant. Thus, the investigation focuses on the NC modification of the polymer resin material only, instead of considering the whole fibre–polymer composite. Therefore, the conclusion of this study is only valid for matrix-dominated material properties, such as the transverse stiffness and transverse damping capability of a unidirectional (UD) laminate.[14,33] The effect of NC on the static material properties of vinyl ester (VE) and epoxy (EP) is investigated specifically for different environmental conditions, such as moisture, UV irritation and the presence of a high electrical field, representative of a composite power transmission pylon in its realistic environment. However, the major subject of this investigation is the damping analysis of different NC-modified polymer configurations at low temperatures (between -20°C and 0°C), low frequencies (≤ 1 Hz) and under the influence of various environmental conditions, representing an aged composite power transmission pylon being affected by galloping-induced vibrations of the attached overhead transmission lines. These material properties have not been investigated so far in relation to the specific environmental conditions mentioned above in combination with the materials used for the analysis.

Experimental methods

This section provides a detailed description about the materials, methods and procedures used to analyse the effect of NC on the static and dynamic material properties of EP and VE. Besides a comprehensive analysis of the dispersion quality in terms of clay–polymer morphology, different mechanical and electrical testing procedures are explained. The experimental setup used for environmental ageing is described at the end of the section.

Materials

The thermoset matrices investigated were a bisphenol-epoxy vinyl ester resin DION IMPACT 9102-683 (VE) and an epoxy infusion system PRIME 20LV (EP). These resin materials are both well suited for use in electrical insulation devices due to their high dielectric properties.[1,40,41] An alkyl ammonium–based NC, commercially available as Garamite 1958 by Byk Additives and Instruments, was used in four weight concentrations (0, 1, 2 and 3 wt%) within the polymer to gradually demonstrate a change in the mechanical properties. This organically modified mixed clay system is a mixture of platelets and ribbon-like clay particles and has been chosen due to its specified usability within EP and VE.[42]

Sample preparation

The NC was added in four different weight concentrations to the thermoset resins relative to the final polymer weight: 0, 1, 2 and 3 wt%. In accordance with Keyoonwong et al.[37] and Ngo et al.,[38] a high-speed homogeniser Ultra-Turrax T25 was chosen to increase the probability of an entirely exfoliated clay–polymer morphology. A maximum of 500 mL resin was mixed during each run with 20.000 rpm for 40 min. The mixing temperature never exceeded 80°C. The final mixing viscosity was dependent on the type of thermoset resin, due to different resin–hardener mixing ratios (VE – 2:100/EP – 26:100). Whereas 98 wt% of the VE resin relative to the final matrix material weight was used for mixing, only 80 wt% of the EP resin was mixed with NC. All dispersions were evacuated for about 90 min under vacuum at 35°C to remove air trapped during mixing. Only for the mixture EP-2 (epoxy with 2 wt% NC), it appeared to be difficult to achieve an air-bubble free dispersion. Additional degassing of the dispersion under vacuum at temperatures of around 50°C for more than 12 h was to little avail. Furthermore, it was observed that VE resin exhibited a loss of mass of about 3% after evacuation, which might be explained by the outgassing of styrene. The resin temperature was raised to 35°C before mixing with the hardener to reduce viscosity. As illustrated in Figure 2, the nanocomposite dispersion was then poured into a vertically orientated mould consisting of two parallel plates to minimize the surface shrinkage pattern. In total, eight

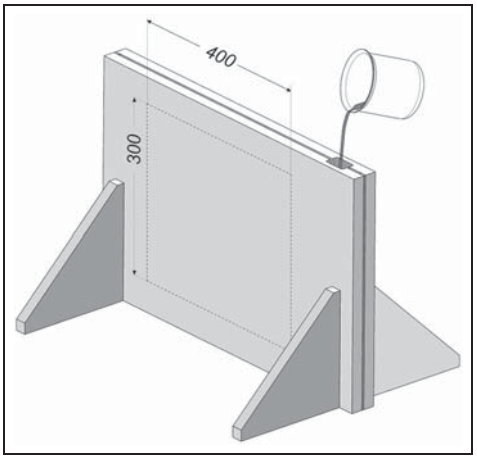

Figure 2. Filling process of the NC-modified resin into the vertically oriented mould.

nanocomposite panels with 300 mm × 400 mm × 2 mm were manufactured to test EP and VE with four NC concentrations. After curing and post-curing, the panels rested for at least 24 h at 40°C and 10 h at 70°C and were then cut by computerized numerical controlled (CNC) milling to samples used for tensile tests and DMTA in test-specific dimensions (see sections 'Mechanical properties' and 'Breakdown strength analysis').

Morphology analysis of nanocomposites

There are several complementary methods typically used for the evaluation of the NC distribution within a polymer, such as scanning electron microscopy (SEM), transmission electron microscopy (TEM), X-ray diffraction (XRD) and rheology analysis.[43] All methods were used in this present investigation.

The SEM analysis was conducted under high vacuum using a Quanta 200 F electron microscope by FEI, while a FEI Tecnai G2 transmission electron microscope was used to generate the TEM images. The required surface treatment of all SEM samples as well as the cutting of 100 nm slices for the TEM analysis was carried out using a Leica Ultracut UCT microtome. To monitor the time-dependent NC distribution within the polymer over a mixing period of 40 min, dispersion samples extracted after every 10 min were cured and then optically analysed.

The XRD method can be used to determine the clay–polymer morphology (see Figure 1) of neat NC and NC-modified polymer materials.[44] Based on the diffraction angle 2θ of the incident and the diffracted X-rays, the interplanar distance d (d-spacing) of two atomic-scale crystal lattice planes can be calculated according to Bragg's law (see Figure 3)

$$n\lambda = 2d \sin \theta \quad (1)$$

The X-ray diffraction investigations on both neat NC and NC composites were performed using a Philips PW 1830 X-ray Generator with Cu Kα radiation ($\lambda_{Cu} = 1.5405$ Å). The specimens were scanned at 45 kV and 40 mA with the diffraction angle of 2θ ranging from 2° to 30° with equidistant increments of 0.1° and a retention time of 3 s.

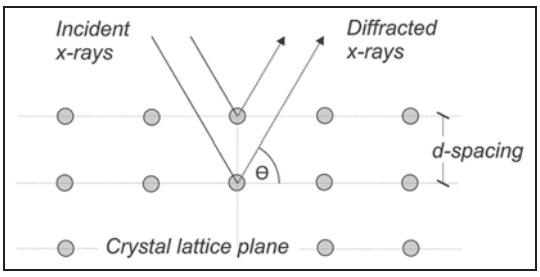

Figure 3. Bragg's diffraction by a crystal lattice plane with the incident and diffracted wave vectors.

A supplementary rheological analysis was carried out using a Rheometer AR 2000 by TA, as this technique is widely used for the evaluation of the dispersion state. While SEM, TEM and XRD methods usually require solid samples, non-cured NC–resin dispersions were used for this rheological investigation. The rheological investigation of all NC–resin dispersions was carried out at 25°C. A parallel plate setup with a gap distance of around 1 mm was used to perform shear rate sweeps for different NC contents in the range from 1 to 100 s^{-1}.

Mechanical properties

The influence of the NC modification on the mechanical properties of the polymer was evaluated based on static tensile tests at room temperature as well as a DMTA at environmental conditions similar to those experienced during transmission line galloping. The static and dynamic results obtained by the tests described below are specifically used to assess the use of NC-modified matrix for high-voltage power pylons.

Tensile test. Uniaxial tensile tests were used to evaluate the effects of NC and various ageing conditions on the static mechanical properties of different thermoset polymers. The tensile test was conducted at room temperature according to the ISO 527-2 Standard.[45] All dog-bone samples with the standardized dimensions of type 1 BA[45] were quasi-statically tested on an MTS Acumen Electrodynamic Test System with a 3 kN load cell at a crosshead speed of 1 mm/min. The displacement was measured by an MTS extensometer with 25 mm gauge length. At least six specimens were used for each configuration.

DMTA. The Dynamic Mechanical Thermal Analyser (DMTA) used for the damping characterization of the nanocomposite samples was a Q800 from TA as shown in Figure 4. The specimens with the dimensions of 60 mm × 5 mm × 2 mm were tested in galloping close environmental conditions according to Liu et al.,[46] at a frequency of 0.5 Hz for the two temperatures of −20°C and 0°C. A three-point bending fixture was used for the analysis.

Breakdown strength analysis

The electrical strength is an important property of an insulating material, as it indicates the maximum electrical field the material can withstand before it fails to work due to the breakdown channel through the material. Thus, electric strength is used to investigate the

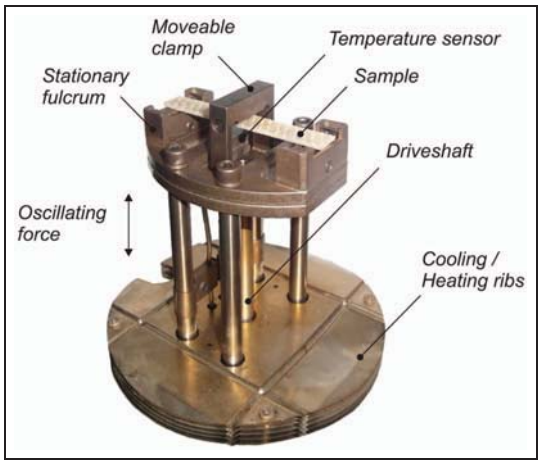

Figure 4. Sample placed in the three-point bending fixture of the DMTA Q800.

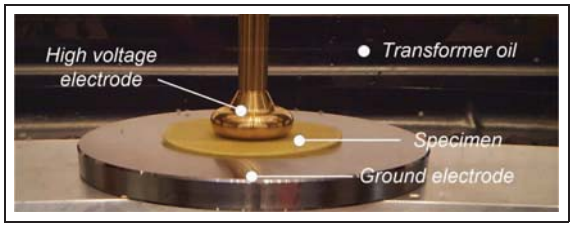

Figure 5. Electric strength test configuration.

effects of different weight percentages of NC particles on the dielectric properties of VE and EP materials. Electric strength tests are performed according to the IEC 60243 Standard[47] to investigate the influence of the NC modification on the dielectric properties of the polymer. Round-plate specimens with the dimensions of 100 mm × 2 mm were tested at ambient atmosphere conditions at 21°C and 50% relative humidity.[48] A cylinder-plate electrode configuration was adopted. Tests were conducted at a grid frequency of 50 Hz in transformer oil. Figure 5 shows the electric strength test configuration.

Environmental ageing test

Artificial weathering tests, such as water immersion and UV exposure, were conducted to investigate the changes in mechanical properties. To shorten the environmental ageing process, high-intensity test conditions were chosen: (a) the samples were placed in a water bath instead of applying realistic condensation conditions and (b) the intensity of UV radiation was about 17 times higher than stated in the ASTM D4329-13 Standard.[49]

Water immersion. The oven-dried nanocomposite samples were immersed in distilled water at room temperature and periodically weight in accordance with the ASTM D570-98 Standard,[50] in order to evaluate the water uptake W_t by

$$W_t(\%) = \frac{(S_t - S_{t_0})}{S_{t_0}} \cdot 100 \qquad (2)$$

where S_t and S_{t_0} are the sample weight at time t_0 and t.

UV exposure. The photoageing process was carried out in a UV exposure chamber as described in Christiansen et al.[51] using UV-lamps from both sides with a relatively broad spectrum centered around 365 nm at 14 mW/cm^3. After measuring the weight, the specimens were randomly redistributed within the chamber. The temperature during UV exposure never exceeded 40°C.

Results and discussion

In this section, the results of the morphological study in terms of dispersion quality are presented first. The sample weight as a result of the sensibility to artificial weathering is then evaluated based on the morphological analysis. Furthermore, the static and dynamic material properties are discussed together with the results of the environmental ageing procedure, leading to an assessment of the applicability of NC-modified thermoset polymers with respect to the use in high-voltage transmission pylons. Finally, the effect of NC on the breakthrough strength, as an indicator for enhanced dielectric properties, is discussed.

Morphology and dispersion quality

The clay–polymer morphology was evaluated by SEM images in Figure 6 for different NC-modified VE configurations. The average agglomerate size was found to depend on the different mixing durations and NC contents (1–3 wt%).

The mixing duration denoted as 0 min corresponds to a brief manual mixing to ensure that all NC particles are bound by resin, and that no loose NC is left on the resin surface. In Figure 6, the bright areas on the back-scattered micrographs represent agglomerated NC particles. The clay portions are continuously being broken up during increased mixing, although a few and small NC agglomerated particles are still present after 40 min of mixing, as shown in Figure 6 for the 3 wt% mixture. The maximal remaining aggregate size is about 5 μm for all three NC concentrations, whereas the density of those max-sized aggregates clearly increases with increasing NC concentration. However, the NC is well dispersed within the polymer after 40 min mixing for all three NC configurations (VE-1, VE-2 and VE-3), although the remaining few clay agglomerates are large and therefore may have a negative influence on the

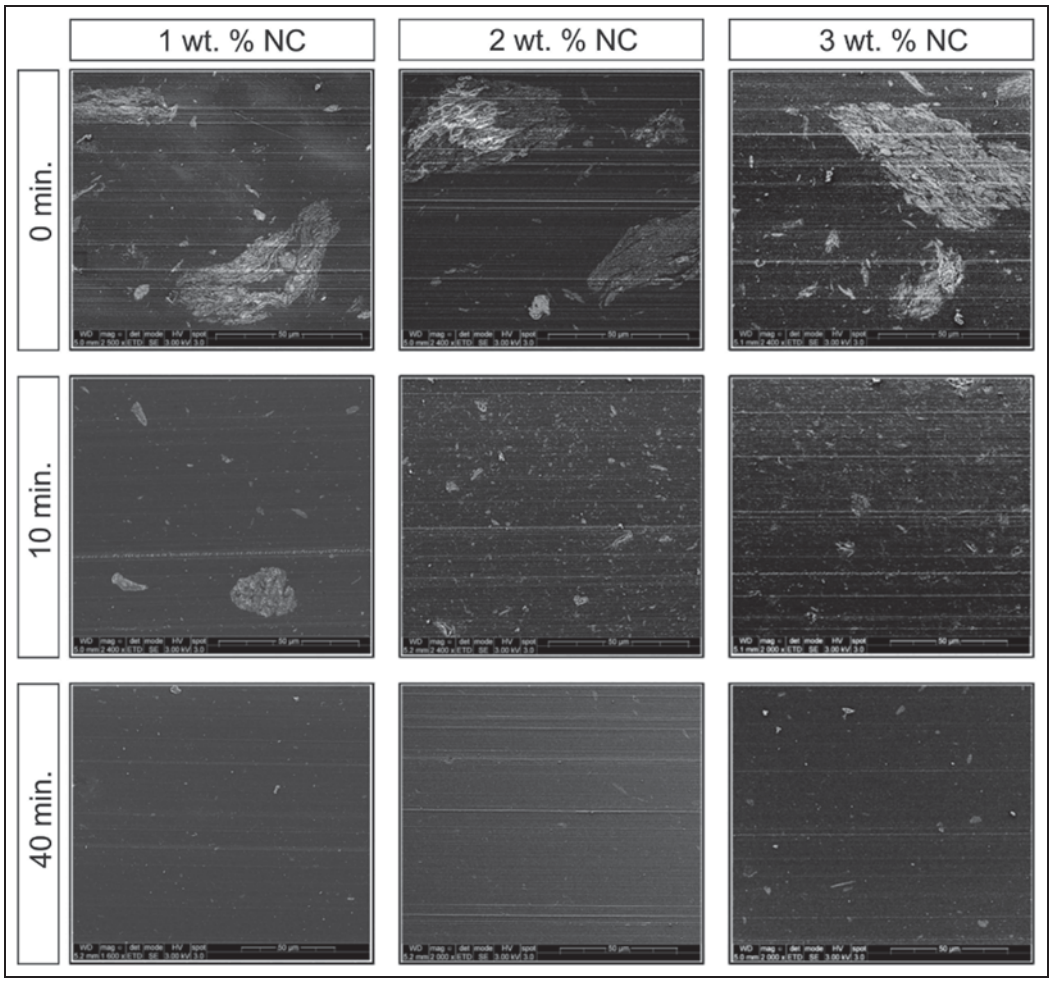

Figure 6. SEM images of VE with respect to different NC contents and mixing durations.

mechanical behaviour of the nanocomposite, due to appearing stress concentrations in these areas.[52,53]

The layered, ribbon-like structure typical for Garamite[37] is shown in Figure 7(a) and (b) obtained by TEM image for VE-2 with 0 and 40 min mixing duration, respectively. Figure 7(a) shows a multi-stack agglomerate consisting of a large number of evenly aligned, tightly packed platelets with small interplanar d-spacing. This phase-separated microcomposite (see Figure 1) with a low d-spacing is typical for an unmixed state and agrees well with the SEM images for 0 min of mixing in Figure 6. In contrast, a well dispersed NC agglomerate with increased d-spacing is seen in Figure 7(b). The remaining average particle size of about four platelets with an increased d-spacing is in good agreement with the observations in Ngo et al.[38] based on an applied high shear mixing method. To support the microscopical results for VE, the broadly used XRD method was performed to evaluate the clay dispersal within the polymer. The results for the neat NC 'Garamite 1958' are in good agreement with Ingram et al.[32] and Huynh et al.[54] and present a mix of minerals dominated by sepiolite (see Figure 8). According to Bragg's law (see equation (1)), the d-spacing of the clay platelets results in $d = 1.194$ nm from the distinct basal peak in Figure 8 at the diffraction angle 2θ of $\sim 7.4°$.

Cured VE- and NC-VE samples were also analysed to determine the clay–polymer morphology, indicating the level of exfoliation. In Figure 8, the broad curve of neat VE with its maximum at around 2θ of $\sim 20.0°$ represents the amorphous structure and it is in good agreement with Pal.[55] The XRD patterns of neat VE with its clay-modified derivatives (VE-1, VE-2 and VE-3) are of similar shape containing no sharp peaks and indicating a complete exfoliation state for all NC-VE dispersions (VE-x). Only for VE-2 and VE-3, an insignificant peak at 2θ of $\sim 7.1°$ can be observed. It may indicate an almost insignificant portion of intercalated NC particles within the exfoliated nanocomposite (see Figure 1). The resulting d-spacing of $d = 1.244$ nm is 4% larger compared to neat Garamite 1958, indicating a

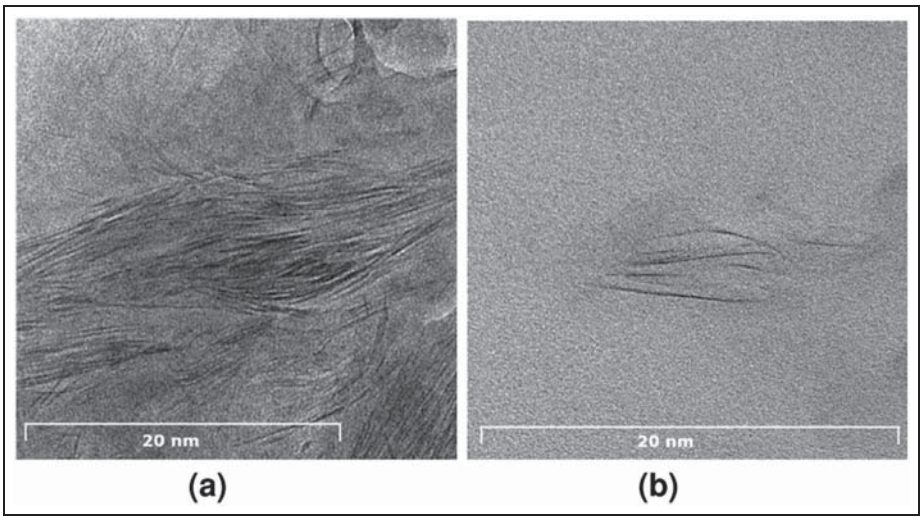

Figure 7. TEM images of VE-2 with different mixing durations: (a) 0 min mixing and (b) 40 min mixing.

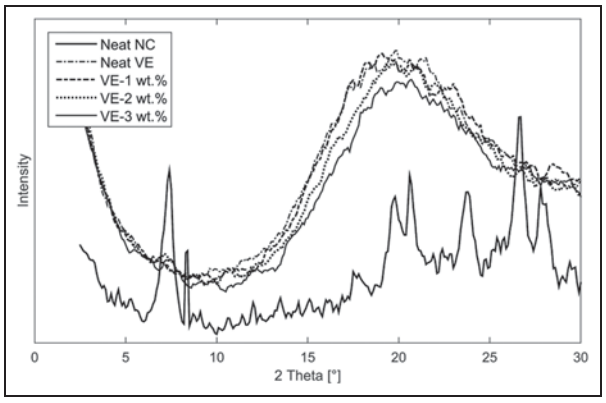

Figure 8. XRD curves of neat Garamite, neat VE and VE-Garamite dispersions.

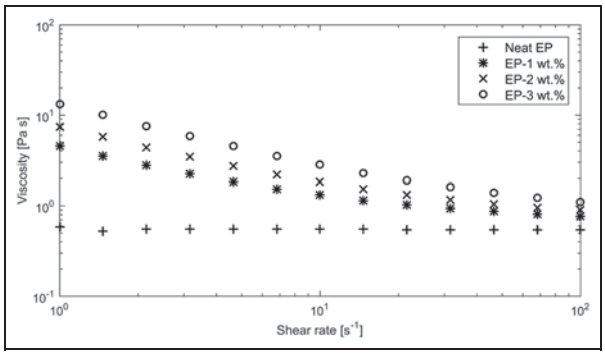

Figure 9. Shear viscosities for neat and NC-modified EP.

negligible increase of polymer molecules between the clay platelets and therefore a higher clay–matrix interaction.

Rheological measurements were carried out for neat and NC-modified EP to evaluate its morphological structure of the nanocomposite. The results for EP are shown in Figure 9. As expected, the initial viscosity increases with increasing NC content due to an enhanced interaction of clay particles within the polymer matrix.[12] At the same time, a viscosity decrease with increasing shear rate is observed, indicating the non-Newtonian behaviour called 'shear thinning'.[56] These phenomena are in agreement with Ingram et al.[32] and Huynh et al.[54] and are found to be directly related to a high grade of exfoliation within the clay–polymer network due to a strong interaction between clay particles and the EP matrix. Consequently, a high level of exfoliated NC particles within the EP is being assumed.

Sample weight as function of ageing duration

The effect of NC on the sample weight related to the ageing duration of polymer matrices, such as moisture and UV irritation, was investigated using water immersion and UV exposure tests. Three different ageing scenarios were developed: (a) UV exposure for 250 h, (b) water immersion for 400 h and (c) combined ageing with 250 h UV exposure and 400 h water immersion. All specimens were regularly weighed to track the sample weight as function of the duration of ageing. The presented curves in Figure 10 comprise an average of six different samples per configuration.

Organoclay, such as Garamite 1958, are capable of water absorption in humid environments[57] and may influence the water uptake characteristics of the nanocomposite when embedded within the polymer. In Figure 10(b), the normalized, time-dependent increase in weight is seen for all material combinations immersed in distilled water for up to 400 h. After a rapid water uptake within the first 100 h, the increase

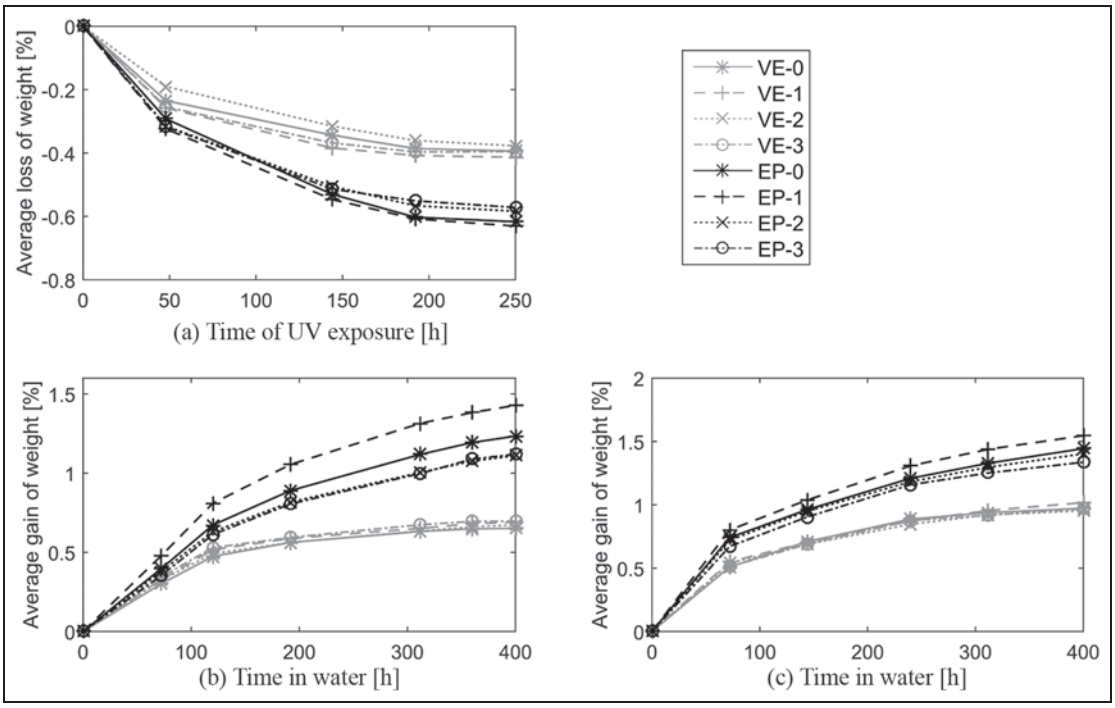

Figure 10. Average weight changes of non-modified and NC-modified VE and EP due to (a) UV exposure for 250 h, (b) water immersion for 400 h and (c) combined ageing condition with UV exposure for 250 h followed by 400 h water immersion.

in weight almost stabilizes for VE at around 0.7% due to saturation. An equilibrium is not reached for EP after 400 h, as the weight steadily increases towards the end of water immersion at 1.2%. No remarkable variation in weight gain for VE and its NC-modified derivatives ($\pm$ 0.02%) is observed, whereas a significant clay dependency is detected for EP ($\pm$ 0.2%). By modifying EP with 1 wt% NC, the water uptake is increased by 14% compared to neat EP. A decrease in weight by 9% can be observed for EP-2 and EP-3 compared to the reference EP-0. The results for EP-1 are partly contradictory to the results in Kusmono et al.[22] and Khanbabaei et al.,[58] as the water uptake should have been reduced with increasing amounts of exfoliated clay structures acting as efficient barriers against the water transport through the polymer. It is assumed that either a few of the larger clay particles remained non-dispersed within the polymer or a higher dispersion porosity of EP-1 due to mixing and manufacturing lead to the increased water uptake.

A similar type of water uptake is observed for samples that had previously been subjected to UV exposure for 250 h (Figure 10(c)). The water uptake for EP-1 is again 7% higher and for EP-2 and EP-3 in average 5% lower compared to EP-0. However, the water uptake capability is significantly increased for both – for VE by 30% and for EP by about 14% compared to the configurations subjected to water immersion only. This phenomenon is caused by micro-cracks as a result of UV exposure, providing pathways for a rapid water ingress.[16,59]

The average weight loss of all analysed VE and EP configurations (VE-x and EP-x) by UV exposure only is shown in Figure 10(a). The mass reduction as a result of UV exposure is caused by the expulsion of volatiles and residual moisture as well as by a physico-chemical degradation.[16,59] After a rapid drop of specimen weight within the first 50 h, the change in weight stabilized after 250 h of photoageing. This trend is apparent for both EP and VE, whereas EP in general is more prone to weight loss with 0.6% than VE with 0.4%. The weight changing characteristics of each polymer configuration due to UV light is inversely proportional to the water uptake behaviour, as shown in Figure 10(a) and (b). EP modified with 1 wt% experiences the highest water uptake, and consequently the highest gain in weight, but also the highest weight loss by UV exposure. The same relation occurs for EP-2 and EP-3. This correlation is not observed for VE, as the water uptake characteristics are found to be similar for all analysed VE configurations. In fact, the NC seems to have a neglectable influence on VE exposed to different environmental ageing conditions. The influence of NC on the mechanical behaviour of VE under environmental conditions will be analysed in the following sections.

It should finally be mentioned that all specimens suffer from discoloration. This phenomena is a result of oxidation reactions due to, for example, photoageing or

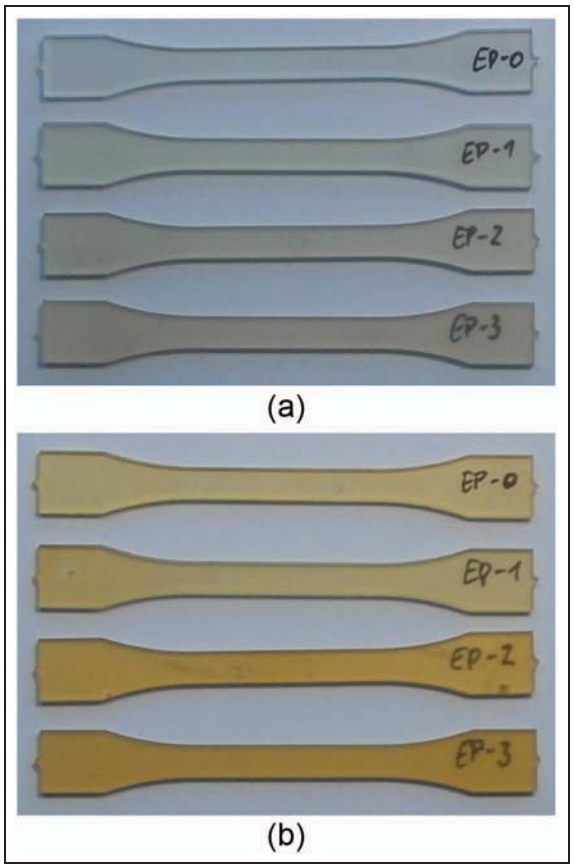

Figure 11. Non-modified and NC-modified EP tensile specimens before and after 250 h of UV exposure: (a) no UV exposure and (b) 250 h of UV exposure.

hygrothermal ageing[59,60,61] and is a nonreversible process based on chemical interactions within the network. The colour changes of the semi-transparent ageing specimens are illustrated by the photos in Figure 11.

Effect on the static mechanical properties

The effect of different ageing conditions, such as moisture and UV light, on the static mechanical properties like stiffness, strength and elongation at break of VE-x and EP-x was evaluated by uniaxial tensile tests according to the ISO 527-2 Standard.[45] It is well established that the environmental ageing conditions, considered in the previous section, may lead to decreased mechanical properties of thermoset polymers, whereas moisture may result in less adverse effects on a polymeric matrix compared to the degradation by UV radiation.[59] Both chain scission and chain cross-linking can take place because of UV irritation. This may result in reduced strength and enhanced brittleness due to a lower molecular weight and the presence of micro-cracks. On the other hand, an ingress of water has been observed to change the thermo-physical, mechanical and chemical characteristics of the polymer, leading to swelling,

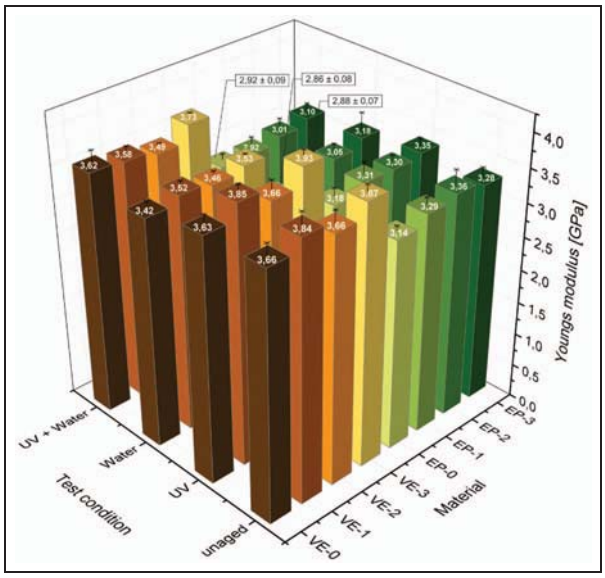

Figure 12. Tensile modulus for NC-modified EP and VE before and after ageing.

plasticization and hydrolysis and thereby resulting in an apparent decrease in the tensile (Young's) modulus.[62,63] A combined ageing of UV exposure and water immersion will couple these effects and may lead to either lower mechanical properties or unchanged stiffness properties due to synergistic effects.[59]

The stiffness of VE-x and EP-x is shown in Figure 12 with respect to different ageing conditions. Supported by a fairly uniform stiffness distribution, the stiffness of VE-x is found to be in average 15% higher compared to the EP-x configurations. A matrix modification by Garamite 1958 leads to a slight increase in stiffness of max. 5% for both VE and EP, although the highest amount of NC not necessarily results in the maximal stiffness.[11] This stiffening effect is found to be consistent for all environmental conditions and is caused by exfoliated or intercalated clay particles restricting the mobility of polymer chains during loading. The highest stiffness is observed for VE-3 and EP-2.

As mentioned above, water immersion of 400 h has a weakening effect on the stiffness of EP-x and VE-x, as shown in Figure 12. The reduction in stiffness is observed to be between 5.5% and 8.7% for VE and 3%–12% for EP.

Surprisingly, a stiffness reduction is not being observed for VE-x and EP-x after combined ageing, although a higher water uptake has been determined after prior UV radiation (see Figure 10(c)). Instead, a constant or slight decrease in stiffness compared to the unaged samples is observed, independent of the NC modification. This indicates the presence of synergistic effects, which seem to positively influence the material properties of specimens exposed to both UV light and moisture. The effect is found to be more pronounced

Table 1. Comparison of the material properties for neat EP and VE based on experiments and datasheet specifications.

Material		Tensile modulus (GPa)	Tensile strength (MPa)	Tensile elongation (%)
VE	Spec.	3.4	79	4.5
	Exp.	3.7 ± 0.2	84.5 ± 3.2	5.07 ± 1.3
EP	Spec.	3.5	73	3.5
	Exp.	3.0 ± 0.1	66.0 ± 0.3	6.4 ± 0.5

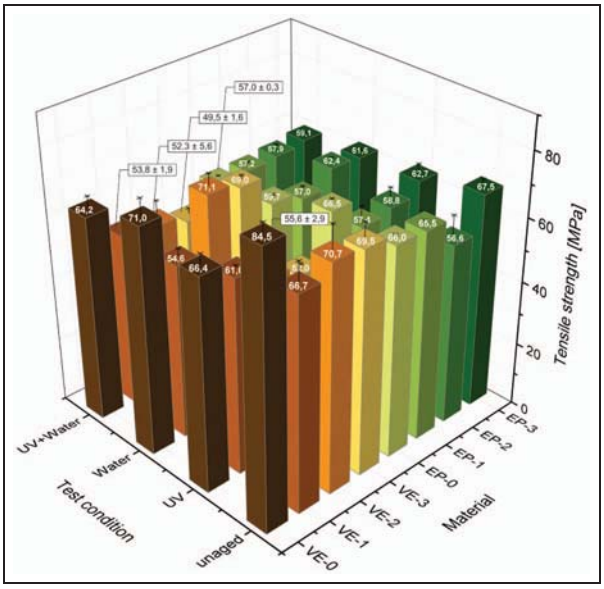

Figure 13. Tensile strength for NC-modified EP and VE before and after ageing.

for VE-x than for EP-x, while UV exposure seems to have no effect on the stiffness, which is in agreement with Thiagarajan et al.[64]

It can be concluded that the stiffness of VE-x and EP-x can be slightly improved by a matrix modification with NC. However, this stiffening effect is found to be independent of any environmental ageing conditions.

The tensile strength results for VE and EP are shown in Figure 13 with respect to varying NC contents and environmental conditions. For any material configuration investigated, the matrix modification by NC leads to a lower strength compared to the neat resin. Only EP-3 demonstrates a negligible increase in strength compared to its non-modified reference (EP-0). These results are in conflict with Chandradass et al.,[26] Ho et al.[65] and Rashmi et al.,[66] reporting an increase in or constant strength by a matrix modification with Garamite 1958. A decrease in strength for NC-modified EP up to a certain threshold concentration of 2 wt% has also been reported in Velmurugan and Mohan.[11] In contrast, a reduction in tensile strength of NC-modified polymers has been claimed in previous studies.[26,39,67,68] The presence of microvoids–proportional to the clay content due to an increased dispersion viscosity–and agglomerated NC particles have been reported to be the main reasons for a reduction in strength. The manufacturing process itself might be another causal factor for the differences, as the specified material properties for neat VE and EP are not properly matching either as indicated by the materials properties in Table 1. As mentioned previously, it is also conceivable that a small amount of NC remained agglomerated after mixing, leading to a reduced final strength of the nanocomposite. However, the dispersion control technologies, such as SEM, TEM, viscosity analysis and XRD used in the analysis, were not detecting any conspicuity in the respective dispersion morphology.

The effect of environmental ageing on the tensile strength varies significantly between VE-x and EP-x. Furthermore, UV exposure leads to considerable strength degradation for VE-x, whereas just a slight reduction in strength is observed for EP-x. On the other hand, water immersion results in slight decreased strength properties for EP-x and VE-x, while the tensile strength of VE-2 and VE-3 is very close to the strength of corresponding unaged samples. The diminishing effect of environmental ageing on the tensile strength of EP-x is plausible and in agreement with the matrix-dominated, transverse tensile properties of UD carbon fibre–reinforced EP samples after ageing.[59] The tensile strength is however found to be less affected by UV light compared to water immersion. Only EP-2 represents an uncommon case, as the reference tensile strength is lower compared to all related specimens exposed to environmental ageing.

It can be concluded that the addition of NC leads to a reduction in tensile strength for almost all analysed polymer configurations. The effect is more pronounced for VE-x than for EP-x. Furthermore, an NC modification seems to have no significant influence on the tensile strength of specimens when exposed to different environmental ageing conditions.

The effect of NC on the ductility of VE-x and EP-x is represented in Figure 14 with respect to the three different environmental ageing conditions. Similar to the strength analysis, the addition of NC to the thermoset polymers leads to a significant reduction in ductility. This NC related loss of ductility by up to 65% can be observed for both VE and EP and is in agreement with Rashmi et al.,[66] reporting an increase in brittleness with

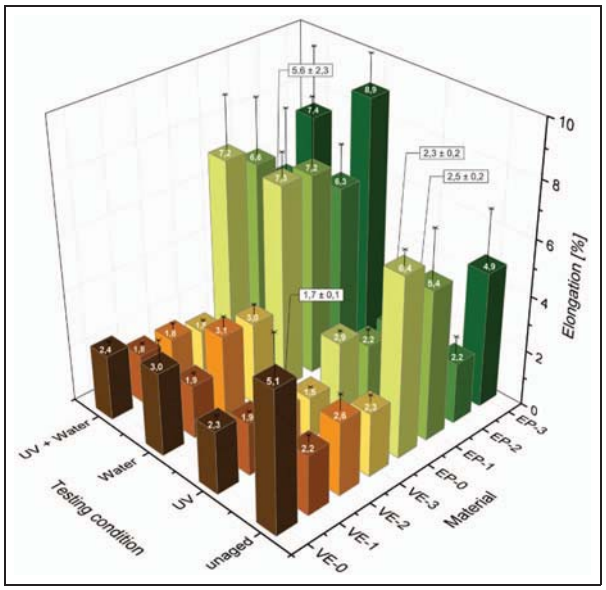

Figure 14. Elongation at break for NC-modified EP and VE before and after ageing.

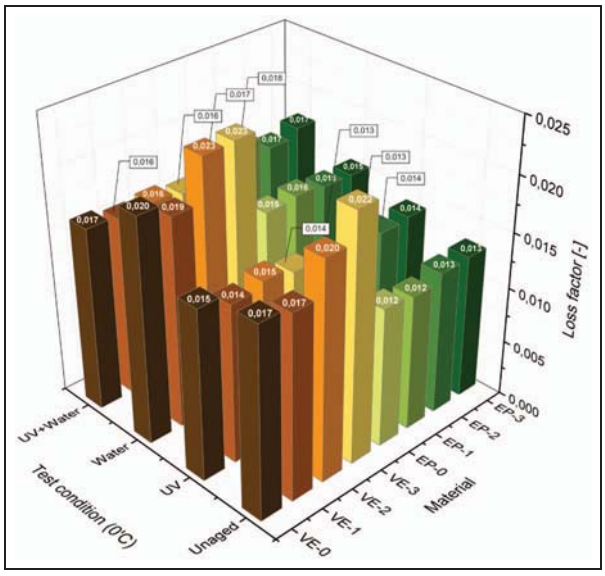

Figure 15. Damping at 0°C for NC-modified EP and VE before and after ageing.

NC content. Again, two mechanisms are believed to be responsible for this partial dramatic drop in ductility: a limitation in mobility of polymer chains under loading and the presence of voids.

When analysing the material-dependent ductility with respect to different ageing scenarios, an opposite tendency of the material-dependent water sensibility is observed for VE and EP. Water immersion only leads to either reduced or slightly increased ductility for VE, depending on the amount of NC. In contrast, a strong increase of ductility independent on the NC content is observed for EP compared to the related non-aged configurations. This individual behaviour has been reported in Zhao and Li[69] for VE and[70] for EP and can be explained by changes on the molecular level of each resin type. The embrittlement of VE and EP by about 55% due to UV exposure is due to the formation of micro-cracks as mentioned before.

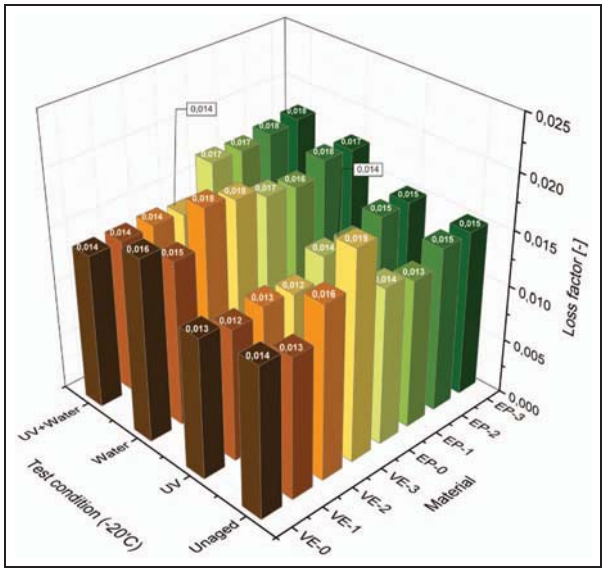

Figure 16. Damping at −20°C for NC-modified EP and VE before and after ageing.

Effect on the dynamic mechanical properties

The effect of NC modification and environmental conditioning on the damping behaviour of VE and EP was investigated using the DMTA with a three-point bending fixture (see Figure 4). The specimen to be analysed was sinusoidally loaded and the response signal was analysed in terms of phase shift between load and response signal. The related phase angle δ is representing the dissipated energy for one load cycle and is used to calculate the damping in the form of the loss factor $\tan\delta$.[71] In Figures 15 and 16, the damping of VE and EP is shown as function of NC content, ageing conditions and temperature. The testing frequency is chosen as a typical galloping frequency of 0.5 Hz. It is observed that the damping characteristics change considerably by varying the NC content and the weathering condition.

The damping capability in general is being reduced for VE by decreasing the temperature of 20°C from 0°C to −20°C, whereas the damping increases for all EP configurations for the same drop in temperature. This effect has been described in Zhang et al.[71] for neat EP and can be explained by the polymer crystallization and its high ordered microstructure at lower

temperatures. This leads to higher damping for VE at 0°C and for EP at −20°C. By modifying VE and EP with up to 3 wt% NC, an increase in the damping characteristics can be achieved at both temperatures. However, the damping enhancement for unaged VE-3 is with 23% at 0°C and with 28% at −20°C much larger compared to unconditioned EP-3 with 4% at 0°C and 6% at −20°C. The reason for this difference in damping increase is assumed to be related to changes in the interaction between clay particles and polymer molecules.

The sensibility of the damping property to different environmental conditions differs to some extent significantly between VE, EP and their NC-modified derivatives. The conditioning of all VE-x samples by UV light results in a decrease to more or less the same loss factor tan δ of about 0.0147 at 0°C and 0.0123 at −20°C. Thus, an NC modification of VE specimens remains without influence on the damping behaviour, when exposed to UV light. This implies the dominating damping effect of UV light–induced micro-cracks, instead of NC-introduced material damping. The same effect is observed by the damping results after combined environmental ageing for all VE-x. The damping of all VE-x is reduced to similar values for the loss factor tan δ of about 0.0162 at 0°C and 0.0140 at −20°C – independent of any NC modification. When considering water immersion only, a slight increase in damping of max. 15% is observed for VE-x compared to the related unaged specimens. This effect is due to the softening and swelling characteristics of the polymer and the absorbed water molecules.[62,63]

Compared to VE-x, the damping behaviour of EP is found to be less sensitive to any NC addition and at the same time much more stable when exposed to different environmental ageing conditions. The increased damping caused by water immersion and UV irritation accumulates to the maximum damping tan $\delta = 0.018$ after combined ageing. The results are valid for both investigated temperatures 0°C and −20°C.

To summarize, the damping behaviour can be increased for VE by up 28% and for EP by 6% due to a modification with NC. The overall damping capability of unaged VE is about 30% higher compared to EP at 0°C, whereas the damping behaviour of the two materials is very similar at −20°C. Compared to VE, it is found that EP is less sensitive to any matrix modification by NC as well as more stable when exposed to different environmental conditions. For example, the beneficial effect on the damping for NC-modified VE is lost when exposed to UV light.

Breakdown strength

Eight groups of specimens, VE-0, VE-1, VE-2, VE-3, EP-0, EP-1, EP-2 and EP-3 in four weight concentrations, 0, 1, 2 and 3 wt% in NC composites, were tested in the electric strength test. Each group contains two or three specimens numbered in sequence. Breakdown voltage was obtained for each specimen and electric strength was calculated by dividing the breakdown voltage (kV) with the specimen thickness (mm). The electric strength of the specimens is presented in Table 2.

Table 2. Test results of the electric strength of VE and EP specimens.

Materials	No. of specimen	Electric strength (kV/mm)
VE-0	# 1	14.4
	# 2	14.7
VE-1	# 1	16.2
	# 2	8.7
VE-2	# 1	16.2
	# 2	16.0
	# 3	16.7
VE-3	# 1	14.9
	# 2	15.4
EP		no results

It is indicated in Table 2 that the electric strength of VE specimens modified by the NC is slightly increased compared with that of the neat VE specimens. For instance, # 2 in group VE-2 has a larger electric strength of 16 kV/mm compared to group VE-0 with strength values of 14.4 and 14.7 kV/mm. This observation agrees with results in the literature.[31,73–76]

The increase in electric strength can be explained by a redistribution of space charge from a modification of NC in the material, resulting in an electrical field uniformity within the nanocomposite. Also, the small distance between NC particles leads to a zigzaging of the electrical tree, that is, it hinders the propagation of the electrical tree in the material. Thus, the specimen can withstand a higher electrical field. However, # 2 in group VE-1 has an unusual low electric strength, even compared with the neat specimens, which may be attributed to weak points (voids, particle agglomeration, etc.) in the material. Thus, this unusual value should be discarded when determining the inherent electrical strength of the VE material. It is also demonstrated based on the limited number of specimens that the electric strength promotion is not proportional to the weight percentage of the NC particles. Specimens with 1 and 2 wt% of NC have similar electric strength of around 16 kV/mm, while the value decreases when the NC concentration increases to 3 wt%. The decrease in electric strength may be the result of clay agglomerates in specimens in VE-3.

In the test, since the distance between the high-voltage electrode and the ground electrode was not

long enough, surface flashover always happened on EP specimens at an electrical field of 19 kV/mm. Therefore, all the EP specimens have a higher electric strength than 19 kV/mm and no effective data about the electric strength were obtained for the EP specimens.

Conclusion

The scope of this investigation was to prove the feasibility and performance of the NC-modified thermoset resin materials VE and EP with respect to high-voltage applications designed for life times of $\geq$50 years. Therefore, various mechanical and electrical material properties have been analysed under harsh environmental conditions such as water immersion, UV exposure and of these combinations. In particular, the effect of NC on the damping behaviour was studied at low temperatures and low frequencies, at which the dangerous cable vibration phenomena galloping typically occurs. In order to eliminate errors during mixing that could negatively affect the material properties at an early stage, various morphology analysis techniques such as SEM, TEM, XRD and rheological measurements were used. It was found that the NC was well dispersed within the polymer mainly consisting of exfoliated clay particles. Results from the experimental study demonstrate the effect of NC on the static, dynamic and electrical material behaviour. The main conclusions are drawn as follows:

- VE has a lower water absorption capacity as well as a lower weight loss due to UV exposure compared to EP. In contrast, VE is more sensitive to environmental ageing. For example, the strength of VE decreased by 22%, when exposed to UV light.
- The sensitivity of VE to the addition of NC is larger compared to EP. For example, an NC modification by 3 wt% led to a strength reduction of 18%, but also resulted in increased damping of up to 26%. This tendency is valid for all investigated environmental conditions.
- The dielectrical properties of VE increased by up to 11%, when modified with 2 wt% NC.
- By adding NC to EP, the tensile strength, stiffness and damping behaviour slightly increased for almost every configuration at all tested environmental conditions.
- The presence of NC led to a significant embrittlement of all investigated VE and EP matrix materials. The brittle behaviour of EP-x slightly changed under the influence of water immersion compared to EP-0.
- The material properties of neat EP were more stable under environmental ageing conditions, but less sensitive to NC compared to VE.

The last point inevitably leads to a design flexibility with respect to the material selection and material properties. Ensuring that all structural components are adequately protected during the life time from environmental impacts, for example, by coatings, the use of NC-modified VE (e.g. VE-3) can significantly enhance the vibrational behaviour – although it also results in some deficiencies in terms of strength and ductility. If special emphasis is on robust design with respect to environmental ageing, the use of NC-modified EP (e.g. EP-3) is preferred and may also result in slightly increased material properties like stiffness, strength and damping compared to neat EP. An embrittlement phenomena is only observed for the unaged and UV exposure test conditions.

The economic feasibility in terms of technical implementation of NC must also be considered and assessed. The long mixing times and the deteriorated flow characteristics during infusion processes due to increased dispersion viscosity are therefore important aspects to consider. Alternative manufacturing methods like filament winding may provide a solution to these drawbacks. Despite the above-mentioned limitations, NC is a promising and suitable additive for the enhancement of mainly dynamic, but also of specific static, material properties to be used in connection with high-voltage power pylons. However, a precise design evaluation and feasibility study has to be done prior to the application of NC-modified thermoset resin materials in composite structures.

Acknowledgements

Thanks are to the Institute of Lightweight Engineering and Polymer Technology of TU Dresden for their kind cooperation in carrying out the experimental dynamic study of this work.

Declaration of conflicting interests

The author(s) declared no potential conflicts of interest with respect to the research, authorship and/or publication of this article.

Funding

The author(s) disclosed receipt of the following financial support for the research, authorship and/or publication of this article: This research is supported by Innovationsfonden Denmark via the project Power Pylons of the Future (PoPyFu) in collaboration with Bystrup and Tuco Marine ApS, which are gratefully acknowledged.

References

1. Arora R and Mosch W. *High voltage and electrical insulation engineering*. New York: Wiley, 2011.

2. Ibrahimbegovic A and Kozar I. *Extreme man-made and natural hazards in dynamics of structures* (NATO security through science series). Rotterdam: Springer, 2007.
3. Li SY and Chen ZQ. Experimental investigation concerning aerodynamic stability of a stay cable incorporated with lamps. In: *Proceedings of the seventh Asia-Pacific conference on wind engineering*, Taipei, 8–12 November 2009, http://www.iawe.org/Proceedings/7APCWE/T3B_4.pdf
4. Boddy D and Rice J. Impact of alternative galloping criteria on transmission line design. In: *Proceedings of the electrical transmission and substation structures*, Fort Worth, TX, 8–12 November 2009, pp.1–12. Virginia: American Society of Civil Engineers.
5. Hu J, Yan B, Zhou S, et al. Parameter study on galloping of iced bundled conductors. In: *Proceedings of the 2010 Asia-Pacific power and energy engineering conference (APPEEC)*, Chengdu, China, 28–31 March 2010. New York: IEEE.
6. Lilien JL. State of the art of conductor galloping (Electra technical brochure 322), 2007, https://orbi.ulg.ac.be/bitstream/2268/17595/1/ELT_232_3.pdf
7. Chen WF and Lui EM. *Handbook of structural engineering*. 2nd ed. Boca Raton, FL: CRC Press, 2005.
8. Mohan TP, Velmurugan R and Kanny K. Damping characteristics of nanoclay filled hybrid laminates during medium velocity impact. *Compos Part B* 2015; 82: 178–189.
9. Kireitseu M, Hui D and Tomlinson G. Advanced shock-resistant and vibration damping of nanoparticle-reinforced composite material. *Compos Part B* 2008; 39: 128–138.
10. Sarathi R, Sahu R and Danikas MG. Understanding the mechanical properties of epoxy nanocomposite insulating materials. *J Electr Eng* 2009; 60: 358–361.
11. Velmurugan R and Mohan TP. Room temperature processing of epoxy-clay nanocomposites. *J Mater Sci* 2004; 39: 7333–7339.
12. Bensadoun F, Kchit N, Billotte C, et al. A comparative study of dispersion techniques for nanocomposite made with nanoclays and an unsaturated polyester resin. *J Nanomater* 2011; 2011: 406087-1–406087-12.
13. Karippal JJ, Murthy HNN, Rai KS, et al. Study of mechanical properties of epoxy/glass/nanoclay hybrid composites. *J Compos Mater* 2011; 45: 1893–1899.
14. Kabir A and Hoa SV. Improvement of vibration damping and flexural fatigue property incorporating nanoclay into glass/epoxy composite. In: *Proceedings of the 26th ICAF symposium*, Montreal, 1–3 June 2011. Berlin: Springer.
15. Kabir A. *Vibration damping property and flexural fatigue behavior of glass/epoxy/nanoclay composites*. PhD Thesis, Concordia University, Montreal, QC, Canada, 2010.
16. Singh RP, Khait M, Zunjarrao SC, et al. Environmental degradation and durability of epoxy-clay nanocomposites. *J Nanomater* 2010; 2010: 352746-1–352746-13.
17. Tcherbi-Narteh A, Hosur M and Jeelani S. Mechanical and thermal properties of carbon/epoxy nanoclay composites exposed to synergistic effect of UV radiation and condensation. In: *Proceedings of the 18th international conference on composite materials*, Jeju Island, Korea, 21–26 August 2011. International Committee on Composite Materials.
18. Hua J, Li X, Gao J, et al. UV aging characterization of epoxy varnish coated steel upon exposure to artificial weathering environment. *Mater Design* 2008; 30: 1542–1547.
19. Signor AW and Chin AW. Effects of ultraviolet radiation exposure on vinyl ester matrix resins: chemical and mechanical characterization. In: *Proceedings of the 16th technical conference on American society for composites*, Blacksburg, VA, 9–12 September 2001.
20. Dasan KP. Nanoclay/polymer composites: recent developments and future prospects. *Adv Struct Mater* 2015; 75: 561–579.
21. Bensadoun F, Kchit N, Billotte C, et al. A study of nanoclay reinforcement of biocomposites made by liquid composite molding. *Int J Polym Sci* 2011; 2011: 964193.
22. Kusmono M, Wildan MW and Ishak ZAM. Preparation and properties of clay-reinforced epoxy nanocomposites. *Int J Polym Sci* 2013; 2013: 690675.
23. Deepak K, Reddy NS and Naidu TVS. Thermosetting polymer and nano clay based natural fiber bio-composites. *Proced Mater Sci* 2015; 10: 626–631.
24. Majeeda K, Jawaidc M, Hassana A, et al. Potential materials for food packaging from nanoclay/natural fibres filled hybrid composites. *Mater Design* 2013; 46: 391–410.
25. Wang K, Chen L, Wu J, et al. Epoxy nanocomposites with highly exfoliated clay: mechanical properties and fracture mechanisms. *Macromolecules* 2005; 38: 788–800.
26. Chandradass J, Kumar MR and Velmurugan R. Effect of clay dispersion on mechanical, thermal and vibration properties of glass fiber-reinforced vinyl ester composites. *J Reinf Plast Comp*. Epub ahead of print 4 June 2008. DOI: 10.1177/0731684407081368.
27. Gilman JW. Flammability and thermal stability studies of polymer layered-silicate (clay) nanocomposites. *Appl Clay Sci* 1999; 15: 34–49.
28. Ozbenli E. Mechanical properties of exfoliated nanoclay/epoxy nanocomposites (University of Oklahoma), http://www.ou.edu/ (2011, accessed 19 September 2016).
29. Kumar M, Kumar V, Muthuraja A, et al. Influence of nanoclay on the rheological properties of PMMA/organoclay nanocomposites prepared by solvent blending technique. *Macromol Sy* 2016; 365: 104–111.
30. Karapappas P, Tsotra P and Scobbie K. Effect of nanofillers on the properties of a state of the art epoxy gelcoat. *eXPRESS Polym Lett* 2011; 5: 218–227.
31. Guevara-Morales A and Taylor AC. Mechanical and dielectric properties of epoxy–clay nanocomposites. *J Mater Sci* 2014; 49: 1574–1584.
32. Ingram S, Dennis H, Hunter I, et al. Influence of clay type on exfoliation, cure and physical properties of in situ polymerised poly(methyl methacrylate) nanocomposites. *Polym Int* 2008; 57: 1118–1127.
33. Chandradass J, Kumar MR and Velmurugan R. Effect of nanoclay addition on vibration properties of glass fibre reinforced vinyl ester composites. *Mater Lett* 2007; 61: 4385–4388.
34. Ho MW. *The mechanical thermal and microstructural behaviors of the strip silicates reinforced epoxy-based*

nanocomposites. PhD Thesis, University of New Orleans, New Orleans, LA, 2006.
35. Lam CK, Lau KT, Cheung HY, et al. Effect of ultrasound sonication in nanoclay clusters of nanoclay/epoxy composites. *Mater Lett* 2005; 59: 1369–1372.
36. Agubra VA, Owuor PS and Hosur MV. Influence of nanoclay dispersion methods on the mechanical behavior of E-glass/epoxy nanocomposites. *Nanomaterials* 2013; 3: 550–563.
37. Keyoonwong W, Guo Y, Kubouchi M, et al. Corrosion behavior of three nanoclay dispersion methods of epoxy/organoclay nanocomposites. *Int J Corros* 2012; 2012: 924283.
38. Ngo TD, Ton-That MT, Hoa SV, et al. Effect of temperature, duration and speed of pre-mixing on the dispersion of clay/epoxy nanocomposites. *Compos Sci Technol* 2009; 69: 1831–1840.
39. Alateyah AI, Dhakal HN, Zhang ZY, et al. Nanoindentation and characterisations of vinyl ester matrix nanocomposites based on layered silicate: effect of voids content. *Int J Mater Eng* 2014; 4: 97–102.
40. Imai T, Sawa F, Nakano T, et al. Effects of nano- and micro-filler mixture on electrical insulation properties of epoxy based composites. *IEEE T Dielect El In* 2006; 13: 319–326.
41. Kandelbauer A, Tondi G and Goodman S. *Handbook of thermoset plastics: 6. Unsaturated polyesters and vinyl esters*. 3rd ed. London: William Andrew, 2013.
42. Datasheet of GARAMITE 1958 by BYK: Additives and Instruments. GARAMITE 1958-rheological additive for epoxy, vinyl ester and unsaturated polyester resins, datasheet (Issue 10), 2013, www.byk.com
43. Bhat G, Hegde RR, Kamath MG, et al. Nanoclay reinforced fibers and nonwovens. *J Eng Fiber Fabr* 2008; 3: 22–34.
44. Chen J and Yan N. Crystallization behavior of organonanoclay treated and untreated kraft fiber – HDPE composites. *Compos Part B* 2013; 54: 180–187.
45. ISO 527-2:2012. Plastics: determination of tensile properties: part 2: test conditions for moulding and extrusion plastics.
46. Liu B, Zhu KJ, Sun XQ, et al. A contrast on conductor galloping amplitude calculated by three mathematical models with different DOFs. *Shock Vib* 2014; 2014: 781304.
47. IEC 60243-1:2013. Electrical strength of insulating materials-test methods – part 1: tests at power frequencies.
48. IEC 60212:2011. Standard conditions for use prior to and during the testing of solid electrical insulating materials.
49. ASTM D4329-13:2013. Standard practice for fluorescent ultraviolet (UV) lamp apparatus exposure of plastics.
50. ASTM D570-98:2010. Standard test method for water absorption of plastics.
51. Christiansen MB, Lopacinska JM, Jakobsen MH, et al. Polymer photonic crystal dye lasers as Optofluidic Cell Sensors. *Opt Express* 2009; 4: 2722–2730.
52. Ferreira JAM, Borrego LP, Costa JDM, et al. Fatigue behaviour of nanoclay reinforced epoxy resin composites. *Compos Part B* 2013; 52: 286–291.
53. Khan SU. *Multiscale carbon fiber-reinforced epoxy composites containing nanofillers*. PhD Thesis, The Hong Kong University of Science and Technology, Hong Kong, 2011.
54. Huynh HT, Benzarti K and Duc M. Role of interfacial chemistry on the rheology and thermo-mechanical properties of clay–polymer nanocomposites for building applications. *Chem Pap* 2012; 66: 519–531.
55. Pal R. *Moisture diffusion through organomodified montmorillonite polymer nanocomposites and resulting property degradations*. PhD Thesis, University of Mysore, Mysore, India, 2014.
56. Vijayan PP, Puglia D, Kennyb JM, et al. Effect of organically modified nanoclay on the miscibility, rheology, morphology and properties of epoxy/carboxyl-terminated (butadiene-*co*-acrylonitrile) blend. *Soft Matter* 2013; 9: 2899–2912.
57. Vosters PJC. *Dual action adhesive composition*. Patent WO 2014033273 A2, 2014, https://patentscope.wipo.int/search/en/detail.jsf?docId=WO2014033273
58. Khanbabaei G, Aalaie J, Rahmatpour A, et al. Preparation and properties of epoxy-clay nanocomposites. *J Macromol Sci B* 2007; 46: 975–986.
59. Kumar BG, Singh RP and Nakamura T. Degradation of carbon fiber-reinforced epoxy composites by ultraviolet radiation and condensation. *J Compos Mater* 2002; 24: 2713–2733.
60. Tcherbi-Narteh A, Hosur M, Triggs E, et al. Viscoelastic and thermal properties of full and partially cured DGEBA epoxy resin composites modified with montmorillonite nanoclay exposed to UV radiation. *Polym Degrad Stabil* 2014; 101: 81–91.
61. Simar A, Gigliotii M, Grandidier JC, et al. Evidence of thermo-oxidation phenomena occurring during hygrothermal aging of thermosetting resins for RTM composite applications. *Composites: Part A* 2014; 66: 175–182.
62. Zai BA, Park MK, Choi HS, et al. Effect of moisture absorption on damping and dynamic stiffness of carbon fiber/epoxy composites. *J Mech Sci Technol* 2009; 23: 2998–3004.
63. Dutta SS. *Water absorption and dielectric properties of epoxy insulation*. Master Thesis, Department of Electrical Power Engineering, Norwegian University of Science and Technology, Trondheim, 2008.
64. Monneya L, Duboisa C, Perreux D, et al. Mechanical behaviour of an epoxy-glass composite under photo-oxidation. *Polym Degrad Stabil* 1999; 63: 219–224.
65. Thiagarajan A, Kaviarasan K, Vigneshwaran R, et al. The nano clay influence on mechanical properties of mixed glass fibre polymer composites. *Int J ChemTech Res* 2014; 6: 1840–1843.
66. Ho MW, Lam CK, Lau KT, et al. Mechanical properties of epoxy-based composites using nanoclays. *Compos Struct* 2014; 75: 415–421.
67. Rashmi, Renukappa NM, Chikkakuntappa R, et al. Montmorillonite nanoclay filler effects on electrical conductivity, thermal and mechanical properties of epoxy-based nanocomposites. *Polym Eng Sci* 2011; 51: 1827–1836.
68. Zunjarrao SC, Sriraman R and Singh RP. Effect of processing parameters and clay volume fraction on the

mechanical properties of epoxy-clay nanocomposites. *J Mater Sci* 2006; 41: 2219–2228.
69. Sobrinho LL, Ferreira M and Bastian FL. The effects of water absorption on an ester vinyl resin system. *Mater Res* 2009; 12: 353–361.
70. Zhao H and Li RKY. Effect of water absorption on the mechanical and dielectric properties of nano-alumina filled epoxy nanocomposites. *Key Eng Mat* 2007; 334: 617–620.
71. Ehrenstein GW, Riedel G and Trawiel P. *Praxis der Thermischen Analyse von Kunststoffen*. Vienna: Hanser Verlag, 1998.
72. Zhang PQ, Ruan JH and Li WZ. Influence of some factors on the damping property of fiber-reinforced epoxy composites at low temperature. *Cryogenics* 2001; 41: 245–251.
73. Ma D, Hugener TA and Siegel RW. Influence of nanoparticle surface modification on the electrical behaviour of polyethylene nanocomposites. *Nanotechnology* 2005; 6: 724–731.
74. Hai-bing H, Hong-Yan L and Bin L. Effect of nanometric fillers on electrical properties of polymers. *Insul Mater* 2006; 5: 36–39.
75. Junguo G, Jinmei Z and Quanquan J. Study on breakdown and partial discharge of polyethylene montmorillonite nanocomposites. In: *Proceedings of the international symposium on electrical insulating materials (ISEIM)*, Yokkaichi, Japan, 7–11 September 2008. New York: IEEE.
76. Zazoum B, David E and Ngo AD. Correlation between structure and dielectric breakdown in LDPE/HDPE/clay nanocomposites. *ISRN Nanomater* 2014; 2014: 612154-1–612154-9.

P2

Damping properties of non-conductive composite materials for applications in power transmission pylons

Mathias Kliem, Marvin Rüppel, Jan Høgsberg, Christian Berggreen, Sina Baier

Journal of Composite Materials,

First published online: March 25, 2018,

DOI: 10.1177/0021998318766635.

Review

JOURNAL OF COMPOSITE MATERIALS

Journal of Composite Materials
0(0) 1–19

DOI: 10.1177/0021998318766635
journals.sagepub.com/home/jcm

SAGE

Damping properties of non-conductive composite materials for applications in power transmission pylons

Mathias Kliem[1], Marvin Rüppel[2], Jan Høgsberg[1], Christian Berggreen[1] and Sina Baier[3]

Abstract

This study aims to characterize the fibre direction dependent damping properties of non-conductive composite materials to be used in newly designed electrical power transmission pylons, on which the conducting cables will be directly connected. Thus, the composite structure can be designed both to insulate and to act as a damper to avoid for example conductor line galloping. In order to predict the damping of the composite materials, a comprehensive analysis on a representative unidirectional laminate was carried out. The fibre direction dependent damping analysis of glass and aramid reinforced epoxy and vinylester, partly reinforced with nanoclay or fibre-hybridized, was investigated using a Dynamic Mechanical Thermal Analysis and a Vibrating Beam Testing procedure for five different fibre orientations (0°, 30°, 45°, 60° and 90°). The focus was on damping behaviour evaluation at low temperatures (−20°C and 0°C) and low vibration frequencies (0.5 Hz, 1 Hz and 2 Hz), in order to represent the environmental conditions of vibrating conductor lines during. The prediction of the damping behaviour for coupon-level-specimens with three balanced laminates was successfully carried out with a maximal deviation of maximal 12.1%.

Keywords

Composite materials, damping, nanoclay, modal strain energy approach

Introduction

The European Network of Transmission System Operators for Electricity (ENTSOE) foresees a need for over 50.000 km of new or overhauled extra high voltage routes in the coming 10 years – with more than half (28.400 km) as new overhead lines.[1] Instead of erecting new standard steel lattice towers, which were developed over 70 years ago without regard to visual appearance, new materials could enable innovative visual expressions and at the same time – through the integration of insulators in the pylon design – reduce the size of the pylons significantly. Using non-conductive raw material components in power pylons would enable the transmission lines to be attached directly to the cross arms of such a composite power pylon. The dynamic interaction between power pylon and transmission lines would however be significantly increased compared to the classic design with long insulators. Consequently, wind-induced vibrations and motion of the transmission lines would then be transferred directly into the composite mast structure. As the self-damping capability of the transmission lines is limited,[2–4] the amplitude level associated with cable vibration phenomena, such as the severe galloping instability, is one of the main design drivers for the overall architecture of large transmission line systems. The long-wave galloping vibration is characterized by very low frequencies of $0.1 - 1$ Hz and temperatures below 0°C.[5,6] Non-symmetrical ice aggregations along the overhead transmission lines in combination with wind speeds between 4 and 20 m/s[7,8] can initiate

[1]Department of Mechanical Engineering, Technical University of Denmark, Denmark
[2]Institut für Kunststofftechnik, Hochschule für Technik, Schweiz
[3]Department of Physics, Technical University of Denmark, Denmark

Corresponding author:
Mathias Kliem, Department of Mechanical Engineering, Technical University of Denmark, Anker Engelunds Vej 1, 2800 Kongens Lyngby, Denmark.
Email: mkliem@mek.dtu.dk

self-excitation which may lead to catastrophic failure of the entire structure due to excessive vibration amplitudes at resonance.[9,10] This issue can be mitigated by increasing the energy dissipation in the material used in the power pylon. The structure would act as a damper itself and thereby reduce the galloping induced vibration amplitudes of the transmission lines. The damping of composite materials can be up to several orders of magnitudes higher compared to traditional engineering materials, such as metals and alloys[11] and mainly depend on the orientation of the fibre reinforcement, the fibre content, the layup of the laminate and the composition of the materials involved.[12] For example, a supplemental nanoclay (NC) modification of the matrix component was shown to enhance specific material properties of different matrix systems like the dielectric properties, the Young's modulus and the damping.[13] Due to the large aspect ratio of the NC, defined by the ratio of surface to volume, the enhanced interaction between the clay surface and the matrix results in a significant improvement of some physico-chemical properties.[14,15] In particular, the damping performance of composite materials in the matrix-dominated off-axis directions may be enhanced by a well dispersed NC. The dispersion technique thereby plays a significant role.[16] Further, a composition of fibre types with different properties such as glass fibre (GF) and aramid fibre (AF) may also be used as hybrid composites to improve the damping properties of laminates.[17] Although a number of studies exist in the literature regarding the dynamic mechanical characterisation of NC-modified or neat composite materials, most publications focus on environmental conditions that are not representative for cable galloping or material compositions not suitable for the use in high-voltage power transmission pylons. The direction dependent damping of glass fibre reinforced polymers (GFRP) for unidirectional (UD) and woven laminates has been investigated only in the frequency domain from 50 Hz to 600 Hz.[18] In a preliminary work the effect of temperature on the damping behaviour was studied in the range of 20°C to 100°C.[19] The natural frequency variation of flat composite beams made of woven Kevlar and polyethylene reinforcement has been evaluated at low and high temperatures.[20] To the best knowledge of the authors, only two investigations have focused on the damping performance of GFRP and AF reinforced plastics (AFRP) at temperatures and frequencies close to galloping environmental conditions, however excluding the off-axis damping characterisation with fibre angles φ between 0° and 90°, which are relevant to compute the shear damping loss factor η_{12}.[21,22] The material damping properties η_{11} (longitudinal), η_{22} (transverse) and η_{12} (shear) fully describe the damping behaviour of a UD composite layer and are therefore input parameters for subsequent analytical and numerical damping analysis of multilayer structures.[23] Given the damping properties of the matrix and fibre, the direction dependent material damping coefficients can be obtained by the classical rule of mixture.[24,25] However, as the obtained results following this method were too inaccurate in comparison to the experimental test data, this approach will no further be discussed in this paper.

To the best knowledge of the authors, a thorough investigation on the damping performance of non-conductive composite materials at temperatures below 0°C and frequencies around 1 Hz has not been addressed in the literature so far. Thus, this study focuses on using nonconductive and NC-modified composite materials with reasonable damping properties such as GFRP and AFRP as structural material in high-voltage power transmission pylons. A comprehensive damping analysis has been conducted under galloping-like environmental conditions for the materials mentioned above. The commonly used dynamic mechanical thermal analyser (DMTA) as well as the vibrating beam test (VBT) have been used to determine the fibre direction dependent damping properties.[26–29] Specimens with unbalanced off-axis stacking sequences, commonly used for the damping characterisation of representative UD layers,[30,31] lead to additional damping due to bend-twist coupling effects caused by the unbalanced layup (off-axis laminate) for fibre angles $0^\circ < \varphi < 90^\circ$ compared to balanced layups (angle-ply laminates).[32]

In order to quantify the unwanted damping-side-effect for the off-axis specimens, a balanced layup configuration for all GFRP specimens has also been included in the test regime. The fibre direction dependent damping properties η_{11}, η_{22} and η_{12} of a representative UD layer made of NC modified and neat GFRP and AFRP have been calculated by the approximate Adams-Bacon method.[31,33] Furthermore, a comprehensive analysis on the parameters effecting the fibre direction dependent damping such as temperature, frequency, change in matrix or fibre materials, NC modification, test method and stacking sequence has been conducted. Finally, a numerical damping prediction of bidirectional hybrid laminates has been carried out based on experimentally obtained damping properties of representative UD layers.

Methods

The fibre direction dependent damping behaviour of non-conductive composite materials was analyzed under low temperature and low frequency conditions. The calculation of damping coefficients is based on the approximate Adams-Bacon damping model.[33] Furthermore, the results are used as input parameters

for the numerical damping analysis with a modal strain energy approach.

Mechanical properties

In this study, the dynamic material properties like stiffness and damping were analysed. The complex dynamic stiffness moduli E^* and G^* of viscoelastic materials such as composite materials contain a real part (storage moduli) E' and G' and an imaginary part (loss moduli) E'' and G'', respectively, representing the elastic and viscous effects

$$E^* = E' + iE'', \quad G^* = G' + iG'' \tag{1}$$

The storage moduli of fibre reinforced plastics (FRP) are assumed to be sufficiently close to the stiffness measurements obtained under quasi-static test conditions at room temperature (RT).[34,35] The stiffness has therefore been characterised by tensile tests.[36,37] The damping properties were analysed by the DMTA (see section 'Dynamic mechanical thermal analysis'). A thin UD-layer may be approximated with transversal isotropy which uses five independent material properties E'_1, $E'_2 \approx E'_3$, $G'_{12} \approx G'_{13}$, G'_{23}, $\nu_{12} \approx \nu_{13}$.[38] The resulting stiffness properties (E'_x, E'_y, G'_{xy}, G'_{yz}, ν_{xy}) may be related to the on-axis material properties (E'_1, E'_2, G'_{12}, G'_{23}, ν_{12}) by loading a lamina in its non-principal off-axis directions φ, according to Figure 1.

The in-plane material properties E'_1, E'_2 and G'_{12} may therefore be calculated by

$$\bar{S}_{11} = \frac{1}{E'_\varphi} = \frac{1}{E'_1}(\cos\varphi)^4\left(\frac{1}{G'_{12}} - \frac{2\nu_{12}}{E'_1}\right) \cdot (\sin\varphi)^2(\cos\varphi)^2 + \frac{1}{E'_2}(\sin\varphi)^4 \tag{2}$$

based on the experimental analysis of the Poisson ratio ν_{12} and the tensile properties E'_φ of UD specimens with five different fibre orientations $\varphi = 0°$, $30°$, $45°$, $60°$ and $90°$.[31,39] The method of least squares has been used in order to minimise the error between the measured stiffness $E'_{\varphi exp}$ and the calculated stiffness E'_φ,

$$\min_{\vec{x}} \sum_{j=1}^{n} \left(E'_{\varphi j exp} - E'_{\varphi j}(\vec{x})\right)^2 \quad with\ \vec{x} = [E'_1, E'_2, G'_{12}]\ and\ n \geq 3 \tag{3}$$

The remaining out-of-plane property G'_{23} may be approximated by the equivalent in-plane property G'_{13}.[29,40,41]

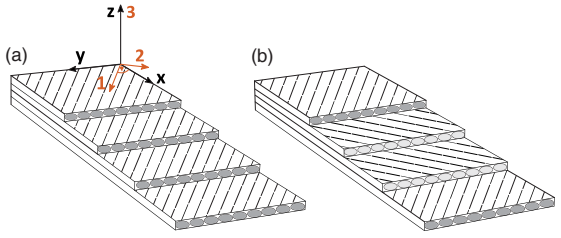

Figure 1. Relation between off-axis and on-axis coordinate systems for unbalanced off-axis (a) and balanced angle-ply laminates (b).

Damping approximation

The loss factor η is a convenient and general damping measurement index often used in material testing or evaluation of composite materials.[42] At low damping levels, the loss factor η is related to other damping definitions by

$$\eta \approx \frac{\psi}{2\pi} \approx \frac{\lambda}{\pi} \approx 2\zeta \approx \tan\delta \approx \delta \tag{4}$$

with ψ, λ, ζ and δ being the specific damping capacity, the logarithmic decrement, the damping ratio and the phase angle, respectively.[43] The damping behaviour of UD composite laminates depends as far the static mechanical properties discussed above, on the fibre direction and may be approximated by the Adam-Bacon-approach[31,33]

$$\eta_\varphi = E'(\varphi)\left[\frac{\eta_1}{E'_1}(\cos\varphi)^4 + \frac{\eta_2}{E'_2}(\sin\varphi)^4 + \left(\frac{\eta_{12}}{G'_{12}} - (\eta_1+\eta_2)\frac{\nu_{12}}{E'_1}\right)(\sin\varphi)^2(\cos\varphi)^2\right]. \tag{5}$$

This assumption is only valid in the 'free flexure' condition: In case a beam is subjected to pure bending, the resulting twist due to bend-twist-coupling is allowed. The direction dependent in-plane damping properties η_{11}, η_{22} and η_{12} are based on the experimentally obtained damping properties η_φ of UD specimens with different fibre orientations $\varphi = 0°$, $30°$, $45°$, $60°$ and $90°$ and are therefore only valid for the specific temperature and frequency conditions used for the experimental testing. The error between the measured damping $\eta_{\varphi exp}$ and the calculated damping η_φ has again been minimised by using the method of least squares

$$\min_{\vec{x}} \sum_{j=1}^{n} (\eta_{\varphi j exp} - \eta_{\varphi j}(\vec{x}))^2 \quad with\ \vec{x} = [\eta_1, \eta_2, \eta_{12}]\ and\ n \geq 3 \tag{6}$$

The out-of-plane damping properties for thin walled structures were approximated by the in-plane equivalents: $\eta_{22} \approx \eta_{33}$, $\eta_{12} \approx \eta_{13} \approx \eta_{23}$.[34] These fibre direction dependent material damping properties have been used as input parameters for the numerical damping analysis described in the following.

Numerical damping analysis by modal strain energy method

The implementation of structural damping in commercially available finite element (FE) software is usually provided by mass and stiffness proportional coefficients in what is known as Rayleigh damping.[44] Since the proportional damping is not suitable to model the orthotropic material damping in composites, the modal strain energy approach is used in the numerical damping analysis.[45] The loss factor η may be calculated by

$$\eta = \frac{1}{2\pi}\frac{\Delta U}{U} \tag{7}$$

where ΔU represents the dissipated energy during a single oscillation, while U is the maximum strain energy stored within that cycle.[22] The strain energy approach may manually be integrated into a commercially available FE-code in order to analyse the modal damping of a multi-layer composite structures. The dissipated energy and the strain energy may be computed separately for the m-th FE in the k-th UD-layer used in the numerical model (see equation (10)). However, the contribution of these energies is direction dependent due to the orthotropic nature of composite material. Therefore, the direction dependency needs to be taken into account by considering the tensor components in all directions ($i, j = 1, 2, 3$)[23,34] by

$$U_{ij}^{[m]} = \frac{1}{2}\sigma_{ij}^{[m]}\epsilon_{ij}^{[m]}V^{[m]} \tag{8}$$

where $\sigma_{ij}^{[m]}$, $\epsilon_{ij}^{[m]}$ and $V^{[m]}$ are the direction dependent stress and strain components within the volume of the m-th element. The equivalent dissipated energy for the m-th FE may then be obtained by

$$\Delta U_{ij}^{[m]} = \eta_{ij} U_{ij}^{[m]} \tag{9}$$

where η_{ij} are the experimentally obtained fibre direction dependent material damping properties, required as input parameters. The modal loss factor of the structure for the n-th mode may then be calculated by

$$\eta_n = \frac{\sum_{m=1}^{N_e}\sum_{k=1}^{N}\sum_{i=1}^{3}\sum_{j=1}^{3}\left(\Delta U_{ij}^{[m](k)}\right)_n}{\sum_{m=1}^{N_e}\sum_{k=1}^{N}\sum_{i=1}^{3}\sum_{j=1}^{3}\left(U_{ij}^{[m](k)}\right)_n} \tag{10}$$

where N_e and N represent the total number of FEs and the number of layers, respectively. The numerical damping analysis based on a representative UD-layer was carried out using the commercial FEM software ABAQUS. The relevant material properties assuming a plane stress state are E_1, E_2, G_{12} and ν_{12}, as shown in equation (2) and later in Table 3. The development of an integrated PYTHON code enables the calculation and plotting of the modal damping η_n at the end of any finite element analysis (FEA) in order to provide a continuous simulation within ABAQUS, thereby avoiding additional post-processing steps.

The aim of the numerical simulation is to model and verify the experimental VBT investigation, in order to predict the first natural frequency f_1 and the related modal damping η of a vibrating cantilever composite beam made of GF-EP-0 with the symmetric and balanced stacking sequence $[+\varphi, -\varphi]_s$, composed of representative UD-layers. The sample dimensions are listed in Table 1 and the static material properties of the representative UD-layer are shown in Table 3. The density of GF-EP and GF-VE has been calculated with $\rho = 1.79\,\mathrm{g/cm^3}$ and $\rho = 1.77\,\mathrm{g/cm^3}$, assuming a fibre-volume-ratio (FVR) $V_f = 0.5$. The modal loss factors η_{11}, η_{12} and η_{22} are used as input parameter in order to calculate the modal damping of the vibrating composite beam. Four different input parameter configurations are used to simulate the VBT analysis, based on varying stacking sequences and test methods: (1) unbalanced, DMTA; (2) balanced, DMTA; (2) unbalanced, VBT; (4) balanced, VBT (see section 'Effect of stacking sequence'). A mesh of fully integrated, 8-node C3D8I hexahedron elements was created to model the vibrating beam in ABAQUS. This element type provides internally added incompatible deformation modes and is therefore a cost effective way to model the bending behaviour of structures, even with only one element through the thickness.[46–48] The composite interface in Abaqus was used to assign the laminate stack and its orientation to the mesh. Selected degrees-of-freedom at the root-end section of the beam were constrained in order to realize the clamped boundary condition of the subsequent experiments.

Experimental investigation

This section provides a detailed description about the materials, methods and procedures used to analyse the fibre direction dependent damping of GFRP and AFRP at low temperatures and low frequencies. Furthermore, the quality and the uniformity of the different laminates were investigated by comparing FVR and images from the computerized axial tomography (CAT). The two common measurement methods for damping characterisation, DMTA and VBT, were used to evaluate the

Table 1. Overview of the different specimen configurations.

Method	Frequency	Fibre material	Stack	Sample size (L × W × T)
DMTA	0.5–2 Hz	GF	$[\varphi]_3$	60 mm × 10 mm × 1.5 mm ± 0.1 mm
		AF	$[\varphi]_5$	60 mm × 10 mm × 0.9 mm ± 0.1 mm
	20 Hz ± 1 Hz	GF	$[\pm\varphi]_s$	220 mm × 15 mm × 2 mm ± 0.1 mm
VBT			$[\varphi]_3$	220 mm × 15 mm × 1.5 mm ± 0.2 mm
(modulus from tensile test)		AF | GF | GF | GF | AF	$[\varphi]_5$	220 mm × 15 mm × 1.9 mm ± 0.1 mm
		GF | AF | GF | AF | GF		

VBT: vibrating beam test; DMTA: dynamic mechanical thermal analyser.

effect of different material and testing parameters on the loss factor η, e.g. matrix material, fibre material, temperature and frequency. The experimental set-ups as well as the testing procedures are described in this section. The data sets of all test results are published separately and freely available.[49]

Materials and sample preparation

Two widely used resin systems, a Bisphenol-Epoxy Vinyl Ester Resin DION IMPACT 9102-683 (VE) and an Epoxy Infusion System PRIME 20LV (EP) as well as their NC modified equivalents, have been used as matrix systems. The NC modification of these resin systems was successfully carried out and evaluated by material testing and microscopic examination in a previous work.[13] The NC Garamite 1958 was thereby dispersed into the neat VE and EP with different weight % (wt.%) using a high-speed homogeniser. An extensive morphology analysis of the nanocomposites using scanning electron microscopy (SEM), transmission electron microscopy (TEM), X-ray diffraction (XRD) and rheology analysis was conducted to evaluate the level of exfoliation. Furthermore, the static and dynamic mechanical properties of the neat VE and EP as well as their modified equivalents, treated with 2 wt.%, were compared. However, the same NC modified VE and EP with 2 wt.% was used right after the dispersion process to manufacture the composite plates for dynamic testing.[13] The specimens are therefore used to verify the transferability of the beneficial effect by NC from polymer level to composite level. A UD GF fabric with an area weight of 475 g/m^2 (incl. 35 g/m^2 of a chopped strand mat) and a UD AF fabric with 109 g/m^2 (incl. 20 g/m^2 AF-weft at $\varphi = 90°$) were used. UD VE- and EP-reinforced GF- and AF-plates, with and without 2 wt.% of NC modification, were manufactured by hand-layup, followed by vacuum bagging, cured at room temperature (RT) and post-cured at 40°C for at least 24 h and then 10 h at 70°C.

As already mentioned in the Introduction section, bend-twist coupling effects are assumed to affect the damping properties of composite laminates.[32] In order to quantify the damping contribution related to these coupling effects of the symmetric, unbalanced GFRP specimens, additional bidirectional, symmetric and balanced GFRP plates were manufactured. Different specimens with regard to testing method, material, dimensions and stack were cut using waterjet for five different fibre orientations, as shown in Table 1. The specimens analysed with VBT were also used for quasi-static tensile tests.

Quality assurance

The fibre volume ratio is a common parameter to verify a homogeneous fibre and matrix material distribution within a composite structure.[50] Three samples per plate in the size of around 80 mm × 20 mm were taken from different locations and burned at 620°C for 4 h according to the standard.[51] The relative weight of the fibre ψ was calculated by

$$\psi = \frac{m_f}{m_{tot}} \tag{11}$$

with m_{tot} and m_f representing the total weight of the specimen (before burning) and the weight of the fibre (after burning). The fibre volume ratio V_f was determined by

$$V_f = \frac{1}{1 + \frac{1-\psi}{\psi}\frac{\rho_f}{\rho_m}} \tag{12}$$

where ρ_m and ρ_f are the densities of the matrix and fibre.[52] The determination of the FVR by combustion is only suited for GF composite, as AF will partly burn and degrade.[53] Furthermore, the CAT device 'ZEISS XRadia 410 Versa' was used to generate cross-sectional images from representative GF and AF specimens, illustrating the sample quality and uniformity with respect to voids, resin rich areas and fibre undulations. The instrument was operated at 40 kV and 60 kV for AFRP and GFRP samples. Image acquisition was

performed using the large field of view objective and 1601 projections with 4 s and 5 s exposure time for AFRP and GFRP samples. Image reconstruction was performed using the inbuilt acquisition and reconstruction software package provided by ZEISS, while for visualization the software 'Avizo9.4.0' from FEI was used.

Static mechanical testing

The static material characterisation was carried out on a servo-hydraulic MTS 312.21 test machine with a 100 kN actuator and a 5 kN load cell. The unbalanced and balanced tensile test specimens were quasi-statically tested at a strain rate of 0.5 mm/ min, which is well below the dynamic test conditions. Hydraulic grips were used to clamp the composite samples, whereof the lower one had a rotational degree of freedom. The calculation of the tensile moduli $E'_{\varphi j exp}$ and the Poisson ratio ν_{12} is based on the ASTM standard D3039.[54] Two specimens were tested per material configuration and fibre orientation. Each specimen was released before repeating the measurement three times resulting in six measurements in total for each configuration.

Dynamic mechanical thermal analysis

The DMTA is a widely used method to analyse the damping behaviour of fibre reinforced composites.[55] The loss factor η was measured in different fibre orientations $\varphi = 0°$, $30°$, $45°$, $60°$ and $90°$. The fibre direction dependent damping properties of a representative UD layer η_{11}, η_{22} and η_{12} were then calculated based on equations (5) and (6). A three-point bending fixture with a span of 50 mm and spherical bearings, allowing rotations around the lengthwise axis of the specimens, were used to minimize clamping effects and in order to fulfil the 'free-flexure' condition required by the Adam-Bacon approach.[33] As polymer materials exhibit a pronounced strain-rate dependency on the mechanical properties, a preliminary strain-rate analysis was carried out in order to determine a vibration amplitude related to the linear region of the amplitude-force-diagram, suitable for all material configurations, environmental test conditions and fibre directions.[56] The results of the strain-rate analysis are demonstrated in Figure 2 for a GF-EP-0 specimen with a $\pm 30°$ configuration at $-20°$C and $+20°$C, and a constant test frequency of 1 Hz.

Due to the linear strain-rate behaviour, a global amplitude of 150 µm was chosen for all DMTA tests. The test conditions were chosen so that they resemble those in a galloping-prone environment with frequencies between 0.5 Hz and 2.0 Hz and temperatures between $-20°$C and $0°$C.[5,6] Additional damping measurements were carried out with the vibrating beam test (VBT) method at 20°C in order to verify the comparability of the two common damping measurement techniques.

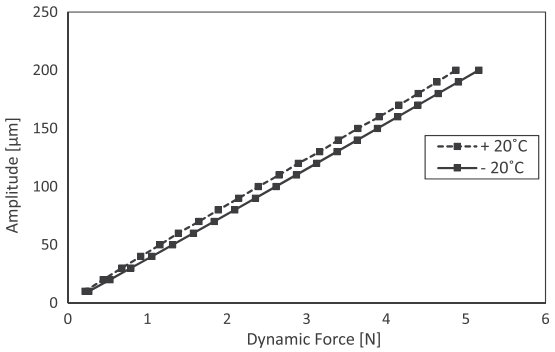

Figure 2. Strain-rate analysis of a GF-EP-0 specimen $[+30°, -30°]_s$ at $-20°$C and $+20°$C and 1 Hz.

Vibrating beam testing

The VBT method is commonly used to analyse the damping properties of under-damped systems such as composite beams by analysing the free vibration decay of an oscillating structure at its first natural frequency f_1.[57–59] Different excitation techniques with various suitability for the damping evaluation have previously been used, such as the excitation by shaker,[60] by impact hammer[17] or by initial displacement.[61–63] The activation of mainly the first mode may be well achieved by an initial displacement, as the focus is on the damping characteristics at the lowest natural frequency. A free-flexural configuration of the test is required to analyse the damping based on the Adam-Bacon approach.[33] The specifications of the test samples are listed in Table 1. The cantilever specimens were horizontally fixed between two clamping plates, screwed together with a tightening torque of 15 Nm. An initial tip displacement was set and released for all specimen configurations and fibre directions. By adjusting the free length of each specimen, all VBT were carried out at a constant vibration frequency f_1 around 20 Hz $\pm$ 1 Hz. The dynamic response of the beam was measured contact-free at a distance of 5 mm from the beam tip by a laser displacement sensor optoNCDT 1402 from Micro-Epsilon at a sampling frequency of 2000 Hz, connected to the analog input module NI 9215 from National Instruments. The dynamic response of the vibrating beam is represented by a declining sine curve, on which an exponential decay curve may be fitted as an envelope. It is assumed that mainly the first mode dominates the behaviour and that any influence from other modes may be neglected. The resulting envelope $g(t)$ for the first mode may therefore be described as

$$g(t) = X_0 e^{-\zeta\omega_1 t} \tag{13}$$

with ω_1, ζ and X_0 being the natural frequency, the damping ratio and the initial displacement, respectively.[64] The loss factor is calculated based on equation (4). Two specimens were tested per material configuration. Each specimen was released before repeating the measurement three times (six measurements in total per material configuration and fibre direction).

Results and discussion

The results of the static mechanical analysis are presented, followed by the results of the experimental damping analysis of relevant composite materials for the use in high-voltage power pylons. The comparability of these results is ensured by verifying the uniformity of the investigated samples with a consistent FVR and representative CAT-scans. The fibre direction dependent damping properties are evaluated with regard to various test and design parameters such as different matrix materials, fibre materials, supplemental NC modification, temperature and frequency variation, as well as different test methodologies and stacking sequences. Finally, the results of the numerical damping analysis of hybrid laminates are compared to equivalent experimental results.

Quality assurance

The uniformity and internal structure of representative specimens were evaluated based on the FVR and X-ray tomograms. The FVR was analysed for all GF samples, whereas only representative GF-EP, GF-VE and AF-EP specimens were CAT-scanned. The results of the relative fibre weight ψ and the FVR V_f are presented in Table 2. The slightly higher relative fibre weight of GF-VE compared to GF-EP may be explained by a lower resin density of VE than EP. The increase of ψ with the application of NC is due to the non-combustible nature of the NC.

Table 2. Results of the relative fibre weights ψ and the FVRs V_f of all GF samples determined by combustion.

Material	GF-0-EP	GF-2-EP	GF-0-VE	GF-2-VE
ZRel. fibre weight ψ (%)	Z67.6 ± 0.8	Z69.0 ± 0.4	Z68.8 ± 0.2	Z70.0 ± 0.7
FVR V_f (%)	47.5 ± 0.9	49.1 ± 0.5	47.6 ± 0.3	49.0 ± 0.9

FVR: fibre-volume-ratio.

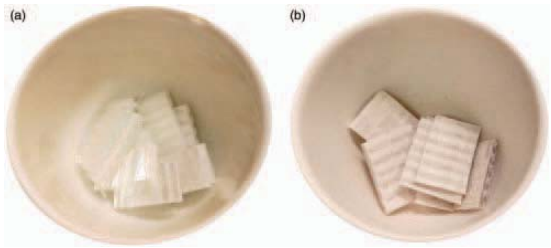

Figure 3. Raw GF without (a) and with (b) a previous NC modification of the resin before combustion.

A visual difference of GF samples with and without NC is also observed with respect to color and cohesion of the remaining fibre bundles (Figure 3). However, the difference in the FVRs and the related standard deviations with regard to the two groups (with NC and without NC) demonstrates a uniform matrix-fibre distribution of the GF sample plates. A comparability of the static and dynamic mechanical properties, determined by DMA and VBT (see section 'Experimental damping investigation'), is thereby ensured.

A quality assurance with regard to voids and undulations was carried out using CAT-scans. X-ray tomograms of AF-EP (A), GF-VE (B) and GF-EP (C) samples were qualitatively analysed. Three representative images are presented in Figure 4, referring to the coordinate system defined in Figure 1.

The poor contrast of the X-ray tomogram A, representing the cross section of AF-EP, is due to similar densities of AF ($\rho = 1.42\,\mathrm{g/cm^3}$) and EP ($\rho = 1.08\,\mathrm{g/cm^3}$). A better contrast is obtained for GF-VE (tomogram B) and GF-EP (tomogram C) due to the density of GF with $\rho = 2.5\,\mathrm{g/cm^3}$. No fibre undulations are observed in tomogram C. Instead, voids with dimensions up to 0.5 mm are identified within all three specimens. Its location between the fibre bundles is due to the use of fibres with a relatively low fineness of 2400 tex. Finer fibre bundles (lower tex) may lead to smaller gaps, resulting in smaller voids.

Furthermore, the manufacturing method (see section 'Materials and sample preparation') is prone to a high void content, due to the manual application of resin. As the same manufacturing method was used for all investigated test sample plates, a similar void characteristics and distribution is assumed for all DMA and VBT specimens. Therefore, the potential effect of the voids on the damping behaviour is assumed to be equal for all investigated specimens.

Static mechanical testing

Quasi-static tensile tests were used to determine the fibre direction dependent tensile moduli $E'_{\varphi i\,exp}$ for all material configurations, with and without the NC modification. The results are presented in Figures 5 and 6 for the GF- and AF-specimens, respectively.

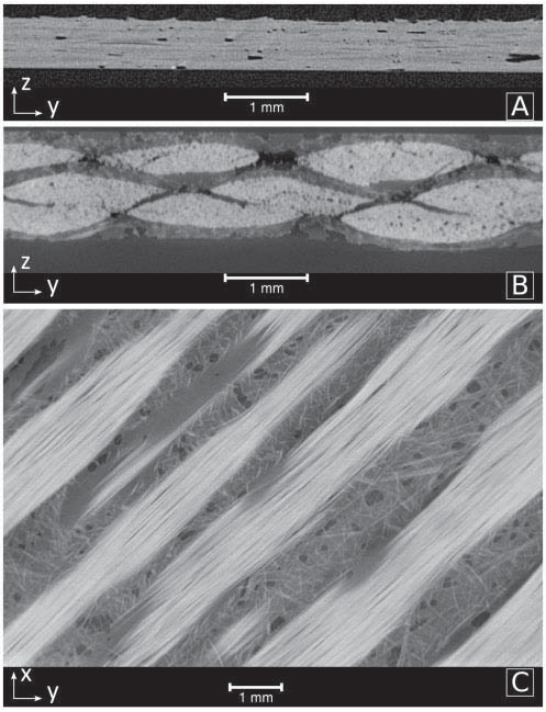

Figure 4. X-ray tomograms of AF-EP (A), GF-VE (B) and GF-EP (C).

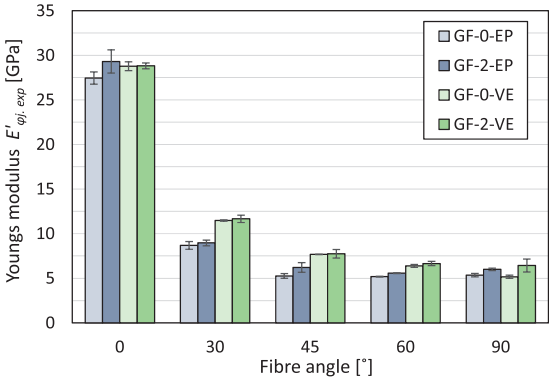

Figure 5. Fibre direction dependent Young's modulus $E'_{\varphi j\,exp}$ for GF-EP and GF-VE (unmodified and modified with 2 wt.% NC).

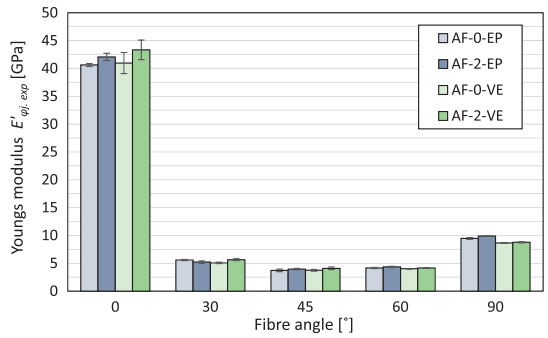

Figure 6. Fibre direction dependent Young's modulus $E'_{\varphi i\,exp}$ for AF-EP and AF-VE (unmodified and modified with 2 wt.% NC).

For both materials and fibre directions, the NC modification has a slight increasing effect on the Young's modulus $E'_{\varphi j\,exp}$, which is consistent with the literature.[13] Independent of the NC content, the matrix material VE shows generally higher stiffness for all GF specimens compared to EP. This effect is not observed for the AF specimens and may be explained by a different sizing-matrix-compatibility of AF to VE and EP.[65]

The stiffness maximum is at $\varphi = 0^\circ$ along the fibre direction for GF and AF specimens. The small amount of weft thread in the AF fabric leads to a stiffness increase for $\varphi = 90^\circ$. The major drop in stiffness between $\varphi = 0^\circ$ and 30° for all AF specimens, independent of the matrix, may be explained by the anisotropic material behaviour of AF.[66,67] A slight fibre misalignment will cause a significant stiffness drop, which explains the larger standard deviation for $\varphi = 0^\circ$. A smoother stiffness drop for the same angle range is observed for GF specimens in Figure 5. Furthermore, no reinforcing effect for $\varphi = 90^\circ$ is observed for GF samples, as pure UD fabrics with chopped strand mats were used (see section 'Materials and sample preparation').

The standard deviation of the fibre direction dependent tensile moduli was considered in the calculation of the material properties in its principle directions by equations (2) and (3). The variation is plotted in a polar diagram (see Figure 7). The resulting material properties for a representative UD-layer E_1, E_2 and G_{12}, obtained from the optimization by equation (3), are shown in Table 3 for all GF-composite configurations. The variation represents the standard deviation of the fibre direction dependent tensile moduli.

However, the fibre direction dependent tensile moduli of unbalanced laminates only represent the apparent stiffness, due to the constrained shear-tension-coupling caused by the hydraulic grips of the test machine.

Experimental damping investigation

The effect of the matrix material, the fibre material, the NC modification as well as the temperature and frequency on the fibre direction damping properties were analysed in galloping-like environmental conditions by DMTA measurements. Although no standard deviation is available for the DMTA measurements, because the analysis only contains a single specimen per material configuration and fibre direction, several DMTA-internal measurements of the loss factor with necessarily consistent results were made before generating an average damping value.

The effect of a balanced and unbalanced stacking sequence on the direction dependent damping properties are analysed by VBT and DMTA at room temperature.

The amplitude-time signal of the VBT measurement is assumed to be related to the first activated bending mode only and the damping ratio may therefore be estimated well by the exponential fit of equation (13) to the envelope of the free decay curve. The good agreement is shown in Figure 8 for GF-EP with 2 wt.% NC and a fibre angle of $\varphi = 60°$.

Effect of matrix material. The damping properties of composite materials are highly dependent on the fibre direction. The loss factor η of a representative UD layer in transverse direction ($\varphi = 90°$) is generally higher compared to its longitudinal direction ($\varphi = 0°$), represented by

$$\eta_{90} = \left(\frac{E''}{E'}\right)_{90} > \left(\frac{E''}{E'}\right)_{0} \tag{14}$$

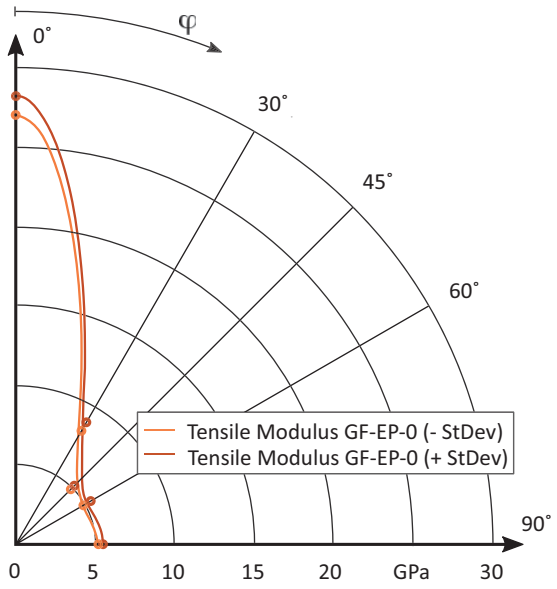

Figure 7. Variation of the fibre direction dependent off-axis tensile moduli of GF-EP-0 (input values for the optimization in equation (3)) with respect to its standard deviation.

This is due to the matrix dominated properties in transverse direction and the much higher damping of the viscoelastic polymer compared to the fibre. Although the loss modulus in longitudinal direction E''_0 may be larger than E''_{90} in transverse direction, the high storage modulus E'_0 in longitudinal direction, dominated by the fibre, leads to a lower loss factor η_0 compared to η_{90} (see equation (14)).[68] Thus, any change or modification with respect to the matrix material composition will mainly affect the off-axis damping properties. According to the DMTA results of GF-VE and GF-EP (measured at 0°C and 1 Hz) presented in Figure 9, the matrix material VE shows significantly higher damping properties of about 20% to 40% for all off-axis fibre directions compared to EP.

Moreover, the loss factor η in fibre direction remains relatively unchanged for EP and VE, as the behaviour is governed by the GF. Furthermore, the off-axis damping properties of GF-VE and GF-EP represent the damping properties of neat EP with $\eta_{EP} = 0.012$ and VE with $\eta_{VE} = 0.017$ at 0°C. These observations are consistent with a previous study.[13] The peak damping is obtained for both materials at an off-axis fibre direction at $\varphi \approx 30°$, since the contribution of damping due to bend-twist-coupling reaches its maximum at fibre angles $\varphi \approx 30°$.[32] As mentioned in section 'Damping approximation', the approach by Adams-Bacon, predicting η_{11}, η_{22} and η_{12}, is only valid for

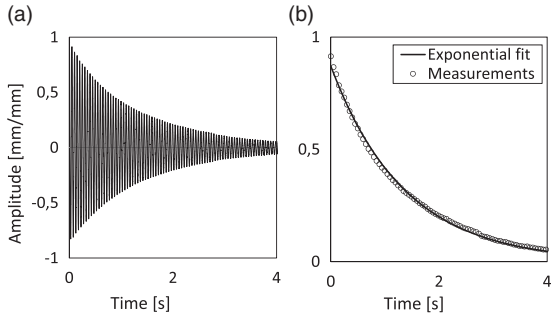

Figure 8. Free vibration of a GF-2-EP-60 specimen (Glass fibre | Epoxy resin | 2 wt.% NC |$\varphi = 60°$). (a) Normalized free decay of a vibrating specimen. (b) Measured data vs. exponential fit.

Table 3. Material properties of a representative UD layer assuming a plane stress state.

Material	wt.% NC	E'_1 (GPa)	E'_2 (GPa)	G'_{12} (GPa)	ν_{12}
GF-EP	0	27.6 ± 0.6	5.3 ± 0.2	2.0 ± 0.1	0.345 ± 0.06
	2	29.9 ± 1.6	5.8 ± 0.2	2.2 ± 0.1	0.324 ± 0.01
GF-VE	0	28.8 ± 0.5	5.3 ± 0.8	2.6 ± 0.1	0.374 ± 0.06
	2	28.8 ± 0.3	6.9 ± 0.5	2.6 ± 0.1	0.330 ± 0.08

UD: unidirectional.

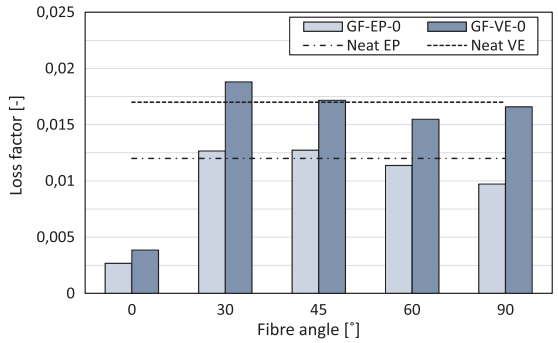

Figure 9. Effect of the matrix material VE and EP on the fibre direction dependent damping behaviour of GF-EP and GF-VE (DMTA, 0°C at 1 Hz).

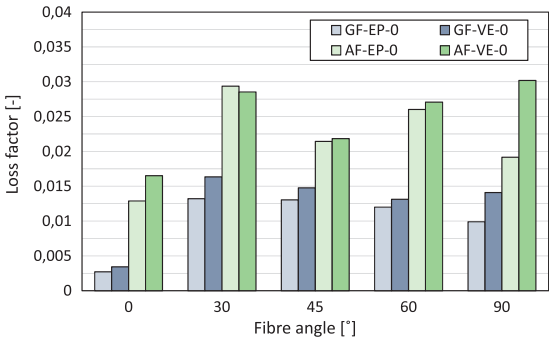

Figure 10. Effect of the fibre material GF and AF on the fibre direction dependent damping behaviour of fibre reinforced EP and VE (DMTA, −20°C at 1 Hz).

the 'free flexure' condition, allowing the beam to twist during bending. This condition is full filled for both the DMTA and VBT. The approach is therefore assumed to successfully predict the additional damping due to the bend-twist-coupling based on several individual measurements of the off-axis damping for various fibre directions φ. However, available data of the predicted fibre direction damping of off-axis laminates under 'free flexure' conditions[33] coincide with the observed trend represented in Figure 9. When applying the modal strain energy approach based on the damping properties of the (unbalanced and symmetric) representative UD layer to a symmetric and balanced multi-layer structure, a systematic error is taken into account due to absence of the structural bend-twisting coupling effects. Therefore, a damping analysis of a symmetric and balanced representative UD layer was carried out in order to quantify the damping caused by bend-twisting effects (see section 'Effect of stacking sequence'). Based on the results shown in Figure 9, VE as matrix material is recommended with regard to damping enhancement.

Effect of fibre material. Investigations of AF composites showed approximately two to four times higher damping properties compared to GF composites at room temperature.[17,31] A similar damping behaviour has been observed for temperatures and frequencies at −20°C and 1 Hz (see Figure 10).

The fibre dominated loss factor for AF composites at $\varphi = 0°$ is with $\eta_{AF_0} \approx 0.015$ up to 5 times larger than the equivalent GF composites with $\eta_{GF_0} \approx 0.003$. In contrast to GF-EP and GF-VE composite specimens, the matrix material VE beneficially contributes to the damping properties in the fibre direction of AF laminates. This behaviour is also observed in Figure 11: A matrix modification of VE by 2 wt.% NC also increases the fibre dominated damping properties at $\varphi = 0°$, whereas the damping properties remain almost unchanged by a NC modification of EP. This might be

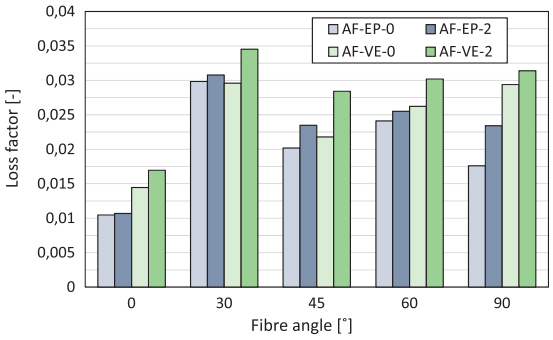

Figure 11. Effect of NC modification on the fibre direction dependent damping behaviour of AF-EP and AF-VE (DMTA, 0°C at 1 Hz).

explained by generally larger damping properties of VE compared to EP and differences in the matrix-fibre interface. In the off-axis fibre directions, the contribution of the AF to the damping behaviour is generally higher compared to GF. The contribution is the lowest at a fibre angle $\varphi = 45°$ due to the fibre reinforcement at $\varphi = 0°$ and $\varphi = 90°$. AF seems to be very well suited for the use in high-voltage power pylons due to its good static and dynamic mechanical properties as well as its non-conductive nature. However, other relevant parameters such as cost, increased moisture absorption and low UV resistance may hinder large scale development.

Effect of NC content. A matrix modification by 2 wt.% NC was observed to be less effective for neat EP than for neat VE.[13] This trend is consistent with the results presented in Figure 11.

The small positive effect of the matrix modification on the damping is mainly observed for the off-axis directions and ranges from + 7% to + 25%, depending on the matrix material and fibre direction. However, the measured damping values in the off-axis directions of

AF composites are with $\eta > 0.02$ significantly larger than the observed damping properties of the individual material components at temperatures at 0°C: neat matrix material (EP-0 ($\eta = 0.012$) | EP-2 ($\eta = 0.013$) | VE-0 ($\eta = 0.017$) | VE-2 ($\eta = 0.02$)) and AF in fibre direction ($\eta < 0.017$ in the fibre direction). The results are consistent with the literature[17,31] and may be explained by the anisotropic material behaviour of AF and its related enhanced damping properties in off-axis directions (see section 'Static analysis').[66,67] That effect is not observed for GF specimens, where the fibres are of isotropic nature. A matrix modification with NC is indeed a viable possibility for increasing the matrix dominated damping properties primarily in the off-axis directions by up to 10% to 20% for AF composites. However, the related restrictions with respect to manufacturability of large composite structures as well as the complex manufacturing process of NC modified resin need to be considered for a realistic cost-to-benefit ratio.

Effect of fibre hybridization. AF and GF may together be used in hybrid-composites in order to combine their properties with respect to static and dynamic mechanical properties.[17,69] Two different AF-GF-EP hybrid stacking sequences, [AF | GF | GF | GF | AF] and [GF | AF | GF | AF | GF], were investigated and compared with its non-hybrid GF-EP and AF-EP counterparts (see Figure 12).

Based on the results already discussed in section 'Effect of fibre material', GF-EP shows in general much lower damping properties compared to AF-EP. The higher the percentage of AF within the laminate, the higher the damping properties in all fibre directions. In case of an equal amount of AF layers within hybrid composites, its location affects the laminate damping behaviour. Laminates with AF layers located furthermost from the neutral axis will exhibit increased damping properties, as these layers will experience larger strains, leading to a proportionally higher damping contribution. The effect is independent of fibre orientation. The hybridization of AF and GF is an effective way to increase the damping properties of composite materials by about 20–30% for off-axis directions and up to 3 times for the fibre direction compared to pure GF composites. However, as discussed in section 'Effect of fibre material', further investigations related to costs and effect on different environmental conditions need to be made.

Effect of temperature. The measured temperature-damping dependency of GF-EP and AF-EP in the range between −20°C and 0°C is shown in Figure 13.

The temperature dependent damping results are consistent with the literature and a previous study on pure EP.[13,21,22,70,71] An increase in temperature from

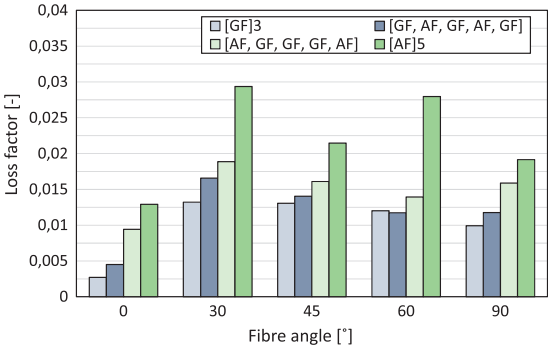

Figure 12. Effect of fibre-hybridization on the fibre direction dependent damping behaviour of GF-EP, AF-EP and AF-GF-EP (DMTA, −20° C at 1 Hz).

−20°C to 0°C leads to a decrease in damping for almost all AF-EP and GF-EP specimens and fibre directions. For AF-laminates, the loss factor is reduced by approximately 8% for $\varphi = 45°$ and 90° as well as 20% for $\varphi = 0°$ and 60°, except for $\varphi = 30°$, which is a potential outlier. The decrease in damping of AF specimens in the fibre direction is in agreement with the observations made in Figures 10 and 11 regarding the influence of matrix dominated properties in the fibre direction (see section 'Effect of fibre material'). This effect may be explained by differences in the matrix-fibre interface compared to GF. The decrease of the damping properties of GF-EP specimens with increasing temperature is with maximum 5% negligible. However, the fibre direction dependent damping characteristics of GF-EP and AF-EP are considered constant within the temperature range relevant for galloping conductor lines.

The fibre direction damping properties η_{11}, η_{22} and η_{12} for a representative UD-layer based on the DMTA measurements and the Adams-Bacon-Approach (see section 'Approximate damping approach') are shown in Table 4 for all GF-composite configurations at different temperatures and NC contents.

Effect of frequency. The effect of frequency on the fibre direction dependent damping is evaluated within the frequency range from 0.5 Hz to 2 Hz, representative for galloping of overhead transmission lines. An increase in frequency from 0.5 Hz to 2 Hz at −20°C leads to slightly increased damping properties in fibre direction for GF-EP and AF-EP, but a decreasing loss factor in the off-axis directions with $\varphi > 0°$ (see Figure 14).

These results are in line with the literature for this particular frequency range and represent the damping behaviour dominated by fibre and matrix, respectively.[21,72] Due to the negligible effect of a frequency change from 0.5 Hz to 2 Hz on the fibre direction damping, the material characterisation with regard to damping is though optimal at a representative

frequency of 1 Hz for the design process of galloping affected composite structures.

Effect of test method. The fibre direction dependent damping properties based on the two different damping measurement methods, DMTA and VBT, are analysed in this section for GF-EP and GF-VE in order to verify the comparability of the two techniques. The test parameters temperature and frequency are therefore kept equal for both tests due to the frequency and temperature dependent damping behaviour of composite materials.[35,62,73] All resonant VBT measurements were carried out at 20°C and 20 Hz with an initial amplitude of 5 mm and 10 mm, the non-resonant DMTA was performed at 20°C with frequencies of up to 10 Hz. The fibre direction dependent damping properties for 20 Hz were obtained by extrapolating the data with a logarithmic approximation function. The results are presented for GF-EP specimens in Figure 15.

The increase of the fibre dominated damping properties ($\varphi = 0°$) and the decrease of the matrix dominated damping properties ($\varphi > 0°$) with higher frequency are in line with existing DMTA results for glass and carbon fibre reinforced plastics.[21,35] In contrast, damping measurements by VBT result in increasing damping with frequency for all fibre directions.[31] These structural damping properties include material damping, friction damping in the clamping area and air damping, which is proportional to frequency and amplitude.[62,74–76] The presence of clamping effects, influencing the overall damping behaviour, is assumed to be higher for cantilever beam configurations (VBT) with a considerably high vibration amplitude compared to simple supported beams in a three-point-bending fixture (DMTA) with vibration amplitudes of 150 µm.

The fibre direction dependent damping properties of GF-EP are shown in Figure 16 for 20 Hz with respect to the two test methods and boundary conditions.

The DMTA results show the characteristic behaviour with its maximum at $\varphi = 30°$, although the decrease in damping at $\varphi = 60°$ and 90° is unusually high (compare to Figure 14). This behaviour may be explained by inaccurately extrapolated data. In contrast, the damping results obtained by VBT measurements increase towards $\varphi = 45°$, followed by constant damping properties for the remaining fibre angles $\varphi \geq 45°$. This behaviour is identical to existing VBT results.[31] However, it is unexpected that the damping properties,

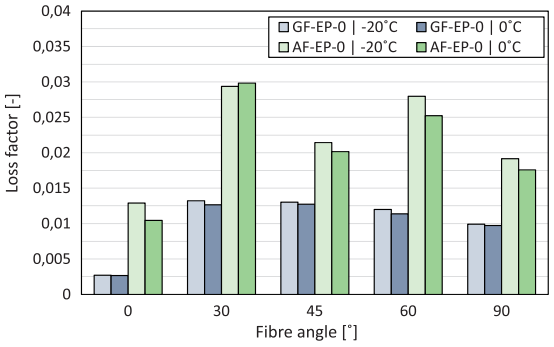

Figure 13. Effect of the testing temperature on the fibre direction dependent damping behaviour of GF-EP and AF-EP (DMTA, −20°C and 0°C at 1 Hz).

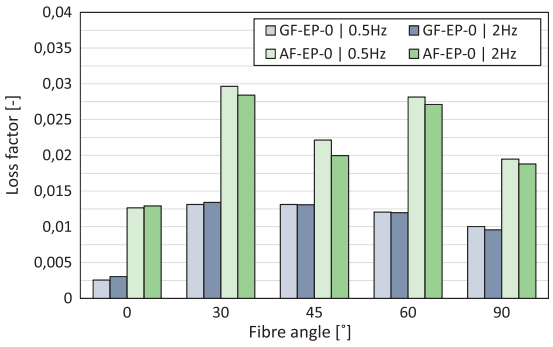

Figure 14. Effect of the testing frequency on the fibre direction dependent damping behaviour of GF-EP and AF-EP (DMTA, −20°C at 0.5 Hz and 2 Hz).

Table 4. Calculated fibre direction dependent damping properties η_{11}, η_{22} and η_{12} based on the Adams-Bacon approach and DMTA measurements at −20°C, 0°C and 20°C at 1 Hz.

Material	wt.% NC	−20°C | 1 Hz			0°C | 1 Hz			20°C | 1 Hz		
		η_{11} (–)	η_{22} (–)	η_{12} (–)	η_{11} (–)	η_{22} (–)	η_{12} (–)	η_{11} (–)	η_{22} (–)	η_{12} (–)
GF-EP	0	0.0028	0.0097	0.0150	0.0027	0.0095	0.0145	0.0033	0.0120	0.0186
	2	0.0039	0.0086	0.0159	0.0036	0.0079	0.0157	0.0038	0.0112	0.0202
GF-VE	0	0.0037	0.0130	0.0174	0.0042	0.0154	0.0200	0.0048	0.0174	0.0219
	2	0.0039	0.0130	0.0167	0.0044	0.0161	0.0201	0.0050	0.0193	0.0230

DMTA: dynamic mechanical thermal analyser;

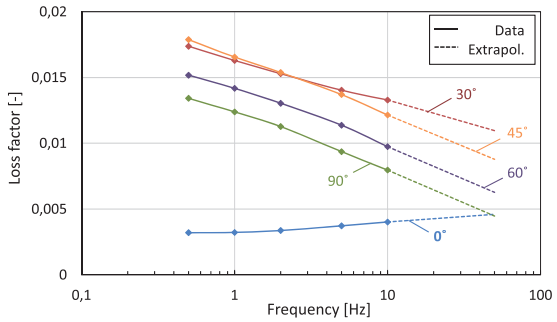

Figure 15. Frequency dependent damping properties of unbalanced GF-EP-0 (DMTA, 20°C).

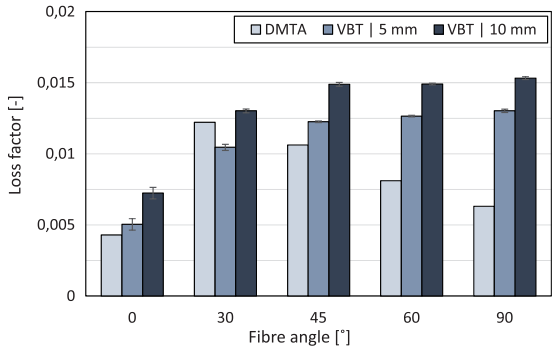

Figure 16. Effect of the test method (DMTA vs. VBT) on the fibre direction dependent damping behaviour of GF-EP at 20°C at 20 Hz.

obtained by VBT and DMTA, do not show similar effects or tendencies, as free-flexure conditions with an unrestricted twist are present in both test methods. Although twist-coupling effects are linked to off-axis laminates, they may contribute differently to the overall damping, depending on varying loading conditions, sample geometries and boundary condition of different test methods. The same tendency of fibre direction dependent damping for GF-EP laminates is observed for GF-VE specimens, tested by VBT and DMTA, using extrapolated data (Figure 17).

The differences in damping due to the different matrix materials VE and EP (compare Figures 16 and 17) vary up to 30% in $\varphi = 30°$ and up to 50% in $\varphi = 90°$ for DMTA measurements, but remain almost constant in the VBT analysis. Thus, the DMTA damping measurements seem to be much more sensitive and may be better suited for analysing different material compositions, temperature and frequency dependencies as well as bend-twist-coupling effects with respect to the damping properties, compared to the resonant VBT method with its larger sample dimensions and vibration amplitudes as well as clamping influence (see Table 1). Furthermore, the increase of initial tip displacement from 5 mm to 10 mm leads to a constant increase of

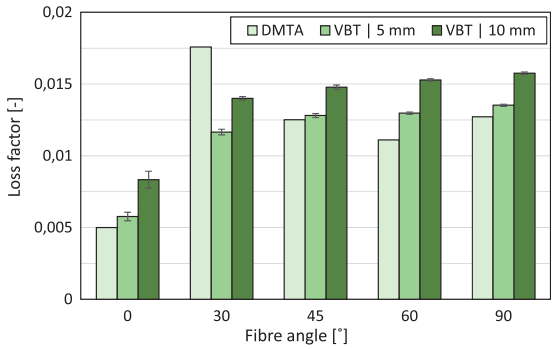

Figure 17. Effect of the test method (DMTA vs. VBT) on the fibre direction dependent damping behaviour of GF-VE at 20°C at 20 Hz.

the damping properties of approximately 20% for both materials due to additional clamping effects and air damping (see Figure 16). In order to reduce these effects, an initial tip displacement of 2.5 mm was investigated. Although the initial displacement may have slightly reduced the influence of air damping even further, the increasing noise in the time-displacement signal from the laser sensor resulted in deviations related to the curve fitting process. The VBT reference damping properties were therefore chosen based on the initial displacement of 5 mm. The generally lower damping properties obtained by DMTA measurements (except for $\varphi = 30°$ due to the bend-twist-coupling effects) can mainly be related to material damping, whereas the damping measurements by VBT consist of material damping, air damping and friction damping and are therefore considered as structural damping. These significant differences between DMTA and VBT with respect to the resulting damping properties should be taken into account when using the data for the dynamic design of composite structures.[62]

Effect of stacking sequence. All samples used for the damping characterisation by DMTA and VBT had a symmetric and unbalanced laminate architecture in order to fulfil the Adams-Bacon-Approach (see Figure 1).[33] Therefore, the damping results obtained by DMTA measurements showed distinct peaks at a fibre angle of $\varphi \approx 30°$ due to bend-twist coupling effects, linked to off-axis laminates (see Figures 11 and 13).[32] This additional damping will artificially overestimate the shear damping property η_{12} of a representative UD layer, from which symmetric, balanced and bend-twist-coupling-free multilayer composite structures are modelled. In order to prevent this systematic error, the coupling related damping needs to be evaluated and quantified. Therefore, the contribution of the coupling effects on the direction dependent damping properties are investigated for GF-EP and GF-VE by

comparing the damping behaviour of unbalanced and balanced laminates, where the latter should be unaffected by bend-twisting effects. The damping results of GF-EP with balanced and unbalanced stacking sequences are shown in Figure 18 based on DMTA and VBT measurements at 20°C and 20 Hz.

No distinction between balanced and unbalanced stacking sequences is made in the fibre directions $\varphi = 0^\circ$ and $\varphi = 90^\circ$, as only balanced laminates will meet these conditions. According to Figure 18 and observations made in section 'Effect of test method', no peaks at a fibre angle of $\varphi \approx 30^\circ$ occur for VBT measurements from specimens with balanced and unbalanced stacking sequence. Instead, the damping increases constantly up to a fibre angle of $\varphi \approx 45^\circ$, followed by a slight increase up to a fibre angle of $\varphi = 90^\circ$. This trend indicates that existing bend-twist coupling effects are superimposed by air damping, friction damping in the clamping zone and other effects. Thus, an assessment of bend-twist coupling effects can not be made by VBT measurements. Furthermore, the specimens with a balanced layup show about 15% lower damping properties for $30^\circ < \varphi < 60^\circ$ compared to specimens with an unbalanced layup. This may also be explained by differences in the specimen thickness, resulting in a change in stiffness and air damping contribution. Specimens with an unbalanced stack were 25% thinner compared to specimens with a balanced stack (see Table 1 and Figure 1). On the other hand, the vibrating length, and therefore the area affected by air damping, were reduced for unbalanced laminates in order to keep the vibration frequency constant at $f_1 = 20$ Hz.

Damping results obtained by DMTA measurements of laminates with an unbalanced stack, exhibit a peak related to coupling effects at $\varphi \approx 30^\circ$. In accordance to the findings above, the highest damping for balanced GF-EP laminates is observed for $\varphi = \pm 45^\circ$. This damping characteristics without bend-twist coupling effects is expected, as shear stresses attain their maximum for this particular stacking sequence. The introduction of an equivalent shear damping $\eta_{12_{eq}}$ for the DMTA damping analysis of balanced laminates may therefore underestimate the damping behaviour of a representative UD-layer: BD laminates with balanced stacking sequences show higher tensile moduli for $\varphi = \pm 30^\circ$, $\pm 45^\circ$ and $\pm 60^\circ$ compared to unbalanced UD laminates, resulting in higher in-plane shear stiffness and thus a reduced equivalent shear damping $\eta_{12_{eq}}$ (see Figure 19).

The calculated shear damping η_{12} (for unbalanced laminate) and the equivalent shear damping $\eta_{12_{eq}}$ (for balanced laminate) based on equations (5) and (6) may result only in small variations: the damping in $\varphi = 30^\circ$ is approx. 20% higher for unbalanced laminates, whereas balanced laminates show approx. 20% higher damping in $\varphi = 60^\circ$ (see Figure 18). Furthermore, the damping properties in $\varphi = 45^\circ$ are in the same range. Thus, the apparent differences in damping for $\varphi = 30^\circ$ and $\varphi = 60^\circ$ may simply cancel out.

Finally, the differences in damping between balanced and unbalanced laminates are less than expected and may not significantly influence the shear damping properties of the investigated materials.

Comparison of numerical and experimental damping analysis

In order to verify the experimentally determined static and dynamic mechanical properties, the first natural frequency f_1 and the related modal damping η of a vibrating multilayer composite beam were predicted by an FEA. Four different input parameter sets with respect to the modal damping were used to simulate the VBT test procedure at room temperature for three GF-EP-0 specimens with $[+30,-30]_s$, $[+45,-45]_s$ and $[+60,-60]_s$, based on the variation of the test method

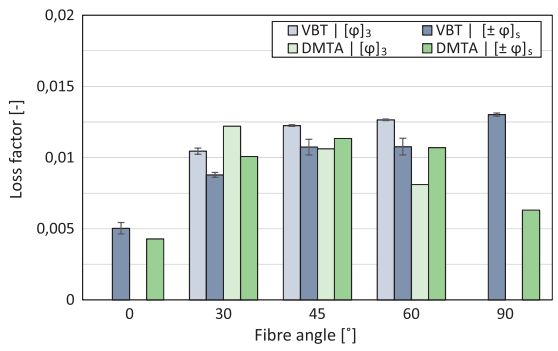

Figure 18. Effect of the stacking sequence (unbalanced $[\varphi]_3$ vs. balanced $[\pm \varphi]_s$) on the fibre direction dependent damping behaviour of GF-EP (DMTA, VBT (5 mm), 20° C at 20 Hz).

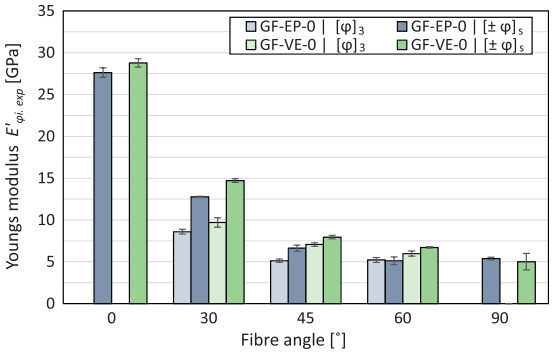

Figure 19. Effect of the stacking (unbalanced $[\varphi]_3$ vs. balanced $[\pm \varphi]_s$) on the fibre direction dependent Youngs modulus of GF-EP and GF-VE.

and a balanced or unbalanced stacking sequence: –(1) unbalanced, DMTA; –(2) balanced, DMTA; –(3) unbalanced, VBT; –(4) balanced, VBT. The results of the numerical analysis are listed in Table 5. Furthermore, a mesh convergence study based on the input parameter set '4. - balanced, VBT' is presented in Figure 20.

The number of elements used for the numerical simulation was set to $n_{el} = 680$. A sufficient mesh refinement was thereby verified. The prediction of the first natural frequency f_1 for GF-EP-0 specimens with a stack of $[+30,-30]_s$ is with a relative deviation of 7.8% slightly overestimated. As no manufacturing imperfections were considered in the simulation, a slight misalignment in the specimen's fibre orientation at $\varphi = 30^\circ$ may explain the reduced natural frequency measured by VBT. A clearly more accurate prediction for laminates with a stack of $[+45,-45]_s$ and $[+60,-60]_s$ was achieved with a relative deviation of maximal 2.9%, both slightly under-predicting f_1.

It is expected that numerical simulations based on VBT-related damping properties over-predict the modal loss factor, as several damping sources such as material damping, friction damping in the clamping area and air damping as an external damping source are included. In contrast, neither friction damping nor air damping are considered in the numerical model. In fact, this assumption has not been borne out by the simulations based on VBT-measurements of laminates with an unbalanced stack. The predicted modal damping is very close to the experimental values and an over-prediction is only observed for specimens with a $[+60,-60]_s$ stack. In contrast, the prediction of the modal damping based on VBT measurements of laminates with a balanced stack lead to high deviations and will therefore not be discussed any further.

Moreover, damping predictions based on DMTA-related damping properties were assumed to result in more precise results, as only material damping is considered in the numerical model. Indeed, a good damping prediction is observed for $[+30,-30]_s$ and $[+45,-45]_s$ with a relative deviation of max. 4.9%, but the calculated modal loss factor for $[+60,-60]_s$ is under-predicted by a maximum of 18.8%. This discrepancy for larger fibre angles ($\varphi \geq 60^\circ$) may be related to an added inaccuracy by the applied extrapolation. The drop in damping for $\varphi = 60^\circ$ and 90° is considered unusually high (see Figure 16), as mentioned in section 'Effect of test method'.

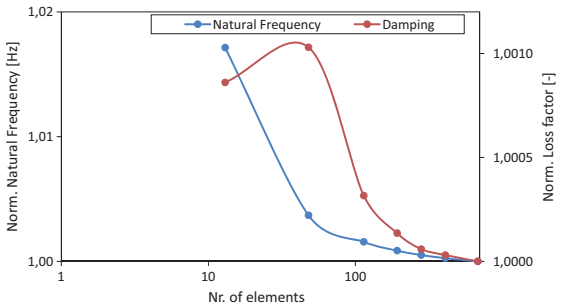

Figure 20. Mesh convergence study of the numerical model with regard to the normalized loss factor and normalized natural frequency.

Table 5. Experimental and FEA-results of a vibrating cantilever GF-composite sample with regard to different damping property input scenarios.

Material	Stack	Free length (mm)	Parameter	VBT	FEA (based on four different damping input parameter sets)			
				Experiment	u.bal–DMTA	bal–DMTA	u.bal–VBT	bal–VBT
GF-EP-0	$[+30,-30]_s$	195.9	f_1 (Hz)	19.90		21.45 ($\Delta f_1 = 7.8$)		
			η (–)	0.0089	0.009	0.0087	0.0087	0.0074
			$\Delta\eta$ (%)	(0.0002)	(0.9)	(2.2)	(2.8)	(16.4)
	$[+45,-45]_s$	179.1	f_1 (Hz)	20.07		19.59 ($\Delta f_1 = 2.4\%$)		
			η (–)	0.0112	0.0108	0.0107	0.0109	0.00918
			$\Delta\eta$ (%)	(0.0001)	(3.5)	(4.9)	(2.9)	(18.0)
	$[+60,-60]_s$	169.1	f_1 (Hz)	20.35		19.77 ($\Delta f_1 = 2.9\%$)		
			η (–)	0.0113	0.0092	0.0096	0.0123	0.0111
			$\Delta\eta$ (%)	(0.0001)	(18.8)	(15.1)	(9.2)	(1.7)
				Mean $\Delta\eta$ (%)	(7.7)	(7.4)	(5.0)	(12.1))

GF: glass fibre; FEA: finite element analysis; VBT: vibrating beam test; DMTA: dynamic mechanical thermal analyser.

In contrast, the VBT-related damping properties are constant for $\varphi \geq 45^\circ$ (see Figure 16), whereby they are slightly over-predicted by 9.2% for the $[+60,-60]_s$ specimens. It is assumed that the 'correct' damping for GF-EP-0 at $\varphi \geq 60^\circ$ is mean value of the VBT and DMTA results.

As expected, only small variations between DMTA-related damping properties with unbalanced and balanced stacking sequences are observed. The difference in loss factor at $\varphi = 30^\circ$ and $\varphi = 60^\circ$ are similar (see Figure 18) and will therefore cancel each other out, when calculating the shear damping η_{12} based on equations (5) and (6). The damping prediction for laminates with stacking sequences at large fibre angles $[+60,-60]_s$ is equally inaccurate for both DMTA-related damping input parameter sets. However, for both unbalanced and balanced stacking sequences, a good damping prediction is obtained for laminates with fibre angles $\varphi < 60^\circ$ based on DMTA measurements. The concerns with regard to bend-twist-coupling related deviations for the simulations are therefore seemingly unfounded. Other effects like friction damping due to clamping may have much higher impact on the modal loss factor.

In fact, the most accurate prediction with $\Delta\eta = 5.0\%$ for all stacking sequences $[+30,-30]_s$, $[+45,-45]_s$ and $[+60,-60]_s$ is based on the VBT-related damping properties with an unbalanced stack. This may be explained by the similarity of the experiment and the numerical model in terms of specimen geometry, boundary condition and the related stress distribution. Thus, VBT-related damping measurements of laminates with an unbalanced stack will further be used to predict the modal damping of more complex composite structures.

Conclusion

The characterisation and prediction of damping properties for non-conductive composite materials such as aramid and GF reinforced plastics have been presented. The direction dependent damping properties have been evaluated under environmental conditions prone for the galloping phenomena, considering different material modifications such as the addition of NC fillers, the variation of matrix materials and the hybridization of glass and AFs. Furthermore, the modal damping was successfully predicted for laminates with different stacking sequences based on damping properties obtained by VBT and DMTA measurements. The main conclusions are as follows:

- AF composites showed up to four times higher damping at -20°C compared to GF composites.
- At 0°C approximately 30% higher damping was obtained for the matrix material VE compared to EP.
- NC led to an increase in the off-axis damping for AF by 10 to 20% at 0°C.
- A fibre hybridization of GF and AF may enhance the damping in the fibre direction by 300% and in the off-axis direction by 20–30% at -20°C.
- The direction dependent damping of GF and AF composites are frequency and temperature dependent. However, at environmental conditions close to galloping, only small changes were observed.
- Damping measurements by DMTA seem to be more sensitive to changes in the stacking sequence.
- The predicted natural frequency and modal damping are in good accordance to the experimental results. The damping properties based on VBT measurements for unbalanced laminates showed the best match.

The latter point raises the question, which damping measurement method to chose for predicting the modal damping of a structure. This may depend primarily on the boundary conditions, due to their substantial influence on the damping. In case of a free-free-boundary condition, no clamping effects will occur and therefore damping values obtained by DMTA measurements may fit well. On the other hand, a free vibrating structure under a clamped-free condition will experience friction damping in the clamping zone. Therefore, damping properties obtained by VBT may better represent the damping behaviour. However, the quality of the clamping is a governing factor of the damping measurements, which must be taken into consideration in each individual case.

In future works, the obtained damping parameters will be applied to more complex composite structures in order to evaluate their modal damping. Therefore, the influence of the clamping effects on the overall damping has to be carefully evaluated. Furthermore, passive and non-conductive constrained layer damping treatments are very promising for the use in high-voltage power pylons. The damping may thereby significantly be increased by viscoelastic intermediate layers, when subjected to shear. The related trade-off between a reduction in natural frequency and an increase in damping and weight may then be investigated using optimization algorithms. However, the design criteria weight will therefore only be of minor importance, as the power pylon is considered mainly as a static structure.

Acknowledgements

Thanks to Prof. M. Gude and Prof. N. Modler of the Institute of Lightweight Engineering and Polymer Technology at TU Dresden for their kind cooperation in carrying out the experimental dynamic study of this work. The 3D Imaging Centre at the Technical University of Denmark is also gratefully acknowledged for their valuable support on image processing.

Declaration of Conflicting Interests

The author(s) declared no potential conflicts of interest with respect to the research, authorship and/or publication of this article.

Funding

The author(s) disclosed receipt of the following financial support for the research, authorship and/or publication of this article: This research is supported by Innovationsfonden Denmark via the project Power Pylons of the Future (PoPyFu) in collaboration with Bystrup and Tuco Marine ApS, which are gratefully acknowledged.

ORCID iD

Mathias Kliem http://orcid.org/0000-0002-0867-5534

References

1. European Network of Transmission System Operators for Electricity. Ten-year network development plan 2012, www.entsoe.eu (2012, accessed 12 March 2018).
2. Guedes AV, Matt CF and Cavalcanti ESC. Experimental investigation of the dynamic behaviour of stockbridge dampers. In: *18th international congress of mechanical engineering*, Ouro Preto, MG, Brazil, 6–11 November 2005.
3. Macdonald JHG and Larose GL. Two-degree-of-freedom inclined cable galloping. Part 1: general formulation and solution for perfectly tuned system. *J Wind Eng Ind Aerodyn* 2008; 96: 291–307.
4. Macdonald JHG and Larose GL. Two-degree-of-freedom inclined cable galloping. Part 2: analysis and prevention for arbitrary frequency ratio. *J Wind Eng Ind Aerodyn* 2008; 96: 308–326.
5. Hu J, Yan B, Zhou S, et al. Parameter study on galloping of iced bundled conductors. In: *2010 Asia-Pacific power and energy engineering conference (APPEEC)*, 2010. USA: IEEE. 28 Mar – 31 Mar 2010, Chengdu, China.
6. Lilien JL (convenor), Van Dyke P (secretary), Asselin JM, Farzaneh M, Halsan K, Havard DG, Hearnshaw D, Laneville A, Mito M, Rawlins CB, St-Louis M, Sunkle D, Vinogradov A (2007) State of the art of conductor galloping. Cigré TFB2.11.06, Électra, technical brochure no 322.
7. Svensson H. *Cable-stayed bridges: 40 years of experience worldwide*. Wilhelm Ernst und Sohn, Verlag für Architektur und technische Wissenschaften GmbH und Co. KG, Berlin, Germany, 2013.
8. Hu N. Composites and their properties. *InTech – Open access,* 2012. Edited Volume, DOI: 10.5772/2816.
9. Ibrahimbegovic A and Kozar I. Extreme man-made and natural hazards in dynamics of structures. Springer, NATO Security through Science Series, 2007.
10. Li SY and Chen ZQ. Experimental investigation concerning aerodynamic stability of a stay cable incorporated with lamps. In: *The seventh Asia-Pacific conference on wind engineering*, Taipei, Taiwan, 8–12 November 2009.
11. Treviso A, Van Genechten B, Mundo D, et al. Damping in composite materials: properties and models. *Composites Part B* 2015; 78: 144–152.
12. Cremer L and Heckl M. *Structure-borne sound: structural vibrations and sound radiation at audio frequencies*. Berlin: Springer-Verlag, 1988.
13. Kliem M, Høgsberg J, Wang Q, et al. Characterization of clay-modified thermoset polymers under various environmental conditions for the use in high-voltage power pylons. *Adv Mech Eng* 2017; 9: 1–16.
14. Bertolino V, Cavallaro G, Lazzara G, et al. Effect of the biopolymer charge and the nanoclay morphology on nanocomposite materials. *Ind Eng Chem Res* 2016; 55: 7373–7380.
15. Makaremi M, Pasbakhsh P, Cavallaro G, et al. Effect of morphology and size of halloysite nanotubes on functional pectin bionanocomposites for food packaging applications. *Appl Mater Interfaces* 2017; 9: 17476–17488.
16. Agubra VA, Owuor PS and Hosur MV. Influence of nanoclay dispersion methods on the mechanical behavior of E-glass/epoxy nanocomposites. *Nanomaterials* 2013; 3: 550–563.
17. Bulut M, Erklig A and Yeter E. Experimental investigation on influence of Kevlar fiber hybridization on tensile and damping response of Kevlar/glass/epoxy resin composite laminates. *J Compos Mater* 2015; 50: 1875–1886.
18. Berthelot JM, Assarar M, Sefrani Y, et al. Damping analysis of composite materials and structures. *Compos Struct* 2008; 85: 189–204.
19. Sefrani Y and Berthelot JM. Temperature effect on the damping properties of unidirectional glass fibre composites. *Composites Part B* 2006; 37: 346–355.
20. Colakoglu M. Effect of temperature on frequency and damping properties of polymer matrix composites. *Adv Compos Mater* 2008; 17: 111–124.
21. Li J, Sun B and Du Y. Damping properties of fiber reinforced composite suitable for stayed cable. In: *Third International Conference on Smart Materials and Nanotechnology in Engineering*, Proc. of SPIE Vol. 8409, doi: 10.1117/12.920368, 5-8 December 2011, Shenzhen, China.
22. Zhang PQ, Ruan JH and Li WZ. Influence of some factors on the damping property of fiber-reinforced epoxy composites at low temperature. *Cryogenics* 2001; 41: 245–251.
23. Zhang HZ and Chen HL. A study on the damping characteristics of laminated composites with integral viscoelastic layers. *Compos Struct* 2006; 74: 63–69.
24. Saravons DA and Chamis CC. Unified micromechanics of damping for unidirectional and off-axis fiber composites. *J Compos Technol Res* 1990; 12: 31–40.
25. Holste C. *Zum Daempfungsverhalten anisotroper Faserverbundstrukturen*. Germany: Dissertation, Technische Universitaet Clausthal, 1998.
26. Stankiewicz B. Durability of glass fiber-reinforced polymer bridge panel based on differential thermal analysis, dynamic mechanical analysis, and differential scanning calorimetry analysis. *J Compos Mater* 2017; 51: 2301–2313.
27. Pothan LA, Potschke P, Habler R, et al. The static and dynamic mechanical properties of banana and glass fiber woven fabric-reinforced polyester composite. *J Compos Mater* 2005; 39: 1007–1025.

28. Fotsing ER, Sola M, Ross A, et al. Lightweight damping of composite sandwich beams: experimental analysis. *J Compos Mater* 2012; 47: 1501–1511.
29. Huang CH and Tsai JL. Characterizing vibration damping response of composite laminates containing silica nanoparticles and rubber particles. *J Compos Mater* 2015; 49: 545–557.
30. Chortis DI. *Structural analysis of composite wind turbine blades – nonlinear mechanics and finite element models with material damping*. Berlin: Springer-Verlag, 2013.
31. Berthelot JM and Sefrani Y. Damping analysis of unidirectional glass and Kevlar fibre composites. *Compos Sci Technol* 2004; 64: 1261–1278.
32. Hwang SJ and Gibson RF. Influence of bending-twisting and extension-bending coupling on damping of laminated composites. *J Mater Sci* 1993; 28: 1–8.
33. Adams RD and Bacon DGC. Effect of fibre orientation and laminate geometry on the dynamic properties of CFRP. *J Compos Mater* 1973; 7: 402–428.
34. Dannemann M. *Zur vibroakustischen Auslegung von Faserverbund-Leichtbaustrukturen*. Germany: Dissertation, Technische Universitaet Dresden, 2012.
35. Melo JDD and Radford DW. Time and temperature dependence of the viscoelastic properties of CFRP by dynamic mechanical analysis. *Compos Struct* 2005; 70: 240–253.
36. Jaroschek C. The end of the flexural modulus. *J Plast Technol* 2012; 8: 515–524.
37. DIN EN ISO 178. *Plastics – determination of flexural properties*. German: German Institute for Standardisation, 2011.
38. Altenbach H, Altenbach J and Kissing W. *Mechanics of composite structural elements*. Berlin: Springer-Verlag, 2004.
39. Staab G. *Laminar composites*. 2nd ed. UK: Butterworth-Heinemann, 2015.
40. Li H, Hu Z, Chandrashekhara K, et al. Reliability-based fatigue life investigation for a medium-scale composite hydrokinetic turbine blade. *Ocean Eng* 2013; 89: 230–242.
41. Samborsky DD, Mandell JF and Agastra P. 3-D static elastic constants and strength properties of a glass/epoxy unidirectional laminate. Technical Report, Montana State University, USA, 2013.
42. Carfagni M, Lenzi E and Pierini M. The loss factor as a measure of mechanical damping. In: *Proceedings – the International Society for Optical Engineering,* 16th International Modal Analysis Conference, Santa Barbara, CA (USA), 2-5 February 1998, Vol. 1, pp. 580–584.
43. Duc F, Bourban PE and Manson JAE. The role of twist and crimp on the vibration behaviour of flax fibre composites. *Compos Sci Technol* 2014; 102: 94–99.
44. ABAQUS. *ABAQUS documentation*. Providence, RI, USA: Dassault Systmes, 2017.
45. Ungar EE and Kerwin M. Loss factors of viscoelastic systems in terms of energy concepts. *J Acoust Soc America* 1962; 34: 954.
46. Heistermann T. *Stiffness of reverse channel connections at room and elevated temperatures*. Sweden: Dissertation, Luleå University of Technology, 2013.
47. Mason BH, Sleight DW and Grenoble RW. *Test and analysis correlation for a Y-joint specimen for a composite cryotank*. Report nos, NASA/TM2015-218967, L-20594, NF1676L-22095, 1 October 2015. Hampton, VA: NASA Langley Research Center.
48. Brown J. Characterization of MSC/NASTRAN and MSC/ABAQUS elements for turbine engine blade frequency analysis. In: *Proceedings of the MSC aerospace user conference,* MSC 1997 Aerospace Users Conference Proceedings, Newport Beach, CA, 17-20 Nov. 1997.
49. Kliem M. Experimental data for analysing the damping behaviour of non-conductive composite materials. *Mendeley Data* 2017; DOI: 10.17632/65t5zzxvm5.1.
50. Messiry ME. Theoretical analysis of natural fiber volume fraction of reinforced composites. *Alex Eng J* 2013; 52: 301–306.
51. DIN EN 2331. *Prüfmethode zur Bestimmung des Harz- und Faseranteils sowie der flächenbezogenen Fasermasse*. Normenstelle Luftfahrt (NL) im DIN Deutsches Institut für Normung e. V, 1993.
52. Schürmann H. *Konstruieren mit Faser-Kunststoff-Verbunden*. Berlin, Heidelberg: Springer-Verlag, 2007.
53. Yi K, Geng D, Shang C, et al. The application of thermogravimetric analysis method in the determination of aramid fiber content in composite. In: *10th international conference on composite science and technology*, Lisbon, Portugal, February 2015.
54. ASTM D3039. *Test method for tensile properties of polymer matrix composite materials*. USA: ASTM International, 2014.
55. Melo JDD and Radford DW. Viscoelastic characterization of transversely isotropic composite laminae. *J Compos Mater* 2003; 37: 129–145.
56. Cogswell FN. *Polymer melt rheology: a guide for industrial practice*. 1st ed. Sawston, Cambridge: Woodhead Publishing Ltd, 1998.
57. Kelly SG. *Mechanical vibrations: theory and applications*, 1st ed. Boston, MA, USA: Cengage Learning, 2011.
58. Assarar M, El Mahi A and Berthelot JM. Damping analysis of sandwich composite materials. *J Compos Mater* 2009; 43: 1461–1485.
59. Guan H and Gibson RF. Micromechanical models for damping in woven fabric-reinforced polymer matrix composites. *J Compos Mater* 2001; 35: 1417–1434.
60. Vanwalleghem J, Baere ID, Loccufier M, et al. Practical aspects in measuring vibration damping of isotropic materials. In: *Proceedings – 15th international conference on experimental mechanics*, Porto, Portugal, July 2012.
61. Borbon FD, Ambrosini D and Curadelli O. Damping response of composites beams with carbon nanotubes. *Composites Part B* 2013; 60: 106–110.
62. Rueppel M, Rion J, Dransfeld C, et al. Damping of carbon fibre and flax fibre angle-ply composite laminates. *Compos Sci Technol* 2017; 146: 1–9.
63. Kiral Z, Malgaca L, Akdag M, et al. Experimental investigation of the dynamic response of a symmetric laminated composite beam via laser vibrometry. *J Compos Mater* 2009; 43: 2943–2962.
64. Beards CF. *Engineering vibration analysis with application to control systems*. 1st ed. Oxford, UK: Wiley, 1996.

65. Petersen HN, Kusano Y, Brondsted P, et al. The influence of removing sizing on strength and stiffness of conventional and high modulus E-glass fibres. *IOP Conf Ser: Mater Sci Eng* 2016; 139: 012040.
66. Herakovich CT. *Mechanics of fibrous composites*. 1st ed. Hoboken, NJ, USA: Wiley, 1997.
67. Wollbrett-Blitz J, Joannes S, Bruant R, et al. Multiaxial mechanical behavior of aramid fibers and identification of skin/core structure from single fiber transverse compression testing. *J Polym Sci Part B* 2015; 54: 374–384.
68. Landel RF and Nielsen LE. *Mechanical properties of polymers and composites*. 2nd ed. Boca Raton: CRC Press, 1993.
69. Sandesh KJ, Umashankar KS, Manujesh BJ, et al. Mechanical characterisation of kevlar/glass hybrid reinforced polymer composite laminates. *Int Adv Res J Sci Eng Technol* 2016; 3: 90–97.
70. Margem FM, Monteiro SN, Neto JB, et al. The dynamic-mechanical behavior of epoxy matrix composites reinforced with ramie fibers. *Rev Mat* 2010; 15: 164–171.
71. Jensen RE, McKnight SH and Palmese GR. Nondestructive evaluation and health monitoring. In: *Proceedings of the SPIE*, San Diego, CA, 7-9 March 2011.
72. Bonakdar M, Seidel GD and Inman DJ. Damping characterization of viscoelastic composites using micromechanical approach. In: *Proceedings of SPIE – the International Society for Optical Engineering,* 2011.
73. Melo JDD and Radford DW. Viscoelastic properties of PEEKIM7 related to temperature. *J Reinf Plast Compos* 2005; 24: 545–556.
74. Baker WE, Woolam WE and Young D. Air and internal damping of thin cantilever beams. *Int J Mech Sci* 1967; 9: 743–766.
75. Stephens DG and Scavullo MA. *Investigation of air damping of circular and rectangular plates, a cylinder, and a sphere*. NASA Technical Note, NASA TN D-1865, Langley Research Center, Langley Station, Hampton, Va, USA 1965.
76. Bleicher A. *Multimodal active vibration control of a stress ribbon bridge using pneumatic muscle actuators*. Germany: Dissertation, Technische Universität Berlin, 2011.

P3

Damping analysis of cylindrical composite structures with enhanced viscoelastic properties

Mathias Kliem, Jan Høgsberg, Joachim Vanwalleghem, Angelos Filippatos, Stefan Hoschützky, Edith-Roland Fotsing, Christian Berggreen

Applied Composite Materials,

Article In Press,

DOI: 10.1007/s1044301896842.

Damping analysis of cylindrical composite structures with enhanced viscoelastic properties

Mathias Kliem[1*], Jan Høgsberg[1], Joachim Vanwalleghem[2], Angelos Filippatos[3], Stefan Hoschützky[4], Edith-Roland Fotsing[5], Christian Berggreen[1].

[1]Department of Mechanical Engineering, Technical University of Denmark, Lyngby, Denmark

[2]Department of Materials Science and Engineering, Ghent University, Belgium

[3]Institute of Lightweight Engineering and Polymer Technology, Technische Universität Dresden, Germany

[4]Leichtbau-Zentrum Sachsen GmbH, Dresden, Germany

[5]Department of Mechanical Engineering, Polytechnique Montréal, Canada

Abstract

Constrained layer damping treatments are widely used in mechanical structures to damp acoustic noise and mechanical vibrations. A viscoelastic layer is thereby applied to a structure and covered by a stiff constraining layer. When the structure vibrates in a bending mode, the viscoelastic layer is forced to deform in shear mode. Thus, the vibration energy is dissipated as low grade frictional heat. This paper documents the efficiency of passive constrained layer damping treatments for low frequency vibrations of cylindrical composite specimens made of glass fibre-reinforced plastics. Different cross section geometries with shear webs have been investigated in order to study a beneficial effect on the damping characteristics of the cylinder. The viscoelastic damping layers are placed at different locations within the composite cylinder e.g. circumferential and along the neutral plane to evaluate the location-dependent efficiency of constrained layer damping treatments. The results of the study provide a thorough understanding of constrained layer damping treatments and an improved damping design of the cylindrical composite structure. The highest damping is achieved when placing the damping layer in the neutral plane perpendicular to the bending load. The results are based on free decay tests of the composite structure.

Keywords: Composite structure; Passive damping treatment; Filament winding; Vibration analysis; Function integration

*Corresponding author: mkliem@mek.dtu.dk

1 Introduction

Glass fibre-reinforced plastics (GFRP) are well suited for use in high voltage applications, such as insulators or overhead transmission pylons, due to the inherent non-conductivity of the raw material. This enables a rigid attachment of overhead transmission lines to the cross arm of each composite pylon, resulting in an increased dynamic interaction. Induced vibrations, such as from the severe cable vibration phenomenon known as galloping, will therefore be directly transferred to the slender composite mast structure and may lead to catastrophic failure of the entire structure due to excessive vibration amplitudes at resonance [1]. These low-frequent galloping vibration amplitudes at frequencies between 0.5 Hz and 2 Hz depend e.g. on the cable vibration mode, the cable tension and the span length [2] and can be reduced by designing the composite power pylon to act as a supportive damper. By introducing passive damping supplements, such as the constrained layer damping (CLD) treatment, the energy dissipation in the composite structure may significantly be increased due to the shear deformation of the integrated viscoelastic material (VEM) damping layer located between two stiff layers: layer 1 - host structure and layer 2 - constraining layer (CL) [3].

In contrast to tuned resonance dampers, such as tuned mass dampers or tuned liquid dampers configured to damp a certain frequency, the passive CLD treatment may be suitable to damp galloping vibrations within a larger frequency range [4]. However, the additional weight of the VEM and the CL may reduce the stiffness and consequently the natural frequency of a structure, when keeping the overall dimensions constant. The trend in the design of passive CLD treatments for lightweight structures is therefore increasing towards damping patches instead of a full damping layer coverage [5]. The VEM-patches are typically located at areas with high shear deformation, which is usually close to the nodes of a mode shape. The added weight of a passive CLD treatment can be reduced by 50 % with respect to full layer damping, while maintaining the overall damping performance [6]. However, many possible locations with high shear deformation exist along a power pylon arm because of the variety of attached conductor line bundles - each with the potential to vibrate by itself or in combination with other cables or cable bundles. Due to the wide range of resulting vibration scenarios of a composite cross arm, the investigation of VEM damping patches is therefore not part of the paper, and has to be addressed in future investigations.

The focus in this paper will be on a full coverage of VEM damping layers in the length wise direction of the generic composite cylinder instead, as the effect of additionally implemented structural elements such as stiffening web on the damping behaviour is investigated. An optimization process regarding a reduction of the amount of applied VEM within a damping-enhanced cross-sectional design concept may be an interesting topic to be investigated further. The cross sectional shape of the structure will also have a great impact on the efficiency of CLD treatments. The proportion of the shear deformed VEM area which is further away from the neutral axis is higher for rectangular cross sections compared to equivalent circular cross sections and will therefore result in better damping [7]. Despite the obvious advantages of rectangular cross sections with regard to damping, the design of the power pylon arm and tower is restricted to a cylindrical outer geometry by the designer. However, no design restrictions are defined for the inside of the composite cylinder, providing a design flexibility with respect to the application of passive CLD treatments within the pylon arm and tower structure [8, 9].

To the best knowledge of the authors, a comprehensive, experimental and numerical analysis of passive CLD treatments with regard to various positions along the cross section of hollow composite cylinders has not been

conducted yet. Therefore, different structural damping-design configurations based on various CLD treatment locations are investigated for eight generic, hollow composite cylinders. The resulting energy dissipation during flexural vibrations is experimentally investigated by analysing the free vibration decay and calculating the loss factor η for the first bending mode.
Furthermore, the experimental results are used to validate a numerical damping analysis based on the modal strain-energy approach, taking the fibre direction material properties into account [10, 11, 12, 13]. A script written in Python enables the calculation of the system modal damping of the composite structure using the finite element analysis (FEA) software package ABAQUS [14].

2 Aim and outline of the paper

The aim of the paper is to provide a method for the dynamic design of generic composite cylinders with maximum vibration damping. Different cross sectional designs are investigated in order to evaluate the location-dependent damping enhancement by CLD treatments. The presented results and properties may be considered in the dynamic design of the next generation of composite power pylon arms.
The damping enhancement of generic composite cylinders is achieved by using viscoelastic damping layers at various locations in the cross section. Eight generic cross section designs are presented and evaluated with regard to its stiffness-weight ratio. Prototypes are manufactured using the filament winding technology and tested statically and dynamically with regard to bending stiffness and damping properties. The results are used to verify the numerical model for the modal damping prediction. Finally, the comparison of experimental and numerical results is presented and discussed.

3 Design of the generic composite tube

This section provides a detailed description of the design and manufacturing of the different generic composite tubes with and without implemented damping layers. The laminate design as well as the load assumptions are derived from the full-scale composite power pylon arm structure at a location close to the root-end.

3.1 Composite power pylon structure

The composite power pylon consists of a tubular column section, supporting a pair of cantilevered and tapered composite cylindrical arms at which three pairs of twin bundle conductor lines are directly attached on each arm (see Fig. 1). The composite arm structure is thereby designed for vertical and transverse bending loads in x and y directions due to the cables weight and common loads from climatic situations such as individual or combined ice and wind loading [16]. Furthermore, vibrating cables due to galloping will introduce dynamic bending loads to the power pylon arms. Based on an optimised, stiffness driven design of the power pylon arms, the laminate thickness gradually decreases from the thick-walled layup configuration at the root-end section to the thin-walled shell-like zone at the tip of the arm.
The power pylon structure will be designed with maximal stiffness, preventing any resonant vibrations of the pylon at typical galloping frequencies. However, any change in cable tension and span length requires a re-examination of the vibration behaviour of the cable-pylon-system and, if necessary, an individual stiffness

Table 1: Geometric and stacking properties of the generic composite tube.

Parameter	Layup and Dimensions
Free specimen length l	950 ± 5 mm
Constant inner diameter D_i	79.0 mm
Wall thickness 'host structure'	4.0 mm
Host structure layup	$[\pm 45\,^\circ, \pm 45\,^\circ, \pm\ 10\,^\circ, \pm 45\,^\circ]$
Constraining layer (CL) layup	$[\pm 10\,^\circ]$
Layer thickness GFRP $[\pm 45\,^\circ]$	0.88 mm
Layer thickness GFRP $[\pm 10\,^\circ]$	1.00 mm (segment) - 1.35 mm (circular)
Layer thickness VEM	0.58 mm
Spacer plate thickness	3.0 mm

adjustment of the power pylon. At the same time, adequate damping of the composite structure is required in order to minimize vibrational amplitudes of the cables and the cross arm due to galloping and thereby prevent severe structural damage.

Tuned resonance dampers are not feasible damper solutions, as they are adjusted to damp only a single frequency instead of typical galloping frequencies in a range between 0.5 Hz and 2 Hz. Furthermore, high electro-magnetic fields do not allow the use of active controlled damping devices.

Instead, non-conductive CLD treatments are well suited for the application in high-voltage power pylons as these are low cost, robust, reliable and maintenance-free structural vibration control methods [17]. However, the application of CLD treatments may considerably reduce the advantage of a lightweight design, defined by the stiffness-weight-ratio, when restricting the geometry [18]. Either the static stiffness of a structure is reduced

Figure 1: Composite power pylon with directly attached overhead transmission line bundles in the global coordinate system [15].

while keeping the weight constant or vice versa.
In this work, the design focus is on maximizing the vibration damping of the composite structure, while keeping the natural frequencies constant. The outer dimension should therefore remain unchanged, so that a potential reinforcement is applied to the inside of the structure. The increase in weight is tolerated and only of minor importance, as the power pylon is considered mainly a static structure not excited at its own resonance frequency. The appearance of galloping overhead transmission lines causing the power pylon to vibrate is a rare but dangerous incident and is therefore considered as an important design criteria for power pylons [19].
The trade-off between an increase in weight and the related increase in costs with regard to material, manufacturing, transportation and installation must also be considered.

3.2 Generic composite cylinder with passive damping treatments

Based on the design of the composite power pylon cross arm, generic composite specimens are developed in the scale of 1:10 with respect to dimensions and stacking sequence of the laminate. The generic composite cylinders represent the cross sectional properties of the cross arm at a position close to the root end section, assuming loading conditions that are free of clamping effects. For reasons of simplicity and comparability, all generic composite specimens are non-tapered, cylindrical and hollow with constant laminate properties along the entire length. The dimensions and layups are specified in Tab. 1.
The efficiency of a damping layer strongly depends on its shear deformation and therefore on the position in the host structure. The VEM is preferably located far from the neutral plane for structures undergoing flexural vibrations, due to the maximum flexural deformation [20].
Alternatively, the positioning of the VEM layer close to the neutral plane also leads to high shear strains in the damping material due to the presence of maximum shear stresses [21]. The damping is thereby most effective when two VEM layers are positioned symmetrically and close to the neutral plane during bending, separated by a stiff mid plane laminate of the host structure [22, 11]. As the design flexibility of CLD treatments is very limited for hollow cylinder structures with regard to its position, a laminated shear web may therefore be introduced into the neutral plane in order to provide a stiff structure for a potential CLD treatment close to the neutral plane (see Fig. 2). The VEM damping layers can then be applied symmetrically to both sides of the neutral plane, representing the most efficient damping scenario described above.
It is assumed that the highest damping performance will be achieved when flexing in the direction perpendicular to the CLD-treated shear web plane. The ribs are positioned in one or two directions in order to possibly damp vibrations of the power pylon arm in x and | or y direction of the global coordinate system (see Fig. 1), caused by the directly mounted overhead transmission line bundles, which are vibrating due to galloping. The resulting loading direction at the pylon arm thereby depends on a symmetric or asymmetric cable vibration mode [23].
The application of VEM damping layers along a the circumference in accordance to the above mentioned positions with maximum shear deformation consequently leads to the following damping layer configurations for the generic composite cylinder: Eight cross-sectional design concepts were investigated (design A to I) in order to evaluate the efficiency of various VEM layer positions along the cross section. An overview of the eight designs is presented in Fig. 2.
The load carrying laminate thickness (section I, II) with $t = 4.0\,\text{mm}$ remains constant for all design concepts, due

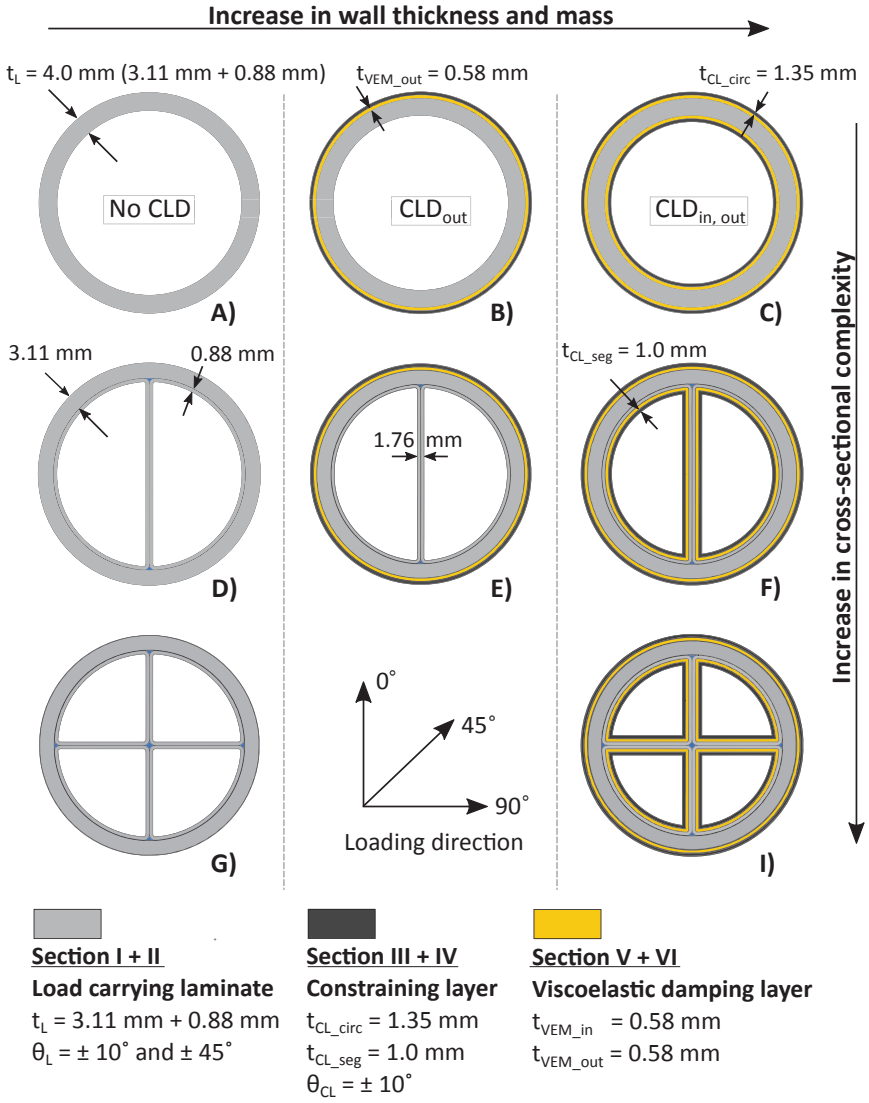

Figure 2: Overview on the different cross-sectional designs with details to the stacking sequence and loading direction (not drawn to scale).

to structural requirements, explained in detail below. The application of viscoelastic damping layers (section V and VI) on the in- and outside in combination with stiff constraining layers (section III and IV) will generate the CLD treatment. An integration of VEM damping layers into the load carrying laminate to further increase the damping is not considered in the present paper, as a safe load introduction of the overhead transmission lines into the cross arm is strongly required over the structural lifetime of 100 years. However, interleaved damping layers may considerably weaken the load carrying laminate so that a reliable load introduction may not be obtained. The alternative approach to reinforce the load introduction areas along the slender composite cross arm in a subsequent step is not as trivial in a filament winding process of a near neat shaped cylindrical structure, and may therefore not considered any further. For the sake of simplicity, a constant wall thickness for all generic composite cylinders is assumed in the present paper for evaluating the effect of various damping layer

configurations on the overall damping behaviour. It is expected that the application of stiff constraining layers may increase the stiffness and vibration behaviour. In order to fairly compare the different design concepts with regard to damping and vibration frequency, the specimens are grouped based on the level of applied CLD treatments (No CLD, CLD_{out}, $CLD_{in,out}$). However, this approach is a trade-off between the implementation of structural requirements and scientific evaluation of damping enhancement treatments. Each cross-sectional designs may be assessed in terms of an 'increase in cross-sectional complexity' and 'increase in weight and wall thickness'. As the complexity of the cross-sectional design is directly related to an expensive, costly and time-consuming manufacturing process, a concept with high complexity (concept G or I) may be chosen when a high damping in combination with a high stiffness-weight ratio is required. In contrast, the application of CLD treatments to specimens with a low cross-sectional complexity leads a considerable increase in wall thickness and weight, when keeping the natural frequency constant (concept A to C).

However, a grouping with respect to an 'increase in cross-sectional complexity' is described in detail as follows: In the first group (A to C), the VEM layer is applied only circumferential on the outside (B) or on the in- and outside (C), covered by a stiff CL, respectively. The CLD treatment applied on the inside of the structure is assumed to be less effective than a CLD treatment on the outside, due to a reduced distance from the neutral plane and thus smaller flexural deformations. However, each CL represents a thin and individual laminate, coupled to the host structure only by the VEM damping layer. When the host structure flexes, the additional laminate deforms, introducing shear strains in the VEM and thereby damping. The laminate of the host structure consists of eight layers, each defined by a fibre direction φ with respect to the axial direction z in the global coordinate system of the cylinder [$\pm 45\,^\circ$, $\pm 45\,^\circ$, $\pm\ 10\,^\circ$, $\pm 45\,^\circ$] (see Fig. 1). The presented fibre orientations of the generic composite cylinder are equivalent to stacking sequence of the composite cross arm, earlier defined by the designer.

In the second group (D to F), a shear web made of two symmetrical GF-EP composite layers with a material orientation of $\varphi = \pm 45\,^\circ$ is introduced, representing the inner layer of the host structure laminate. A fibre direction of $\varphi = \pm 45\,^\circ$ was chosen since mainly shear stresses occur during bending and a reliable manufacturability of that fibre angle is feasible by filament winding. The remaining $\pm 45\,^\circ$, $\pm 10\,^\circ$ and $\pm 45\,^\circ$ layers of the host structure are of cylindrical shape. The layup and thickness of the host structure is thereby kept constant for all design concepts A to I. For concept E, the CLD treatment is only added to the outside of the structure. In order to further increase the damping of the generic composite structure, VEM damping layers are also placed close to the neutral plane with its maximum shear stresses. Thereby, two individual and hollow half cylinders are generated by the inner CL.

In the third group (design G and I), two perpendicular shear webs are introduced the same way as described for the one-web design concept D to F, resulting in four individual quarter cylinders. A rotation of the shear web with respect to the loading direction leads to a variation in static stiffness, natural frequency and damping. Therefore, the two significant loading directions $0\,^\circ$ and $90\,^\circ$ with regard to the shear web plane will be investigated for design concept D, E and F. The composite cylinders of concept G and I are only loaded in $45\,^\circ$, as a loading in $0\,^\circ$ and $90\,^\circ$ is equivalent to the conditions investigated for the design concepts D, E and F. The concept and the loading is specified in its notation, where the cross sectional design concept is defined by a letter (A to I) and the loading direction ($0\,^\circ$, $45\,^\circ$ or $90\,^\circ$) is stated by a number (e.g. I.45).

3.3 Materials

The materials used for manufacturing the generic composites cylinders are considered to be the same as for the composite power pylon arms. A glass fibre (GF) roving EC17-2400-352 with 2400 tex and a sizing suitable for epoxy and vinyl-ester from PD Fibre Glass was used in combination with the PRIME 20 epoxy (EP) resin and the slow hardener from Gurit [24, 14]. The static material properties of GF-EP were determined based on a planar unidirectional (UD) composite plate, made up of a UD GF fabric with an area weight of 475 g/m^2 (incl. 35 g/m^2 of a chopped strand mat) and the Prime 20 Epoxy [14]. The static GF-EP properties at room temperature are given as follows: $E_{11} = 27.6$ GPa, $E_{22} = 5.3$ GPa, $G_{12} = 2.0$ GPa, $\nu_{12} = 0.345$ and $\rho = 1.79$ g/cm^3 [14]. The particular polyurethane (PU) material DYAD 601 from Soundcoat with a thickness of 0.58 mm was selected as VEM damping layer for the damping investigation of the generic composite cylinder, due to its optimised damping performance at temperatures prone for galloping vibrations around 0 °C. However, any other VEM may be selected, depending on the required damping performance. The surface of the elastomer was initially coated with a B-Flex epoxy formulation, assuring a high adhesive quality [25].

PU materials are the most commonly used VEM's for vibration control. However, these materials exhibit frequency and temperature dependent material properties with an optimal damping characteristics of a narrow frequency and temperature range [26]. The dynamic stiffness and damping properties of DYAD 601 are therefore discussed in more detail in section 5.1. However, the Poisson's ratio is assumed to be constant with $\nu = 0.49$ for the investigated frequency and temperature range [27]. The density of DYAD 601 was determined as $\rho = 1.04$ g/cm^3.

3.4 Manufacturing of test specimens

The damping behaviour of GF-EP was determined at coupon and structural level with two different sets of GF-EP specimens: 1) Unidirectional (UD) composite coupons were used to characterise the fibre direction dependent damping behaviour. 2) Various composite cylinders with different cross section designs were manufactured by filament winding in order to demonstrate the potential of VEM damping layers with regard to a vibrating power pylon arm.

3.4.1 Manufacturing of coupons

The same coupon specimens, used for a previous damping investigation [14], were dynamically tested to characterise the fibre direction damping at room temperature between 20 Hz and 60 Hz. The first natural frequency of the investigated composite cylinders lies within this frequency range. The static and dynamic properties of the two different sets of specimens are thereby assumed to be of the same order of magnitude, due to the use of similar UD GF materials. A detailed description of the generic composite cylinder manufacturing is presented in the following.

3.4.2 Manufacturing of generic composite cylinders

Filament winding is a well suited manufacturing process for cylindrical composite parts with a constant layup throughout the whole specimen due to its high efficient, automated and low cost fabrication characteristics [28]. Although a typical range of fibre layup angles for filament winding is between 20 ° and 85 °, local reinforcement with very low winding angles can be implemented during the manufacturing process by the use of pins for fibre redirection at each end of the mandrel [29]. This layup modification might be used to reinforce the compression side of slender composite power pylon arm structures subjected to bending loads in order to prevent buckling. A segmentable aluminium mandrel was designed and CNC-milled in order to manufacture the different cross-sectional designs using a wet filament winding process (see Fig. 3).

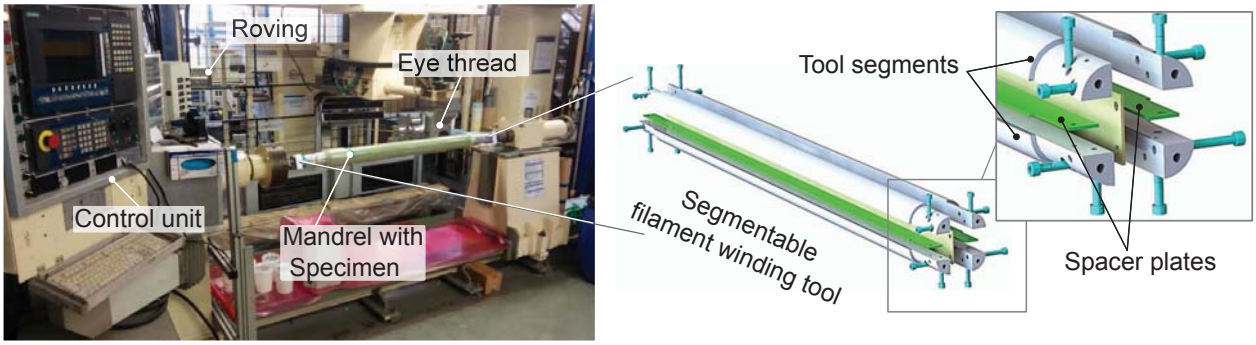

Figure 3: Manufacturing of the generic tubular composite structure using a filament winding machine and the tool segments.

Thereby, a wet GF, impregnated by a resin bath prior to the placement process, was positioned and cured on the mandrel (tool). By either winding on a single tool segment, a 'two-segment assembly' or a 'four-segment assembly', generic composite specimens consisting of two shear webs (design concepts G to I), one shear web (design concepts D to F) or no shear web (design concepts A to C) may be manufactured. In case of a composite cylinder with only one shear web and no VEM damping layer (design concept D), the manufacturing process consists of five stages:

1. Assembly of two tool segments and a 3 mm thick spacer plate, forming a cylinder half,
2. Filament winding of the first layer of the host structure laminate with $\varphi = \pm 45\,^\circ$ on the two cylinder halves respectively (see Tab. 1),
3. Mounting of the two cylinder halves to a 'two-segment assembly',
4. Finalizing the winding process with the three remaining host structure layers with $\varphi = \pm 45\,^\circ$, $\pm\ 10\,^\circ$, and $\pm\ 45\,^\circ$,
5. Thickening the end section for clamping, curing and mandrel removal.

The manufacturing process for composite cylinders without shear webs (design concept A to C) significantly simplifies, as the mounting procedure described in step 3.) vanishes. The fully assembled, cylindrical mandrel

with its 3 mm thick spacer plates, representing the shear webs, may be used directly. For design concepts with shear webs (concept D to I), the shear webs vary in thickness, depending on the presence of VEM damping layers (shear web thickness of concept D: 1.76 mm | concept F: 4.9 mm). This causes an ovalization of the cross section, which may lead to a slight change in bending stiffness compared to its equivalent circular concept (concept A, B or C). Therefore, the ovalization of the cross section was considered in the numerical model in order to fairly compare the different damping designs.
Dependent on the cross-sectional design (concept B, C, E, F or I), the VEM damping layer was applied by wrapping a 70 mm wide stripe of DYAD 601 helically and gap-free on the wet GF-EP structure. The final layup was cured under constant rotation in a climate chamber for 10 hours at 70 °C before pulling out the mandrel. The end sections were thickened and subsequently lathed to an outer diameter of $D_o \approx 100$ mm in order to provide constant clamping conditions. The reinforcement is about 100 mm long and made of n GF-EP layers, each with a fibre direction of $\varphi = \pm 85\,^\circ$, as shown in Fig. 4.

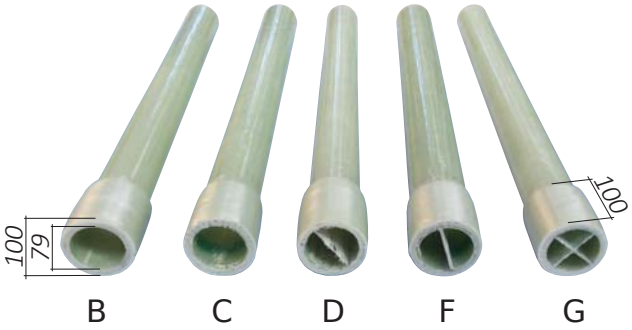

Figure 4: Selection of different manufactured cylindrical composite design concepts, where the inner area is visible.

Due to the constant outer diameter of the mandrel with $D_M = 79$ mm, the outer diameter of the cylindrical composite structure increases by applying CLD treatments, when keeping the laminate thickness of the host structure constant (e.g. concept A to C). This violates the initial design restriction (see section 3.1) because such restrictions are simply hard to realize with a single mandrel. Therefore, the results will be appropriately normalized in order to ensure comparability between the different concepts (see section 3.2).
The weight and fibre volume content of the manufactured specimens with regard to their different cross-sectional design concepts are listed in Tab. 2. The fibre volume content was calculated by the known total weight of the structure, the amount of the used fibre (and VEM material) as well as the related densities.
In Fig. 5 the inner and the outer damping layer distribution is shown for the cross-sectional design concept I.45 by a schematic and a realistic micro-section.

4 Numerical damping calculation

The numerical prediction of the modal loss factor of a vibrating composite cylinder is based on the modal strain-energy approach [30], manually implemented into the commercially available finite element (FE) software

Table 2: Design-related properties of the different generic composite cylinders.

Parameter	Cross-sectional design							
	A	B	C	D	E	F	G	I
Mass [kg]	2.04	3.00	3.69	2.32	3.36	4.67	2.56	5.30
Fibre volume content [%]	51.0	45.6	51.3	50.4	53.4	48.4	48.8	42.4

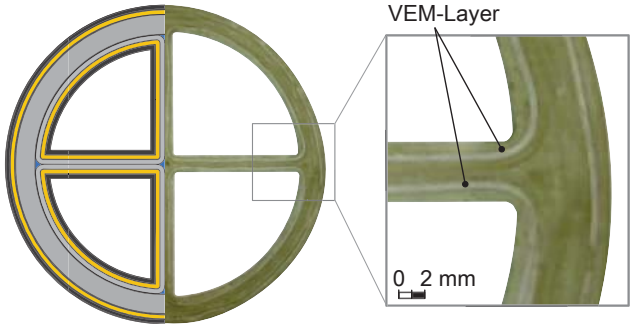

Figure 5: Distribution of the VEM for the cross-sectional design concept I.45 (left) and zoom into the interesting area (right).

ABAQUS [31, 14]. The loss factor η can be calculated as

$$\eta = \frac{1}{2\pi} \frac{\Delta U}{U}. \tag{1}$$

The dissipated energy and the stored energy with regard to a single oscillation is represented by ΔU and U, respectively. The energies are fibre direction dependent, due to the orthotropic nature of composite materials. The element-wise calculation of ΔU and U is therefore based on the local material coordinate system ($i, j = 1$, 2, 3) [11] by

$$U_{ij}^{[m]} = \frac{1}{2} \sigma_{ij}^{[m]} \epsilon_{ij}^{[m]} V^{[m]}, \tag{2}$$

with $\sigma_{ij}^{[m]}$, $\epsilon_{ij}^{[m]}$ and $V^{[m]}$ representing the stress and strain components as well as the m-th element volume, respectively. The modal loss factor for the first natural frequency η_1 of a composite structure with N layers, each with a total number of elements N_e, may then be computed by

$$\eta_1 = \frac{\sum_{m=1}^{N_e} \sum_{k=1}^{N} \sum_{i=1}^{3} \sum_{j=1}^{3} (\eta_{ij} U_{ij}^{[m](k)})}{\sum_{m=1}^{N_e} \sum_{k=1}^{N} \sum_{i=1}^{3} \sum_{j=1}^{3} (U_{ij}^{[m](k)})}. \tag{3}$$

The finite element (FE) model of the generic composite cylinder is composed of fully integrated, 8-node hexahedron elements. Adjacent layers with equal thickness were section-wise modelled using the composite layup

module provided by ABAQUS [32]. The results of the numerical damping prediction and the experimental decay test are compared in order to verify the FE model.

5 Experimental test setup

This section provides a detailed description of the procedures used to experimentally determine the dynamic mechanical properties of the VEM damping layer, the unidirectional (UD) composite coupons and the generic composite cylinder at room temperature. The Dynamic Mechanical Thermal Analysis (DMTA) and the Vibrating Beam Test (VBT) were used to investigate the damping properties on the material and structural level. All experimental data sets are published and freely available [33].

5.1 Dynamic mechanical analysis of viscoelastic material

The Dynamic Mechanical Thermal Analyser (DMTA) used for the damping characterisation of the DYAD 601 samples was a Q800 from TA with shear sandwich clamps, as shown in Fig. 6.

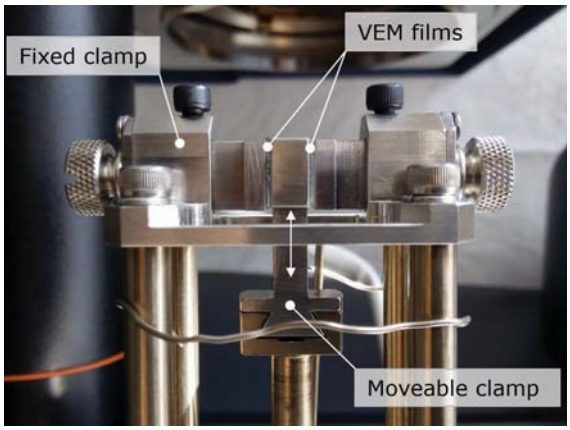

Figure 6: Clamped VEM films to analyse the shear damping by DMTA using the Q800 from TA.

The dynamic mechanical properties were analysed under two environmental conditions: I) conditions prone for cable galloping (-20 ° and 0 ° | from 0.5 Hz to 2 Hz) and II) conditions for generic composite cylinder testing (20 ° | 50 Hz). The frequency dependent complex shear modulus G^* of the VEM may be calculated by

$$|G^*(f)| = \sqrt{[G'(f)]^2 + [G''(f)]^2}\,. \tag{4}$$

where $G'(f)$ and $G''(f)$ represent the frequency dependent shear storage and shear loss modulus, respectively [34].

All DMTA shear tests have been performed within the linear viscoelastic range of the elastomer, so that constant material properties can be assumed. An approximately linear viscoelastic behaviour of DYAD 601 was quasi-statically determined for shear strains below 1.5 % with regard to the three different test temperatures -20 °C, 0 °C and 20 °C (see Fig. 7).

The dynamic characterisation of DYAD 601 was therefore carried out at strains well below 1.5 % (see section

5.1). The calculation of the frequency dependent complex E-modulus E^* of elastomer materials such the DYAD 601 may be calculated by

$$E^*(f) = 3\,G^*(f), \tag{5}$$

assuming incompressibility ($\nu = 0.5$) [35].

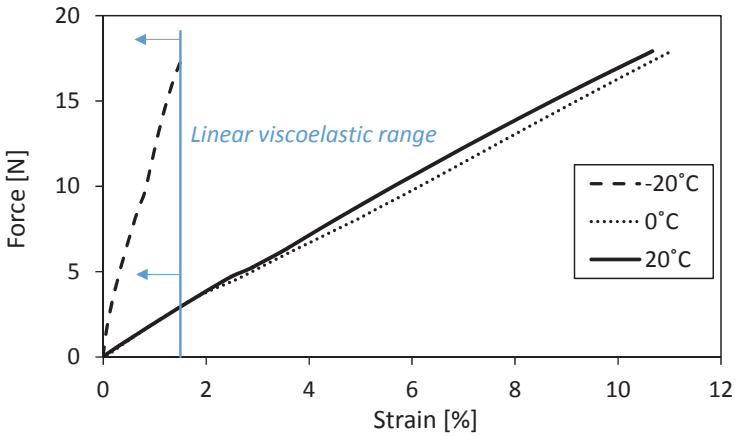

Figure 7: Strain sweep of DYAD 601 for the relevant temperatures: -20 °C, 0 °C and 20 °C.

5.2 Damping analysis of unidirectional GFRP coupons

Due to the relatively low damping of fibre-reinforced thermoset materials at room temperature compared to viscoelastic elastomers, the dynamic moduli E^* and G^* for GF-EP is considered to be constant within the studied frequency range and therefore assumed to be equivalent to the static moduli (see section 3.3) [36]. The fibre direction dependent damping properties were determined using the vibrating beam test method (VBT), which was successfully verified in a previous investigation [14]. An initial tip displacement of 5 mm was used for all investigated specimens. Furthermore, the free length of the vibrating coupon specimens were adjusted in order to determine the damping at different frequencies.

Two GF-EP specimens were tested per fibre direction without readjusting the clamped sample before repeating the measurement three times (six measurements in total per fibre direction and frequency). A logarithmic trend line was applied for each fibre direction in order to visualize the trend of the frequency dependent damping.

5.3 Damping analysis of generic composite cylinders

All cylindrical composite specimens were provided with an end-sectional outer diameter of $D_o = 100$ mm for constant clamping conditions. Metallic inserts with circular, semicircular or quarter-circular cross sections were pressed into each end section of the composite specimens in order to prevent the cross section to become oval during clamping and loading. The reinforced end of the cylinder was fixed to a strong table by two pairs of steel half shells, screwed together with four screws, each with a tightening torque of 200 Nm. The half shells were

designed with an interference fit with regard to the outer diameter of the composite cylinder, in order to obtain constant clamping conditions by press fit. The clamping half shells were supported by four bracing elements in order to further stiffen the clamping area.

The static stiffness was determined by applying a bending load with a hydraulic lifting device. The signal was logged using a 3 kN load cell in combination with an analog input module NI 9237 from National Instruments. In contrast, the excitation of the flexural vibration for the dynamic investigation of the composite cylinder occurred by impulse. The cylinder was therefore hit by a rubber block mounted on a bracket in vertical direction. The test setup is shown in Fig. 8.

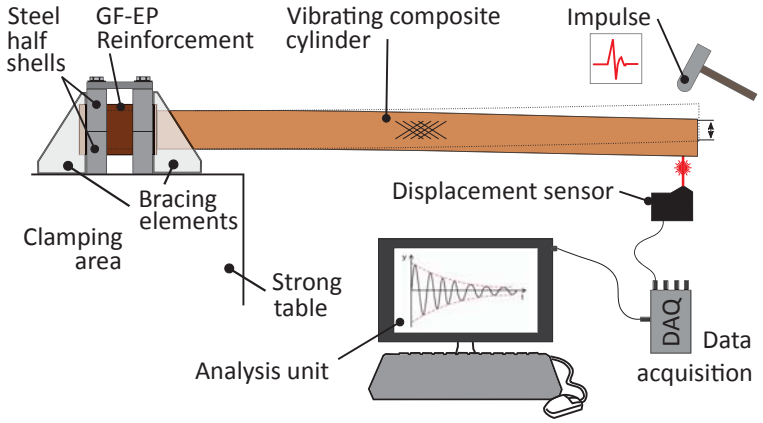

Figure 8: Schematic free vibration test rig for composite cylinders.

The resulting vibration amplitudes were kept below 0.8 % of the free cylinder length of $l = 960\,\text{mm} \pm 3\,\text{mm}$, depending on the bending stiffness of each composite structure. It is assumed that air damping is constant within this range. A laser displacement sensor optoNCDT 1402 from Micro-Epsilon with a sampling frequency of 2000 Hz together with an analog input module NI 9215 from National Instruments were used to log the declining sine curve of the freely vibrating cylinder. The accuracy of the measurement parameters were verified in a previous damping investigation [14].

It is assumed that mainly the first mode dominates the dynamic behaviour of the structure. The first 10 periods were neglected in order for activated higher modes to die out. Any influence from other modes are thereby neglected. An exponential curve may be fitted as an envelope $g(t)$ on the response signal, which can be described for the first mode as

$$g(t) = X_0 e^{-\zeta \omega_1 t}\,. \tag{6}$$

The first natural angular frequency, the damping ratio and the initial displacement are thereby represented by ω_1, ζ and X_0 respectively [37]. The loss factor of the vibrating composite structure may be calculated by

$$\eta \approx 2\,\zeta\,. \tag{7}$$

In order to evaluate the influence of the clamping, which is typically leading to a frequency dependent viscous behaviour, dead weights were mounted to the tip of the cylinder. The resulting variation of the first natural

frequency $f_1 = \omega_1/2\pi$ in the range between 20 Hz and 60 Hz is not supposed to strongly effect the damping of the composite structure. Each composite cylinder, representing a specific cross-sectional design, was tested without readjusting the clamped specimen before repeating the measurement at least 12 times.

6 Results and Discussion

The dynamic mechanical properties of the composite structure as well as its individual materials are presented, followed by the comparison with the numerical model.

6.1 Dynamic properties on material level

The cylindrical composite structures listed in Fig. 2 are composed of unidirectional GFRP layers with various orientation and to some extent with viscoelastic damping layers. In order to predict the modal loss factor η_1 of the vibrating composite structure by the modal strain-energy method, the damping of each individual material involved must be known. The dynamic mechanical properties of the VEM and the UD-GFRP have therefore been analysed at temperatures and frequencies of different environmental conditions.

6.1.1 Viscoelastic material

The loss factor as well as the storage and loss moduli of the VEM were investigated by DMTA at conditions close to structural testing of the composite cylinder (20 °C and 50 Hz) and conditions close to galloping (-20 °C and 0 °C, 0.5 Hz, 1 Hz and 2 Hz). The damping results are presented in Fig. 9 and are in line with the literature [38].

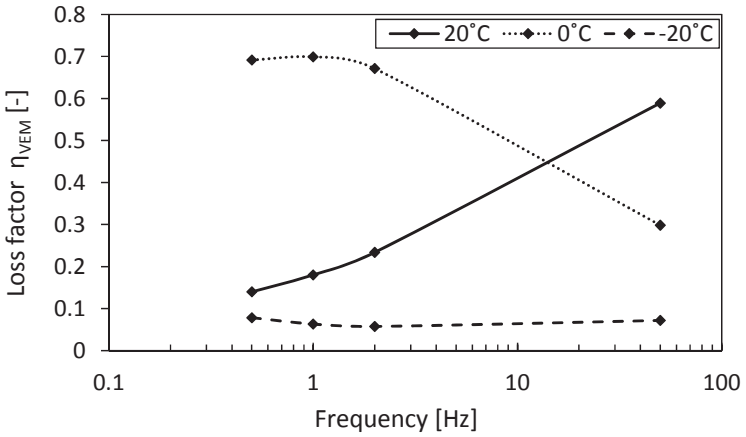

Figure 9: Frequency dependent loss factor of the VEM η_{VEM} for -20 °C, 0 °C and 20 °C.

As expected, the dynamic material properties of DYAD 601 show a strong frequency and temperature dependency, which is typical for VEM's. The maximum damping is observed at 0 °C and low frequencies up to 2 Hz, verifying the proposed temperature range in the data sheet [25]. The glass transition temperature range is therefore assumed to be close to 0 °C at low frequencies. An increase in frequency leads to a different behaviour of the loss factor depending on the temperature. While the damping decreases with increasing frequency at

0 °C, the damping increases at 20 °C and remains constant at -20 °C. The maximum damping capacity of the DYAD is therefore assumed to be between 0 °C and 20 °C, as at higher frequencies the glass transition and therefore the peak damping shifts to higher temperatures [39].

In Fig. 10 the storage and loss moduli for DYAD 601 are presented for different temperatures and frequencies. An increase in frequency from 0.5 Hz to 50 Hz only slightly changes the storage modulus at -20 °C and 20 °C, whereas the storage modulus quadruples at 0 °C. Furthermore, the loss modulus at 0 °C is slightly higher compared to -20 °C and increases with increasing frequency. The glass transition temperature Tg is therefore assumed to be between -20 °C and 0 °C for low frequencies, shifting towards 0 °C with higher frequencies.

The observations are coherent with the literature, as Tg is always below the temperature of the peak damping

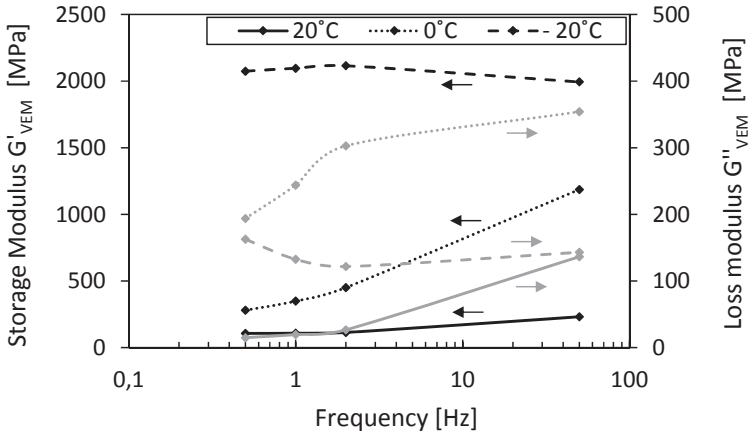

Figure 10: Frequency dependent storage and loss modulus of the VEM for -20 °C, 0 °C and 20 °C.

[34]. Based on the results above, the viscoelastic material properties of DYAD 601 may be approximated by

$$G'(f) = 29.07\ \ln(f) + 111.93\ \text{[GPa]}, \tag{8}$$

$$G''(f) = 28.00\ \ln(f) + 22.03\ \text{[GPa]}, \tag{9}$$

as a function of the frequency at 20 °C.

6.1.2 UD-composite coupons

The fibre direction dependent modal damping of GF-EP was investigated at room temperature using the VBT method for coupon specimens with five fibre directions 0 °, 30 °, 45 °, 60 ° and 90 °. The frequency dependency is evaluated by distributed measurements between 20 Hz and 60 Hz, whereas the results at 20 Hz are based on a previous investigation [14].

The modal damping was determined at higher frequencies by gradually reducing the free length of the clamped composite coupons. The first 50 periods were considered for analysing the damping by Eq. (6) and (7). The fibre direction dependent damping properties for the five fibre directions at 20 °C are presented in Fig. 11 with respect to frequencies in the range between 20 Hz and 60 Hz.

A slight increase in the loss factor with frequency is observed for all investigated fibre directions. The trend and magnitude of the damping for GFRP is in accordance to the literature [40]. The direction dependent

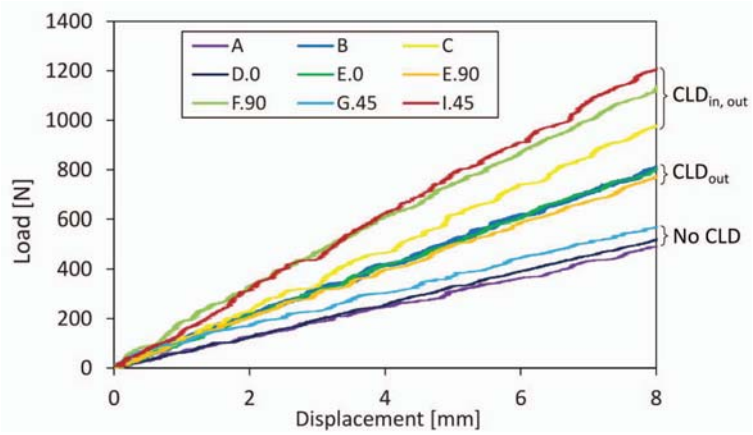

Figure 12: Static load-displacement curves for a selection of specimens with different cross-sectional designs.

The bending stiffness of all cross-sectional design concepts behaves linearly within the analysed range of deflection of approximately 0.8 % of the free cylinder length. The noise-like pattern of each curve may be explained by stick-slip effects relative to the clamping fixture or the load introduction elements close to the tip of the cylinder. The presented curves may be assigned into three groups in order to fairly compare the effect of additionally implemented stiffening webs, as the application of constraining layers to the in- and outside, purely floating on the VEM, have a major impact on the bending stiffness: 1.) specimens without CLD treatment (concepts A, D and G), 2.) specimens with a CLD treatment only on the outside (concept B and E) and 3.) specimens with a CLD on the in- and outside (concept C, F and I).

The difference in bending stiffness between the groups originates mainly from the increase in wall thickness by the application of CLD treatments or the increase of diameter of the host structure (load carrying laminate) by adding a CLD treatment on the inside of the cylinder (concept B and C) (see Fig. 2).

The differences in bending stiffness within the groups may be explained by the presence of shear webs or the slight ovalization of the cross section (see section 3.4.2). The variation of the free vibration length of 960 mm within the range of ± 3 mm may also lead to a slight impact on the static bending stiffness.

However, the reference structure (design concept A) shows the lowest bending stiffness, followed by the concept D.0 and concept G.45. The slight increase is due to the vertical oriented shear web with its well suited fibre orientation of $\varphi = \pm 45\,^{\circ}$. The presence of two shear webs, inclined by ± 45 ° to the loading direction (concept G.45), leads to a slightly higher bending stiffness compared to one shear web parallel to the loading direction (concept D.0).

The bending stiffness increases further by adding a circumferential CLD treatment on the outside (concept E.0, E.90 and B). A stiffening effect by an additional, vertical oriented shear web (concept E.0) is not observed at this magnitude of bending stiffness. However, the slight decrease in bending stiffness for design concept E.90 compared to the concepts B and E.0 may be due to its slight ovalized cross section. The differences in stiffness between concept C and F.90 are also assumed to be due to the ovalized cross section, resulting in a higher effective diameter when loading in the direction of 90 ° (see Fig. 2). As already shown for concept G.45, two inclined shear webs with an inclination of ± 45 ° to the loading direction lead to a further increase of bending

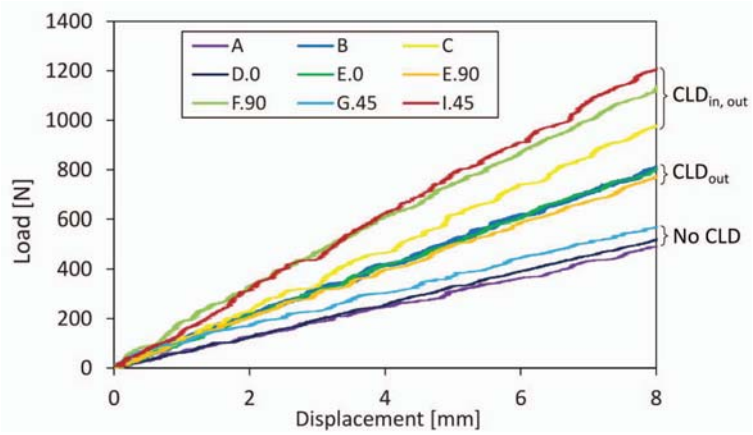

Figure 12: Static load-displacement curves for a selection of specimens with different cross-sectional designs.

The bending stiffness of all cross-sectional design concepts behaves linearly within the analysed range of deflection of approximately 0.8 % of the free cylinder length. The noise-like pattern of each curve may be explained by stick-slip effects relative to the clamping fixture or the load introduction elements close to the tip of the cylinder. The presented curves may be assigned into three groups in order to fairly compare the effect of additionally implemented stiffening webs, as the application of constraining layers to the in- and outside, purely floating on the VEM, have a major impact on the bending stiffness: 1.) specimens without CLD treatment (concepts A, D and G), 2.) specimens with a CLD treatment only on the outside (concept B and E) and 3.) specimens with a CLD on the in- and outside (concept C, F and I).

The difference in bending stiffness between the groups originates mainly from the increase in wall thickness by the application of CLD treatments or the increase of diameter of the host structure (load carrying laminate) by adding a CLD treatment on the inside of the cylinder (concept B and C) (see Fig. 2).

The differences in bending stiffness within the groups may be explained by the presence of shear webs or the slight ovalization of the cross section (see section 3.4.2). The variation of the free vibration length of 960 mm within the range of ± 3 mm may also lead to a slight impact on the static bending stiffness.

However, the reference structure (design concept A) shows the lowest bending stiffness, followed by the concept D.0 and concept G.45. The slight increase is due to the vertical oriented shear web with its well suited fibre orientation of $\varphi = \pm 45\,^{\circ}$. The presence of two shear webs, inclined by ± 45 ° to the loading direction (concept G.45), leads to a slightly higher bending stiffness compared to one shear web parallel to the loading direction (concept D.0).

The bending stiffness increases further by adding a circumferential CLD treatment on the outside (concept E.0, E.90 and B). A stiffening effect by an additional, vertical oriented shear web (concept E.0) is not observed at this magnitude of bending stiffness. However, the slight decrease in bending stiffness for design concept E.90 compared to the concepts B and E.0 may be due to its slight ovalized cross section. The differences in stiffness between concept C and F.90 are also assumed to be due to the ovalized cross section, resulting in a higher effective diameter when loading in the direction of 90 ° (see Fig. 2). As already shown for concept G.45, two inclined shear webs with an inclination of ± 45 ° to the loading direction lead to a further increase of bending

stiffness (concept I.45).

6.2.2 Dynamic structural testing

The modal damping of the composite structure was determined by a free vibration test at room temperature. The test rig with a mounted I.45 specimen is shown in Fig. 13, superimposed by its equivalent numerical FE-model.

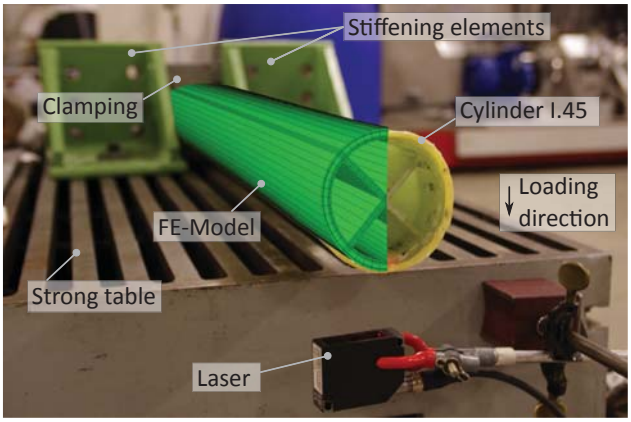

Figure 13: Test rig with clamped cylindrical specimen (design concept I.45).

The free vibration was initiated by an impulse in vertical direction, using a rubber block mounted on a bracket. The orientation of the shear webs was thereby adjusted with regard to the excitation direction for each specimen. It is assumed that the response signal is mainly related to the first activated bending mode. Therefore, an envelope may be exponentially fitted on the free decay curve of the vibrating composite structure, resulting in the damping ratio by Eq. (6). However, the first 10 periods were neglected in order for potentially activated higher modes to die out (see Fig. 14a and 14b).

In order to verify the dominance of the first flexural mode, a Fourier analysis of the experimental time-history was carried out for the cross-sectional concept A. As expected, the resulting frequency plot, shown in Fig. 15, verifies the dominance of first flexural mode at about 50 Hz and a neglectable peak at about 450 Hz.

The natural frequencies of composite specimens with different cross-sectional designs were determined in order to evaluate the influence of additional CLD treatments. However, a quantitative comparison is not appropriate, as the diameter increases between the groups, each with a similar outer geometry (No CLD to CLD_{out} to $\mathrm{CLD}_{in,out}$) (see section 6.2.1).

Therefore, the first natural frequencies were compared qualitatively for the different groups, supported by the stiffness-weight-ratio (see Fig. 16). The free specimen length of $l = 960\,\mathrm{mm} \pm 3\,\mathrm{mm}$ was kept constant for all investigated composite structures. The first natural frequency varies with $f_1 = 50\,\mathrm{Hz} \pm 6\,\mathrm{Hz}$ only slightly for all investigated specimens. The increasing outer dimensions between group 'NoCLD' and 'CLD_{out}', each represented by concept A and B, is demonstrated by an increase in the stiffness-weight-ratio, respectively.

However, a clear increasing stiffness-weight-ratio also implies that the VEM damping layer is too stiff. The

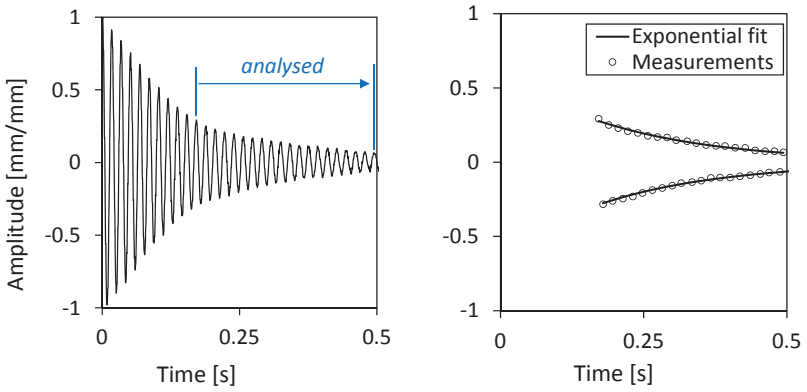

(a) Normalized free decay for the analysed period range $P_{10} < P_{analysed} < P_{30}$.

(b) Comparison of measured data with its exponential fit in the range $P_{analysed}$.

Figure 14: Normalized free decay (a) of a vibrating composite cylinder with the cross-sectional design concept B, on which an exponential decay curve was fitted (b).

VEM simply transfers the shear stresses to the floating and stiff constraining layer and therefore unintentionally contributes to the structural stiffness, instead of deforming in shear. A reduction of the VEM shear stiffness is thereby assumed to enhance the shear deformation and thus the energy dissipation. A variation in the VEM stiffness will be discussed in more detail in section 6.2.3. However, the application of the CLD treatment to the inside of the cylinder (concepts B and C) is verified to be less effective due to an unchanged stiffness-weight-ratio. Furthermore, the application of shear webs parallel to the loading direction is not an effective method to increase the stiffness with respect to weight, demonstrated by a decreased stiffness-weight-ratio (concept A vs. D.0 | B vs. E.0 | C vs. F.0). The purely cylindrical cross section is therefore the most effective with regard to

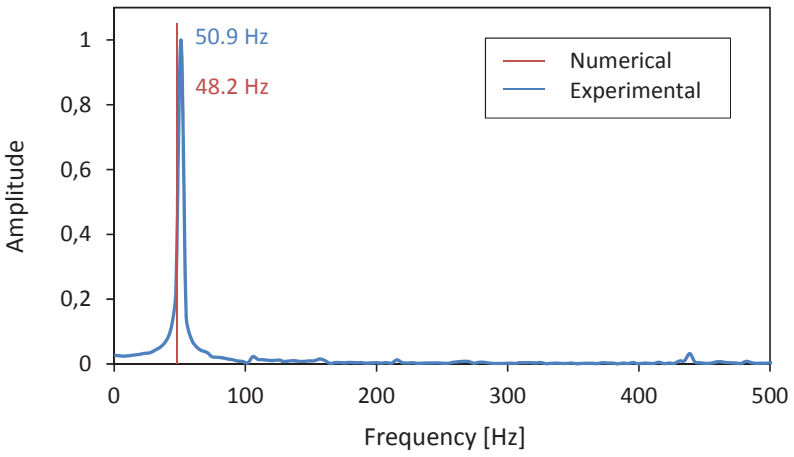

Figure 15: Results of the Fourier analysis with regard to the experimental time history of the cross-sectional concept A for the range $P_{10} < P_{analysed} < P_{30}$.

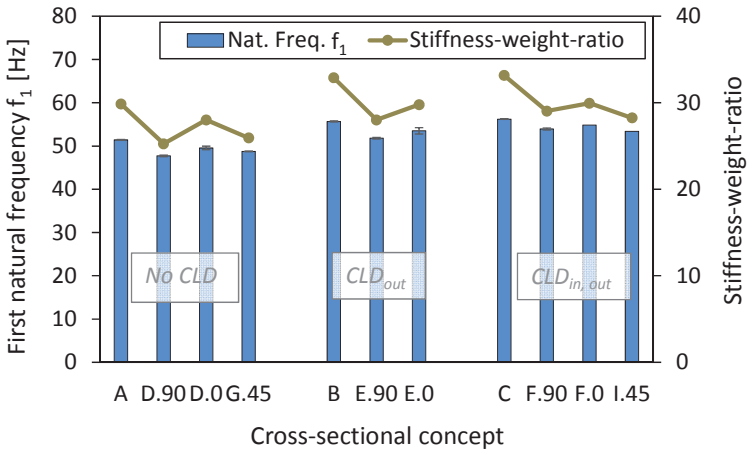

Figure 16: Results of the first natural frequency f_1 for all cross-sectional design concepts in relation to its stiffness-weight-ratio.

the investigated cross-section designs, represented by concept A, B and C and its highest natural frequency f_1 within each group.

Shear webs with a 90 ° orientation (concept D.90, E.90 and F.90) lead to lower natural frequencies compared to shear webs in 0 °, due to the vanishing contribution to the structural stiffness but increase in weight. A shear web in 90 ° may therefore only be used for the application of CLD treatments close to the neutral plane in order to increase the damping of a vibrating composite cylinder.

Although a considerable potential of the CLD treatment is assumed to be untapped due to the high VEM stiffness, the resulting damping is shown for all cross-sectional designs in Fig. 17.

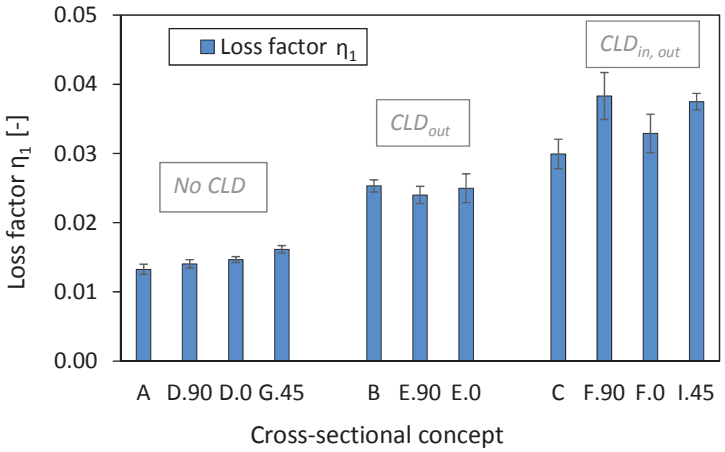

Figure 17: Results of the modal loss factor η_1 related to the first bending mode.

As expected, the damping of composite cylinders without CLD treatments (concept A, D and G) is significantly below the damping of specimens with a CLD treatment on the outside (concept B and E), followed by specimens with CLD treatments on the in- and outside (concept C, F and I). The reference design concept A exhibits

thereby the lowest damping. In the group of specimens without VEM damping layers, a slight increase is observed for specimens with shear webs (design concepts D and G).

Furthermore, the specimen with two shear webs, inclined by $\pm 45\,^\circ$ to the loading direction (concept G.45), shows slightly higher damping compared to specimens with one shear web parallel to the loading direction (concept D.0). This may be explained by the fibre direction of $\varphi = \pm 45\,^\circ$ of the shear webs and its matrix dominated, high damping properties.

A significant increase in damping is achieved by introducing CLD treatments. An application on the outside of the cylinder (concept B and E) leads to an increase of ca. 90 %. A shear web parallel to the loading direction (concept E.0) has no effect on the loss factor at this level of damping, generated by a CLD treatment on the outside of the structure. The highest damping, compared to the reference concept A, is observed for specimens with CLD treatments on the in- and outside (concept C, F, and I), corresponding to the largest amount of applied VEM. The damping increases by ca. 130 % for concept C and ca. 190 % for concept F.90.

The specimen with the highly complex cross-sectional design I.45 leads to an increase of ca. 180 %. Only a slight increase in damping is observed for concept F.0 compared to C, as only a small portion of VEM is located within the neutral plane, experiencing shear, compared to F.90. As expected, the highest damping is observed for concept F.90, which represents the largest amount of VEM subjected to shear deformation: at the shear web close to the neutral plane and along the circumference, far away from the neutral axis.

It is expected that composite structures, which are composed of viscoelastic materials, show the same trend of frequency dependent behaviour as each individual material involved (see Fig. 9 and 11). Therefore, the modal damping of all cylindrical composite specimens was determined at three different frequencies by attaching tip masses. The results are plotted in Fig. 18.

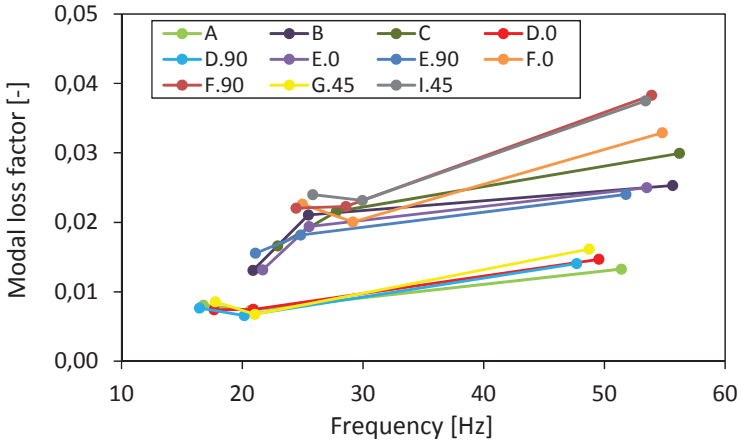

Figure 18: Variation of the test frequency for all cross-sectional design concepts at room temperature.

The same trend of frequency dependent damping is observed compared to the raw materials used for the cylindrical composite structure: GFRP and VEM. The damping decreases with decreasing frequencies. Furthermore, the significant damping enhancement by introducing CLD treatments is clearly demonstrated for a frequency range between approximately 20 Hz and 60 Hz.

As the modal loss factor η_1 was determined for all investigated specimens at varying frequencies with 52 Hz $\pm$ 5 Hz

(see Fig. 16), the loss factors and natural frequencies were normalized by the results of the reference concept A in order to enable comparability. The ratio of normalized damping to the normalized frequency therefore describes an equivalent damping, which refers to the first natural frequency of concept A. The results are shown in Fig. 19.

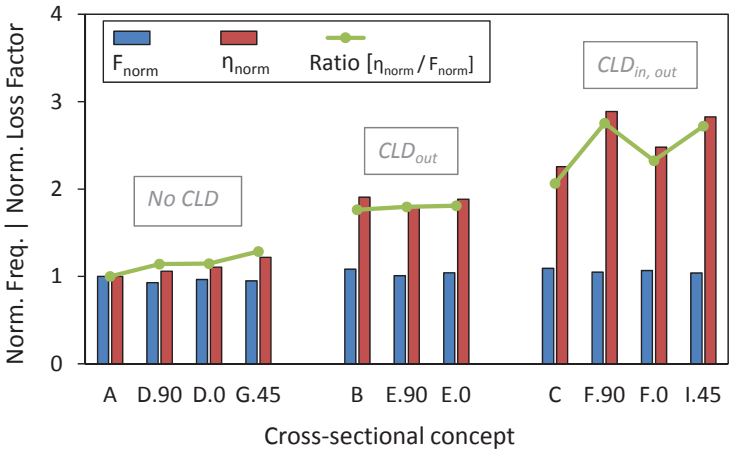

Figure 19: Results of the normalized frequency and loss factor (with respect to the reference design concept A) and its related damping-frequency-ratio.

The equivalent damping represents the damping behaviour at a frequency $f_{1_A} = 51.4\,\text{Hz}$ and therefore facilitates comparability between the specimens. Only slight changes in the trend are observed between the equivalent damping (Fig. 19) and the results of the first loss factor η_1 (Fig. 17). In general, the damping increases directly proportional to the amount of VEM used for the CLD treatment.
For specimens without CLD treatments, the damping slightly increases by adding shear webs with a fibre orientation of $\varphi = \pm\,45\,°$, as its matrix dominated damping values enhances the overall damping. As expected, the increase in number of shear webs from 1 to 2 leads to an increase in the equivalent damping (concept D.0 to G.45). However, this effect is hardly observed for specimens with a CLD treatment on the outside (concept B, E.90 and E.0) due the dominating effect of VEM. The equivalent damping increases even further when considering a CLD treatment to the in- and outside (concept C, F.90, F.0 and I.45). The highest damping is

Table 4: Increase in damping with regard to the reference design concept A or the representative design concept of each group A, B or C.

Increase in	Cross-sectional design concept										
damping [%]	Group 'No CLD'				Group 'CLD$_{out}$'			Group 'CLD$_{in,out}$'			
with respect to ...	A	D.90	D.0	G.45	B	E.90	E.0	C	F.90	F.0	I.45
... A	Ref.	14.2	14.7	28.4	76.2	79.7	81.0	106.3	175.3	132.6	172.0
... A, B or C	Ref.				Ref.	2.0	2.7	Ref.	33.4	12.7	31.8

Table 5: Results of the numerical frequency analysis of the cross-sectional design concept A.

Mode	1	2	3	4	5	6	7	8
Frequency [Hz]	48.2	48.2	285.1	285.1	468.2	699.6	699.6	708.3
Mode type	Bending (out-of-plane)				Torsion	Bending (in-plane)		Axial

therefore observed for concept F.90, demonstrating the potential of the additional CLD treatment close and in parallel to the neutral plane.

The percentage-wise increase of the damping is represented in Tab. 4, with regard to either the reference design concept A or the representative design concept of each group A, B or C.

6.2.3 Comparison of numerical and experimental results

The experimental results were used to verify the numerical model, which predicts the first natural frequency f_1 and the related modal damping η_1 of the cylindrical composite structures with varying cross-sectional design (see section 4). The experimental and numerical results of the first natural frequency are presented in Fig. 20. A good correlation of the experimental and numerical results of the first natural frequencies for all investigated cylinder concepts is observed with the trend of a slight under-prediction by the FEA. The consistency of the under-prediction indicates an inaccuracy related to the material properties or the manufacturing process. The material properties, used for the numerical analysis, may be too conservative although the same GF and resin were utilized (see section 3.3).

Another source of error may be related to the manufacturing process: constant change of fibre direction by a few degrees or a slightly different layer thickness may result in a lower predicted natural frequency.

In order to verify the experimental results of the Fourier analysis, demonstrating the dominance of the first flexural mode, a numerical frequency analysis was carried out (see Tab. 5). As expected, the numerically

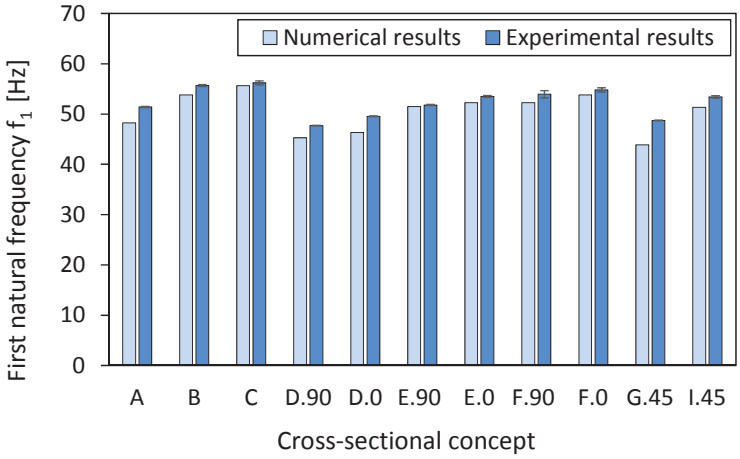

Figure 20: Numerical and experimental results of the first natural frequencies.

and experimentally determined natural frequencies of the first flexural mode coincide with an error of about 5 %, demonstrated for the cross-sectional design concept A (see Fig. 15). The observed peak at about 450 Hz is associated with the first torsional mode. However, the intensity is very low, so that any influence may be neglected. The comparison of the experimental and numerical damping is based on the presented loss factors in Fig. 21. The numerical predicted loss factors are considerably lower than the experimental values. However, the same trend of the damping is captured by the simulation for all cross-sectional design concepts, although the differences increase disproportionally with the application of VEM damping layers (concept B, C, E, F and I). The predicted damping for concepts without CLD treatments are maximum 39 % lower than the experimental results (concept G.45), compared to maximum 64 % for concepts with CLD treatments (concept F.90). The increased mismatch may be attributed to a much softer clamping area, caused by the continuous VEM, compared to concepts without CLD.

Although metallic inserts were used to allow each end section to be compressed and clamped, a continuous VEM layer can deform and creep in axial direction of the specimen, leading to a reduced clamping pressure and therefore to an increased friction damping. These clamping effects, substantially increased by an applied VEM, lead to higher experimental damping values, which are not captured in the numerical model.

Furthermore, a variation in the tolerance of the lathed end section of the composite cylinders may lead to different clamping conditions and therefore to a different contribution of friction damping. An enhanced specimen stiffness may also result in an increase in clamping effects and therefore in damping. The horizontal displacement of the metallic clamping were measured, while specimens with different bending stiffness were loaded: a maximum displacement of 0.005 mm or 0.06 mm was observed at a bending load of 0.85 kN or 1.6 kN for concepts A or I, respectively. This leads to an enhanced friction damping relative to the strong table and therefore an increase in the measured decay.

A correction factor may be applied in further investigations to account for the discrepancies in the clamping area mentioned above, causing differences between the experimentally and numerically determined loss factor. Several displacement measurements at various locations in the clamping area may therefore be considered in

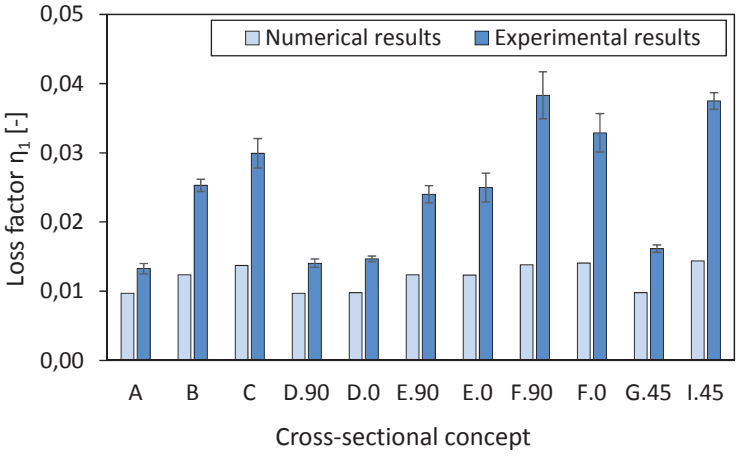

Figure 21: Numerical and experimental results of the modal loss factor related to the first bending mode.

order to understand the phenomenon and to determine the relative displacement between the points of interest. However, the highest damping was observed for the specimen with the cross-sectional design concept F.90. This result is expected, since a large area of VEM is well located where the largest shear stresses appear (see section 3.2). As mentioned in section 6.2.2, the VEM DYAD 601 is seemingly too stiff in order to allow sufficient shear deformations. Instead, the occurring stresses may simply be transferred to the constraining layer, leading to an increase in structural stiffness but no damping. Therefore, the effect of the VEM stiffness on the modal damping η_1 and first natural frequency f_1 was numerically investigated for the design concept F.0 and F.90 using the modal strain-energy method. A decrease of the storage modulus G', while keeping the loss factor η constant, will relatively adjust the loss modulus G'' by

$$\eta = \frac{G''}{G'} \quad . \tag{10}$$

The results are presented in Fig. 22.

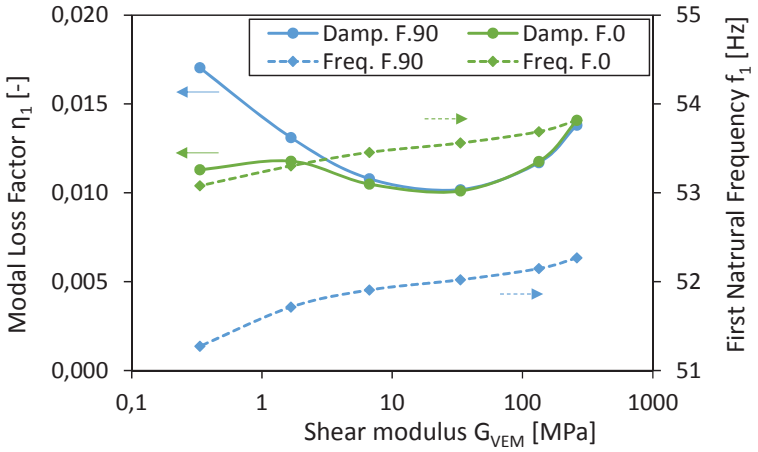

Figure 22: Effect of the shear modulus of the VEM on the first natural frequency f_1 and the related structural modal loss factor η_1 for the concepts F.0 and F.90.

As expected, the reduction of the VEM stiffness results in the same constant decrease of the first natural frequency for both concepts. The initial decrease in loss factor is unexpected, but may be explained by the non-appearance of shear deformation within the VEM, located on the circumference. The trend is the same for both concepts, where the only difference is the orientation of the shear web.
However, the modal loss factor increases for both concepts below the shear modulus G_{Vem} of about 30 MPa, but slightly decreases with a shear modulus lower than 1 MPa only for concept F.0. In contrast, the loss factor for concept F.90 continuously increases and exceeds its initial value of $\eta_1 = 0.0138$. The shear deformed VEM is plotted in the x,z plane in Fig. 23 for the concept F.90, when a shear modulus of $G = 0.33$ MPa was used. The shear deformation of the VEM is equally distributed between the top, bottom and middle section, close to the neutral plane of the composite cylinder. This is expected as the four individual composite sections (1x Host structure, 2x inner CL, 1x outer CL), only coupled by the VEM, deform the same way as the load carrying host structure. The deformation plot verifies the higher loss factor compared to the concept F.0 with its shear web

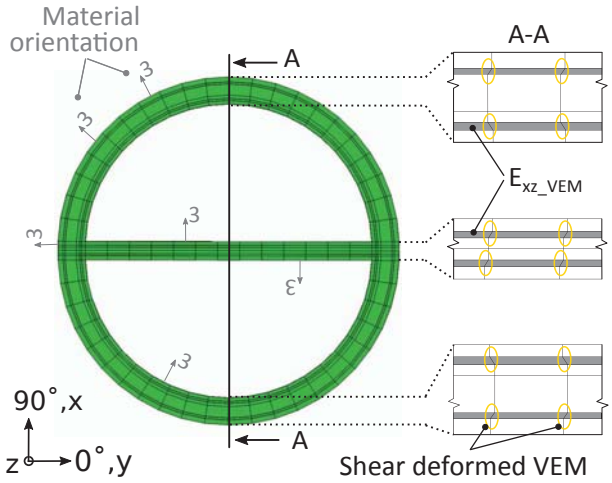

Figure 23: Numerical model of concept F.90 (vibrating in 90 °) with its shear deformed VEM layers (E_{xz}).

oriented perpendicular to the neutral plane. The efficiency of a CLD treatment within the neutral plane has hereby been demonstrated successfully.

7 Conclusion

The present paper provides a method for the design of highly damped cylindrical composite structures under dynamic loading with passive CLD treatments, which can be used as sound basis for the design of the next generation of composite power pylon arms. The enhanced damping design is demonstrated by the experimental and numerical investigation of various cross-sectional design concepts, which differ in their complexity and weight. Furthermore, the manufacturing of generic composite cylinders by filament winding, the experimental modal analysis and the determination of the modal damping is thoroughly described.

A numerical damping model based on the modal strain-energy method finally confirms the trend of the experimental results with regard to the first natural frequency f_1 and the related modal loss factor η_1. Depending on the design requirements with respect to stiffness and weight, different levels of damping can be achieved in relation to cost and manufacturing capabilities.

The application of circumferential CLD treatments lead to a considerable increase of weight and wall thickness, while keeping the cross-sectional complexity constant. In contrast, shear webs with or without CLD treatments lead to an increase of the cross-sectional complexity, while keeping the change in stiffness and mass low. The maximum damping is achieved for the cross-sectional design concept F.90 with its high complexity and weight. However, a CLD treatment close to the neutral plane of the cylindrical composite structure is found to significantly increase the modal damping. A low stiffness of the VEM is thereby of crucial importance for a maximum shear deformation and damping. The main conclusions are drawn as follows:

- The damping of cylindrical composite structures can be enhanced by integrating shear webs (max. $+28\,\%$) without applying CLD treatments. The complexity of the cross section thereby increases directly proportional, causing extra costs and effort during manufacturing.

- The application of circumferential CLD treatments leads to an increase in damping of max. 106.3 % (concept C) compared to the reference design concept A.
- An additional increase in damping is observed by max. 33 % (concept C to concept F.90), when applying CLD treatments in parallel and close to the neutral plane.
- The damping prediction of clamped composite cylinders, using the modal strain-energy method, leads partly to large deviations depending on the amount of applied VEM, due to different clamping conditions. The damping of specimens without CLD treatments can be predicted with deviations of max. 39 %, due to the disregard of friction damping in the clamping zone.

Acknowledgement

Thanks to Prof. M. Gude and Prof. N. Modler from the Institute of Lightweight Engineering and Polymer Technology of TU Dresden for their kind cooperation in manufacturing the cylindrical specimens. The authors are also indebted to The Soundcoat Company, providing the viscoelastic material for the vibrational tests.

Declaration of conflicting interests

The author(s) declared no potential conflicts of interest with respect to the research, authorship and/or publication of this article.

Funding

The author(s) disclosed receipt of the following financial support for the research, authorship and/or publication of this article: This research is supported by Innovationsfonden Denmark via the project Power Pylons of the Future (PoPyFu) in collaboration with Bystrup and Tuco Marine ApS, which are gratefully acknowledged.

References

[1] Yang F, Yang J, Zhang Z, Xing H (2012) Dynamic Simulation on a Broken Test of Conductors. *Procedia Engineering, International Conference on Advances in Computational Modeling and Simulation* 31: 435-440.

[2] Dang HX, Yang FL, L XM, Yang JB (2012) Galloping Characteristics of Conductor Accreted with Crescent-Shaped Ice. *Applied Mechanics and Materials* 226-228: 158-161.

[3] Hujare PP, Sahasrabudhe AD (2014) Experimental Investigation of Damping Performance of Viscoelastic Material Using Constrained Layer Damping Treatment. *Procedia Materials Science, International conference on Advances in Manufacturing and Materials Engineering, Kuala Lumpur, 2014* 5: 726-733.

[4] Trindade MA (2011) Experimental analysis of active-passive vibration control using viscoelastic materials and extension and shear piezoelectric actuators. *Journal of Vibration and Control* 17: 917-929

[5] Sasikumar KSK (2015) Vibration control of Beam with Composite Constrained Layer Treatment. *International Journal of Latest Trends in Engineering and Technology* 5: 176-184

[6] Fotsing ER, Sola M, Ross A, Ruiz E (2012) Lightweight damping of composite sandwich beams: Experimental analysis. *Journal of composite materials* 47: 1501-1511

[7] Gallimore CA (2006) Passive Viscoelastic Constrained Layer Damping Application for a Small Aircraft Landing Gear System. *Master thesis* Virginia Polytechnic Institute and State University, 30.09.2008

[8] Ruzicka J (1961) Damping Structural Resonances Using Viscoelastic Shear-Damping Mechanisms: Part IDesign Configurations. *Journal of Engineering for Industry* 83: 403-413

[9] March ER, Hale LC (1998) Damping of Flexural Waves With Imbedded Viscoelastic Materials. *Journal of Vibration and Acoustics* 120: 188-193

[10] Huang CY, Tsai JL (2015) Characterizing vibration damping response of composite laminates containing silica nanoparticles and rubber particles. *Journal of Composite Materials* 49: 545-557

[11] Zhang SH, Chen HL (2006) A study on the damping characteristics of laminated composites with integral viscoelastic layers. *Composite Structures* 74: 63-69

[12] Wollmann T, Modler N, Dannemann M, Langkamp A, Nitschke S, Filippatos A (2017) Design and testing of composite compressor blades with focus on the vibration behaviour. *Composites Part A: Applied Science and Manufacturing* 92: 183-189

[13] Filippatos A, Dannemann M, Wohlfahrt D, Modler N (2016) Design of highly damped fibre-reinforced lightweight mast for automated storage systems in logistics. *In Proceedings of the 23nd International Congress on Sound and Vibration ICSV* 10.-14.July 2016, Athens

[14] Kliem M, Rueppel M, Høgsberg J, Berggreen C (2017) Damping properties of Nanoclay modified Glass and Aramid composites at low temperature and low frequencies. *submitted* 2017.

[15] Skouboe H (2017) Power pylon of the Future, BYSTRUP Design, *E-mail: hs@bystrup.dk* 16.11.2017.

[16] DIN EN 50341-1:2013-11 (2013) Overhead electrical lines exceeding AC 1 kV - Part 1: General requirements - Common specifications. *Beuth Verlag* 2013-11

[17] Trindade MA, Benjeddou A (2002) Hybrid Active-Passive Damping Treatments Using Viscoelastic and Piezoelectric Materials: Review and Assessment. *Journal of Vibration and Control* 8: 699-745. 10.1177/1077546029186

[18] Klein B (2013) Leichtbau-Konstruktion: Berechnungsgrundlagen und Gestaltung . *Springer Vieweg* 10th edition

[19] Mengjin W (1990) Conductor Galloping and Control Measures. *High Voltage Engineering* 4: 1-22

[20] Moreira RAS, Rodrigues JD (2006) Partial Constrained Viscoelastic Damping Treatment of Structures: A Modal Strain Energy Approach. *International Journal of Structural Stability and Dynamics* 6: 397-411.

[21] Cortes F, Elejabarrieta MJ (2008) Structural vibration of flexural beams with thick unconstrained layer damping. *International Journal of Solids and Structures* 45: 5805-5813.

[22] Dannemann M (2012) Zur vibroakustischen Auslegung von Faserverbund-Leichtbaustrukturen. *Dissertation* Technische Universitaet Dresden, 2012.

[23] Gurung CB, Yamaguchi H, Yukino T (2003) Identification and Characterization of Galloping of Tsuruga Test Line Based on Multi-Channel Modal Analysis of Field Data. *Journal of Wind Engineering and Industrial Aerodynamics* 91: 903-924.

[24] Kliem M, Høgsberg J, Wang Q, Dannemann M (2017) Characterization of clay-modified thermoset polymers under various environmental conditions for the use in high-voltage power pylons. *Advances in Mechanical Engineering* 9: 1-16.

[25] Soundcoat (2017) Data sheet of damping products. *Material data sheet* Retrieved from http://www.soundcoat.com/soundcoatdamping.pdf

[26] Lin W (2016) Creation and Evaluation of Polymer/Multiwall Carbon Nanotube Films for Structural Vibration Control and Strain Sensing Properties. *Dissertation* Florida International University, 2016. 10.25148/etd.FIDC001208

[27] Pai R, Lumsdaine A, Parsons M (2004) Design and Fabrication of Optimal Constrained Layer Damping Topologies. *Proceedings Volume 5386, Smart Structures and Materials: Damping and Isolation* 2004, doi: 10.1117/12.540065

[28] Peters S (2011) Composite Filament Winding. *ASM International* 1st Edition.

[29] Skinner ML (2006) Trends, advances and innovations in filament winding. *Reinforced Plastics* 50: 28-33.

[30] Ungar EE, Kerwin M (1962) Loss factors of viscoelastic systems in terms of energy concepts. *The Journal of the Acoustical Society of America* 34: 954.

[31] ABAQUS (2017) ABAQUS Documentation. *Dassault Systmes* Providence, RI, USA.

[32] Qi X, Zhao X, Rose JL (2010) Ultrasonic guided wave simulation toolbox development for damage detection in composites. *AIP Conference Proceedings* 1211, 1095, doi.org/10.1063/1.3362163

[33] Kliem M (2017) Data for: Damping investigation of cylindrical composite structures with enhanced damping properties. *Mendeley Data* doi:10.17632/jxy3m76dg5.1

[34] Ehrenstein GW, Riedel G, Trawiel P (1998) Praxis der Thermischen Analyse von Kunststoffen. *Hanser-Verlag, Muenchen, Wien.*

[35] Gohl W, Spies KH (2003) Elastomere Dicht- und Konstruktionswerkstoffe: Gummitechnik, Richtlinien und Anwendungsbeispiele für Konstruktion und Praxis. *Expert Verlag*, 5th edition.

[36] Melo JDD, Radford DW (2005) Time and temperature dependence of the viscoelastic properties of CFRP by dynamic mechanical analysis. *Composite Structures* 70: 240-253.

[37] Beards CF (1996) Engineering Vibration Analysis with Application to Control Systems. *Wiley - Technology and Engineering*, 1st edition.

[38] Leibolt MF (2009) Noise control of an acoustic cavity coupled with a vibrating plate treated with a spatially varying constrained viscoelastic layer. *Dissertation* University of Maryland, 2009.

[39] Turi EA (1997) Thermal Characterization of Polymeric Materials. *Academic Press, Brooklyn, New York*, 2nd edition, P.529

[40] Berthelot JM, Sefrani Y (2004) Damping analysis of unidirectional glass and Kevlar fibre composites. *Composites Science and Technology* 64: 1261-1278

[41] Adams RD, Bacon DGC (1973) Effect of Fibre Orientation and Laminate Geometry on the Dynamic Properties of CFRP. *Journal of Composite Materials* 7: 402-428.

P4

Mitigation of conductor line galloping by enhanced damping in composite power pylons

Mathias Kliem, Daniel Johansen, Jan Høgsberg

- submitted -

Mitigation of conductor line galloping by a direct cable-connection to non-conductive composite power pylons

Mathias Kliem[1*], Daniel Johansen[1], Jan Høgsberg[1].

[1]Department of Mechanical Engineering, Technical University of Denmark, Lyngby, Denmark

Abstract

Steel lattice towers with suspended insulator strings are typically used to carry high-voltage overhead transmission lines. The installation of non-conductive power pylons made of glass fibre reinforced plastics enables a direct cable-pylon connection, as the composite structure acts as an unibody insulator. At the same time, wind-induced vibrations, such as the severe cable vibration phenomenon galloping, will consequently be directly transferred to the slender composite mast structure, potentially leading to extensive damage. The aim of the study is therefore to investigate the galloping behaviour of iced conductor lines with regard to different cable support conditions. Furthermore, additional damping in the composite power pylon structure is assumed to mitigate conductor line galloping and therefore reduce the risk of phase flash-overs between adjacent conductor lines. A numerical galloping simulation is carried out in order to evaluate the effect of a rigid cable-pylon connection with enhanced damping properties on the cable vibration amplitudes. A pylon-cable system, consisting of 3 x 300 m spans, is investigated. It was found that the support conditions of the conductor lines have a significant influence on the galloping mode, the vibration amplitudes and the orientation of the characteristic galloping ellipse. The addition of damping to the pylon decreases the vibration amplitudes slightly and leads to a re-orientation of the galloping ellipse.

Keywords: Non-conductive composite power pylons; Galloping conductor lines; Numerical galloping simulation; Direct cable-pylon connection

1 Introduction

National electrical grid systems are facing significant transformations: The increasing demand for alternative and renewable energy solutions and, at the same time, the ageing of high-voltage infrastructure are just a few examples, demonstrating the need for renewed and expanding electrical grid systems [1, 2, 3, 4]. As a result, a beautification of the 400 kV network has been decided by a national directive 2008 in Denmark [5]. The standard steel lattice towers with its long insulator strings, basically unchanged in visual their appearance for decades and dominating today's landscape, are planned to be replaced by power pylon

*Corresponding author: mkliem@mek.dtu.dk

structures based on composite materials. The use of non-conductive composite materials, such as glass fibre reinforced plastics (GFRP) or aramid fibre reinforced plastics (AFRP), allows an innovative design and a significantly reduction in size, due to the possibility of integrating the insulators directly on the pylon arm. However, this direct and stiff connection of the conductor lines to the non-conductive composite structure may lead to an increased dynamic interaction.

Wind-induced vibrations and motions, such as the cable vibration phenomenon called galloping, may therefore be directly transferred to the power pylon, potentially leading to structural damage due to excessive vibration amplitudes at resonance [6]. Conductor line galloping is a severe cable vibration phenomenon typically occurring at temperatures below the freezing point and at frequencies between 0.1 Hz and 1 Hz with large amplitudes of up to 0.03 times the span length [7, 8]. The aerodynamic instability is initiated by asymmetric ice aggregations along the conductor, when subjected to moderate or strong cross winds. The galloping motion typically describes a vertically oriented ellipse with a small horizontal component, also known as the galloping ellipse. Depending on the wind conditions, the ice aggregations and the related dynamic characteristics of the conductor lines, a single loop or a few loops of a standing wave may be represented [8] over a time period of up to 24 h. Thus, fatigue damage in the cable, the structure or the clamping may potentially be induced. The design for the severe galloping vibration phenomenon is therefore an important dynamic load case for high voltage power pylons.

Furthermore, the galloping instability is a governing factor in determining the spacing between the conductors. A mitigation in galloping amplitudes may potentially allow a decrease in spacing between adjacent phase conductors due to a reduced risk of phase flash overs. This may consequently lead to a desired downsizing of the composite power pylon, giving it a smaller footprint in its environment. A mitigation of conductor line galloping is assumed to be achieved by the direct cable-tower attachment, compared to the much more flexible standard cable connection with insulator strings [9].

Additional damping in the load carrying pylon structure, potentially obtained by using materials with enhanced damping properties or by the application of damping treatments, may further lead to a mitigation of wind induced galloping vibrations in the cable. Therefore, special regard is given to the dynamic mechanical material behaviour of the non-conductive composite materials, like GFRP and AFRP, used for the power pylon structure. Due to the viscoelastic nature of the polymer resin material, the damping behaviour is up to several magnitudes larger compared to traditional engineering materials such as metals [10]. The damping properties of various polymer resin materials and composite materials have thoroughly been investigated at environmental conditions typical for conductor line galloping [11, 12]. The damping depends highly depends on the fibre direction of the laminate. The lowest damping is obtained in the direction parallel to the fibres, whereas the damping is maximized at fibre angles $\varphi \approx 30\,^{\circ}$ - $45\,^{\circ}$. Furthermore, the application of additional damping treatments may enhance the overall damping behaviour of the entire structure. The passive constrained layer damping treatment, suitable for high-voltage applications, was experimentally and numerically studied on generic composite mast substructures [13].

Several analytical, numerical and experimental investigations have been carried out on galloping conductor line cables over the last 90 years, when galloping

was observed and documented the first time. A fundamental formulation of galloping was proposed by Den Hartog, describing the vertical oscillation mechanism of asymmetrically iced conductor lines [7]. A potential mitigation of cable galloping was studied using external devices, such as spiral wires and circular rings, locally mounted to the cables [14]. Other options to reduce galloping effects are seen in the use of twisted conductors, the reduction of the span length and the adjustment of the cable tension to a certain level, minimizing a potential lateral movement of the conductor line [15].

To the best knowledge of the authors, an investigation on a potential mitigation of conductor line galloping by connecting the cable directly to the non-conductive power pylon has not been conducted yet. The aim of this study is therefore to analyse the effect of different cable support conditions and additional damping of the pylon on the vibration amplitudes of galloping conductor lines. A numerical galloping analysis of a representative 3 x 300 m cable-pylon system is carried out in order to compare the resulting cable vibration behaviour with respect to the different support conditions and properties.

2 400 kV network with improved visual design

The required expansion and upgrade of national grid systems, due an ageing infrastructure or the increasing demand for renewable energies, provides the opportunity to install visually improved power pylons compared to standard steel lattice towers, which are basically unchanged in their design for the last 60 years (see Fig. 1).

The use of the non-conductive composite materials for the design of high-voltage power pylons offers several advantages [17] compared to steel:

1) Visually improved and compact design.

Figure 1: Visual impact of the composite-based power pylon (computer aided image) [16].

2) Cost competitive due to reduced transportation effort, a monopile foundation and a shorter construction time.

3) Unibody insulator by using non-conductive composite materials like GFRP and AFRP.

4) Enhanced damping properties due to the viscoelastic nature of the polymer.

The composite pylon and the related span properties and dimensions are described in more detail in the following sections.

2.1 Composite power pylon

The composite power pylon is developed in a multi-material design, exploiting the unique properties of each individual material. The pylon consists of a tubular and tapered steel tower, carrying a pair of cantilevered, tapered and hollow composite cylinders at which three pairs of double cable bundles are directly attached, equally distributed at each side (see Fig. 2). The composite cross arms with an inclination of 30 ° are designed for static and dynamic bending loads in x- and y- direction, such as the static self weight of the (iced) conductor line and the dynamic wind or galloping loads [18].

The laminate of the cylindrical composite structure with the stacking sequence $[\,0\,^\circ, \pm 20\,^\circ, 0\,^\circ]_n$, shown in Fig. 3, gradually decreases in thickness from a

Table 1: Dimensions and properties of composite pylon.

Parameter	Symbol	Unit	Value
Height tower	h_T	m	21.6
Wall thickness tower	t_T	m	30.0
Wall thickness cross arm	t_A	mm	8.0 - 29.0
Length cross arm	l_A	m	13.6
Inclination cross arm	α_A	(°)	30
Lamina orientation (cross arm)		(°)	$[\,0, \pm 20, 0]_n$
Lamina thickness (quadriaxial woven fabric)	t_L	mm	1.0
	E_x	GPa	34.9
Smeared lamina properties	E_y	GPa	10.8
(based on Fig. 3)	G_{xy}	GPa	5.6
	ν_{xy}	-	0.43

thick-walled root-end section ($t_{A_1} = 29\,\text{mm}$) to a thin-walled shell-like zone at the tip of the arm ($t_{A_2} = 8\,\text{mm}$).

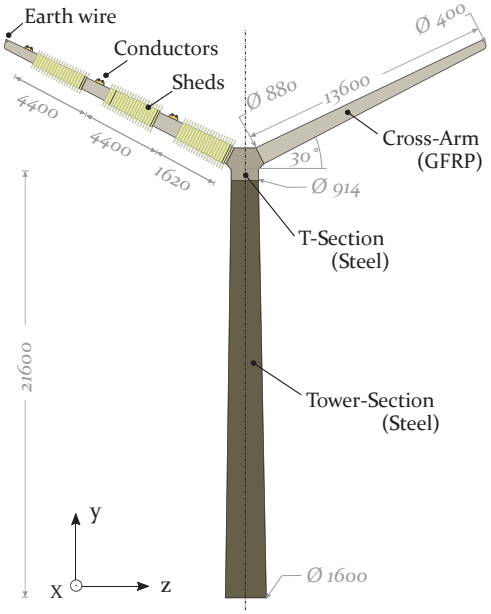

Figure 2: Multi-material design of the power pylon.

The pylon structure is designed for maximum stiffness in order to prevent any resonant vibrations of the structure due to galloping conductor lines at frequencies between 0.1 Hz and 1 Hz [8]. At the same time, enhanced damping properties of the composite cross arms are desired to potentially damp wind induced cable vibrations, which are directly transferred to the pylon due the rigid cable-tower connection. Furthermore, damping of the composite cross arm is assumed to mitigate conductor line galloping and thereby prevent any structural damage. The dimensions and mechanical properties of the composite power pylon structure are listed in Tab. 1. The material properties of the representative unidirectional (UD) GFRP lamina are given in the literature [19].

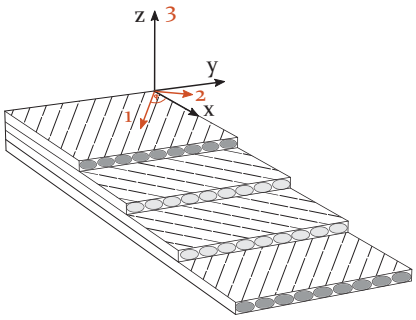

Figure 3: Global coordinate system (COS) and local material COS.

Table 2: Mechanical properties and dimensions of iced conductors similar to the properties of an ACSR conductor line type 'Martin' [20].

Parameter	Symbol	Unit	Value
Axial stiffness	EA	10^6 N	20.23
Torsional rigidity	GI	$\mathrm{Nm}^2/\mathrm{rad}$	101.0
Diameter bare conductor	d_c	10^{-3} m	28.6
Height of the D-shaped ice [21]	h_{ice}	10^{-3} m	63.5
Mass per unit length (incl. ice)	m	kg/m	2.38
Moment of inertia per unit length	J	10^{-4} kg m	3.33

2.2 Representative span properties and dimensions

The composite power pylon is designed to carry transmission lines with two 400 kV circuits on each side. The initial span length is defined by 300 m, using ACSR conductor lines of the type 'Martin' [9]. The physical properties of iced conductor lines with a similar characteristic are given in Tab. 2. A typical sag configuration of a 300 m span at -17.7 °C (0 ° F) was modelled, expecting galloping to happen at temperatures below 0 °C [22].

3 Numerical modelling of cable galloping

Galloping vibrations are sensitive to specific parameters, such as wind velocity, cable sag and cable damping. Any change may affect the vibration characteristics of the conductor line significantly [23]. Several numerical sensitivity studies are reported, investigating the influence of such parameters: galloping vibrations are amplified by an increased wind speed and a decreased cable damping and cable sag [24]. However, strong winds are not necessarily a sufficient condition to initiate conductor line galloping. It is possible that even extremely strong winds may not lead to galloping, when the instability criteria is not met [25].

In this numerical galloping analysis, typical values for the wind velocity, the cable sag and the cable damping were chosen and kept constant throughout the numerical galloping analysis, in order to maintain comparability. The focus of the study is to analyse the effect of different cable support conditions on the vibration behaviour of galloping conductor lines, with regard to the stiffness and damping properties of the supporting structure. It is assumed that a stiff cable-pylon connection in combination with additional damping, introduced for example by a passive constrained layer damping treatment, may lead to mitigation of the galloping vibration amplitudes [26].

A realistic 400 kV three-span system was modelled, containing two cable attachment points (CAP) and one representative conductor line over the whole range of 3 x 300 m. Two cable connections are investigated: 1) cable attachment to a flexible insulator string and 2) cable attachment directly to a stiff power pylon structure. The latter configuration is shown in Fig. 4.

The representative conductor line is thereby rigidly connected to the composite cross arm at its outer most position. The remaining cables are represented by point masses and equivalent spring stiffnesses. The numerical galloping analysis was conducted using the commercially available finite element (FE)

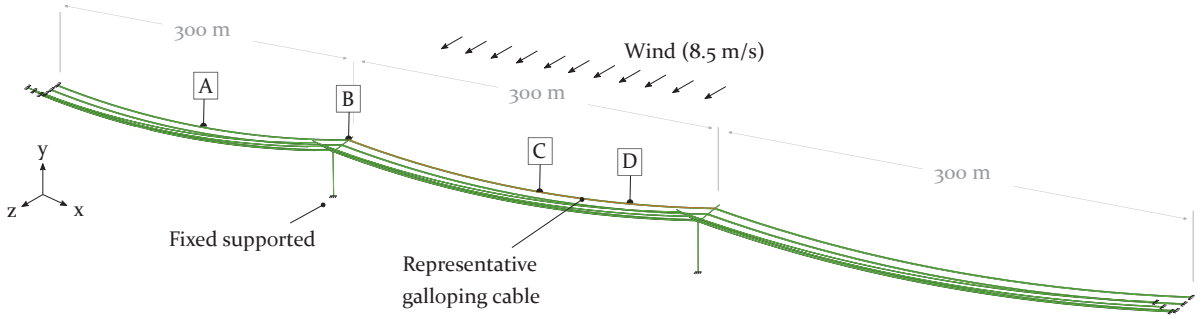

Figure 4: Representative double 400 kV three-span system of 3x 300 m with a representative center-span-cable exposed to aerodynamic forces | Displacements due to galloping are analysed at the center (1/2) of an adjacent cable [A], at the cable attachment point (CAP) of the power pylon [B], at the center (1/2) of the galloping cable [C] and at a quarter (1/4) of the galloping cable [D].

software Abaqus. A user-subroutine, written in Fortran, was used to subject the representative conductor line to aerodynamic loads only on the intermediate 300 m span, thereby initiating a galloping event. Prior to that, the numerically obtained static equilibrium of the pre-tensioned conductor line, calibrated to a typical sag condition, was verified by the analytical expression, calculating the cable sag

$$k = \frac{1}{8}\frac{mgL_x^2}{H_x}\,, \tag{1}$$

where m, g, L_x and H_x are the mass per unit length of the cable, the constant of gravity, the span length and the horizontal cable tension, respectively. Furthermore, a numerical frequency analysis of the single power pylon and the entire three-span system was carried out in order to identify the first natural frequencies. Finally, the galloping analysis of the cable-pylon system was conducted. The numerical analysis is based on the following steps:

1) Static: Pretension of the cable in the global x-direction (see Fig. 4),
2) Static: Application of gravity to the conductor lines and pylon structures in the global y-direction,
3) Dynamic: Galloping analysis by applying aerodynamic loads to the representative mid-span section of the conductor line.

Beam elements with a hybrid formulation were used to model the cable and the pylon, specially recommended for slender structures with a high axial stiffness compared to its bending stiffness [27, 28, 29].

3.1 Conductor line model

The schematic cross section of a conductor line with a D-shaped ice accretion, frequently used in numerical galloping studies [30, 31], is represented in Fig. 5. The related properties and dimensions are listed in Tab. 2. D-shapes with their vertical front facing the wind are found to behave very unstable and are therefore highly prone to galloping [8, 24].

To simplify the D-shaped cross section of the conductor line for the numerical simulation, a circular cross section with equivalent properties is assumed in order to maintain the same axial stiffness EA, torsional rigidity GI, moment of inertia J and the mass per unit length m (see Tab. 3) [20].

Although the level of self-damping in transmission lines is low [33, 34, 35], mainly caused by friction

Table 3: Equivalent properties of the presented iced conductor lines (see Tab. 2) used as input parameters for the numerical simulation [20].

Eq. diamter d_c'	Eq. density ρ'	Eq. E-modulus E'	Eq. G-modulus G'
0.0335 m	2706.36 kg/m^3	$23.02 \cdot 10^9$ Pa	$821.2 \cdot 10^6$ Pa

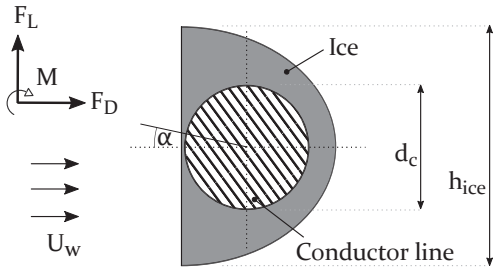

Figure 5: Schematic conductor line with a D-shaped ice accretion and the resulting aerodynamic loads (F_L, F_D and M) due to wind loading with the velocity U_W [32].

between the strands, the damping of additional ice may influence the galloping behaviour and is therefore taken into account in the numerical simulations. Damping ratios in the wide range between 0.4 % and 6 % are typically used to simulate the galloping vibration of iced conductor lines, depending on the type of conductor line and ice accretion [36, 37, 38, 39]. An average damping ratio of $\zeta_c = 3.2\,\%$ was employed, applicable to Abaqus using the Rayleigh model. The mass and stiffness proportional Rayleigh damping coefficients α_R and β_R are described as

$$\alpha_R = \zeta_c \frac{2\,\omega_i\,\omega_j}{\omega_i + \omega_j} \quad , \quad \beta_R = \zeta_c \frac{2}{\omega_i + \omega_j} \ , \qquad (2)$$

with ω_i and ω_j representing the two adjacent angular frequencies of the cable vibration mode, respectively. The aerodynamic loads F_L, F_D and M, acting on an iced transmission line (see Fig. 5), are defined in (3) by the aerodynamic coefficients C_L, C_D and C_M, the density of the air ρ_{air}, the velocity of the wind U_w and the height h of the wind-exposed object.

$$\begin{bmatrix} F_L \\ F_D \\ M \end{bmatrix} = \frac{1}{2}\rho_{air} U_w^2 h \begin{bmatrix} C_L(\alpha) \\ C_D(\alpha) \\ h\,C_M(\alpha) \end{bmatrix} \qquad (3)$$

For conductor lines with a U-shaped ice accretion, the height is equivalent to the diameter of the bare conductor d_c, whereas for D-shaped ice accretions the height h is assumed to be the height of the ice front h_{ice} [40] (see Fig. 5).

The wind velocity is a sensitive parameter with a significant impact on the galloping vibration amplitudes [23]. A wind velocity of $U_w = 8.5$ m/s was used for the numerical galloping analysis, representing a typical wind speed in Denmark [41]. The aerodynamic coefficients C_L, C_D and C_M, experimentally determined in wind tunnel tests for the specific D-shape of the iced conductor lines [21], are shown in Fig. 6.

The aerodynamic coefficients are independent of the wind velocity [42] and only depend on the instantaneous angle of attack α, which is constantly changing due to the dynamics of a galloping system. The angle of attack can be approximated by

$$\alpha \approx \theta_0 - \left(\frac{R\dot{\theta} + \dot{V}}{U_w} \right) , \qquad (4)$$

where R, θ_0, $\dot{\theta}$ and $\dot{V}$ represent the radius of the

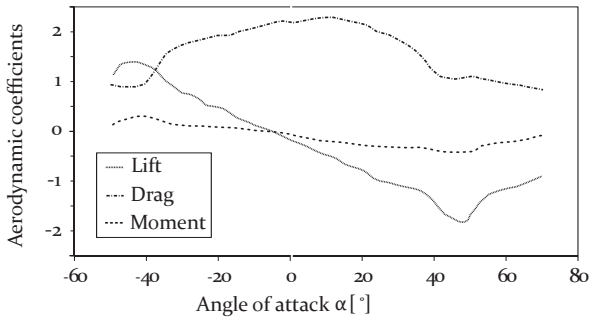

Figure 6: Aerodynamic coefficients for lift C_L, drag C_D and moment C_M as a function of the angle of attack α, specifically determined for an iced conductor line with a characteristic D-shape [21].

bare conductor, the initial angle of attack, the torsional angular velocity and the vertical velocity of the conductor line, respectively [43, 44]. The latter two properties and the nodal displacement and the torsional angle, describing the time dependent state of motion of the conductor line, are obtained for each time step by numerical time integration. A user-defined element (UEL) subroutine is therefore introduced into Abaqus [20], generating user elements without mass and stiffness to share the same nodes as the beam elements used for modelling the conductor line (see Fig. 7).

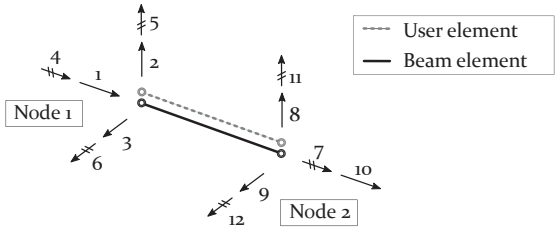

Figure 7: Schematic beam elements and user elements.

As the bending stiffness of cables is usually low, the bending degrees-of-freedom (DoF) may be released (DOF 5 and 6 at Node 1; DOF 11 and 12 at Node 2). Based on a previously conducted sensitivity analysis, a release was found to only change the static deflection of the cable by 0.8 % [45], simultaneously leading to numerical instabilities. The bending DOFs were therefore not released for the conducted numerical galloping analysis.

The implementation of a user-defined element subroutine enables access on the state-of-motion parameters for each cable element at time t and $t + \Delta t$. This allows the calculation and prediction of the angle of attack α by (4) and the application of the aerodynamic loads F_L, F_D and M by (3)at time t and $t + \Delta t$. The Hilber-Hughes-Taylor time integration method is used in Abaqus by default [46]. The user element, introduced by the UEL, is defined to share the same nodes as its equivalent cable element, exhibiting no mass and stiffness. The required input in the Abaqus-specific matrix AMATRX for the UEL, containing the mass matrix M, the damping matrix C and stiffness matrix K, can therefore be set to zero for the user element. The residual load vector RHS, also required as input parameter for the UEL, is defined by

$$\text{RHS} = (1+\nu)[F_L\ F_D\ M]^T_{t+\triangle t} - \nu[F_L\ F_D\ M]^T_t\ , \quad (5)$$

with ν = -0.05, F_L, F_D, and M representing the slight numerical damping and the aerodynamic loads for lift, drag and moment at time t and $t + \Delta t$ [20]. The predicted aerodynamic loads at time $t + \Delta t$ are applied to the two shared nodes of the beam and user element, in order to calculate the nodal 'state-of-motion' properties at time $t + \Delta t$.

The initial angle of attack θ_0, required in Eq. (4) to calculate the angle of attack $\alpha_{t+\Delta t}$, was set to 10 °.

3.2 Model of the insulator strings

In order to compare the effect of different cable support conditions on the galloping vibration amplitudes,

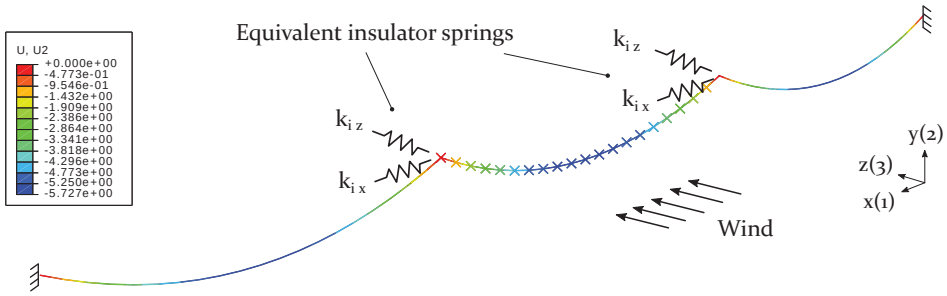

Figure 8: Simplified support conditions for standard conductor line connection using hanging insulator strings at static equilibrium (contour plot: deflection U_2).

a simplified three-span-system with a standard cable-insulator string connection is modelled. The hanging insulator strings are thereby represented by linear static springs in the x-z plane [47], determined by

$$k_{i_x} = \frac{1}{L_i}\left(mgL_x + \frac{m_i g}{2}\right), \tag{6}$$

$$k_{i_z} = k_{i_x} + \frac{2H_x}{L_x}, \tag{7}$$

where L_i and m_i represent the length and the weight of the insulator string, respectively. It is assumed that the insulator string and the load carrying tower structure are entirely stiff. The support conditions used in the numerical galloping simulation are schematically shown in Fig. 8.

3.3 Model of the power pylon structure

Spatial beam elements were used to model the power pylon with its multi-material-design. The material properties of steel were assigned to the tapered tower section, whereas the composite cross arm is defined by the smeared lamina properties (see Tab. 1). The tower and the cross arm is divided into several sub-sections to represent the decreasing wall thickness and diameter towards each tip. In order to evaluate potential resonant vibrations due to a galloping event, a frequency analysis of the power pylon was carried out. The conductor lines are thereby represented by point masses and equivalent springs, acting to both sides of each cable attachment point (CAP) in the global x-direction. As the present sag-to-span ratio is smaller than 1/8, the equivalent spring stiffness k_x of a taut conductor line may be calculated by

$$k_x = k_e \left[1 + \frac{mgL_x^3 k_e}{12H_x^3\left(1 + \frac{8}{3}\left(\frac{s}{L_x}\right)^2\right)}\right]^{-1}, \tag{8}$$

where k_e and s represent the horizontal stiffness of a perfectly taut cable and the cable sag, respectively [48]. The horizontal stiffness of a perfectly taut cable k_e is described as

$$k_e = \frac{AE}{L_x}\cos^2(\varphi), \tag{9}$$

with AE and φ representing the axial stiffness of the conductor line and the angle between the chord line and a horizontal reference [48].

The numerical galloping simulation is based on a preliminary power pylon design [49], considering a variation of wind-ice-loading scenarios [50, 51] and a maximum allowable static deflection in the vertical y-direction of 200 mm, defined by the architects.

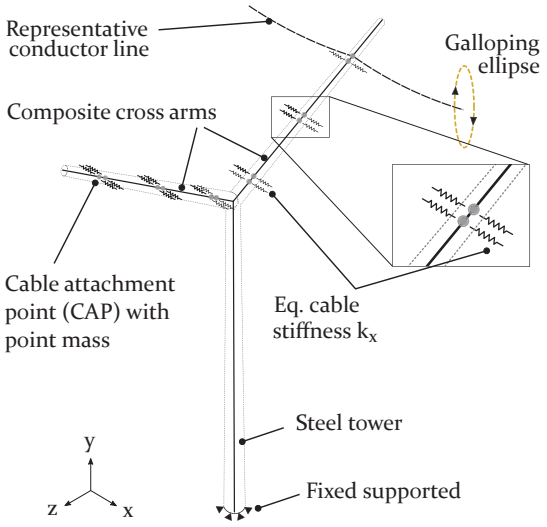

Figure 9: Boundary conditions for the composite power pylon with cables represented by springs and point masses.

In order to investigate the effect of damping on the cable vibration amplitudes due to galloping, a reasonable damping ratio is therefore assigned to the composite cross arm section of the power pylon model. The damping properties of GFRP composite materials significantly decrease with decreasing temperature [11] and may not offer sufficient damping at galloping-prone temperatures below the freezing point. However, the application of constrained layer damping treatments, using viscoelastic materials with its peak damping in that temperature range, may considerably increase the damping of the composite structure [26]. A damping ratio of $\zeta_{CA} = 0.03$ is therefore assigned to the composite cross arm section in the numerical galloping analysis. The damping is implemented using the Rayleigh damping coefficients, calculated by Eq. (2), where ω_i and ω_j represent the two angular frequencies, at which the composite cross arm vibrates during the galloping event.

3.4 Model of the cable-tower system

The numerical galloping analysis was carried out using the three-span model with different cable support conditions. Only one conductor line is fully modelled, subjected to aerodynamic loading in the center span (see section 2.2). The remaining cables are represented by point masses and equivalent horizontal springs in the global x-direction (see section 3.3). All relevant codes in order to reproduce the numerical galloping analysis, such as the Fortran-code for the UEL, the Python-code for extracting and post-processing the displacement data from Abaqus and the input files for Abaqus, are published and freely available [52].

4 Results numerical simulation

The results of the numerical galloping simulation of the three-span system are presented in this section. The results of the static deflection and the horizontal reaction forces are discussed before presenting the natural frequencies of the system and the power pylon with its equivalent cable springs and point masses. Furthermore, the effect of the cable support condition on the cable vibration amplitudes are investigated by comparing the direct cable attachment with the standard cable-insulator string connection. Finally, the potential mitigation of conductor line galloping by the implementation of additional damping in the composite cross arm is discussed.

4.1 Static deflection of cable-pylon system

The results of the static deflections of a three-span-system are shown in Figs. 8 and 10. The latter figure represents the direct cable-pylon connection approach, containing a set of power pylons and a representative 3x300 m long conductor line with ice accretion, positioned at the outer most CAP on the

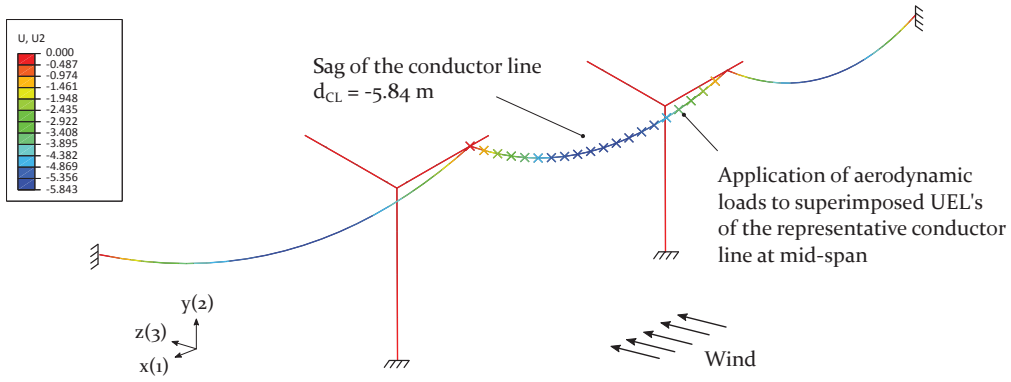

Figure 10: Maximum static deflection of the three-span-system with the representative conductor line subjected to aerodynamic loads.

composite cross arm. The user elements (UEL) are assigned to the conductor line at mid-span, representing the point of attack of the aerodynamic loads. The results of the equilibrium condition of a single, 300 m long cable span are listed in Tab. 4. The maximum cable sag at the center with $s_{num} = 5.727\,\text{m}$ corresponds to the analytical solution based on (1) with $s_{an} = 5.730\,\text{m}$. In order to considerably reduce the computational effort for the numerical galloping simulation, the remaining 11 cables of the system are represented by equivalent springs (based on (8)) and point masses (see Fig. 9). The properties are listed in Tab. 4.

4.2 Frequency analysis

The results of the natural frequencies of the individual power pylon and the entire cable-pylon-system are discussed in the following.

4.2.1 Composite Power Pylon

The mode shapes and the natural frequencies of the individual power pylon - with and without equivalent cable masses and stiffness - are presented in Fig. 11. The consideration of 12 taut cables significantly changes the vibration behaviour of the power pylon. The equivalent cable masses lead to a decrease of the first natural frequency by 55 % while maintaining its bending mode shape in the yz-plane, compared to the power pylon without equivalent cable attachments. However, the resulting first natural frequency of the power pylon $f_{p_1} = 1.32\,\text{Hz}$ (bending mode in the yz-plane) is very close to the galloping induced pylon vibration $f_{g_p} = 1.23\,\text{Hz}$ (bending mode in xz-plane), discussed in more detail in section 4.3.1. An increase in the vertical bending stiffness by locally reinforcing the cross arm and the tower in the yz-plane may reduce a potential resonance vibration of the pylon due to galloping. The natural frequencies of the higher modes are above 2 Hz and therefore not prone to resonance due to galloping induced vibrations.

4.2.2 Conductor line-pylon system

The natural frequencies of the entire cable-pylon-system are dominated by the conductor lines. The results are listed in Tab. 5. The mode shape related to the lowest frequencies of the 3x300 m span system corresponds to a single, horizontally oriented loop in the xz-plane. As conductor line galloping occurs in most of the cases as a vertically oriented single loop,

Table 4: Static conditions of an iced conductor line with a span length of 300 m, based on the properties shown in Tab.2 and 3.

	Per cable			Per cable attachment point (CAP)	
	Tension H_x	Sag s	Cable inclination α_c	Eq. Stiffness k_x	Eq. Point mass m_c
Numerical	45840 N	5.727 m	4.01 °	$1.3 \cdot 10^5$ N/m	714 kg

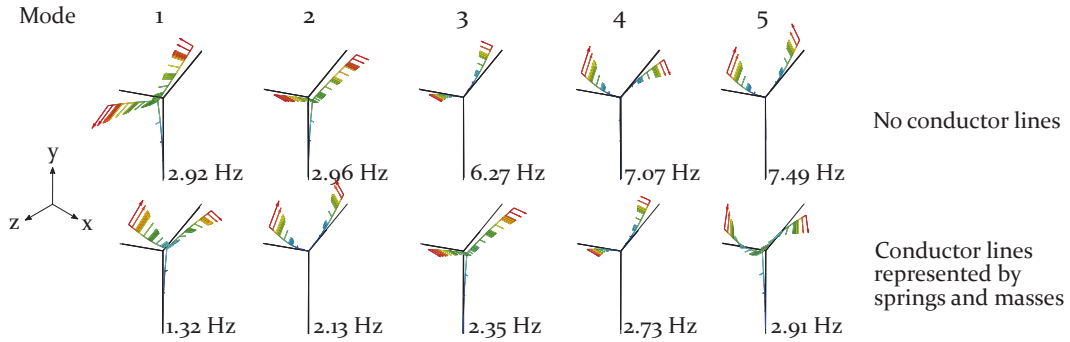

Figure 11: Frequency analysis of the composite power pylon - without and with attached cables (represented by eq. springs k_x and point masses m_c at each CAP as shown in Fig. 9).

the initial guess of the numerically simulated galloping frequencies was set to the corresponding mode 4-6 with its natural frequencies between 0.286 Hz and 0.312 Hz for the calibration of the Rayleigh damping coefficients (see section 4.3.1 and Tab. 6).

4.3 Galloping analysis

In the following the results of the numerical galloping simulation for a three-span conductor line system with different cable boundary conditions are presented. The parameters like wind speed U_w, initial angle of attack α, cable sag s, damping of the iced conductor line ζ_c and horizontal tension force H_x remain unchanged throughout the entire analysis (see section 3).

In the first section, the calibration of the Rayleigh coefficients is described, as the damping for the cable and the cross arm is implemented using Rayleigh damping. Three galloping models

- Model 1: Standard cable-insulator string connection,
- Model 2: Direct cable-pylon connection ($\zeta_{CA} = 0$),
- Model 3: Direct cable-pylon connection ($\zeta_{CA} = 0.03$),

are studied and discussed in the following sections. Each galloping simulation was carried out over a period of 1500 s, in order to reach a steady state condition. Finally, the vibration amplitudes of the three models with regard to the mid-span are compared and discussed in more detail in the section 'Comparison of vibration amplitudes'.

Table 5: Natural frequencies of three-span system (3x300 m conductor lines, each with a sag $s = 5.73$ m and a horizontal reaction force $H_x = 45.84$ kN).

	Mode	1-3	4-6	7-9	10-12	13-15	16-18	19-21
Natural frequencies	min	0.231	0.286	0.459	0.461	0.687	0.690	0.908
of the system f_{s_n} [Hz]	max	0.231	0.312	0.460	0.461	0.688	0.690	0.910
Nr. loops per span (plane)		1 (xz)	1 (xy)	2 (xy)	2 (xz)	3 (xz)	3 (xy)	3 (xz | xy)

4.3.1 Calibration of Rayleigh coefficients

The calibration of the Rayleigh damping coefficients α_R and β_R for the cable and cross arm was carried out iteratively, based on Eq. (2). The iteration is needed, as the galloping characteristics may change when introducing a change in the damping level.

1) Galloping analysis of a cable, fully constrained at each end; Calibration of the initial Rayleigh coefficients based on an expected single loop (in xy-plane) at frequencies close to the natural frequencies of the 3x300 m cable-pylon system (see Tab. 5),

2) Re-calibration of the Rayleigh coefficients based on the resulting galloping frequencies of a cable-pylon-system (shown in Fig. 12 for Model 2), representing a three-span-model (3x300 m) with a galloping cable in the center span (see Fig. 10),

3) Verification step of the galloping analysis, based on Rayleigh coefficients calibrated in step 2), showing galloping frequencies in the same range.

The Rayleigh coefficient for the cable, used in the numerical galloping analysis, are shown in Tab. 6 and are based on the galloping frequencies presented in Fig. 12. The galloping frequencies were determined by using a Fast Fourier Transformation (FFT) of the time histories at the CAP (location B) and the galloping conductor lines (location D) at steady state in horizontal and vertical direction (see Fig. 4).

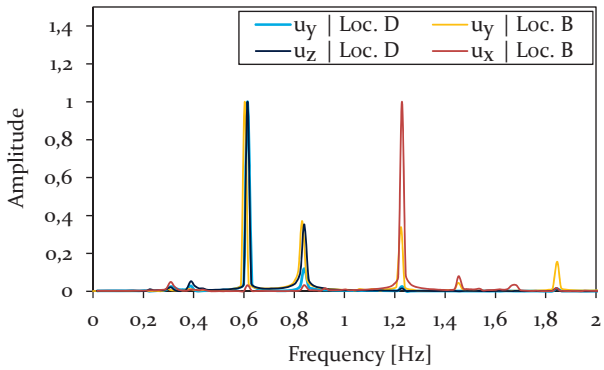

Figure 12: Results of the FFT of Model 2, based on the time histories of displacements in vertical u_y and horizontal u_x, u_z directions at location B (CAP) and D (1/4) of the galloping cable span).

The location D along the galloping conductor line of the reference model was chosen instead of location C, as the iced cable was galloping in a 2-loop constellation with its anti-nodes at 1/4 of the span. As expected, the CAP of the power pylon vibrates in vertical direction with mainly the same frequencies as the galloping conductor line ($f_1 = 0.61$ Hz and $f_2 = 0.84$ Hz) and the horizontal vibration of the CAP ($f_2 = 1.23$ Hz). The latter is basically twice the vertical galloping frequency of the cable, as the power pylon is pulled sidewards when the cable vibrates between its maximum and minimum.

The Rayleigh coefficients of the cross arm are determined with $\alpha_R^{pylon} = 0.152$ and $\beta_R^{pylon} = 0.005$, based on the galloping induced vibrations frequencies of the

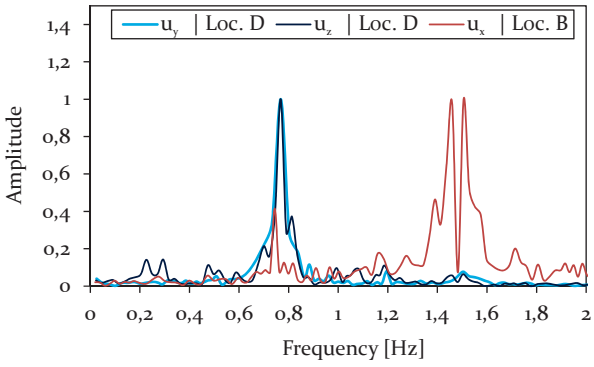

Figure 13: Results of the FFT of Model 1, analysing the time histories of displacements in vertical u_y and horizontal u_x, u_z directions at location B (Insulator string connection) and D (1/4 of the galloping cable span).

structure and its damping ratio of $\zeta_{CA} = 0.03$ (see section 3.3).

The Rayleigh coefficients for the cable, used in Model 1, were determined as $\alpha_R^{cable} = 0.154$ and $\beta_R^{cable} = 0.0066$, based on the FFT-plot represented in Fig. 13. The slightly increased galloping frequencies of Model 1 compared to Model 2 (see Fig. 12) are due a galloping mode with 3 loops, instead of a 2-loops condition at steady state.

4.3.2 Model 1: Cable-Insulator connection

The spring stiffnesses used to represent the hanging insulator strings (see Fig. 8) are defined by $k_{i_x} = 8.61\,\text{kN/m}$ and $k_{i_z} = 8.36\,\text{kN/m}$ [9]. Time histories of the vertical and horizontal cable vibration amplitudes due to galloping are shown in Figs. 14 and 15 for different locations along the three-span system.

After a period of about 200 s, denoted as phase I, the galloping instability reaches steady state (phase II), in which a 3-loop galloping mode is identified (see Fig. 16).

The observation is in agreement with the determined

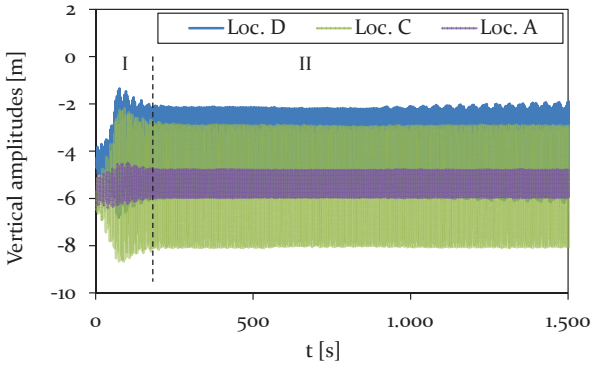

Figure 14: Model 1 - Time history plot of vertical displacements at location A (Center, adjadent span), location B (CAP, insulator string), C (Center, mid span) and D (1/4, mid span) (see Fig. 4), representing different vibration conditions (phase I - II).

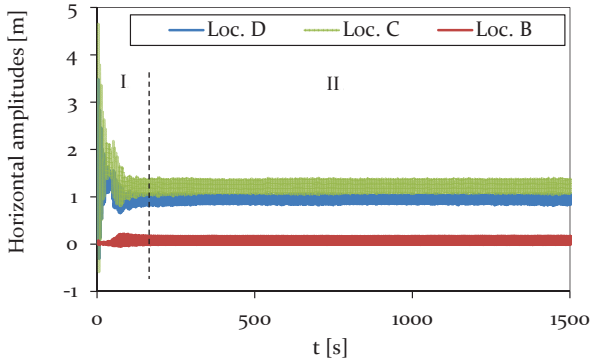

Figure 15: Model 1 - Time history plot of horizontal displacements at location A (Center, adjadent span), location B (CAP, insulator string), C (Center, mid span) and D (1/4, mid span) (see Fig. 4), representing different vibration conditions (phase I - II).

Table 6: Calibration of the Rayleigh coefficients α_R^{cable} and β_R^{cable} for the galloping cable for Model 2 and 3.

Model	Galloping mode (steady state)	Damping ζ_c [-]	Galloping frequencies [Hz]		Rayleigh coefficients	
		Cable	Cable	Tower	α_R^{cable}	β_R^{cable}
Initial (1x300 m)	1-Loop (xy-plane)	0.032	0.29 - 0.31	-	0.060	0.017
Iteration 1 (3x300 m)	2-Loop (xy-plane)	0.032	0.61 | 0.84	0.60 | 1.23	0.143	0.007
Iteration 2 (3x300 m)	2-Loop (xy-plane)	0.032	0.52 | 0.61	0.57 | 1.01	No re-calibration	

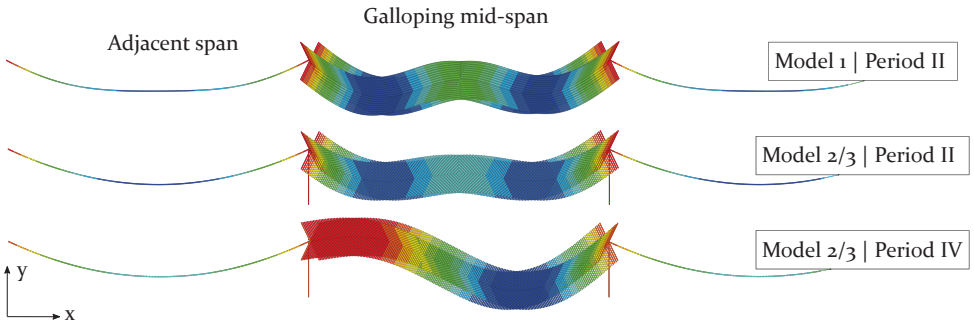

Figure 16: Comparison of the scaled galloping modes of Model 1 at steady state (phase II) and Model 2 and 3 with a 3-loop (phase II) and a 2-loop galloping mode (phase IV).

galloping frequencies, presented in Fig. 13. The natural frequencies of the system, corresponding to a vertical 3-loop mode in the xy-plane, are with $f_{s_{16-18}} = 0.69\,\text{Hz}$ close to the galloping frequencies of the cable with $f_{g_c} \approx 0.76\,\text{Hz}$ (see Tab. 5).

The vertical amplitudes at the center and at the quarter point of the galloping mid-span (Loc. C and D) are determined as 4.9 m and 3.6 m in phase II, respectively. It is clearly observed that the adjacent span (Loc. A) is excited by the galloping conductor lines at mid-span to vibrate in the vertical direction, leading to amplitudes of about 1.1 m. The pronounced coupling is due to the cable connection by the hanging insulator strings, which are free to move in the xz-plane and only restricted by the stiffness from the adjacent cables.

The horizontal amplitudes in the mid-span at steady state (phase II) are with maximum 0.4 m much smaller

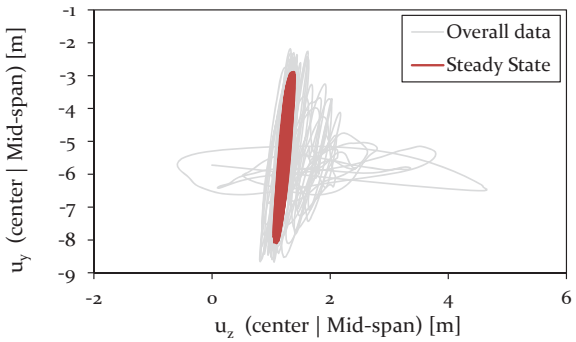

Figure 17: Model 1 - Galloping ellipse traced at Loc. C (center, mid-span) during 3-loop galloping.

compared to the vertical amplitudes. However, an excitation of the adjacent spans to vibrate in the z-direction is also observed. The trace of the galloping conductor line in yz-plane at the center of the mid-span (Loc. C) is presented in Fig. 17, showing the chaotic build-up phase (phase I) and the clearly vis-

ible galloping ellipse during steady state (phase II).

4.3.3 Model 2: Cable-pylon-connection (no cross arm damping)

The galloping behaviour of the conductor line, rigidly attached to the composite cross arm, is much more unsteady compared to Model 1, demonstrated by the vertical and horizontal time history plots in Fig. 18 and 19.

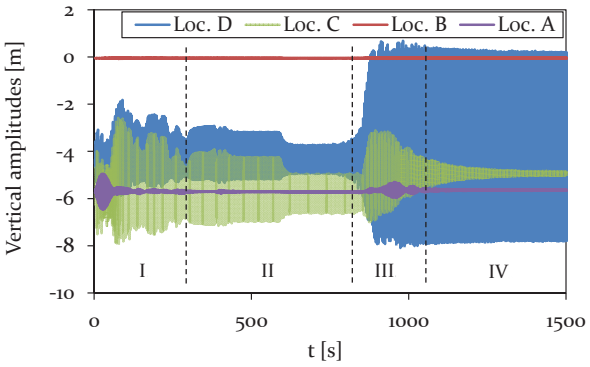

Figure 18: Model 2 - Time history plot of vertical displacements at location A (Center, adjacent span), location B (CAP, pylon), C (Center, mid span) and D (1/4, mid span) (see Fig. 4), representing different vibration conditions (phase I - IV).

After the initial build-up phase with a chaotic vibration behaviour of the cable, a 3-loop condition is observed (phase II) over a range of about 500 s. The vertical amplitudes at the center of the mid-span are with 2.7 m about 30 % higher compared to the location D at one-quarter of the mid-span. The steady state (phase IV) is reached after about 1050 s, representing a 2-loop galloping mode with a maximum vertical amplitude of 7.6 m at location D. The vertical and horizontal amplitude almost vanishes at the center of the mid-span, demonstrating a well-balanced 2-loop condition (see Fig. 16).

The vibration response of the cable consists of a dominating part at the frequency $f_{g_c1} \approx 0.6$ Hz and a minor portion at $f_{g_c1} \approx 0.81$ Hz (see Fig. 12).

The unsteady vibration behaviour of the cable in vertical (y-axis) and horizontal (z-axis) direction is assumed to be due to the direct power pylon connection with its high bending stiffness, resulting in a limited displacement at the CAP in the xy-plane. This leads to a delayed and irregular excitation of the adjacent spans, which consequently effects the vibration behaviour of the galloping cable at mid-span.

The observed vibration amplitudes of the adjacent spans (see Loc. A in Fig. 18 and 19) exhibit the same magnitude compared to Model 1, but only in the transient phases I and III and just over a short period of 150 s. In phase I and III of Model 2, the observed and steady vibration amplitudes in vertical direction with maximum 0.1 m, which corresponds to only 9 % of the vertical amplitudes in Model 1 with its standard insulator string connection (compare with at Loc. A in Fig. 14). The horizontal

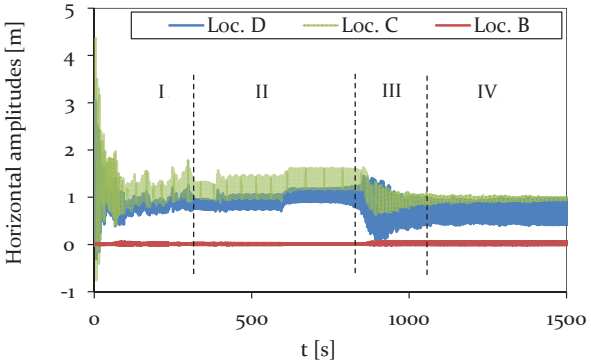

Figure 19: Model 2 - Time history plot of horizontal displacements at location B (CAP, pylon), C (Center, mid span) and D (1/4, mid span) (see Fig. 4), representing different vibration conditions (phase I - IV).

vibration amplitudes of the adjacent spans of Model 1 and 2 also vary in magnitude. In Model 1, the amplitudes are with 0.18 m about 90 % higher compared to Model 2. The variation in vibration amplitudes of

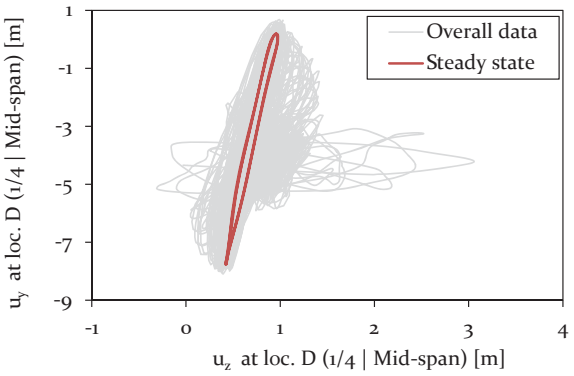

Figure 20: Model 2 - Galloping ellipse traced at Loc. D (1/4, mid-span) during 2-loop galloping.

the different models at mid-span is discussed in more detail in section 4.3.5. In Fig. 20, the characteristic galloping ellipse at Loc. D is shown for the 2-loop galloping condition at steady state.

4.3.4 Model 3: Cable-pylon-connection with cross arm damping

Additional damping in the composite cross arm of the power pylon is assumed to mitigate the galloping induced cable vibration amplitudes. A damping ratio of $\zeta_{CA} = 0.03$ is thereby implemented to the cross arm by Rayleigh damping, calibrated based on the vibration frequencies at Loc. B (CAP) shown in Fig. 12. The results of the time dependent cable displacements in vertical and horizontal direction are presented in Fig. 21 and 22 for different locations along the three-span system.

The difference in the time history plots of the vertical and horizontal amplitudes of Model 2 and 3 is mainly related to a changed duration of the different phases. Whereas the durations of the transition phases I and III are increased, the period of phase II with its 3-loop galloping mode is reduced.

However, the overall vibration behaviour with the 2- and 3-loop mode is the same for Model 2 and 3. No significant difference in horizontal and vertical vibra-

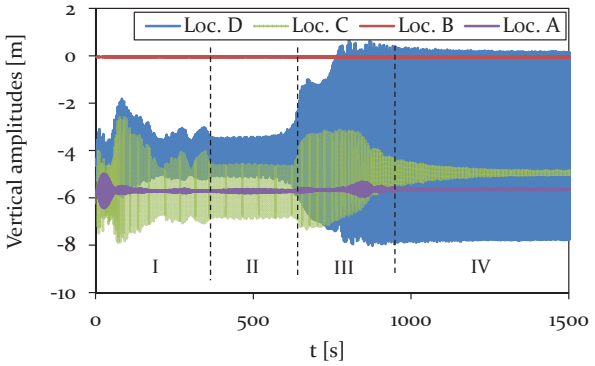

Figure 21: Model 3 - Time history plot of vertical displacements at location A (Center, adjacent span), location B (CAP, Power pylon), C (Center, mid span) and D (1/4, mid span) (see Fig. 4), representing different vibration conditions (phase I - IV).

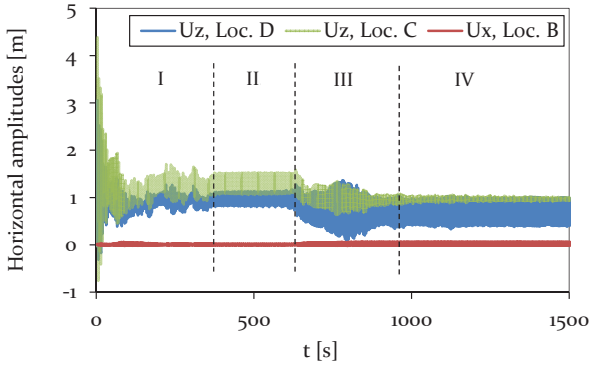

Figure 22: Model 3 - Time history plot of horizontal displacements at location B (CAP, pylon), C (Center, mid span) and D (1/4, mid span) (see Fig. 4), representing different vibration conditions (phase I - IV).

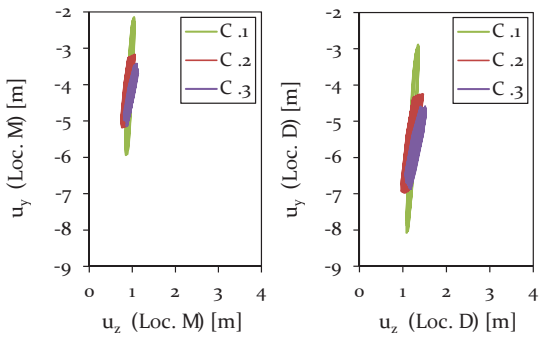

Figure 23: Comparison of the galloping ellipses of Model 1 (Insulator string connection), Model 2 (direct connection without cross arm damping) and Model 3 (direct connection with cross arm damping $\zeta_{CA} = 0.03$) with regard to a 3-loop condition at Loc. C and D, each at about 500 s (phase II).

tion amplitude of the adjacent spans is observed. A comparison of the vibration amplitudes of the mid-span is discussed in more detail in the following section.

4.3.5 Comparison of vibration amplitudes

As expected, the vertical vibration amplitudes at steady state are larger during a 2-loop galloping mode (see Fig. 20) compared to a 3-loop mode (see Fig. 17). In order to fairly compare the effect of the cable support condition on the vibration amplitudes of the galloping cable, the vibration conditions needs to be similar. Therefore, the galloping ellipse of Model 1, representing a standard cable-insulator string connection, is compared to the galloping ellipses of the models with a direct cable-tower connection (Model 2 and 3) at a time of about 500 s in phase II (see Fig. 18 and 21). At this state, the cables of all three models vibrate in a 3-loop mode with its local maxima in the center and close to one-quarter and three-quarter at mid-span. The resulting galloping ellipses for Model 1, 2 and 3 at Loc. C and D are therefore shown in Fig. 23.

A change in cable support condition from an insulator string to a stiff pylon structure leads to a significant change in the vibration behaviour with respect to the xz-plane in the center (Loc. C) and close to one-quarter (Loc. D) at mid-span. Two phenomena are thereby observed at both locations: 1) a change in length of the major axis of the galloping ellipse and 2) a rotation of the ellipse towards the z-axis. The length of the major axis of the galloping ellipse significantly reduces from Model 1 to Model 2, resulting in a reduced vertical vibration amplitude of about 48 % due to the increased stiffness at the CAP. The application of damping to the cross arm with $\zeta_{CA} = 0.03$ in Model 3 leads to an additional reduction in vertical amplitudes by 15 % for the 3-loop condition at Loc. C.

At the same time, a gradually rotating galloping ellipse towards the z-axis is observed for Model 1 to 2 by 7 % and for Model 2 to 3 by additional 2.3 %. This consequently leads to an increase in horizontal amplitude by 53 % from Model 1 to Model 2. A further increase in horizontal vibration amplitude is not observed for Model 3. Instead, the application of damping to the composite cross arm leads to a reduction of the galloping ellipse in horizontal direction by 8 %.

In summary, it can be stated that a change from a flexible cable-insulator string connection to a stiff cable-pylon connection seems to considerably reduce the size of the galloping ellipse, while slightly increasing the horizontal vibration amplitude. Additional damping in the composite cross arm further reduces the vertical vibration amplitudes and, at the same time, the horizontal vibration amplitude compared to Model 2 without any damping.

5 Conclusion

Wind-induced vibrations, such as the severe galloping cable vibration phenomenon, may lead to extensive damage at the cable attachment point or even for the entire mast structure. The objective of this research was to investigate a potential mitigation of conductor line galloping by rigidly connecting the conductor line to a non-conductive composite power pylon with enhanced damping properties.

A numerical galloping analysis of a representative 3 x 300 m span system was carried out in order to evaluate different cable-support conditions with respect to the resulting vibration amplitudes. The outer most cable of the mid-span was therefore subjected to aerodynamic loading in order to initiate conductor line galloping. The remaining cables were represented by equivalent spring stiffnesses and point masses. The main conclusions are drawn for the conducted simulations:

1) The vibration behaviour of a galloping conductor line, directly attached to a stiff pylon structure, is with a 3-loop and 2-loop condition much more complex compared to a flexible cable-insulator string connection with a constant 3-loop condition.

2) By changing the cable support conditions from an insulator string to a stiff power pylon, the vertical vibration amplitude at the location of maximum deflection may be reduced by 48 %, while the small horizontal vibration amplitude increases by 53 %.

3) The addition of damping to the composite cross arm with ζ_{CA} =0.03 leads to a reduction of vertical and horizontal vibration amplitudes by 15 % and 8 %, respectively, compared to the model without any damping in the composite cross arm.

Acknowledgement

Thanks to the Innovationsfonden Denmark for the financial support of the project 'Power Pylons of the Future' (PoPyFu) in collaboration with Bystrup and Tuco Marine ApS.

Declaration of conflicting interests

The author(s) declared no potential conflicts of interest with respect to the research, authorship and/or publication of this article.

Funding

The author(s) disclosed receipt of the following financial support for the research, authorship and/or publication of this article: This research is supported by Innovationsfonden Denmark via the project Power Pylons of the Future (PoPyFu) in collaboration with Bystrup and Tuco Marine ApS, which are gratefully acknowledged.

References

[1] D. Gardiner, *Report: Transmission upgrades and expansion - Keys to meeting large customer demand for renewable energy*, A Renewable America, 2018.

[2] Z. Liu, *Global Energy Interconnection*, Academic Press, 1st Edition, 2015.

[3] A. Bettencourt, *The Global Smart Grid Federation Report*, SmartGrid Canada, 2012.

[4] A. Feltus, Ageing grid poses problems, *Petroleum Economist*, **69**:15, 2002.

[5] Danish Energy Agency, *Nye retningslinjer for kabellægning og udbygning af transmissionsnettet*, 8. October 2008, j.nr. 022520/78028-001.

[6] K.J. Zhu, B. Liu, H.J. Niu, Statistical analysis and research on galloping characteristics and damage for iced conductors of transmission lines in China,

2010 International Conference on Power System Technology: Technological Innovations Making Power Grid Smarter, Powercon2010, doi: 10.1109/POWERCON.2010.5666025, 2010.

[7] J.P. Den Hartog, *Mechanical Vibrations*, McGraw-Hill Book Company, Inc., 4th Edition, 1956.

[8] J.L Lilien, M. Farzaneh et al., *State of the Art of Conductor Galloping - A complementary document to EPRI Orange Book*, CIGRÉ Publication, Technical Brochure no. 322, June 2007.

[9] N. Krog, Numerical Modeling of Conductor Line Galloping. *Master thesis* Technical University Denmark, Mechanical Engineering, 2015.

[10] A. Treviso, B.V. Genechten, D. Mundo, M. Tournour, Damping in Composite Materials: Properties and Models. *Composites Part B* doi: 10.1016/j.compositesb.2015.03.081, 2015.

[11] M. Kliem, M. Rueppel, J. Høgsberg, C. Berggreen, Damping properties of Nanoclay modified Glass and Aramid composites at low temperature and low frequencies. *submitted to Journal of Composite Materials*, 2017.

[12] M. Kliem, J. Høgsberg, Q. Wang, M. Dannemann, Characterization of clay-modified thermoset polymers under various environmental conditions for the use in high-voltage power pylons. *Advances in Mechanical Engineering* **9**:1–16, 2017.

[13] M. Kliem, J. Høgsberg, S. Hoschützky, J. Vanwalleghem, A. Filippatos, Experimental analysis of passive constrained layer damping treatments for composite power pylon structures. *Canadian-International Conference on Composites, Cancom* Ottawa, Canada, 17-20 July 2017.

[14] H. D. Vo, H. Katsuchi, H. Yamada, M. Nishio A wind tunnel study on control methods for cable dry-galloping. *Frontiers of Structural and Civil Engineering* **10**:72–80, 2016.

[15] S. Kalaga, P. Yenumla, *Design of Electrical Transmission Lines: Structures and Foundations*, CRC Press, 1st Edition, 2016.

[16] H. Skouboe, BYSTRUP Design, Power Pylons of the Future, *E-mail: hs@bystrup.dk*, 16.11.2017.

[17] Bystrup Architects, *Power Pylons of the Future*, Commercial booklet, 3rd Edition, 2015.

[18] J. R. Offersen, Udbygning og forstærkning af Energinet.dk's 400 kV linje Idomlund-Tjele. *Diplomingeniør projekt* Aalborg Universitet, Mechanical Engineering, 2016.

[19] R.A. Hayder, *Strengthening design of reinforced concrete with FRP*, Taylor and Francis, 1st Edition, 2015.

[20] J. Hu, B. Yan, S. Zhou, H. Zhang, Numerical Investigation on Galloping of Iced Quad Bundle Conductors. *IEEE TRANSACTIONS ON POWER DELIVERY* **27**:784–792, 2012.

[21] P. Yu, Y. M. Desai, N. Popplewell, A.H. Shah, Three-degree-of-freedom model for galloping. Part II: Solutions. *Journal of Engineering Mechanics* **119**:2426–2448, 1993.

[22] M. Walker, *Aluminum Electrical Conductor Handbook*, Aluminum Association, 3rd Edition, 1989.

[23] A. Borna, Prediction of Galloping of Transmission Line Conductors by a Computational Aeroelastic Approach. *Dissertation* McGill University, Mechanical Engineering, Montreal, 2014.

[24] H. Xu, K.-J. Zhu, B. Liu, C.-L. Liu, J.-L. Yang, A study of influencing parameters on conductor galloping for transmission lines. *Journal of Vibro-Engineering* **16**:ISSN1392-8716, 2014.

[25] M. T. Stickland, T. J. Scanlon, An investigation into the aerodynamic characteristics of catenary contact wires in a cross-wind. *Proc Instn Mech Engrs* **215**, Part F, 2001.

[26] M. Kliem, J. Høgsberg, J. Vanwalleghem, A. Filippatos, S. Hoschützky, E. R. Fotsing, C.

Berggreen, Damping investigation of cylindrical composite structures with enhanced damping properties. *submitted to the Journal of Applied Composite Materials*, 2018.

[27] G. J. Davies, Numerical Analysis of Cables in the Offshore Environment. *Master thesis* University of Cape Town, South Africa, 1988.

[28] B. Yan, X. Lin, W. Luo, Z. Chen, Z. Liu, Numerical Study on Dynamic Swing of Suspension Insulator String in Overhead Transmission Line under Wind Load. *IEEE TRANSACTIONS ON POWER DELIVERY* **25**:248–259, 2010.

[29] W. Dai, F. Gao, Y. Bai, FEM analysis of deepwater drilling risers under the operability and hang-off working conditions. *J. Marine. Sci. Appl.* **8**:156–162, 2009.

[30] X. M. Li, K. J. Zhu, L. Bin, Experimental Simulation on Aerodynamic Character of D-Shaped Iced Conductor. *Applied Mechanics and Materials* **614**:622–627, 2013.

[31] D.G Havard, J.L Lilien, *Conductor galloping*, Tutorial given at IEEE ESMOL and TPC Meeting, Las Vegas, January 2008.

[32] B. Liu, K. J. Zhu, X. M. Li, X.P. Zhan, Hysteresis Phenomenon in the Galloping of the D-Shape Iced Conductor, *Mathematical Problems in Engineering* **784239** doi.org/10.1155/2013/784239, 2013.

[33] A. V. Guedes, C.F. Matt, E. S. C. Cavalcanti, Experimental investigation of the dynamic behaviour of stockbridge dampers. *18th International Congress of Mechanical Engineering* November 6-11, 2005, Ouro Preto, MG.

[34] J. H. G. Macdonald, G. L. Larose, Two-degree-of-freedom inclined cable gallopingPart 2: Analysis and prevention for arbitrary frequency ratio. *J. Wind Eng. Ind. Aerodyn.* **96**:291–307, 2008.

[35] J. H. G. Macdonald, G. L. Larose, Two-degree-of-freedom inclined cable gallopingPart 1: General formulation and solution for perfectly tuned system. *J. Wind Eng. Ind. Aerodyn.* **96**:308–326, 2008.

[36] M. B. Waris, T. Ishihara, M. W. Sarwar, Galloping response prediction of ice-accreted transmission lines. *The 4th International Conference on Advances in Wind and Structures(AWAS'08)* Jeju, Korea, May 29-31, 2008.

[37] H. Zhang, X. Liu, L. Zhang, L. He, Theoretical and Numerical Analysis of Galloping of Bundle Conductors. *Asia-Pacific Power and Energy Engineering Conference* Wuhan, China, March 25-28, 2011.

[38] C. B. Gurung, H. Yamaguchi, T. Yukino, Identification of large amplitude wind-induced vibration of ice-accreted transmission lines based on field observed data. *Engineering Structures* **24**:179–188, 2001.

[39] B. Yan, X. Liu, X. Lv, L. Zhou, Investigation into galloping characteristics of iced quad bundle conductors. *Journal of Vibration and Control* **22**:965–987, 2014.

[40] R. Clark, D. Cox, H. Curtiss, J. W. Edwards, K. C. Hall, D. A. Peters, R. Scanlan, E. Simiu, F. Sisto, T. W. Strganac, *A Modern Course in Aeroelasticity*, Springer Science an Business Media, 4th Edition, 2006.

[41] J. Swinkels, L. v. d. Eijnden, A journey towards sustainable energy security - Lessons learned from Denmark, *Interdisciplinary research* Utrecht University, Mechanical Engineering, 2014.

[42] R. Keutgen, J. L. Lilien, Benchmark cases for galloping with results obtained from wind tunnel facilities validation of a finite element model. *IEEE Transactions on Power Delivery* **15**:367–374, 2000.

[43] R. D. Blevins, *Flow-induced vibration*, Van Nostrand Reinhold, New York, 2nd Edition, 1990.

[44] D. Srivastava, D. Chandra, Transmission Line Conductor Galloping Analysis using FEM. *International Journal of Applied Engineering Research* **11**:6972–6982, 2016.

[45] D. Johansen, Mitigation of Conductor Line Galloping by Enhanced Damping in Composite Power Pylons. *Master thesis* Technical University Denmark, Mechanical Engineering, 2018.

[46] *'Implicit dynamic analysis' in the ABAQUS Theory Manual* ver. 6.14.

[47] A. S. Veletsos, G. R. Darbret, Dynamic stiffness of parabolic cables. *Earthquake Engineering and Structural Dynamics* **11**:367–401, 1983.

[48] M. K. S. Madugula, *Dynamic Response of Lattice Towers and Guyed Masts*, Amer Society of Civil Engineers, 1st Edition, 2001.

[49] T. S. Odgaard, C. Corfitzen, Statisk design og analyse af hjspndingsmast i glasfiber, *Diplom thesis* Technical University Denmark, Mechanical Engineering, 2017.

[50] DS/EN 50341-1:2013, Elektriske luftledninger, der overstiger 1 kV AC - Del 1: Generelle krav - Flles specifikationer, *Dansk Standard*, 2013.

[51] DS/EN 50341-3-5:2001, Elektriske luftledninger, der overstiger 45 kV AC - Del 3: Nationale normative aspekter, *Dansk Standard*, 2013.

[52] M. Kliem, Fortran-, Python- and Abaqus-Codes for: Mitigation of conductor line galloping by a direct cable-connection to non-conductive composite power pylons, *Mendeley Data*, doi:10.17632/3gg4mc2n8t.1.

DTU Mechanical Engineering
Section of Solid Mechanics
Technical University of Denmark

Nils Koppels Allé, Bld. 404
DK-2800 Kgs. Lyngby
Denmark
Phone (+45) 4525 4250
Fax (+45) 4593 1475
www.mek.dtu.dk
ISBN: 978-87-7475-522-7

DCAMM
Danish Center for Applied Mathematics and Mechanics

Nils Koppels Allé, Bld. 404
DK-2800 Kgs. Lyngby
Denmark
Phone (+45) 4525 4250
Fax (+45) 4593 1475
www.dcamm.dk
ISSN: 0903-1685